National Aeronautics and Space Administration

John F. Kennedy Space Center

2005 Annual Report

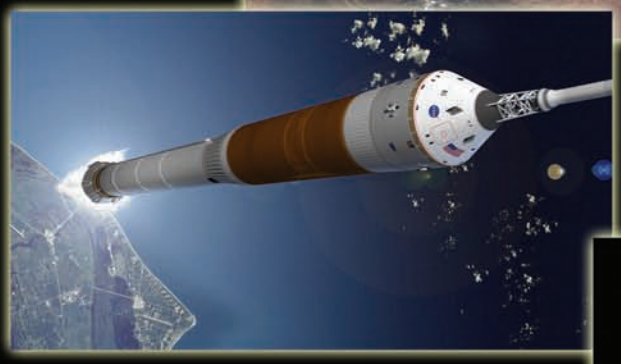

technology development and application

Technology Development and Application 2005 Annual Report

John F. Kennedy Space Center

Foreword

Successful technology development and application projects are critical to maintaining and enhancing KSC capabilities. Advanced technologies are required to solve technical problems, resolve operational issues, and optimize designs of flight and ground systems. When new technologies are infused in KSC systems and processes, the outcomes are safer, more efficient, and more responsive spaceport and range operations for our customers.

The KSC technology development team includes a wide variety of partnerships among civil servants, contractors, academic institutions, and commercial industries. KSC focuses its advanced technology activities on a list of KSC high-priority technology needs defined by our primary stakeholders, including current operational programs, future programs, and institutional technical programs. We focus and align our technology investments, personnel investments, new project proposals, and strategic partnerships with the technology needs most important to the programs supporting our Nation's Vision for Space Exploration.

This report highlights the results of KSC's applied technology work during 2005. Dr. Dave Bartine, Director, Applied Technology, is responsible for publication of this report and is the point of contact for any desired information. Contact him at 321-867-7069 or <David.E.Bartine@nasa.gov>.

James W. Kennedy
Director
John F. Kennedy Space Center

Contents

Contents (continued)

Contents (continued)

* 2005 Center Director's Discretionary Fund Project

Primary Stakeholders for KSC Technology Development and Application Activities

Reusable-Spacecraft Processing

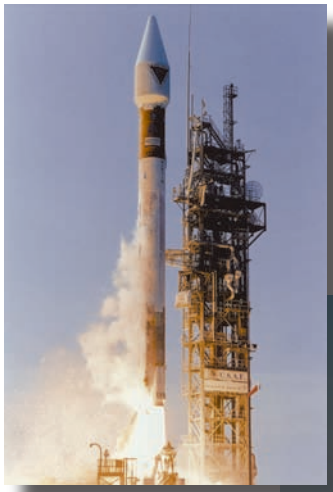

Launch Services Program

International Space Station/ Payload Processing

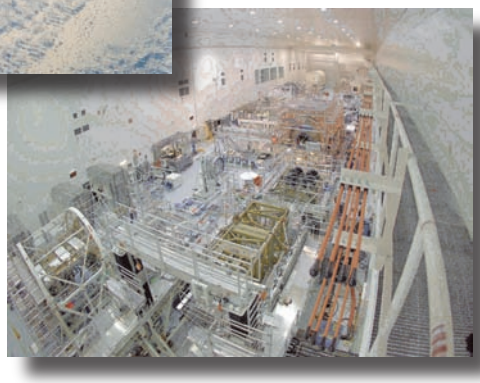

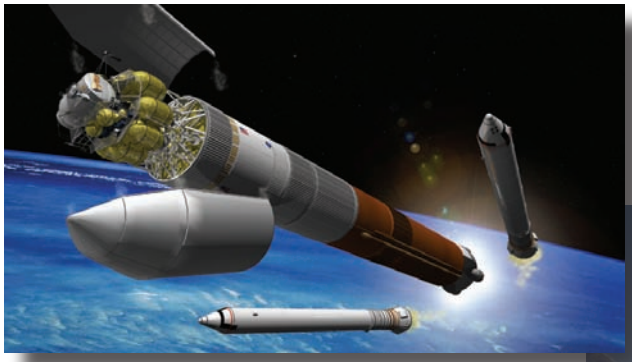

Constellation Systems

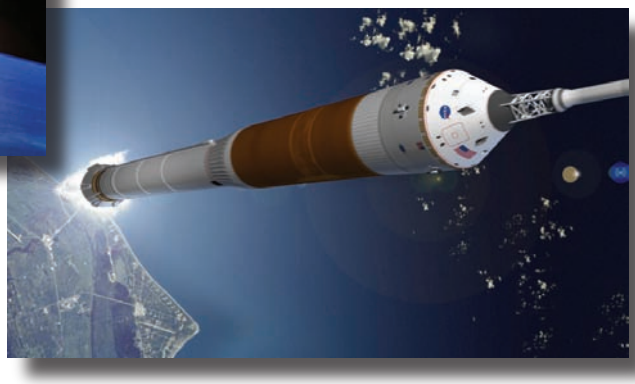

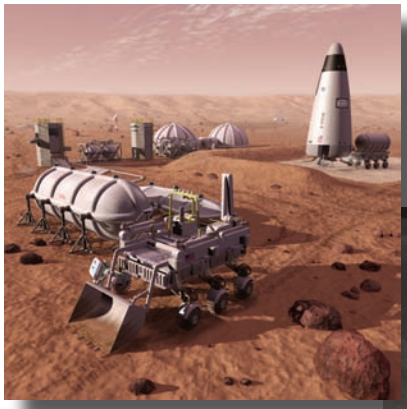

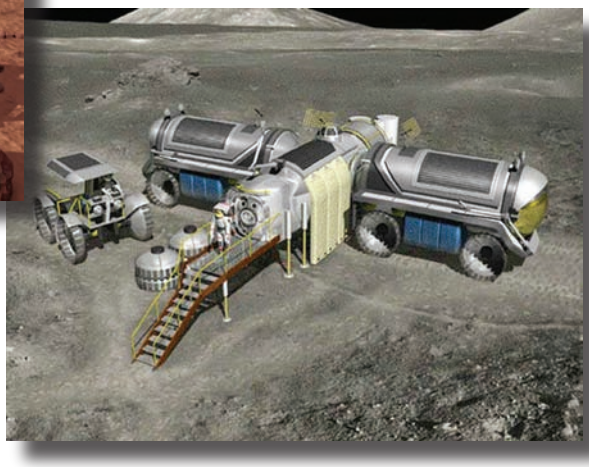

Extended Human and Robotic Exploration

Institutional Technical Programs

- Safety and Mission Assurance
- Institutional Facilities and Equipment
- Information Technology and Communication Services

Introduction

John F. Kennedy Space Center (KSC) technology development efforts support NASA's goals of increased safety, reduced cost of space access, and expansion of commercial markets by applying new technologies in current and future Space Transportation Systems.

KSC's role as the nation's premier launch site creates requirements for new spaceport and range technologies. KSC's people use our unique institutional resources to provide technologies to NASA program customers, including designers and operators of spaceports on Earth, lunar bases, and Mars bases. KSC has extensive expertise in designing, building, and operating a spaceport with all of its complex technologies and systems.

KSC technology development activities are categorized by six Spaceport Technology and Science Product Lines: Spaceport Structures and Materials; Range Technologies; Fluid System Technologies; Biological Sciences; Process and Human Factors Engineering Technologies; and Command, Control, and Monitoring Technologies. This report is organized by KSC's Spaceport Technology and Science Product Lines.

The primary stakeholders for spaceport and range technologies are current operational programs, future programs, and institutional technical programs. These stakeholders are illustrated on pages vi and vii. KSC focuses and aligns its technology investments, personnel investments, new project proposals, and strategic partnerships with the technology needs most important to our stakeholders in order to maximize benefits for the Agency and the nation. Articles describing technology results supporting KSC High-Priority Technology (HPT) Needs display the HPT icon. The complete list of KSC HPT Needs appears in Appendix A.

Through its Innovative Partnership Program, KSC seeks industry participation and collaboration in its technology development initiatives. Additional information on the Innovative Partnership Program is included in Appendix B. KSC reaches out to transfer expertise and technologies to the commercial sector and academic community. Programs and commercialization opportunities available to American industries and other organizations are described in the KSC Technology Transfer Office Internet Web site at <*http://ksc.nasatechnology.com/*>. University faculty and postdoctoral fellowship opportunities are described in the KSC University Programs Internet Web site at <*http://education.ksc.nasa.gov/educators/faculty.htm*>. Efforts to transfer NASA technology and content into high school classrooms are highlighted in Appendix C.

The U.S. Government controls exports of sensitive equipment, software, and technology as a means to promote our national security interests and foreign-policy objectives. This document has been reviewed for export control and intellectual property. Additional information on KSC's export control function appears in Appendix D.

An electronic version of this report is available at <*http://rtreport.ksc.nasa.gov*>.

Spaceport Structures and Materials

Advanced structures and materials are critical to achieving the goals of reduced costs, increased reliability, and higher flight rates for future spaceports. Spaceport structures and materials technology development areas include corrosion abatement, static charge dissipation, nondestructive evaluation (NDE), reduction of vibroacoustic loads during launch, and nonflammability. Sources of corrosion and material degradation include humid saltwater environments surrounding launch structures and aggressive ozone and hard radiation environments of Earth orbit. Static charge buildup on payloads, spacecraft, and launch structures can present significant safety issues for personnel and equipment. NDE technologies are critical to obtaining rapid status analysis of flight hardware. Passive sound mitigation techniques to replace active noise reduction methods such as water suppression systems are desirable for future launch vehicle pads. Advanced nonflammable materials are desirable to enhance the safety of crew and ground personnel during operations. Since materials are ubiquitous in spaceflight, the reach of this technology thrust area will encompass launch structures, payload processing, spacecraft design, and vehicle maintenance.

Technology focus areas include the following:

- launch structures and mechanisms,
- corrosion science and technology,
- electromagnetic physics,
- materials science and technology, and
- nondestructive evaluation.

The goals and objectives of Spaceport Structures and Materials include the following:

- ensuring safe, efficient, and reliable structures techniques;
- enhancing reliability and reducing maintenance cost of infrastructure;
- improving safety and reliability of operations through detection, mitigation, and prevention of electrostatic generation on equipment; and
- developing specialty materials in support of future structures and materials initiatives.

For more information regarding Spaceport Structures and Materials, please contact Dr. Carlos I. Calle <Carlos.I.Calle@nasa.gov>, NASA KT-E3, (321) 867-3274.

Vacuum-Gasketed, Crevice-Free Electrochemical Corrosion Cell

Corrosion Control

Crevice corrosion in electrochemical corrosion cells is a common source of error in corrosion measurements. This type of corrosion occurs at the interface that joins the sample of interest, the electrolyte, and the sample mounting device. The presence of crevice corrosion during electrochemical corrosion measurements significantly alters current/voltage responses, leading to error in the determination of both the thermodynamic and kinetic aspects of corrosion.

Efforts to address this problem have yielded several different crevice-free corrosion cell designs:

- The flooded gasket cell, despite being the gold standard for accurate electrochemical corrosion measurements, is expensive and prone to clogging and requires large volumes of electrolytes to keep the influx of distilled water from altering the electrolyte concentration.
- The flag working electrode is designed to be completely immersed in the electrolyte except for a thin flaglike section. This design eliminates any masking agent and most crevice-associated error but is not reliable for samples with multiple surfaces that exhibit different corrosion properties.
- Knife point polytetrafluoroethylene (PTFE) gaskets reduce but do not eliminate crevice corrosion and are usable for only one measurement.

In response, the vacuum-gasketed, crevice-free electrochemical corrosion cell (VGC) was designed to eliminate all crevice corrosion during corrosion measurements (Figure 1). This novel design prevents the development of crevices between the sample of interest and the masking agent by using pressure differences to hold the electrolyte in place. This pressure difference is generated by creating a sealed volume of gas above the electrolyte. The cell allows for the complete gas purging of electrolytes before and during electrochemical measurements. The cell is easy to operate, uses small volumes of electrolyte (10 to 25 mL), accommodates samples of various sizes, does not leave residue on samples, can be used for gas-purged electrolytes, and is easy to clean up. Waterline corrosion could cause error during measurements, but this error can be considered negligible. Simple modifications allow the cell to be used in special crevice-free applications, such as measuring the critical pitting temperature. Since gas can quickly diffuse into the electrolyte, it is important to select purging gases carefully for reliable results.

Cyclic polarization experiments were performed in 0.5M sodium chloride solution using a traditional knife point PTFE electrochemical cell and the new VGC to evaluate the likelihood of crevice corrosion in the different cells. Three tests using 304 stainless steel were performed on each cell. The knife edge PTFE gasket created crevice corrosion in all three measurements, as shown in Figure 2. Only pitting corrosion was observed in the three measurements using the VGC (Figure 3).

Contacts: Paul E. Hintze <Paul.E.Hintze@nasa.gov>, NASA KT-E, (321) 867-3751; and Dr. Luz Marina Calle <Luz.M.Calle@nasa.gov>, NASA KT-E, (321) 867-3278

Participating Organization: Ohio State University (Andrew P. Bonifas)

Figure 1. Vacuum-gasketed, crevice-free corrosion cell.

Figure 2. Sample after testing with knife point PTFE gasket cell.

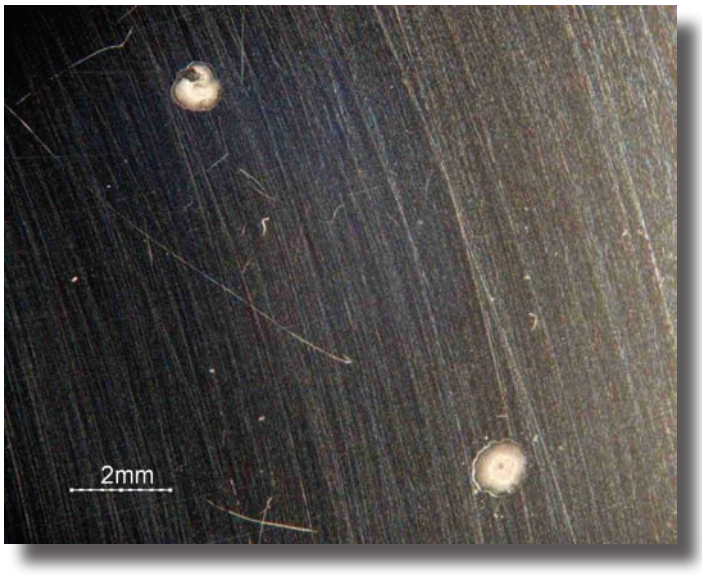

Figure 3. Sample after testing with VGC.

Microelectrochemical Cell for Evaluating Corrosion on Small Areas

Corrosion Control

The NASA Corrosion Technology Laboratory has built a microelectrochemical cell (MEC) for measuring electrochemical properties with high spatial resolution. This cell was used to investigate the corrosion properties of a friction stir weld (FSW).

An MEC measures the electrochemical properties of small areas. This type of measurement does not expose the entire sample to the electrolyte or another masking agent. This allows for many measurements to be run on a single sample, unlike conventional electrochemical tests. The MEC (Figure 1) consists of a Teflon body for the electrolyte and ports for the capillary tube, counter electrode, and reference electrode. The electrolyte makes contact with the sample through the capillary tube. The MEC is mounted on a microscope objective (Figure 2) so that the area being tested can be seen. The cell can be rotated in and out of the optical path. In this experiment, the tip measured an area of approximately 0.2 mm^2. Figure 3 shows a sample after measurement. All common electrochemical measurements may be made with the MEC.

FSW is a relatively new process invented by The Welding Institute in 1991. In this technique, two pieces of metal are placed together and the FSW bit is put in contact with the seam. The frictional heat formed where the rotating bit touches the metal softens the metals and allows them to be joined. The FSW process has advantages over other welding processes: lower temperature than other welds; defect-free welds; and a weld zone with the same composition as the bulk material. The FSW process produces an asymmetrical weld since the bit rotates as it moves across the two pieces of metal. The two sides of the weld are referred to as the advancing and receding sides. The advancing side is the side where the direction of rotation and translation are the same. The microstructure of an aluminum 6061-T6 FSW cross section is shown in Figure 4. On the advancing side, the left, the weld nugget reaches the surface of the metal.

The MEC was used to investigate the properties of an FSW of aluminum 6061-T6. Measurements of the pitting potential versus Standard Calomel Electrode at different distances from the center of the weld are shown in Figure 5. Negative distances are on

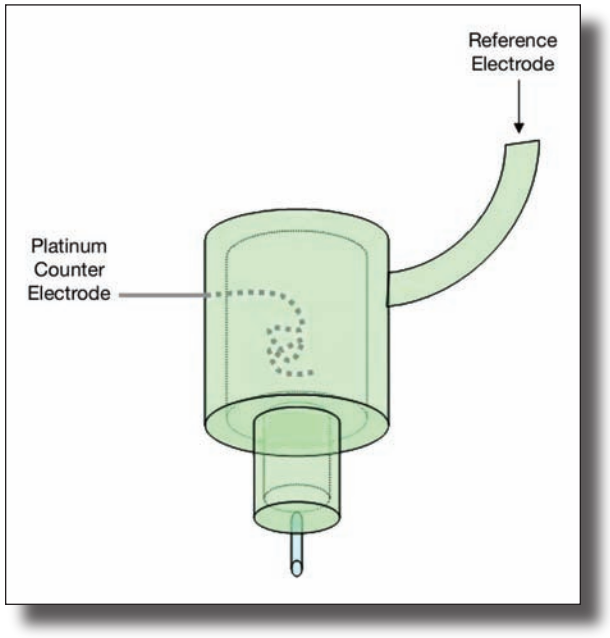

Figure 1. Schematic of MEC.

Figure 2. The MEC mounted on a microscope.

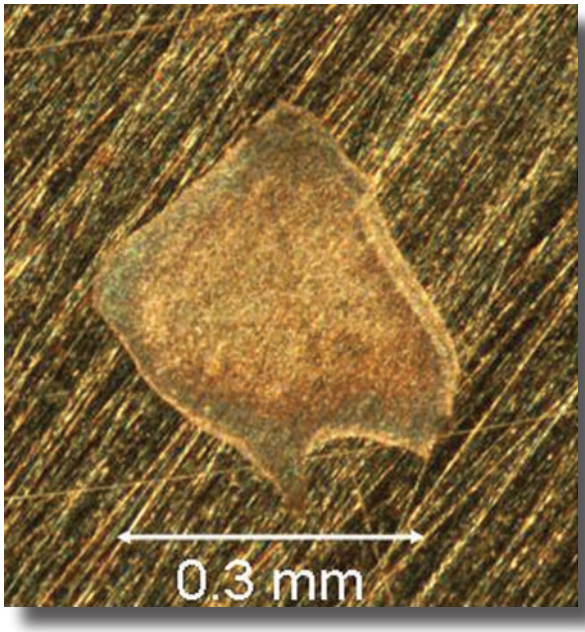

Figure 3. Metal sample after testing with the MEC.

the advancing side of the weld. At a large distance from the center of the weld, –12 mm, the pitting potential is that of the bulk metal. The pitting potential drops at about –5 mm from the weld, about where the weld nugget appears in Figure 4, indicating a decrease in corrosion resistance. The pitting potential stays low through the center of the weld. At 5 mm from the center on the receding side of the weld, the pitting potential has returned to a value very close to that of the bulk metal. This shows that the FSW process affects the corrosion properties of the metal in a very small region close to the weld. The MEC is actually able to measure the asymmetrical properties caused by the weld.

Contacts: Paul E. Hintze <Paul.E.Hintze@nasa.gov>, NASA KT-E, (321) 867-3751; and Dr. Luz Marina Calle <Luz.M .Calle@nasa.gov>, NASA KT-E, (321) 867-3278

Participating Organization: Ohio State University (Andrew P. Bonifas)

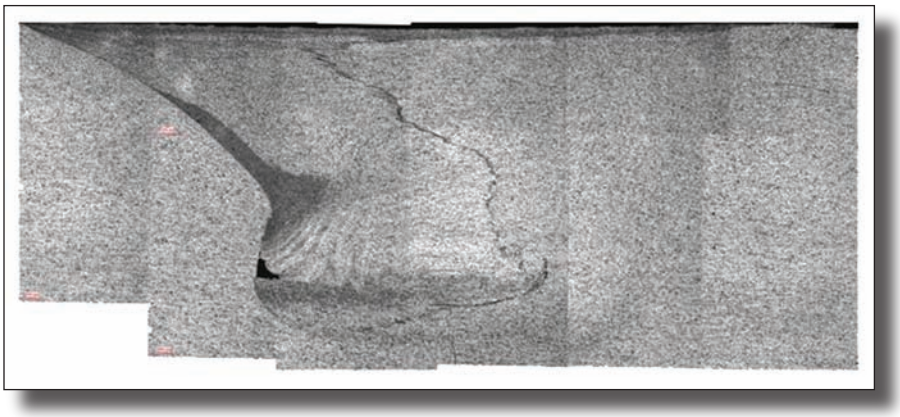

Figure 4. Microstructure of an aluminum 6061-T6 FSW.

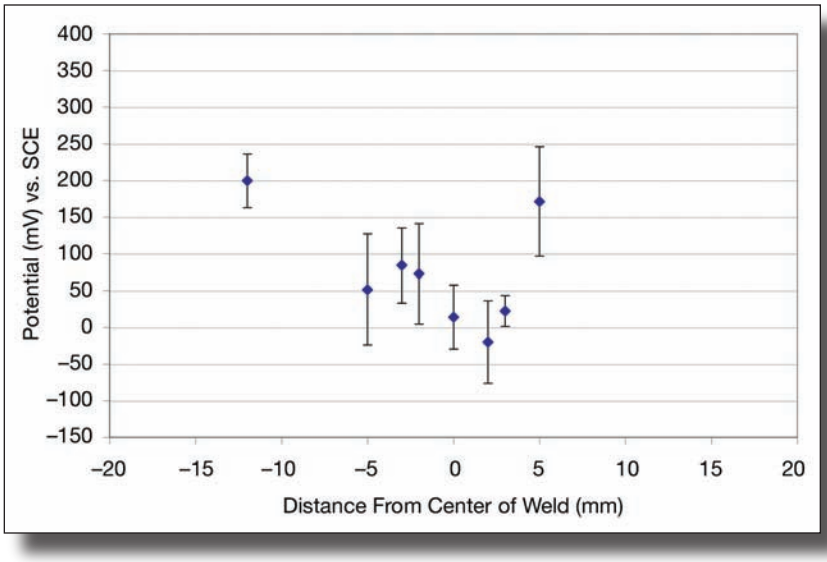

Figure 5. Pitting potentials measured at distances from the center of the FSW.

Smart Coating for Corrosion Detection and Protection

2005 Center Director's Discretionary Fund Project

Corrosion Control

Corrosion is a safety and economic concern worldwide. The direct cost of corrosion in the United States has been estimated as $276 billion, which is 3 percent of the 1998 U.S. gross domestic product (GDP). About one third of corrosion failures are caused by pitting, which is a form of localized corrosion (Figure 1). Undetected localized corrosion can result in catastrophic failures.

The objective of this work was to develop a smart coating that can detect localized corrosion at an early stage and repair it to prevent its growth. The intelligence of this smart coating relies on its ability to transform through its interaction with the corrosive environment. Such transformation can be used for early corrosion detection and prevention of its propagation.

This new smart coating system consists of microcapsules that can detect the chemical changes involved in the localized corrosion process. The diameter of these microcapsules can be 1 μm or larger, and their content can be completely released in a relatively short time, such as 4 hours, when the pH changes at the onset of localized corrosion. When localized corrosion occurs, the anode area often has an acidic pH and the cathode has an alkaline pH.

The microcapsules were prepared using the Zenaca microencapsulation process, wherein the polymer wall is formed by interfacial polymerization and condensation of a mixture of a prepolymer and a crosslinking agent.

The response of the microcapsule is due to the irreversible hydrolysis reaction of ester under basic pH conditions, which causes the polymer wall of the microcapsule to break down. The pH-triggered release microcapsules can be used to deliver healing agents, such as corrosion inhibitors, or film-forming agents to the localized corrosion sites to terminate the process at its early stage, or they can be used as corrosion indicators themselves by releasing dyes (color or fluorescent) at the localized corrosion sites. Figure 2 shows microcapsules indicating basic pH condition in solution. Figure 3 shows microcapsules that changed color in response to the onset of localized corrosion on a carbon steel surface.

Contacts: Dr. Luz Marina Calle <Luz.M.Calle@nasa.gov>, NASA KT-E, (321) 867-3278; and Dr. Wenyan N. Li <Wenyan.N.Li-1@nasa.gov>, National Academies at NASA, Kennedy Space Center

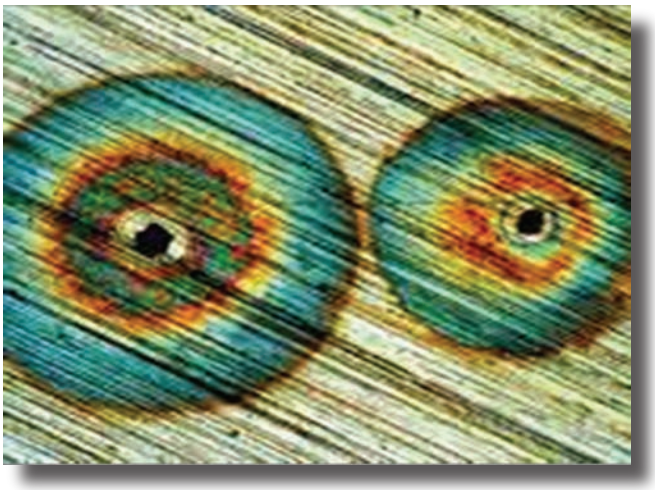

Figure 1a. Typical pitting corrosion.

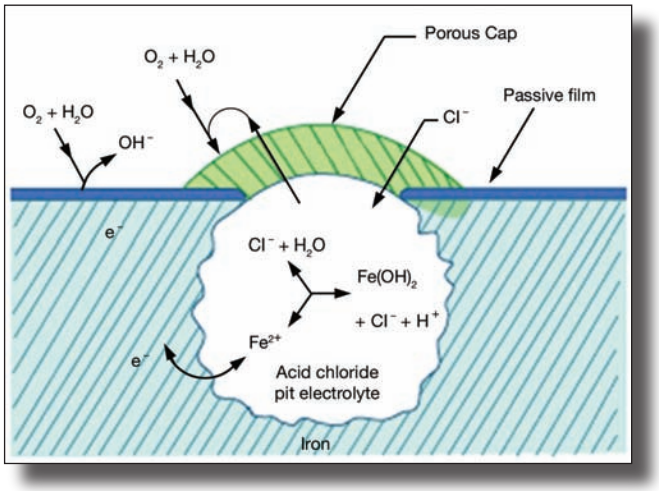

Figure 1b. Schematic illustration of pitting corrosion.

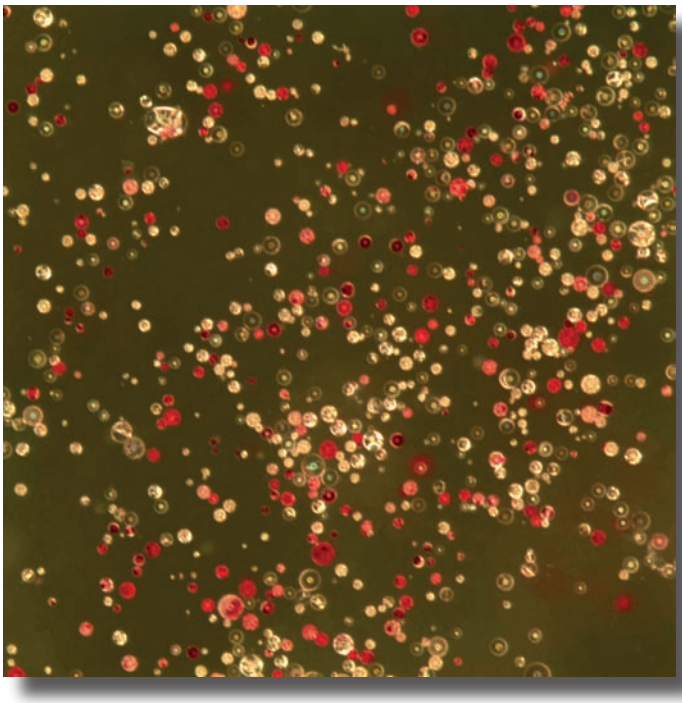

Figure 2. Microcapsules in solution responding to basic condition.

Figure 3. Microcapsules indicating localized corrosion through color change.

Electrochemical Characterization of Tubing Alloys in Simulated Space Shuttle Launch Pad Conditions

Corrosion Control

Type 304L stainless-steel (304L SS) tubing is used in various supply lines that service the Orbiter at the KSC launch pads. The atmosphere at the launch site has a very high chloride content caused by the proximity of the Atlantic Ocean. In addition, during a launch, concentrated hydrochloric acid (HCl) is produced by the fuel combination reaction in the Solid Rocket Boosters. The acidic chloride environment is aggressive to most metals and causes severe pitting in many of the common stainless-steel alloys. 304L SS tubing is susceptible to pitting corrosion that can cause cracking and rupture of both high-pressure gas and fluid systems. The failures can be life-threatening to launch pad personnel in the immediate vicinity. Outages in the systems where the failure occurs can also affect Shuttle launch schedules. The use of a new tubing alloy for launch pad applications would greatly reduce the probability of failure, improve safety, decrease maintenance costs, and reduce downtime losses.

In a previous investigation to find a suitable replacement for the 304L SS in vacuum-jacketed cryogenic supply lines at the Space Shuttle launch sites, several nickel-based alloys, among the 19 alloys included, were found to have very high resistance to the highly corrosive environment at the launch pads.

In the present investigation, electrochemical impedance spectroscopy (EIS) was used to study the corrosion performance of 254SMO, AL6XN, and 304L SS. Alloy 304L SS was included as a control. The EIS measurements were carried out under three different electrolyte conditions: neutral 3.55 percent NaCl, 3.55 percent NaCl in 0.1N HCl, and 3.55 percent NaCl in 1.0N HCl. These conditions were expected to be, respectively, less severe than, similar to, and more severe than the conditions at the launch pad. To better understand the surface chemistry behind the electrochemical data on 304L SS, 254SMO and Al6XN samples, scanning electron microscopy (SEM), x-ray photoelectron spectroscopy (XPS), and auger electron spectroscopy (AES) were used. A parallel study was carried out in which tubes fabricated with the alloys were exposed to the atmosphere at the KSC Corrosion Test Site near the Space Shuttle launch pads.

Figure 1 shows the variation of polarization resistance (R_p) with immersion time for the three alloys in the three electrolyte solutions. Figure 1a shows the R_p increases with time for all three alloys in a neutral salt solution with time. 254SMO significantly increased its R_p toward the end of the study. Figure 1b shows that, when the concentration of HCl in the solution is increased to 0.1N, the R_p values for the alloys are not significantly different during the first 72 hours of immersion, and they all increased. It was observed that the R_p values of 304L SS start to decrease thereafter, while the more highly alloyed 254SMO and AL6XN stabilize to a degree at approximately 10^7 Ωcm^2. Figure 1c shows the polarization resistance versus time when the concentration of the acid in the electrolyte is further increased to 1.0N. The alloy 254SMO shows the highest resistance at all times of measurement. Both 254SMO and AL6XN show approximately three orders of magnitude more polarization resistance than 304L.

The table shows the value for the final polarization resistance measured for all three alloys in different 3.55 percent NaCl acidic conditions. The R_p values decreased for all three alloys with increasing concentration of HCl. The alloy 254SMO has the highest R_p value of 3.79×10^5 Ωcm^2 in 3.55 percent NaCl 1.0 N HCl solution when compared to 304L SS and AL6XN in the most acidic condition.

Final polarization resistance measured for all three alloys in different 3.55 percent NaCl acid concentrations.

Alloy	R_p in 3.55% NaCl (Ωcm^2)	R_p in 3.55% NaCl in 0.1N HCl (Ωcm^2)	R_p in 3.55% NaCl in 1.0N HCl (Ωcm^2)
304L SS	2.12×10^7	1.49×10^4	1.58×10^2
254SMO	2.24×10^8	9.44×10^6	3.79×10^5
AL6XN	7.77×10^7	6.10×10^6	7.66×10^4

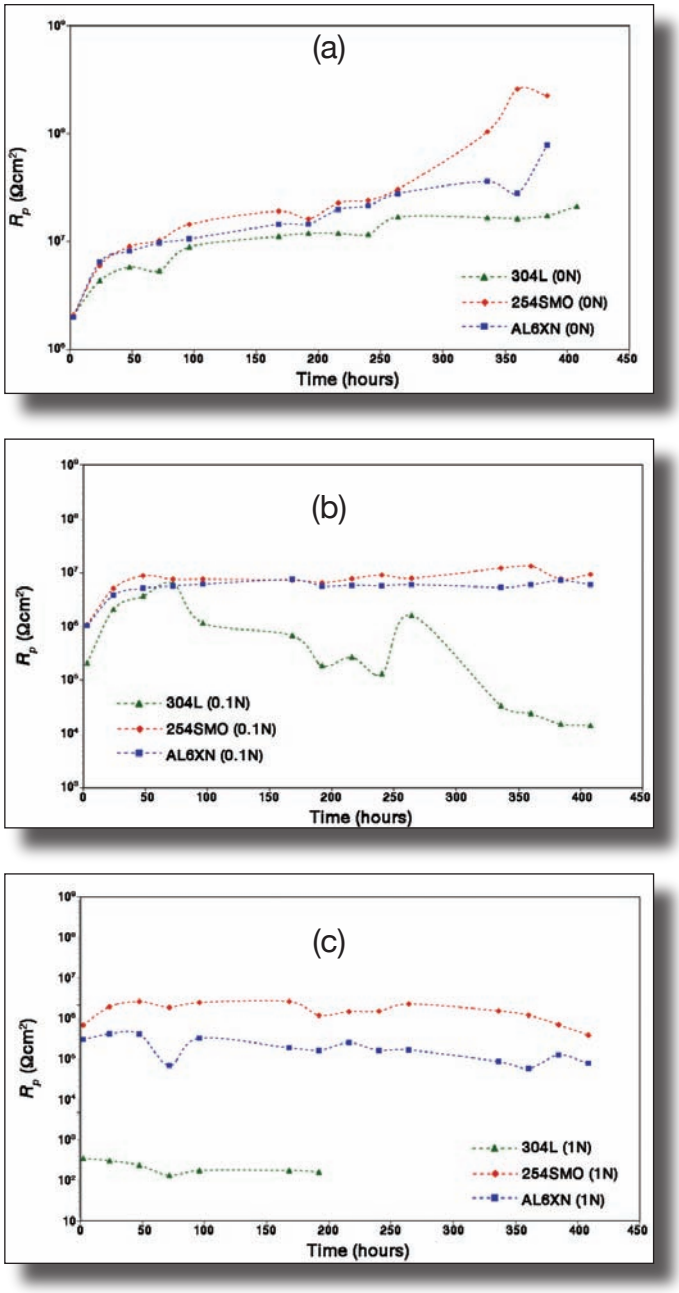

Figure 1. Average R_p at different immersion times: (a) in neutral 3.55% NaCl, (b) in 3.55% NaCl-0.1N HCl, and (c) in 3.55% NaCl-1.0N HCl.

Figure 2 shows SEM images of several pits of various sizes that developed around the area where the o-ring touched the surface of the 304L-0.1N sample while mounted in the electrochemical cell during the EIS analysis.

Contact: Dr. Luz Marina Calle <Luz.M.Calle@nasa.gov>, NASA KT-E, (321) 867-3278

Participating Organizations: ASRC Aerospace (Rubiela D. Vinje and Dr. Mark R. Kolody), University of Central Florida (Dr. Mary C. Whitten), and National Academies at NASA, Kennedy Space Center (Dr. Wenyan N. Li)

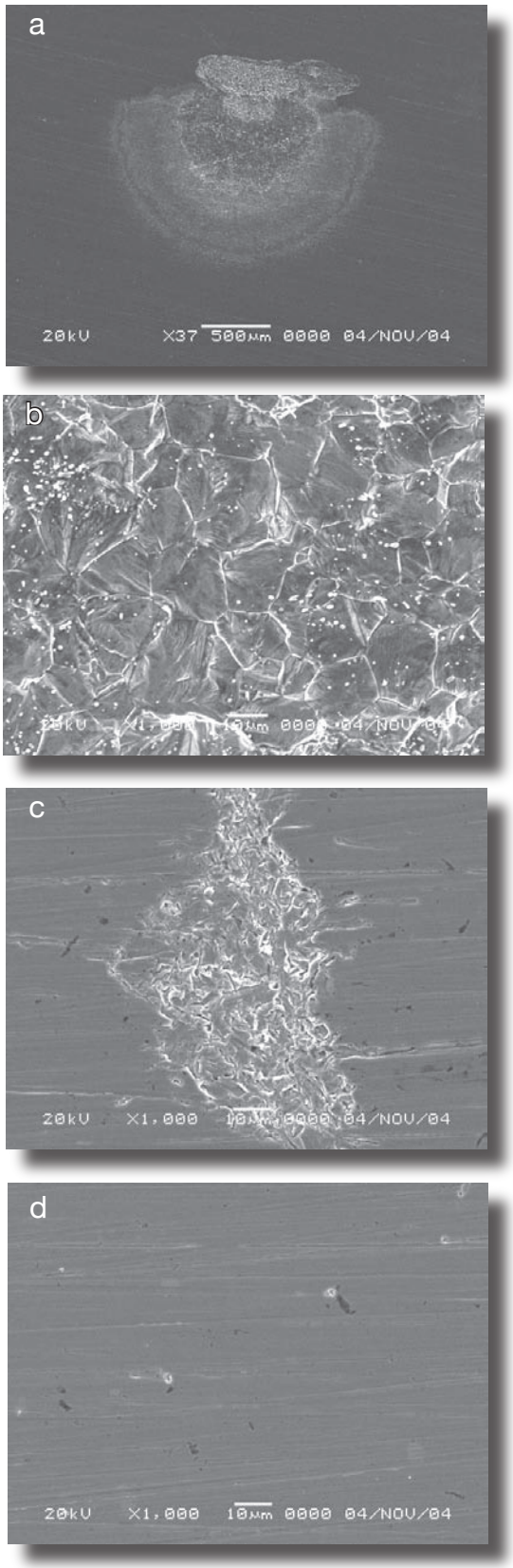

Figure 2. SEM images of 304L-0.1N-pit sample showing different pit sizes. (a) 37 × image of a large pit A, (b) 1,000 × image of a close-up pit A, (c) 1,000 × image of a middle size pit, and (d) 1,000 × image of small pits.

Alternative Refractory Materials for the Main Flame Deflectors at KSC Launch Complexes

Corrosion Control

The launch facilities at KSC are critical support facilities required for the safe and successful launch of vehicles into space. Most of these facilities are over 25 years old and are experiencing deterioration. As deterioration of the materials in the launch complex continues, the chance of these deteriorated materials failing and breaking from their base structures during launches increases. When these materials fail and break away from the steel base structure during a launch, the exhaust from the launch vehicle often turns these materials into high-speed projectiles. These projectiles can jeopardize the safety of the launch complex and vehicle. Materials that exhibit long-term resistance to the Florida coastal environment and the launch environment are needed to ensure safe launches at KSC.

To address these problems, the condition of the Solid Rocket Booster (SRB) flame deflector at KSC was characterized before and after the launch of STS-113 and revealed significant increases in spalling, abrasion, and erosion (Figure 1). As part of this environmental and load characterization, the optimum placement (number and location) of strain gauges and thermocouples in the SRB flame deflector was determined.

Two candidate refractory products—Fondu Fyre and WRP—to protect the steel base structures during launch were evaluated in three conditions: cured, dried, and fired. Cured samples were cast, demolded, and kept moist until the test time (3 and 7 days). The dried samples were cured for 24 hours and then placed in an oven at 225 °F for approximately 24 hours. Samples were allowed to cool in the oven until the following day. The fired samples were cured for at least 24 hours, dried for 24 hours, and then heated to 1,800 °F and 225 °F for approximately 20 hours. Data on compressive strength, tensile strength, modulus of rupture (MOR), shrinkage, and abrasion were obtained for samples that were cooled after the firing (fired: room temperature [RT]) and for samples that were removed from the oven and immediately tested (fired: elevated temperature [ET]).

Figure 1. A location in the SRB flame deflector before (left) and after (right) the launch of STS-113.

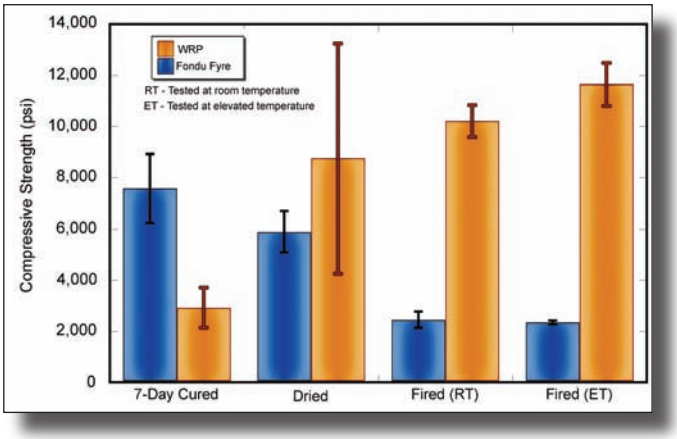

Figure 2. Compressive-strength values of Fondu Fyre and WRP with different processing.

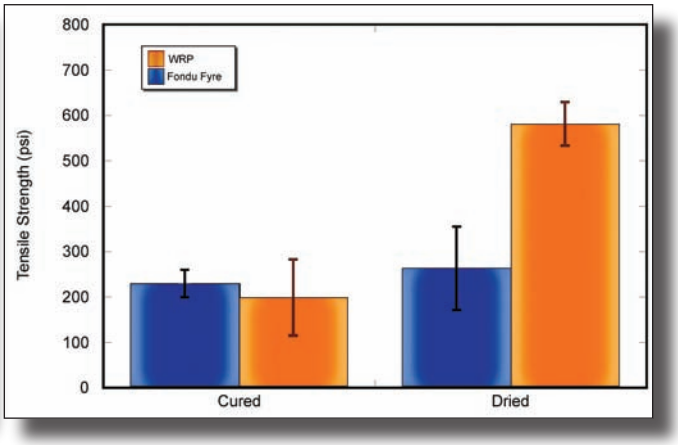

Figure 3. Tensile-strength values of Fondu Fyre and WRP with different processing.

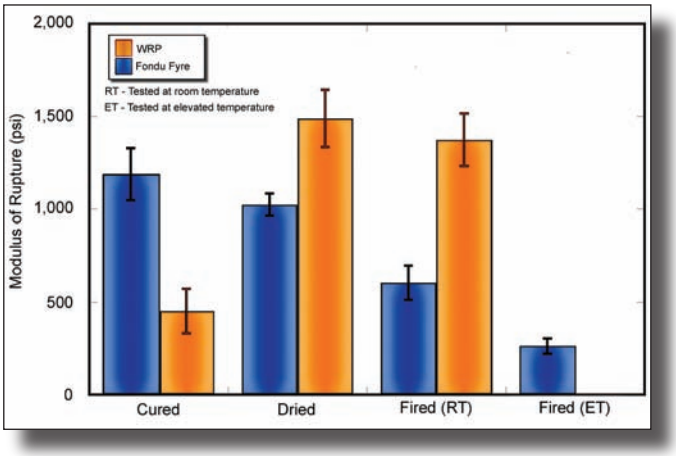

Figure 4. MOR-strength values of Fondu Fyre and WRP with different processing.

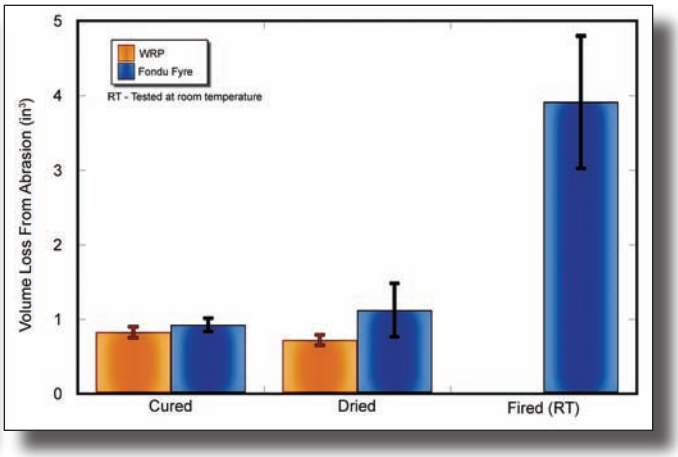

Figure 5. Abrasion results for Fondu Fyre and WRP with different processing.

With the exception of the compressive strength and MOR for cured samples, this preliminary study found that the performance of WRP exceeded that of the Fondu Fyre refractory product (Figures 2 through 6). Further study of candidate refractory materials, together with the installation of sensors in the SRB flame deflector in the identified configuration and a comprehensive revision of the KSC specification used to qualify refractory concrete, will lead to better protection of this launch structure at a substantial cost savings.

Contacts: Dr. Luz Marina Calle <Luz.M.Calle@nasa.gov>, NASA KT-E3, (321) 867-3278

Participating Organization: Texas A&M University (Dr. David Trejo and Justin Rutkowsky)

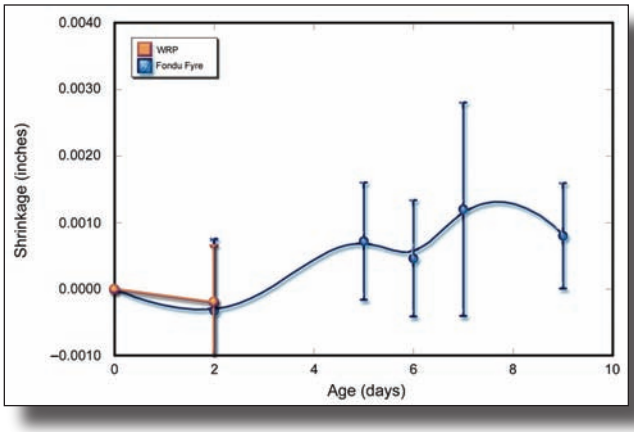

Figure 6. Shrinkage measurements of Fondu Fyre and WRP.

Polyurethane Replacement Coatings

Corrosion Control

Most metals require periodic maintenance and coatings to guard against corrosion, which is particularly problematic at KSC. Some of the most commonly used coating systems contain polyurethane, and though they perform well in the field, they contain isocyanates, which are carcinogenic. The Occupational Safety and Health Administration states that isocyanate exposure can also irritate the skin and mucous membranes and cause chest tightness and difficulty breathing. Because of this, NASA Stennis Space Center has banned the use of such coatings. The objective of this effort is to demonstrate and validate alternatives to aliphatic isocyanate polyurethanes.

The test procedure required 2,000 4-inch by 6-inch test panels, along with several nonstandard test-specific samples. The test panels consisted of several different steel substrates and one aluminum substrate.

Ten different coating systems were applied to the substrates, two of which were polyurethane controls currently in use at the Center. The coatings were applied according to manufacturer specifications at the KSC Coating Application Laboratory. In addition, a field test is being conducted on a rocket engine test stand at Stennis Space Center (Figure 1). The substrate was prepared by sponge jet-blasting to white metal conditions and coating with the same systems applied in the KSC Coating Application Laboratory, using the manufacturer specifications.

To qualify an alternative coating for use, evaluation was divided into two phases. Phase I qualified coatings based upon ease of application, appearance, pot life, long-term stability, curability, and cure time. Once coated, the test panels were performance-tested (solvent rub and adhesion). An example of a test specimen after being subject to an adhesion test is shown in Figure 2.

Phase II testing is being performed and includes tests for abrasion, filiform corrosion, accelerated weathering, and cleanability. The performance-based testing also includes marine exposure evaluation at the KSC Atmospheric Test Site.

Contact: Christina M. Brown <Christina.M.Brown@nasa.gov>, NASA KT-F, (321) 867-8463; and Kevin S. Andrews <Kevin.Andrews-1@ksc.nasa.gov>, Intl. Trade, ITBINC, (321) 867-8479

Participating Organization: ASRC Aerospace (Jerome P. Curran)

Figure 1. Rocket test stand at Stennis Space Center.

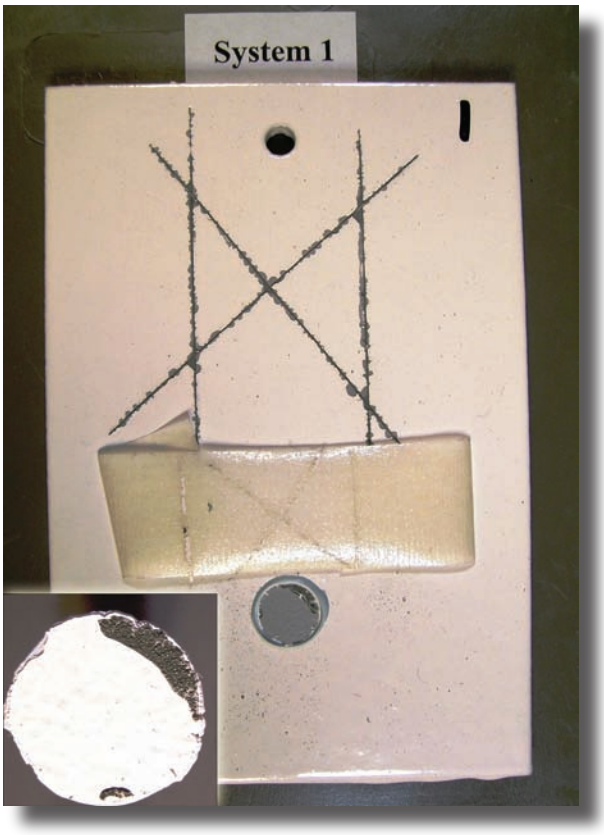

Figure 2. Test specimen after adhesion test.

Chromate Coating Replacement for Military Aircraft

Corrosion Control

To enhance corrosion resistance of aluminum alloys, hexavalent chromium-based products are presently used. Because of their carcinogenic effects and danger to the environment, tighter restrictions are being placed on the use of these coatings.

The objective of this project is to expose 960 experimentally formulated nonchromate-coated coupons to a harsh, outdoor marine environment at the KSC Beach Corrosion Test Site (BCTS) while tracking the deterioration of the surface pretreatments and coatings. In essence, the project aims to protect multimillion-dollar assets, while retaining the integrity of the equipment protecting U.S. military personnel.

The 960 coupons form a matrix of four aluminum alloys having nine pretreatments, each of which has five coating systems. Racks were fabricated for exposure of the nonstandard samples at the BCTS (Figure 1). All coupons were inspected upon arrival and defects were noted. Three sets of baseline photographs were taken; one set of all initial defects, one set of one coupon from each set of five, and one set of an overview of each rack. The third coupon from each set was chosen to represent its respective set. A portable camera stand (Figure 2) was developed and designed to enable the photographs to be taken from the same focal point, directly over the coupon in the field, during each photography session.

Each coupon was received scribed by the customer and was evaluated in accordance with American Society for Testing Materials (ASTM) D 1654, "Standard Test Method for Evaluation of Painted or Coated Specimens Subjected to Corrosive Environments." This standard uses a rating system of 0 (worst) to 10 (best) depending on the distance of creepage from the scribe. The coupons were observed every 6 weeks and intensively evaluated at 4, 8, and 12 months using ASTM D 1654 ratings for blister sizes. All blisters were measured one-sided, that is, from the scribe to the creepage front. All blister measurements were recorded for each coupon in millimeters. The maximum, minimum, and representative means were recorded along with each blister measured. All coupons with an ASTM rating of 2 or less were considered failures. Failures were removed from the site and sent back to the customer for evaluation.

Key accomplishments:

- Built panels to hold 960 nonstandard-sized coupons.
- Installed approximately 960 coupons at the BCTS.
- Completed 1-year evaluations and photodocumentation.
- Developed a portable camera stand for taking consistent coupon photographs.
- Compiled 12-month reports of the test evaluation.

Contact: Dr. Luz Marina Calle <Luz.M.Calle@nasa.gov>, NASA KT-E3, (321) 867-3278

Participating Organization: ASRC Aerospace (Jerome P. Curran and Francis E. Gryn)

Figure 1. Fabricated exposure racks at the Beach Corrosion Test Site.

Figure 2. Camera mount fabricated for photo-documentation of samples.

Protocol Development and Selection of Coatings for Vehicle Assembly Building Siding

Corrosion Control

The siding on the Vehicle Assembly Building (VAB) sustained damage during the 2004 hurricane season, which resulted in the replacement of numerous panels. As part of the refurbishment project, it was necessary to recoat the existing and recently installed polyfluoromer-coated siding. The newly coated materials had to exhibit a durability and appearance representative of NASA and the attention to detail required of a landmark facility. Of greater importance was further assurance that the coating processes and preparative techniques would protect the integrity of NASA assets for future vehicle needs. Consequently, manufacturer-recommended preparation and coating techniques, as well as the coating systems themselves, were evaluated to meet these needs.

Because the panels are already coated with Kynar by the manufacturer, different surface preparation and coating application protocols (using coatings from three different manufacturers) were tested to determine the adhesion and surface appearance of coatings on siding specimens. One major concern for this test was the environmental effect of the surface preparation required. The test panels were sorted and inspected. This process included photodocumentation to assess and record anomalies on the substrates prior to coating. Anomalies on the specimens provided were not unlike those that may be experienced in the field and therefore provide valuable information for field-applied processes.

The coatings were applied to the test panels using manufacturer-recommended techniques. Surface preparations and coating application techniques were evaluated throughout the application process. These evaluations included film thickness measurements and quality checks performed in accordance with NACE International-recommended test practices and manufacturers' specifications. A coated siding specimen is illustrated in Figure 1.

The table shows the test panel attributes that were evaluated and the applicable standards.

Evaluated test panel attributes and standards.

Attribute	Standard
Specular gloss	ASTM D 2244-02, Standard Practice for Calculation of Color Tolerances and Color Differences from Instrumentally Measured Color Coordinates
Adhesion tape	ASTM D3359-02, Standard Test Methods for Measuring Adhesion by Test Tape
Tensile adhesion	ASTM D4541-02, Standard Test Method for Pull-Off Strength of Coatings Using Portable Adhesion Testers
Initial film thickness measurement	SSPC-PA2, Measurement of Dry Coating Thickness with Magnetic Gages

Figure 1. Test specimen with coating applied.

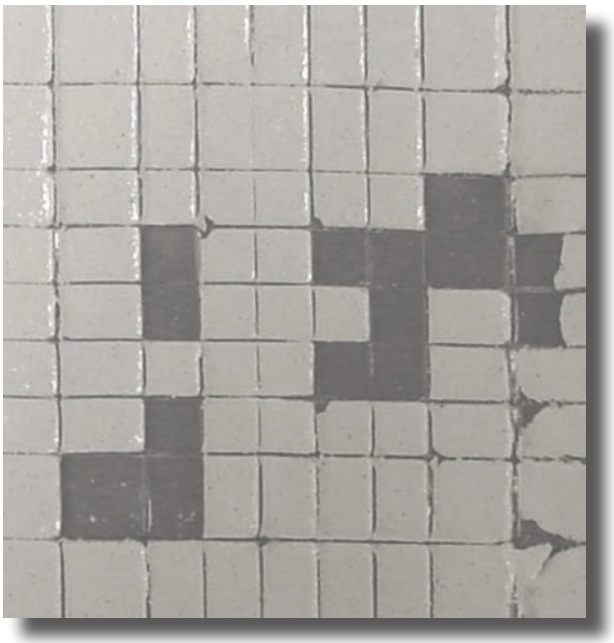

Figure 2. Rejected coating system showing adhesion failures on test specimen. Each rectangle measures 2 mm × 2 mm.

At the end of the project, it was strongly advised to remove one of the manufacturer-recommended coating systems from consideration. Figure 2 illustrates the poor adhesive characteristics that were exhibited for that specimen.

Contact: Roger J. Sarkovics <Roger.J.Sarkovics@nasa.gov>, NASA KT-E2, (321) 867-5517

Participating Organization: ASRC Aerospace (Jerome P. Curran and Francis E. Gryn)

New Test Method for Measuring the Safety of Spaceport Materials, Using the Spark Incendivity Probe

Contamination Detection/Reduction/ Cleaning

For many years, scientists and engineers have searched for the proper test method to evaluate electrostatic risk for materials used in hazardous environments. The new test is a promising addition to conventional test methods used throughout industry. This new test, called the Spark Incendivity Test, created by the International Electrotechnical Commission (IEC) has been successful for evaluating the safety of flexible intermediate bulk containers (FIBCs), which are widely used to store, transport, and handle powdered, flaked, or granular material. The mishandling, improper grounding, and poor electrostatic dissipation (ESD) properties of FIBCs have caused injury and/or death to workers. However, the use of the new IEC test standard has greatly decreased the number of incidents by properly addressing the ESD hazard.

Essentially, the test method is to charge a material by corona charging, triboelectric charging, or both and then purposely discharge the surface of the test material (in the form of a spark), using a metal sphere while in the presence of a flammable gas mixture. If the spark has energy equal to or exceeding the minimum ignition energy (MIE) of the gas mixture, then the resulting discharge will ignite the gas mixture. This test method directly measures a material's propensity to extract sufficient ignitable charge from its surface when a worker and/or object is nearby.

To perform this test, a Spark Incendivity Probe is used. Gases with a known MIE enter a polycarbonate mixing chamber full of glass beads. The glass beads ensure uniform mixing and serve as a flame arrestor to prevent back propagation. The gas mixture passes first through fine copper mesh and then into the mixing chamber before passing through a second copper mesh and a perforated metal plate. The gases then surround the brass electrode, which is electrically grounded. It is here that the ignition occurs.

The proposed test standard normally calls for gas mixtures of 13 percent ethylene in air, which have an MIE of 0.14 mJ. This is the case for FIBCs in the presence of methanol environments, as seen normally in industry. Here however, testing was performed using hydrogen in air at stoichiometric mixtures (30 percent hydrogen and 70 percent dry air as before) having a much lower MIE of 0.02 mJ to represent the worst-case scenario of a charged material in the presence of a hydrogen-enriched atmosphere. Hydrogen and other flammable gases and liquids are commonly used in spaceport operations; hence, electrostatic charging could pose a problem if incendive discharges exist. Tribocharging occurs in several ways and can be due to the presence of charged personnel, charged payloads or equipment, or charged liquids and vapors during typical Orbiter processing and operations.

Samples are typically mounted on an insulating frame using clips. Once mounted, the materials were acclimated for up to 2 days at both 20 percent ±5 percent relative humidity and 50 percent ±5 percent relative humidity. Charge was applied to the materials in two ways. The first method was corona charging. A high-voltage power supply was connected to a corona needle plate to create ions in the air that deposit onto the surface of the test material. The voltage was set to –30 kV to deposit charge levels similar to those seen in FIBCs. The second method was tribocharging with wool. The wool cloth was repeatedly rubbed against the test materials until they were saturated with charge. After deposition onto the surface, the resulting surface potential was measured using a JCI 140 Fieldmeter and recorded. After the test material was fully

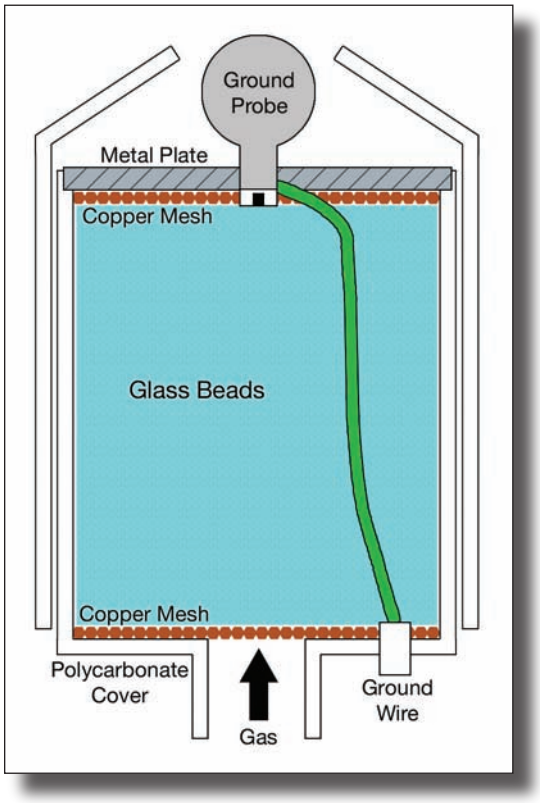

Schematic of the Spark Incendivity Probe.

charged, the gas mixture was allowed to flow through the probe for at least 30 s. The probe then approached the charged material at about 0.75 ±0.25 m/s. Too slow an approach caused corona to reduce local charge levels, and too fast an approach quenched the nascent flame kernel. When the extracted charge was sufficient to cause an ignition of the hydrogen-air mixture, the ignition event was recorded.

Key accomplishments:

- Built an environmental clean room to house the Spark Incendivity Test.
- Successfully evaluated the Spark Incendivity Test using a variety of spaceport materials.

Key milestone:

- The new test method is currently being proposed as a new test standard required for all materials used throughout NASA.

Contact: Dr. Carlos I. Calle <Carlos.I.Calle@nasa.gov>, NASA KT-E3, (321) 867-3274

Participating Organizations: ASRC Aerospace (Dr. Charles R. Buhler, Mindy L. Ritz, and Jeffrey W. Starnes) and Appalachian State University (Dr. Sid Clements)

Application of Glow Discharge Plasma To Alter Surface Properties of Materials

2005 Center Director's Discretionary Fund Project

Contamination Detection/Reduction/ Cleaning

Some polymer materials that are considered important for spaceport operations are rendered noncompliant when subjected to KSC standard electrostatic testing (Standard Test Method for Evaluating Triboelectric Charge Generation and Decay, MMA-1985-79, Rev. 4). Treating materials that fail electrostatic testing and altering their surface properties so they become compliant would reduce costs and improve safety for the Space Shuttle, International Space Station, and Launch Services Programs. The goal of this project was to use Atmospheric Plasma Glow Discharge (APGD) to alter the surface properties of polymers for improved electrostatic dissipation characteristics.

The advantages of an APGD are that it can be used in atmosphere, eliminating the need for an expensive vacuum chamber, and it operates at low temperatures, minimizing heat damage to the polymer surface. The depth of surface modification depends upon the power level and time of treatment, typically several hundred angstroms for polymers. After plasma treatment, the effects of aging, caused primarily by the environment and temperature, can be detrimental to the modification. Once a surface is modified, the effect on the surface is monitored.

The plasma treatment procedure (Figure 1) was optimized on Saf-T-Vu (failed KSC test), Herculite 20 white (borderline KSC test), and Rastex (a polytetrafluoroethylene [PTE] material that did not dissipate charge) with different gases (O_2, air, O_2+H_2O, and He+O_2) at 47±3 percent relative humidity and at 72 °F.

He+O_2 produced the most significant effect, determined by monitoring the increase in the O:C ratio on the surface by x-ray photoelectron spectroscopy. Figure 2 shows the effect of He+O_2 on Saf-T-Vu.

Results on Rastex after APGD with O_2 showed a decrease in the amount of surface voltage, but the material still failed the test. Samples of Rastex and Herculite 20 white were submitted to AST Products Inc., where a chemical treatment (Hydrolast) was applied after plasma treatment that locks in the surface modification. The subsequent tribocharging data for the two materials in Figure 3 shows that a hydrophobic material such as Rastex (basically a woven PTFE cloth) can be made electrostatically dissipative compared to untreated material that charged up and retained a high voltage (approximately – 6 to –7 kV).

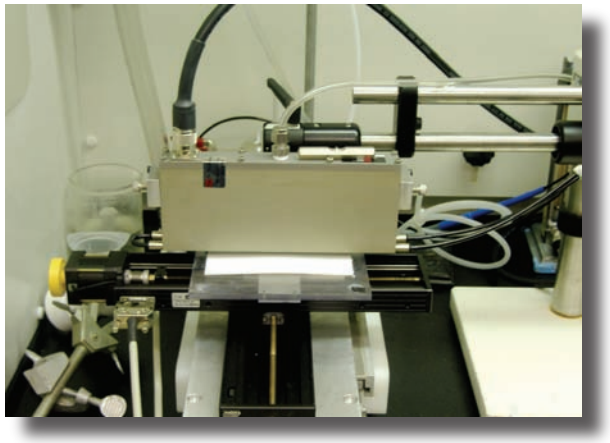

Figure 1. O_2 and He plasma head shown treating PTFE sheet.

Current research is extending the work to metals (stainless steel and aluminum) and the effects of APGD on spaceport materials on bacterial growth.

Key accomplishments:

- Optimized APGD treatment for various spaceport materials so they were rendered compliant with the KSC electrostatic test.
- Continuing to monitor aging effects (not evident 6 weeks after treatment).
- Presented results at the Electrostatics Society of America 33rd Annual Meeting in Edmonton, Canada, in June 2005.
- Submitted findings for publication in the *Journal of Electrostatics*.

Contact: Dr. Carlos I. Calle <Carlos.I.Calle@nasa.gov>, NASA KT-E3, (321) 867-3274

Participating Organization: ASRC Aerospace (Dr. Charles R. Buhler, Dr. Steve Trigwell, Mindy L. Ritz, and Jeffrey W. Starnes)

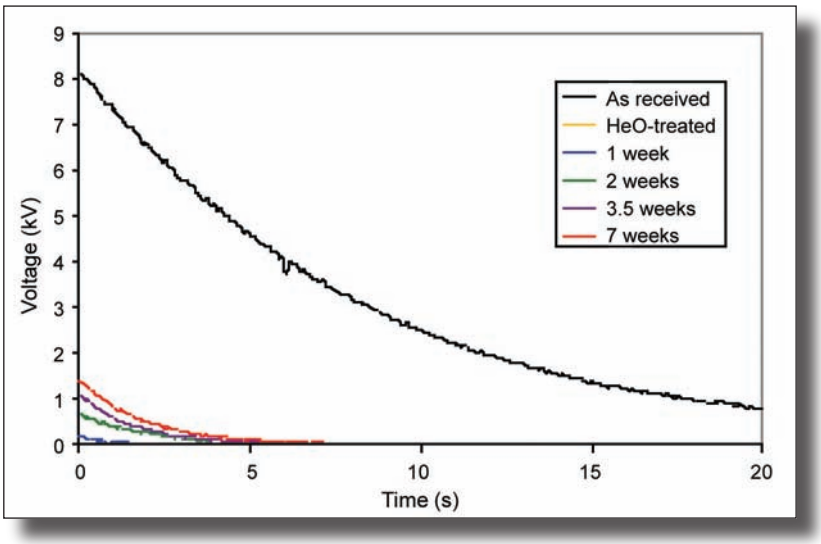

Figure 2. Effect of He+O_2 APGD on Saf-T-Vu. The curve clearly shows that, for the as-received material, the surface voltage after tribocharging failed to reach <350 V after 5 seconds, required by the standard. After APGD treatment, and after 7 weeks, the material passes the standard test.

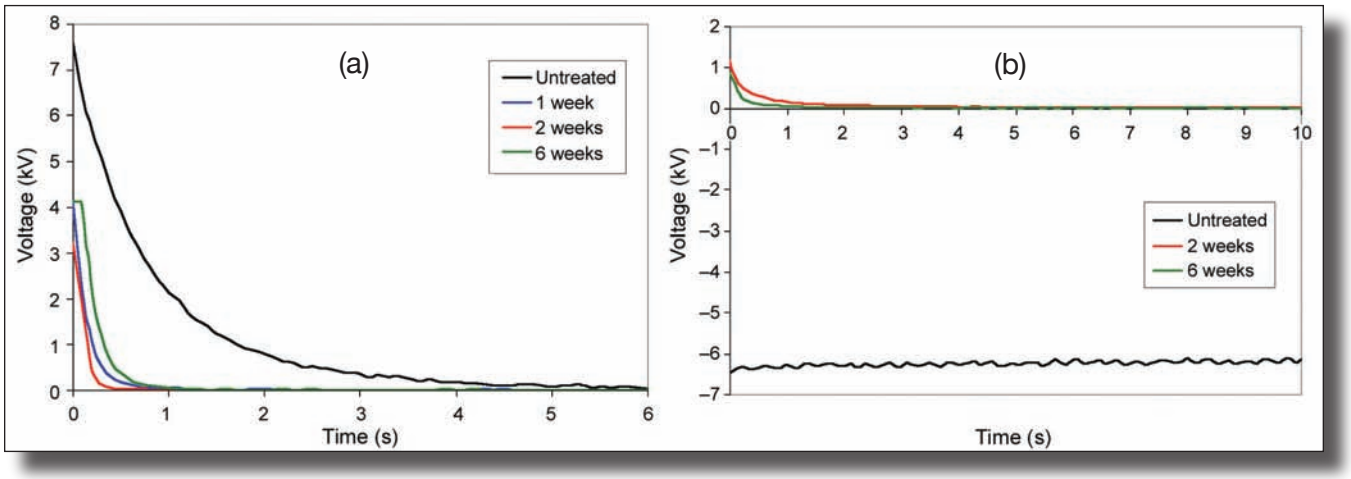

Figure 3. (a) Herculite 20 white showing material easily passes the test and (b) Rastex also passes the test 6 weeks after APGD and Hydrolast treatment.

Electrostatic Screen for Martian and Lunar Dust Mitigation

Contamination Detection/Reduction/ Cleaning

The Martian and lunar environments both contain granular regolith that may be transported through many different mechanisms. In the Martian atmosphere, aeolian processes readily deposit dust onto all surfaces. In the lunar environment, since the atmosphere is around 10 to 12 torr, regolith is only transported ballistically, as a result of direct mechanical erosion, rocket exhaust, etc. In both the lunar and Martian environments, dust contamination on surfaces is a tremendous obstacle to long-duration missions. Dust obscuration of the solar arrays is the leading limiting factor for mission longevity of the Mars Exploration Rover missions and has been somewhat mitigated by the fortunate occurrence of dust devils that clear accumulation. On all six Apollo manned lunar exploration missions, dust accumulation was so tenacious that additional excursions would have been impossible because of contamination of the space suit seals.

One promising technology for dust mitigation being developed at KSC is the electrostatic screen. The screen consists of alternating patterns of interdigitated conductive fingers that form distinct phases, typically three. The screen phases are subjected to a timed pattern of high voltage on the order of 1 kV. A three-phase, 3-inch by 3-inch screen with Martian simulant is shown in Figure 1. Upon application of the high-voltage pulse pattern to the screen, the dust is transported to the edges of the screen. Figure 2 shows the same screen after 100 cycles of the Moesner and Higuchi pattern at 10 Hz, 900 V. The Martian simulant has been transported to the upper-right and lower-left edges of the screen. A small amount of the simulant remains adhered to the grid over the traces.

The performance of the screen is highly dependent on the number of phases, trace width, electrode spacing, dust particle size, screen voltage, pulse pattern, insulator thickness, and conductive material. Optimization of these parameters for lunar and Martian conditions with simulant is currently under way. Each environment has its own challenges. The Martian regolith is easily transported in Earthlike atmospheric conditions, but the Martian environment has a very low Paschen breakdown voltage, limiting the upper operation voltage range. The lunar environment has a very high Paschen breakdown voltage, allowing much higher operation voltages, but the chemical and morphological nature of the regolith presents greater challenges for removal. Despite the additional challenges, preliminary tests indicate that the screen operates effectively in both environments.

To adapt the screen technology for use over solar panels, the screen must be transparent. Indium tin oxide (ITO) is a transparent conductor commonly found in touch screens, liquid crystal displays, heaters, etc. The KSC team has developed a technique to pattern ITO and is pursuing fabrication of electrostatic screens of ITO on polyester films that can be readily applied over solar panels. Preliminary tests show that transparent ITO/ polyester film has minimal effect on solar panel operation while still providing adequate cleaning capability at Earth-ambient conditions.

Key accomplishments:

- Designed and constructed two distinct three-phase, high-voltage power supplies.
- Optimized the clearing factor for screen parameters in Earth atmosphere.
- Demonstrated screen clearing of lunar and Martian simulant in their respective environments.
- Developed a method for patterning indium tin oxide on polyester films.
- Prototyped a transparent electrostatic screen.

Key milestones:

- Optimize screen parameters for their respective environments.
- Optimize transparent screens for installation over solar panels.
- Develop technology to embed screens in fabric (for use on space suits).

Contact: Dr. Carlos I. Calle <Carlos.I.Calle@nasa.gov>, NASA KT-E3, (321) 867-3274

Participating Organizations: ASRC Aerospace (Dr. Christopher D. Immer, Mindy L. Ritz, Jeffrey W. Starnes, and Dr. Charles R. Buhler), Appalachian State University (Dr. Sid Clements), and NASA KT-E3 (Ellen E. Arens)

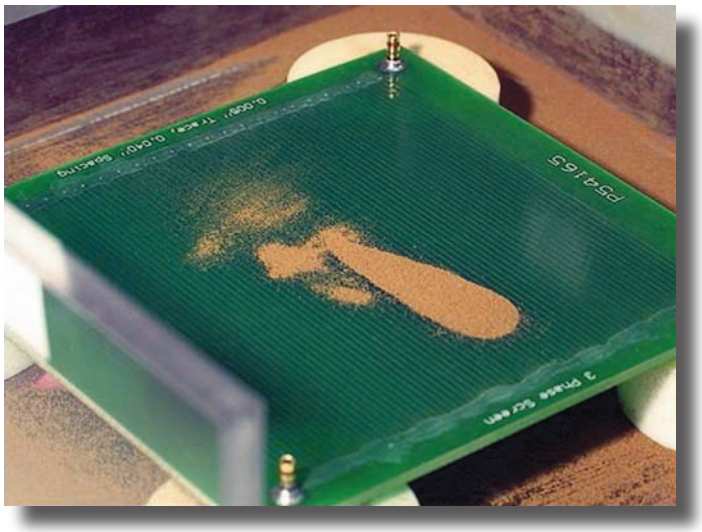

Figure 1. Three-phase electrostatic screen with JSC-1 Martian simulant. The copper conductors are coated with a thin layer of insulative material. The traces are 0.005 inch wide and are spaced 0.04 inch apart.

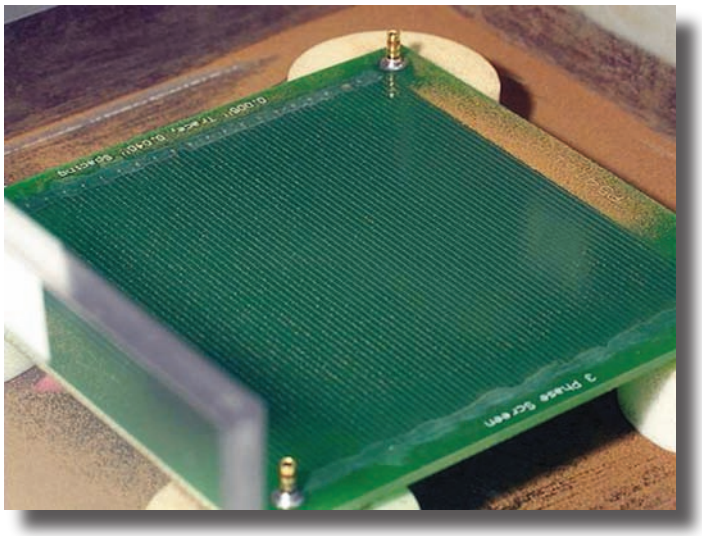

Figure 2. Screen from Figure 1 after 100 cycles of Moesner and Huguchi pattern at 10 Hz, 900 V.

Modified Millikan Dust Particle Analyzer for Mars

Contamination Detection/Reduction/ Cleaning

Experience in extraterrestrial exploration thus far has indicated that the dust on the Moon and Mars can be problematic and potentially hazardous to human health. There are projects currently under way to deal with these problems, but first, the properties of the dust itself must be understood. Therefore, a modified Millikan dust particle analyzer (DPA) was designed and constructed to measure the equivalent aerodynamic diameter and charge of Martian dust particles in the 0.3- to 20.0-μm size range.

The DPA uses a low-light charge-coupled device camera and a 5× microscope objective to capture images of simulated (JSC-1) Martian dust particles illuminated with a diode laser as they fall under gravity's influence and oscillate horizontally as the result of an applied alternating electric field. The images (Figure 1) are analyzed by a program written in LabVIEW. The automated-analysis version of the program uses algorithms to find the peaks of the particle's sinusoidal track. The manual version requires the user to mark the peaks of the track by clicking the image with the mouse. The particle's oscillation amplitude, terminal velocity, and phase lag are obtained from the images and are used to calculate the size and charge of the dust particle.

The DPA is placed inside a vacuum bell jar containing a simulated Martian atmosphere (~95 percent CO_2 at 7.6 torr, a pressure 100 times as low as that on Earth). The test dust is tribocharged and pumped into the chamber using simulated Martian gas and is allowed to settle through the DPA. As shown in Figure 2, the DPA contains high-voltage and ground electrodes that create the alternating uniform electric field (E) at the center of the camera's field of view. The cylindrical brass electrodes are placed end to end and embedded in dielectric to prevent glow discharges that occur easily at these low gas pressures.

The charged particle oscillates at the same frequency as E, but its motion lags E because of the particle's inertia. The diode laser illuminating the particle is pulsed synchronously with E so that the phase lag (φ) can be observed. The particle's aerodynamic diameter (d) can be obtained from φ and the charge (q) is obtained from the peak-to-peak oscillation amplitude (A). For particles less than 2 μm in size and/or with low amounts of charge (or neutral), φ is too small to be measured. Therefore, in these cases, the terminal velocity method is used to obtain the size. Terminal velocity is reached when the gravitational force ($F_g = mg$) is canceled by the drag force. The drag is obtained from Stokes' law, except at the low pressures on Mars, the drag force must be corrected by dividing by the Cunningham slip factor $C(d)$ for CO_2. This yields $F_d = 3\pi\eta vd/C(d)$, where F_d is the drag force, η is the gas viscosity, and v is the particle velocity. Setting the gravitational and drag forces to an equal value yields the terminal velocity $v_t = BF_g = Bmg$, where the particle mobility $B = C(d)/3\pi\eta d$. Using $m = \rho V$ for the particle gives

$$v_t = \frac{C(d)d^2\rho g}{18\eta} \quad (1)$$

which can be solved by bisection for d if v_t is measured.

While oscillating, the charged particle also reaches terminal horizontal velocities (migration velocities, v_m), which are obtained in an analogous manner by replacing the

gravitational force (F_g) with the Coulomb force $F_c = qE$. Thus, $v_m = BF_c = BqE$, that is, $v_m = C(d)qE/3\pi\eta d$.

The peak-to-peak oscillation amplitude is $A = \frac{2v_m}{\omega}$, where $\omega = 2\pi f$. Substitution yields

$$q = \frac{3\pi^2 \eta d f A}{EC(d)} \qquad (2)$$

which gives the particle charge if A is measured. The phase lag is given by, $\phi = \arctan(\omega\tau)$ where the particle relaxation time constant $\tau = mB$. In practice, phase lag is measured and d is obtained by numerical bisection (τ is a function of d). The Cunningham slip factor used in the above equations is given by

$$C(d) = 1 + K_n\left[\alpha + \beta e^{\frac{-\gamma n}{K_n}}\right] \qquad (3)$$

where the Knudsen number $K_n = \frac{2\lambda}{d}$, with λ being the mean free path of the gas molecules and α, β, and γ gas parameters that depend on the composition, temperature, and pressure of the gas.

Key accomplishments:

- Built and tested a dust particle analyzer that can measure the size and charge of JSC-1 Martian simulant particles under simulated Martian atmospheric conditions. The manual-analysis version of the software is fully functional and very reliable.

Key milestones:

- A preliminary version of the automated-analysis software is working, and the full version should be completed within a few months.

Contact: Dr. Carlos I. Calle <Carlos.I.Calle@nasa.gov>, NASA KT-E3, (321) 867-3274

Participating Organizations: Appalachian State University (Dr. Sid Clements), ASRC Aerospace (Dr. Charles R. Buhler, Mindy L. Ritz, and Jeffrey W. Starnes), Oklahoma Baptist University (Dr. Albert Chen), University of Arkansas at Little Rock (Dr. Malay Mazumder), and NASA KT-E (Ellen E. Arens)

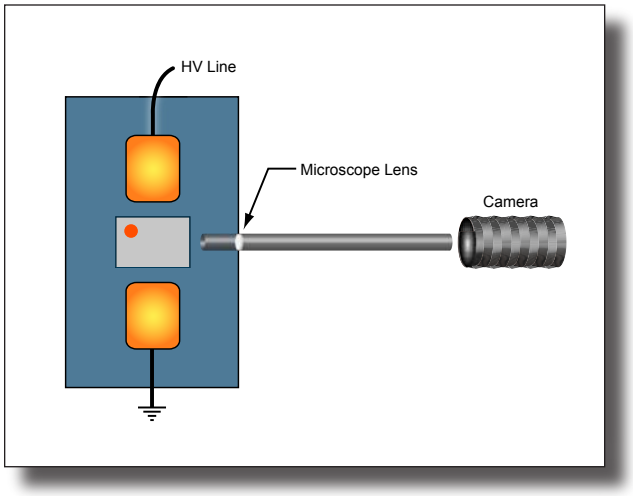

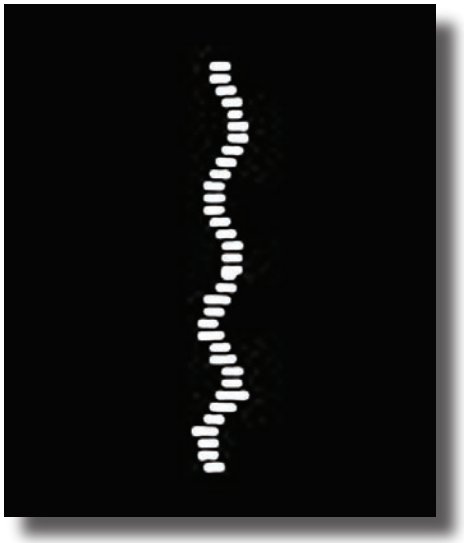

Figure 1. Image of a charged dust particle oscillating horizontally as it falls through the DPA at terminal velocity.

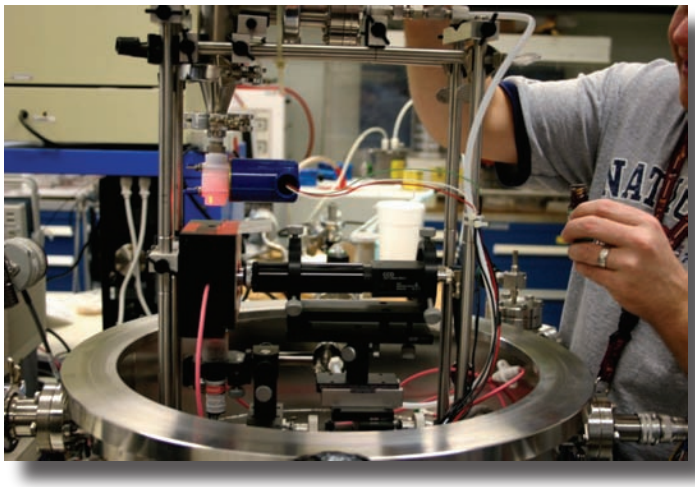

Figure 2. (Top) Top-view schematic of the system, showing a particle (in red) being viewed by the camera while being acted on by the oscillating electric field generated by brass electrodes (orange) embedded in dielectric (gray).(Bottom) The prototype DPA housed inside a bell jar.

Electro-Optic Method of Surface Charge Measurement

2005 Center Director's Discretionary Fund Project

Contamination Detection/Reduction/ Cleaning

Current methods for measuring charge are either impractical in the field or do not give a true value of charge distributed over a surface. Most devices in current use measure the electric field over a large surface area. By understanding how charge is spread over a material (concentrated in small areas or evenly distributed over a large surface), we can better determine the properties of the materials and the electrostatic-discharge risks posed by those materials.

We have developed an electro-optic method, based on the Pockel's effect, to visualize electric fields emanating from surfaces. The direction of polarized light is changed in certain birefringent crystals depending on the strength of the electric field across the surfaces of the crystal. If we pass the reflected light back through a polarizer before imaging, the intensity of the light will have changed depending on the strength of the electric field. In the longitudinal mode, the electric field to be measured is parallel to the light traveling through the crystal and the resolution of the imaged surface is on the same scale as the thickness of the crystal. We are using a 25-mm-diameter, 0.5-mm-thick $Bi_{12}GeO_{20}$ (BGO) crystal to image charged surfaces two dimensionally.

An advantage of this system over current methods of electric-field and charge measurement is that it can distinguish between positive and negative charge on a surface. By inserting a quarter wave plate between the first polarizer and the beam splitter, the light intensity output by the system is offset to its halfway mark. Positive fields will increase the light intensity, while negative fields will decrease the intensity.

The goals of this project are to develop an instrument to visualize surface charge on insulators for material characterization and to calculate the minimum obtainable resolution to determine if the system can detect surface defects. For initial measurements, we are applying known voltages to a needle electrode near the surface of the crystal to determine the sensitivity of the system. The system responds well to electric-field changes, and currently the range is limited only by the sensitivity of the camera used. The next step is to test the system response to different electrode configurations and then test the system response to charged insulators.

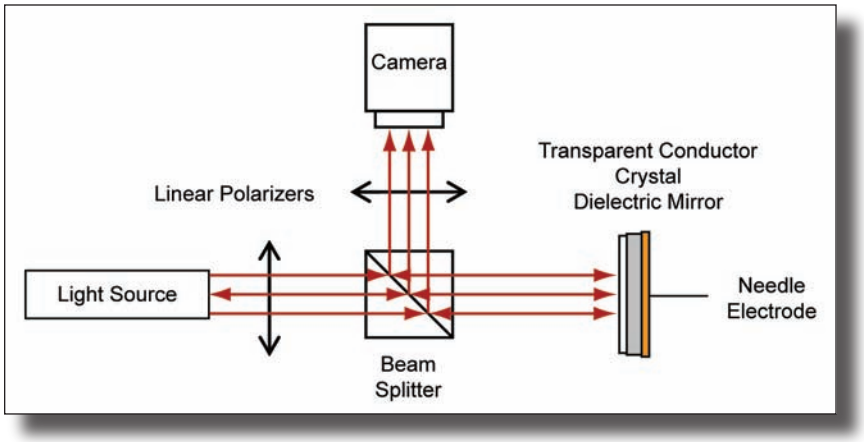

Electro-optic system design schematic.

How the crystal responds to the changing electric field of a needle electrode. The bottom image is with –1,000 V, and the top image is with +1,000 V (100-V increments between images) applied to a needle electrode near the center of each image.

Key accomplishments:

- Completed an optical board layout of components and an image acquisition system for a laboratory-based device.
- Developed an image processing program for comparing image statistics.
- Calculated the intensity shift to calibrate the crystal's response to electric fields.
- Made initial measurements with BGO crystal and a needle electrode.
- Started using more complicated electrode configurations to test the system response and resolution when the electrode is at various distances from the surface of the crystal.

Contacts: Dr. Carlos I. Calle <Carlos.I.Calle@nasa.gov>, NASA KT-E, (321) 867-3274; and Ellen E. Arens <Ellen.E.Arens@nasa.gov>, NASA KT-E, (321) 867-4861

Participating Organization: ASRC Aerospace (Andrew W. Nowicki)

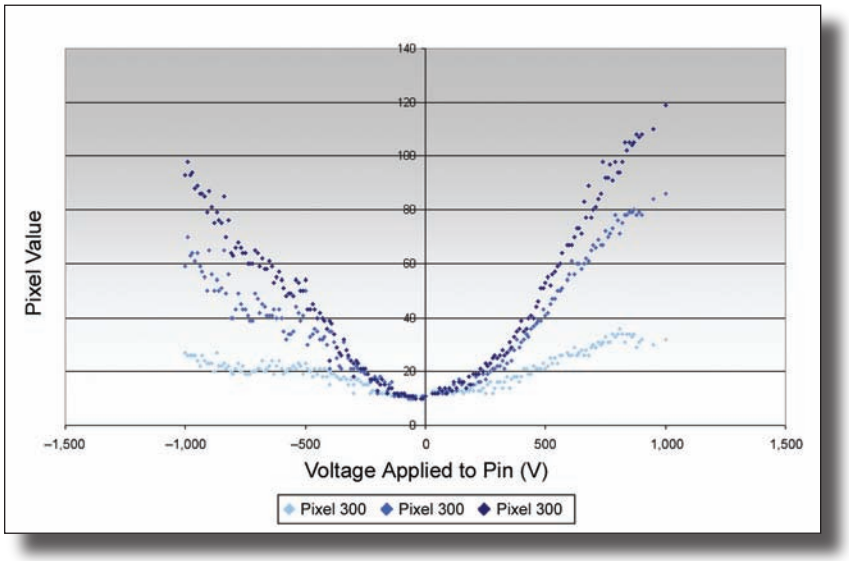

Output intensity (pixel value) at different points along a line. As the pixel gets farther from the electrode, the electric field decreases and so does the output intensity.

Depainting Technologies for Structural Steel

Contamination Detection/Reduction/ Cleaning

When a structural component is recoated, the substrate profile must be compatible with its intended coating. Therefore, the right surface preparation/depainting technique must be chosen. Often, the depainting methods liberate copious amounts of hazardous materials, such as lead. The high quantities of airborne dust and waste generated are of great environmental concern at KSC and Air Force bases. Existing processes to contain the contaminants and reduce the amount of waste generated, while effective, have resulted in significantly higher project costs.

The objective of this project is to qualify candidate alternative low-emission surface preparation/depainting technologies for structural-steel applications. This collaborative effort of the Air Force Space Command (AFSPC) and NASA compares surface preparation/depainting performance of the proposed alternatives to existing methods.

The test article consisted of a rocket motor test stand flame deflector located at Stennis Space Center. This stand was previously coated with a two-coat paint system, as illustrated in Figure 1. Additional samples were prepared from 12-inch by 12-inch substrate panels (Figure 2). The coupon matrix consisted of rusted mill-scale steel, coated steel, and coated aluminum. The mill-scale coupons were placed at the KSC Beach Corrosion Test Site and allowed to form a layer of rust. A Devoe zinc epoxy urethane coating system was applied to an additional set of prepared steel panels and a direct-to-metal urethane was applied to the aluminum panels. Once prepared, the panels and sections of the Stennis test stand were used to measure strip rate, substrate damage, surface profile, and cleanliness of depainting methods in accordance with

Figure 1. Flame deflector used for depainting technology evaluation at Stennis Space Center.

NACE-International and SSPC standards. An example of a region efficiently stripped with a blast medium is shown in Figure 3.

The procedures for surface preparation included three different blast media, hand tool cleaning, and high-pressure liquid-hydrogen blasting. The hand tool and high pressure liquid-hydrogen methods proved to be inefficient and were subsequently discarded from further testing. The blast media used in the evaluation consisted of plastic, steel, and sponge. All three media were evaluated for their effectiveness in removing corrosion products and coatings from the sample surfaces, as well as their ability to limit airborne dust. Additional testing is being performed and includes metallurgical evaluation, air contamination evaluation, and research into other methods of surface preparation.

Contacts: Christina M. Brown <Christina.M.Brown@nasa.gov>, NASA KT-F, (321) 867-8463; and Kevin S. Andrews <Kevin.Andrews-1@ksc.nasa.gov>, Intl. Trade, ITBINC, (321) 867-8479

Participating Organization: ASRC Aerospace (Jerome P. Curran and Francis E. Gryn)

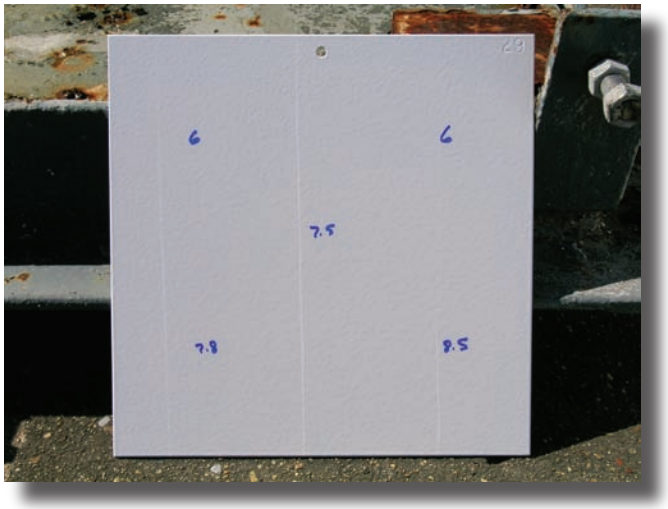

Figure 2. Sample test panel.

Figure 3. Test region after being stripped with blast media at Stennis Space Center.

Next-Generation Wiring: Polyimide Wire Insulation Repair Material

Wire Inspection and Repair

Early efforts to assess the viability of using modified polyimides and polyimide precursors (polyamic acids [PAAs]) as repair materials for aging polyimide (Kapton) electrical wire insulation were successful (see *Kennedy Space Center Research and Technology 2004 Annual Report*). Continued research in this area has advanced this concept on a number of fronts: developing several PAAs with melting points below 170 °C, using these materials in simulated wire repair procedures, developing several electrical and chemical heating systems, and using low-melting-point polyimides (as opposed to the PAA precursors) as repair materials.

The table provides a generic description of several potential repair materials. A wide range of melting temperatures exists for these experimental materials, from 90 to 170 °C. These temperatures are low enough that conventional methods of electrical or chemical heating can be used to aid in the repair process. In addition to exhibiting good melting properties, a repair material must meet other important criteria. It must adhere well to the damaged polyimide substrate, exhibit good flexibility, be easy to work with, and possess good electrical insulating properties. One method of applying a repair material that is being investigated is using thin films of the polymer. Such a film can be wrapped around the wire and then heated to melt, flow, and if necessary, cure the repair to its final state. A number of materials listed in the table form excellent films that can be used in simulating repairs of polyimide-coated wires. Some of these repairs also exhibit excellent adhesion and flexibility.

Characteristics of modified repair materials.

Polymer	Type	Temp. (°C)	Film-Forming Ability	Simulated Repair Results	Comments
A	PAA	>200	very good	very good	Kapton H Precursor PAA
B	PAA	170	poor	fair	
C	PAA	90	poor	fair	
D	PAA	160	good	fair/good	
E	PAA	115	poor	good	
F	Imide of E	—	fair	fair	
G	PAA	90	failed	—	
H	Imide of G	—	good	good	rubberlike
I	PAA	150	failed	—	
J	Imide of I	—	good	fair/good	

The method for heating a repair using this type of repair material is also being investigated. A number of methods for melting, flowing, and curing are available using electrical-resistance heating. There is concern, however, that a source of power to operate an electrical heater may not always be available. Therefore, a number of chemical heating methods using materials that meet several important criteria are being evaluated for this heating application. Such a heater will have to deliver peak temperatures of at least 180 °C and maintain a temperature above approximately 130 °C for several minutes to melt, flow, and cure these repair polymers, using minimal amounts of chemical reaction medium (several grams maximum). This heater must

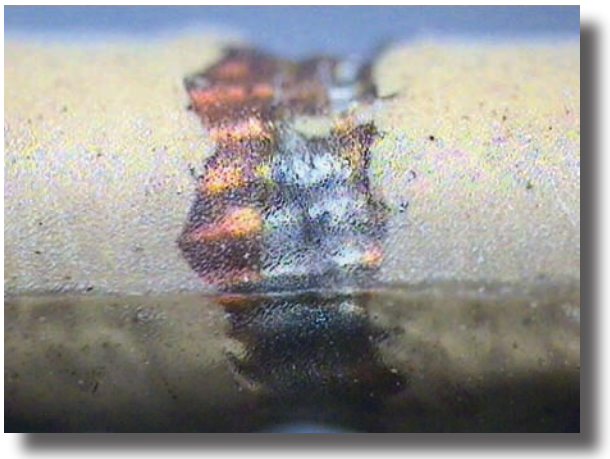

Figure 1. Wire repair.

Figure 2. Bent wire.

be reproducible and easy to use, and must not generate any toxic by-products. The following are some of the chemical-heater systems evaluated:

- potassium permanganate/glycerin,
- magnesium chloride/water,
- calcium oxide/ethylene glycol,
- acid/base interactions,
- magnesium/cupric chloride, and
- potassium chlorate/iron/acid.

Many of these systems can generate heat in excess of 180 °C for several minutes when used in quantities from 1 to 5 g.

Simulated wire repairs were carried out using a number of candidate polymer films. Several of these produced repairs that exhibited excellent melt and flow characteristics, adhesion to the repair surface, and flexibility when bent. Figures 1 and 2 show one such repair carried out using an electrical aluminum block. Figure 1 details good melt and flow into the scored area of the wire piece. Figure 2 shows this repair piece after bending. The repair polymer exhibited excellent flexibility such that no cracking or delamination of the repair surface occurred.

Key accomplishments:

- Prepared low-melting-point PAAs.
- Developed chemical heaters.
- Simulated wire repairs.
- Accomplished wire repair via a chemical heater.
- Evaluated electrical properties.
- Investigated Teflon adhesion.

Contacts: Dr. Tracy L. Gibson <Tracy.Gibson-1@ksc.nasa.gov>, ASRC Aerospace, ASRC-15, (321) 867-7572; and Dr. Scott T. Jolley <Scott.Jolley-1@ksc.nasa.gov>, ASRC Aerospace, ASRC-15, (321) 867-7568

Participating Organizations: NASA KT-D (Dr. Clyde F. Parrish) and ASRC Aerospace (Lilliana Fitzpatrick)

ATR-FTIR Analysis of Aging Space Shuttle Wire

Wire Inspection and Repair

Kapton is a polymer known for its desirable qualities, such as thermooxidative stability and chemical resistance, although it is susceptible to degradation over long periods. Kapton has been widely used to insulate wires in aircraft as well as in the Space Shuttle's electrical system. While the deterioration of wire insulation poses a serious problem for the Orbiter, as well as aircraft, a reliable method to determine the remaining lifetime of the wire insulation does not exist.

The purpose of this research is to correlate the changes observed in the infrared spectra of wire insulation with its mechanical properties as aging occurs. The aged polymer insulation becomes increasingly susceptible to arc tracking and radial cracking, posing an increased risk to delicate electrical systems. The goal is to develop a nondestructive *in situ* tool for determining the useful remaining lifetime of the wire. Fourier transform infrared (FTIR) spectroscopy is an ideal analytical tool for several reasons: it is nondestructive and surface-sensitive and can be noninvasive when used with attenuated total reflection (ATR). ATR employs an evanescent wave that occurs at a reflective crystal interface. The wire sample surface is placed on the crystal surface and the infrared evanescent wave is used to interrogate the surface of the wire insulation. The unique nature of ATR probes the surface of the sample, which is ideal for this case where the degradation will initially occur at the exposed surface.

There are two main types of wire typically used in electrical systems, shielded and unshielded. Both sets of wire consist of two Kapton layers wrapped around the wire to maintain at minimum of 50 percent overlap. A fluorinated polymer (FEP) is used as a glue between the Kapton layers that allows for some flexibility of the wire while maintaining its insulating characteristics.

Several sources of degradation are known and affect the polyimide in different ways. Quantifying this degradation is an important first step in an effort to determine the lifetime of wire insulation. Water in the form of humidity can degrade the FEP coating and cause hydrolysis of the polyimide, converting the Kapton back to the intermediate poly(amic acid). This conversion can be monitored with the use of FTIR because of the strong OH absorption band. Other changes in the spectra may indicate degradation of a different mechanism.

Several aging techniques were employed to artificially age the wire samples in an effort to re-create the degradation measured over a longer period in the Shuttle/aircraft environments. The wire samples were subjected to boiling water, a high-humidity environment (100 °C, 95 percent relative humidity), and a small ultraviolet/ozone chamber. In addition to these laboratory studies, samples were placed at NASA's Corrosion Technology Testbed Beach Site, where they were subjected to sunlight, sea spray, rain, wind, and temperature cycling.

A careful analysis of the accelerated aging over a week indicated a drastic difference between the samples subjected to boiling water and a humid environment. After a day of exposure to boiling water, the FEP coating had completely degraded and the ATR-FTIR spectra exhibited the absorbance bands of the underlying Kapton no longer protected by the FEP (Figures 1 and 2). Further exposure to boiling water yielded an increase in the OH absorption band, suggesting degradation of the underlying Kapton polymer to the polyamic acid.

Exposure of the shielded wire to humid conditions also degraded of the FEP (Figure 3); however, the change was not as drastic as observed with exposure to boiling water. The absorption bands of the FEP were present in the spectra taken throughout the week, but

new absorption features appeared, indicating a change in the surface insulation of the wire. These bands were relatively small and existed alongside the FEP doublet absorption. Since ATR-FTIR probes into a small depth on the surface, this trend indicates the FEP coating is decreasing in thickness, allowing the evanescent IR wave to probe the underlying Kapton insulation. Because the humid environment is not as harsh as the boiling water, the artificial aging is slower and the change in the spectra from FEP to Kapton is visible.

Further investigation is under way to determine a predictive model that accounts for the accelerated aging for changes observed in the ATR-FTIR spectra. There are several challenges that must be overcome to effectively correlate the observed changes to wire aging. One of these challenges is taking a spectrum of a curved surface since the absorption of the IR beam changes with contact angle.

To use this as a predictive tool for wire insulation lifetime, aged wires will be mechanically tested to determine the deterioration of the mechanical properties of the Kapton. This will provide the ability to correlate the changes observed in the ATR-FTIR spectra with the mechanical properties of the aged wires and ultimately enable this predictive tool to determine the remaining lifetime of the wire insulation.

Contacts: Dr. Janine E. Captain <Janine .E.Captain@nasa.gov>, NASA KT-D2, (321) 867-6970; and Dr. Clyde F. Parrish, NASA KT-D

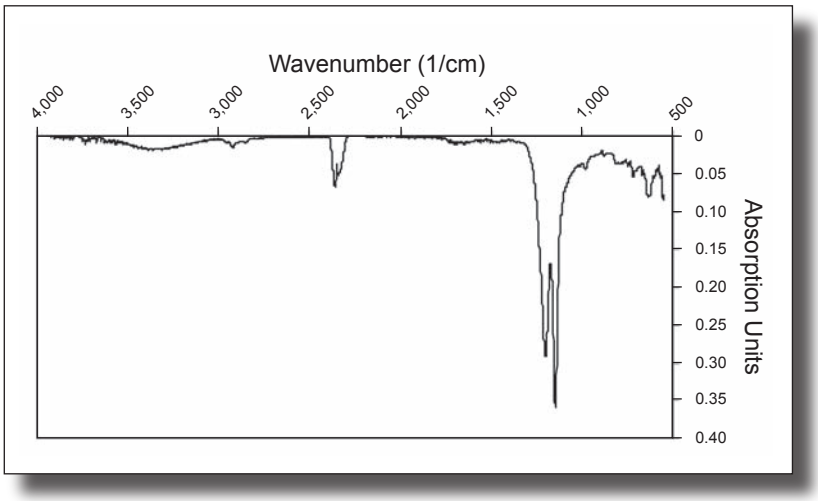

Figure 1. Initial ATR-FTIR spectrum of shielded-wire sample (untreated).

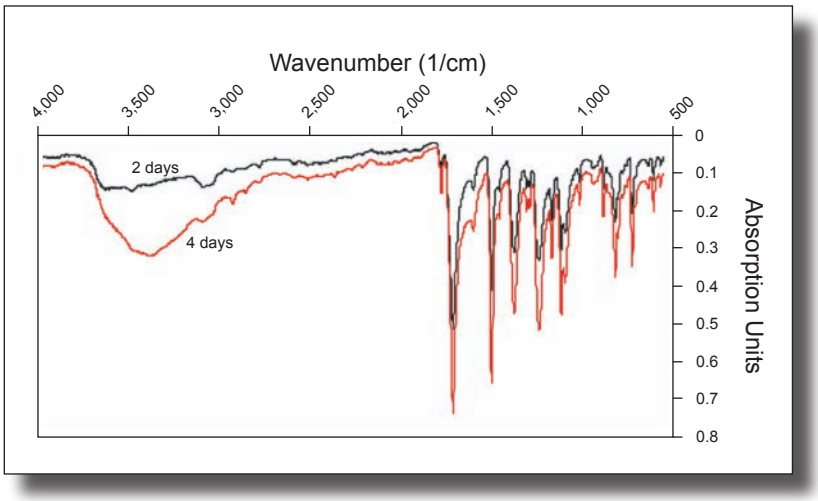

Figure 2. ATR-FTIR spectra of shielded-wire sample exposed to boiling

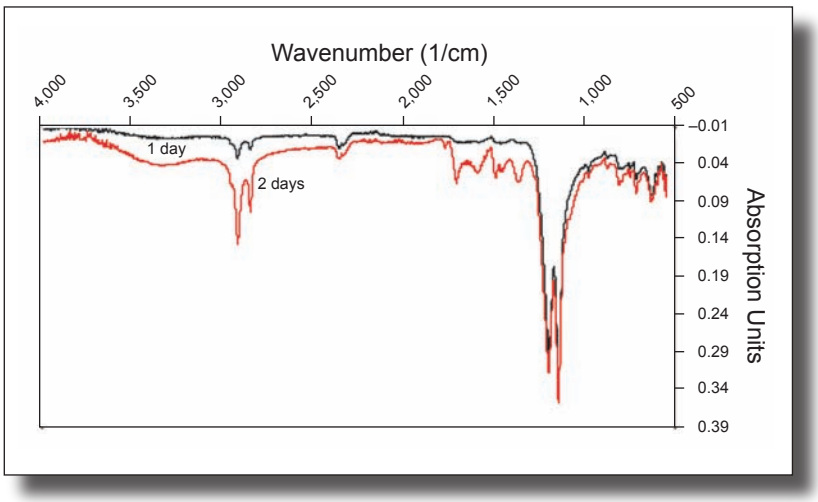

Figure 3. ATR-FTIR spectra of shielded-wire sample exposed to air at 100 °C and 95 percent relative humidity.

Variable-Pulse-Width Time Domain Reflectometry

Wire Inspection and Repair

KSC has developed an innovative time domain reflectometry (TDR) technique that uses a time-varying narrow pulse width with a fast rise/fall time. The front and back edges of a narrow TDR pulse generate a reflection pair from cable defects. By observing the delay time between the reflection pair as a function of pulse width, the effective signal-to-noise ratio of the measurement may be significantly improved.

This variable-pulse-width TDR (VPW-TDR) generates a function, $R(\tau,t)$, of two variables, pulse width (τ) and time (t), where $R(\tau,t)$ is the TDR voltage containing the reflections of interest. However, $R(\tau,t)$, as with traditional TDR, may also contain many features that could mask the signal of interest.

A digital-signal processing (DSP) technique to postprocess VPW-TDR data has also been developed as part of the R&D investigation. The goal of this filter processing algorithm is to suppress features that are not directly related to cable damage. Two filter algorithms, denoted by $D_1(\tau,t)$ and $D_2(\tau,t)$, are mathematically described by (1) and (3), respectively. The primary strategy behind these algorithms is to take advantage of the fact that cut wires in the cable (shield and/or core) create a positive-going pulse at the beginning of the TDR pulse and a negative-going pulse at the end of the TDR pulse. Correlating the first half of the pulse with the negative of the second half results in a processing method that is similar to a detection filter in that it suppresses unwanted data while allowing data of interest to pass. Detection filter 1 exhibits a narrower response, whereas detection filter 2 requires fewer mathematical instructions to compute, but at the expense of a broader response.

Detection filter 1:

$$D1(\tau,t) = \int_{t}^{t+\tau/2} (R(\tau,t') - \bar{R}(\tau,t)) \cdot (\bar{R}(\tau,t) - R(\tau,t+\tau-t'))dt'$$

$$\text{if } (\bar{R}_{-}(\tau,t) > 0) \text{ and } (\bar{R}_{+}(\tau,t) > 0). \qquad (1)$$

$$D1(\tau,t) = 0$$

if otherwise.

where

$$\bar{R}(\tau,t) \equiv \frac{1}{t}\int_{t}^{t+\tau} R(\tau,t')dt'$$

$$\bar{R}_{-}(\tau,t) \equiv \frac{2}{t}\int_{t}^{t+\tau/2} R(\tau,t')dt' \qquad (2)$$

$$\bar{R}_{+}(\tau,t) \equiv \frac{2}{t}\int_{t}^{t+\tau/2} R(\tau,t+\tau-t')dt'$$

Detection filter 2:

$$D_2(\tau,t) = \int_{t}^{t+\tau/2} (R(\tau,t') - R(\tau,t+\tau-t'))dt' \qquad (3)$$

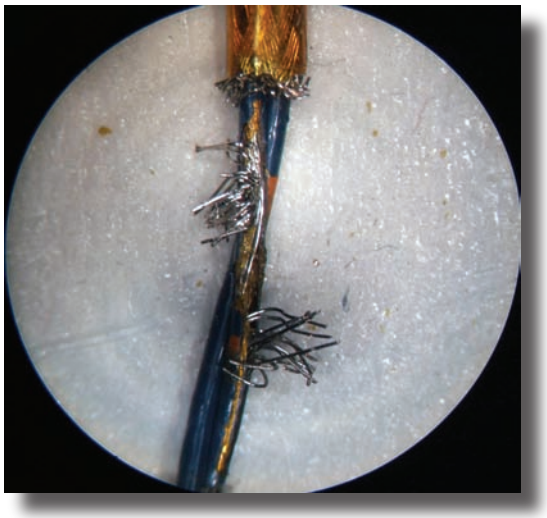

Figure 1. Kapton cable test: shield is cut away completely (and not connected). The ground and signal is connected through the twisted pair. The signal wire is cut so that only one strand remains.

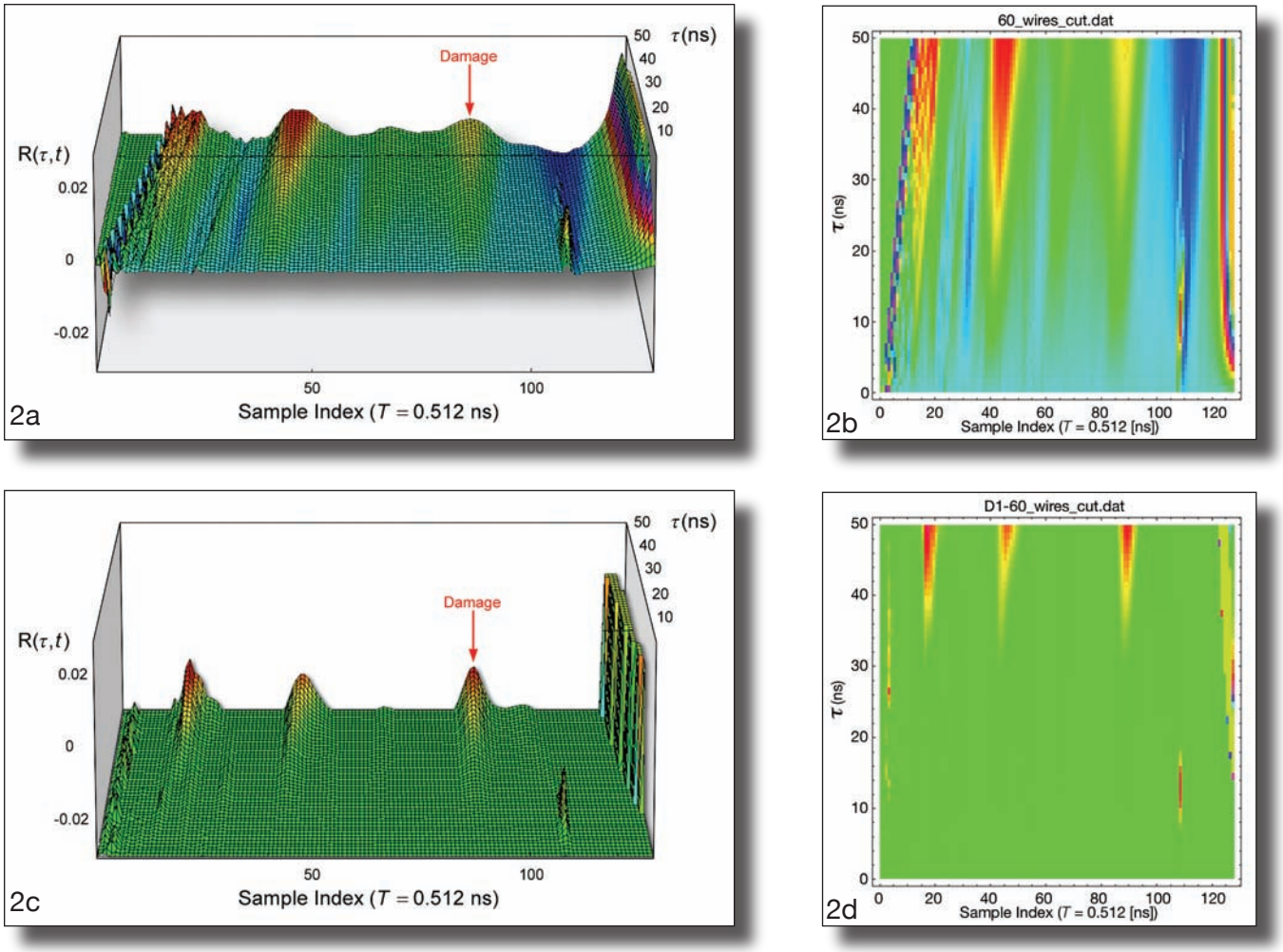

Figure 2. Cut Kapton shield test (4 out of 64 wires remaining): (a) raw TRD data, 3-D plot; (b) raw TDR data, 2-D plot; (c) processed TDR data, 3-D plot; (d) processed TDR data, 2-D plot.

Figure 1 shows a typical Kapton cable test where all but one of the core multistrand conductor wires have be severed. Note that in this context, Kapton implies wire that is commonly used in the Space Shuttle wiring systems. Figure 2 shows the result of applying the detection filter algorithm described in (1) to VPW-TDR data corresponding to a cable with a cut shield (4 wires out of 64 of the shield remain).

Key accomplishments:

- Developed a novel TDR measurement technique using a VPW excitation signal.
- Developed a signal processing algorithm to postprocess VPW-TDR data.

Contacts: Angel R. Lucena <Angel.R.Lucena@nasa.gov>, NASA DX-E3, (321) 867-6743; and Dr. John E. Lane <John.Lane-1@ksc.nasa.gov>, ASRC Aerospace, ASRC-25, (321) 867-6939

Participating Organizations: NASA DX-E (Pamela A. Mullenix, Josephine B. Santiago, and Po Tien Huang) and ASRC Aerospace (Dr. Carlos T. Mata, Dr. Pedro J. Medelius, and Carlos E. Zavala)

Analysis of a Lunar Base Electrostatic Radiation Shield Concept

The use of passive versus active radiation shielding is a topic that will be debated more frequently as the prospect of returning to the Moon for long-duration missions becomes a reality. Based on the research to date, one might conclude that both types of shielding strategies will be needed to effectively solve the lunar radiation problem.

Active shielding is based on deflecting charged particles by means of the Lorentz force:

$$\mathbf{F} = q\mathbf{E} + q\mathbf{v} \times \mathbf{B} \tag{1}$$

where q is the charge of a single radiation particle, $\mathbf{v}$ is the particle velocity, $\mathbf{E}$ is the electric field of the shield, and $\mathbf{B}$ is the magnetic-field component of the shield. The field component determines the shield type:

- electrostatic shield – electric field only (time-independent),
- magnetic shield – magnetic field only (time-independent), or
- plasma shield – both electric and magnetic fields.

Passive shielding simply stops charged particles by multiple collisions with the shield material. The force involved is primarily the Coulomb force, $\mathbf{F}$ in (1), on an atomic spatial scale. Multiple collisions generate radiation by-products in the form of additional charged particles, each with less energy than the previous collision, until all kinetic energy is dissipated.

The magnitude of biological damage caused by charged-particle radiation is proportional to the kinetic energy of the particle, as well as the particle cross section. Even though biological damage will increase with an increase in kinetic energy, as well as cross-sectional area, some researchers assert that at some point of increasing kinetic energy, biological damage will begin to decrease because the interaction time of the particle with the biological media will decrease, resulting in fewer collision by-products. This effect needs to be better understood in the general context of shielding strategies.

The primary hurdle in implementing a practical electrostatic radiation shield, such as that shown in Figures 1a and 1b, is proving out the voltage generation system and preventing voltage breakdown of the system components. In addition, if the spheres are fabricated from thin polymer materials with high dielectric and high tensile strengths, can brehmsstrahlung radiation (high-energy x rays) be eliminated or sufficiently reduced? Will the power consumed by the shield be small enough to be practical? In other words, what is the leakage current caused by the capture of charged particles?

The combined electrostatic and magnetostatic shield system represented by Figures 2a and 2b includes a magnetic component, which unfortunately introduces many of the problems associated with a magnetic-only shield system, such as weight and power. However, it does have the potential of eliminating the negative electrostatic spheres, as well as eliminating secondary brehmsstrahlung radiation.

The next logical step is to carefully investigate material properties of conductive coated polymers for the spherical balloons. Simulations and experiments need to be performed to determine the feasibility of creating an ultrahigh-voltage system on the lunar surface. Future work would be approximately half material and high-voltage experiments. Continued simulations of optimized shield geometry would be performed in parallel.

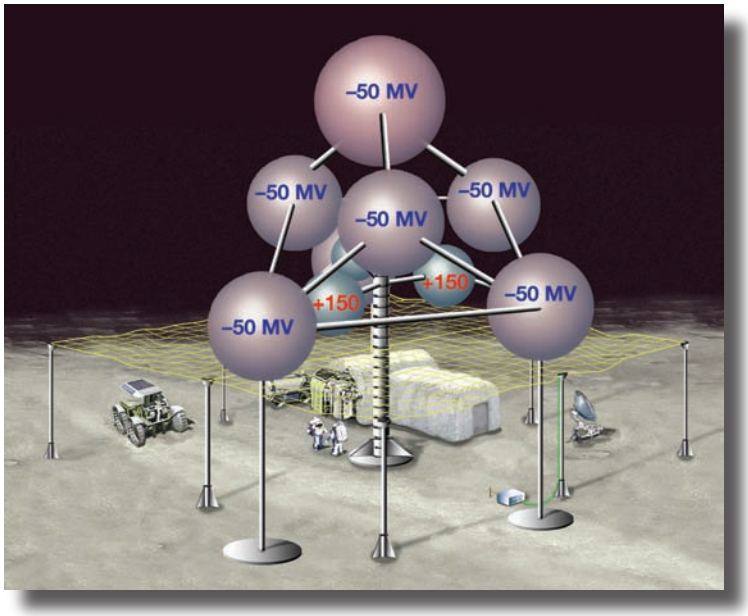

Figure 1a. Artist's concept of sphere tree, consisting of positively charged inner spheres and negatively charged outer spheres. The screen net is connected to ground potential (at infinity).

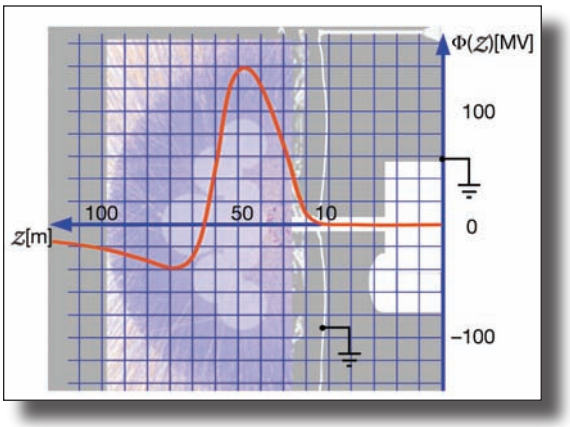

Figure 1b. Electric-field potential profile along the vertical axis of symmetry (z axis) for the sphere configuration shown in Figure 1a.

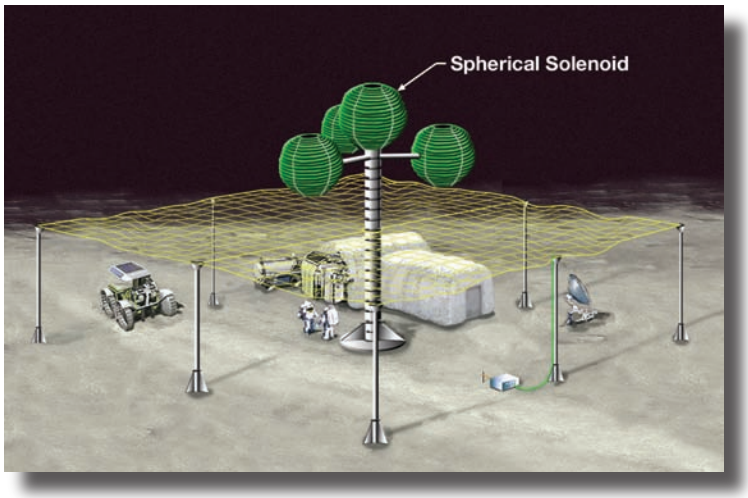

Figure 2a. Electrostatic-shield concept using only positively charged spheres, wrapped with a current-carrying wire. Electrons are repelled by the magnetic field generated in the spherical wire loops.

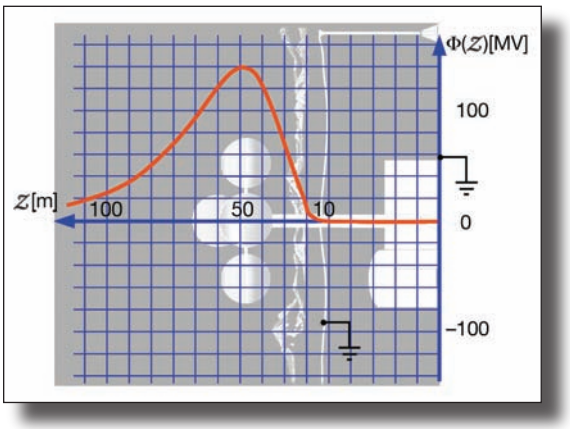

Figure 2b. Electric-field potential profile along the vertical axis of symmetry (z axis) for the sphere configuration shown in Figure 2a.

Key accomplishments:

- Developed a Monte Carlo-based charged-particle radiation trajectory model to test lunar base electrostatic-shielding concepts. Implemented the math model in FORTRAN 90.
- Added a magnetostatic simulation for testing a direct-current-carrying solenoid, wrapped around an electrostatic sphere.
- Designed and simulated several potential geometries.
- Presented results to the NASA Institute for Advanced Concepts (NIAC) meeting in Atlanta, Georgia, in March 2005.

Contact: Dr. Robert C. Youngquist <Robert.C.Youngquist@nasa.gov>, NASA KT-D1, (321) 867-1829

Participating Organization: ASRC Aerospace (Dr. Charles R. Buhler and Dr. John E. Lane)

Analytical/Numerical Approximation of the Electric Field of a Conducting Torus

This work was originally motivated by an ongoing investigation into electrostatic radiation-shielding strategies. Previously, the shield components (high voltage electrodes) were composed of conducting spheres or screens. The spheres were modeled by analytical techniques and custom software, while the screens were modeled using finite-element software. A new direction was recently proposed to surround a single electrostatic sphere with a negatively charged electrostatic torus.

The current version of the radiation-shielding simulation model, the Spacecraft Electrostatic Shield (SES), is based on analytical computation of the electric field at any point in space, generated by a cluster of negatively and positively charged conducting spheres. To add a conducting torus to the SES, it was necessary to develop and test similar analytical formulas for the torus geometry.

A solution to the electrostatic-field problem of the torus was available using commercial off-the-shelf finite-element software. However, what was really needed was a closed-form solution (or at least a good approximation of a closed-form solution) that could be incorporated into the SES model. Even though an analytical solution using toroidal coordinates was derived in 1953 by Morse and Feshbach, to incorporate a torus solution into the previous version of SES, a more efficient method had to be devised. The results are described below.

In cylindrical coordinates (r, θ, z), define

$$\alpha^2 \equiv (r - a_w)^2 + z^2 \qquad \beta^2 \equiv (r + a_w)^2 + z^2 \tag{1}$$

where a_w is the radius of the wire loop and ρ is the charge density per unit length.

Electrical potential:

$$\Phi(r,z) = \frac{a_w \rho}{\pi \varepsilon_0 \alpha} \mathrm{K}\left(-\frac{4 a_w r}{\alpha^2}\right) \tag{2}$$

where $\mathrm{E}(k^2)$ and $\mathrm{K}(k^2)$ are the complete elliptic integrals of the first and second kind, respectively. The wire loop radius a_w can be computed from the toroid parameters a and b, with the following empirical formula:

$$a_w \cong a \cdot \frac{1+u}{1+c_0\ u} \qquad u \equiv \left(\frac{x}{c_3}\right)^{c_2} \tag{3}$$

where $x \equiv b/a$, and $c_0 = 0.48044$, $c_1 = 1$, $c_2 = 0.7096$, $c_3 = 0.73764$.

This approximation for a_w is obtained by applying the following boundary conditions:

$$\Phi(a+b,0) = \Phi(a-b,0) = V_0 \tag{4}$$

leading to two formulas for the line charge density, ρ:

$$\rho_1 = \left.\frac{V_0 \pi \varepsilon_0 \alpha}{a_w \mathrm{K}\left(-\frac{4a_w r}{\alpha^2}\right)}\right|_{r=a-b} = \frac{V_0 \pi \varepsilon_0 (a_w + b - a)}{a_w \mathrm{K}\left(-\frac{4a_w (a-b)}{(a_w + b - a)^2}\right)} \qquad \rho_2 = \left.\frac{V_0 \pi \varepsilon_0 \alpha}{a_w \mathrm{K}\left(-\frac{4a_w r}{\alpha^2}\right)}\right|_{r=a+b} = \frac{V_0 \pi \varepsilon_0 (a + b - a_w)}{a_w \mathrm{K}\left(-\frac{4a_w (a+b)}{(a + b - a_w)^2}\right)} \quad (5)$$

Since ρ_1 and ρ_2 should be equal, within numerical noise, the final value for line charge density is taken as the algebraic sum: $\rho = \frac{1}{2}(\rho_1 + \rho_2)$.

Electric field:

$$\boldsymbol{E}(r,z) = \frac{a_w \rho}{2\pi\varepsilon_0 r \alpha \beta^2}\left((r^2 - z^2 - a_w^2)\mathrm{E}\left(-\frac{4a_w r}{\alpha^2}\right) + \beta^2 \mathrm{K}\left(-\frac{4a_w r}{\alpha^2}\right)\right)\hat{\boldsymbol{r}} + \frac{a_w z \rho}{\pi\varepsilon_0 \alpha \beta^2}\mathrm{E}\left(-\frac{4a_w r}{\alpha^2}\right)\hat{\boldsymbol{z}} \quad (6)$$

Total charge:

$$Q_T = 2\pi a_w \rho \quad (7)$$

Key accomplishments:

- An accurate, and simple model for the electric field of a conducting torus was developed, by replacing the torus by a wire loop of radius a_w and line charge ρ.
- Approximation formulas to compute a_w and ρ were developed, and analytical formulas for the electric field and potential of a wire loop were derived.

Contact: Dr. Robert C. Youngquist <Robert.C.Youngquist@nasa.gov>, NASA KT-D1, (321) 867-1829

Participating Organization: ASRC Aerospace (Dr. John E. Lane)

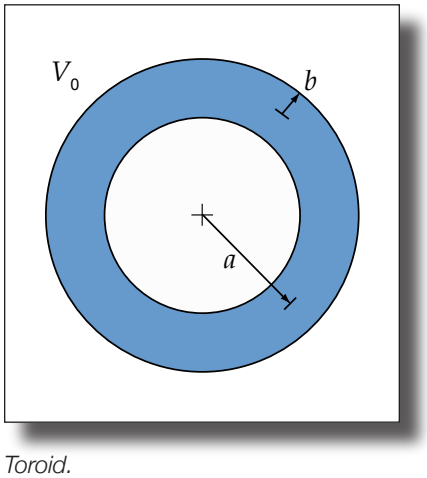

Toroid.

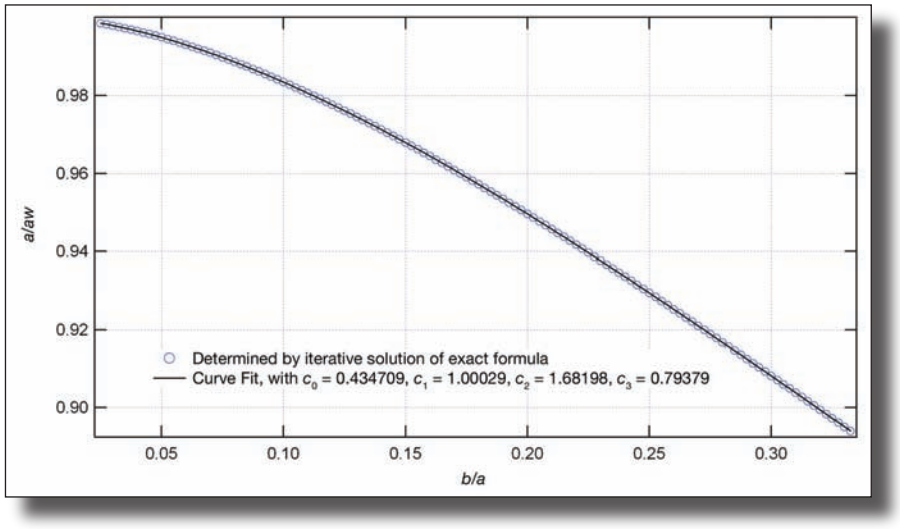

Fit leading to coefficients in (3).

Computational Fluid Dynamics Analysis of Wind Flow Impact on the Vehicle Assembly Building

Decision/Data Models and Analysis

In an attempt to explain the inordinate loss of siding panels from the south face of the Vehicle Assembly Building (VAB) during Hurricane Frances, a 3-D computational fluid dynamics (CFD) model was developed to simulate local velocity and pressure distributions resulting from the wind flow field. A preconditioned compressible Navier-Stokes flow solver was used to compute the flow field around the VAB complex, including the Launch Control Center, the low and high bays of the VAB, and several surrounding buildings. The mapping of the forces and velocities on and along the affected faces of the VAB correlated surprisingly well with the extensive damage areas seen on both the south face and the southeast section of the roof. The model results were also consistent with the minimal damage seen on the east, north, and west faces of the structure.

A viscous, Reynolds-averaged Navier-Stokes (RANS) with k–ε turbulence model was selected for the simulation. The flow is assumed to be uniform, with wind speed and direction prescribed as the freestream boundary conditions. Because of the complexity of the building geometry and surrounding structures, an unstructured grid system was used. A grid-independence study was performed with two grid levels: coarse mesh with 501,025 cells, and fine mesh with 884,382 cells. To speed up the convergence, a multigrid scheme was also used. The computations were made on the Beowulf cluster using parallel processors at the KSC Launch Systems Testbed. Several case studies were made for different wind speeds and flow directions.
Figure 1 shows the computational domain and the wind direction considered for the simulations. A parametric study was performed with different wind magnitudes and directions.

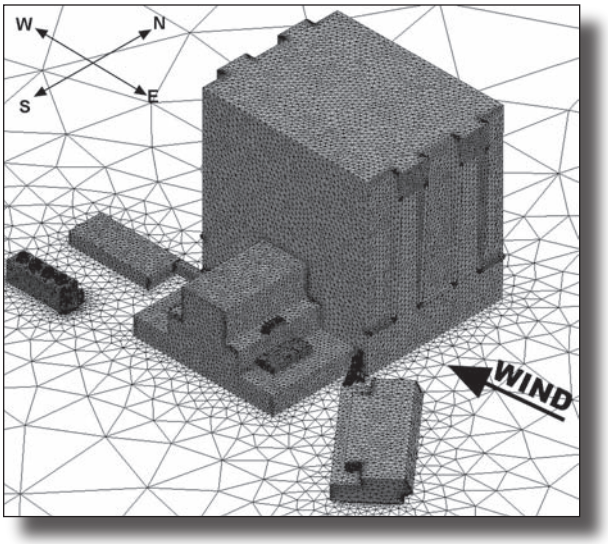

Figure 1. VAB computational geometry.

The CFD analysis explained the flow phenomena around the VAB. The results agree well with actual damage seen after the hurricane. The south wall of the VAB sustained the most damage as a result of pressure interactions with the adjoining low bay. Flow visualizations also help explain what actually happened during the hurricane: streamlines and velocity vectors reveal strong vortices near the south face of the VAB (Figures 2, 3, and 4). The flow reversals, as seen in the velocity vectors (Figure 5), explain why the panels were stripped off the surface in two different directions. Finally, the area of the pressure gradients on the south face are consistent with the location and size of the area of failed panels, even though the magnitude of the wind was much lower than what was anticipated for failure. The combination of the pressure and velocity distributions suggests that the panel failures were caused by shear, peeling, and tension, rather than compression. Inspection of the panels corroborated the failure modes and that corrosion of the panels and fasteners suggests material degradation may have played an important role in the panels failing in winds far weaker than hurricane force. CFD analysis is an important tool for understanding potential or actual

Figure 2. Panel loss from Hurricane Frances on the south face of the VAB.

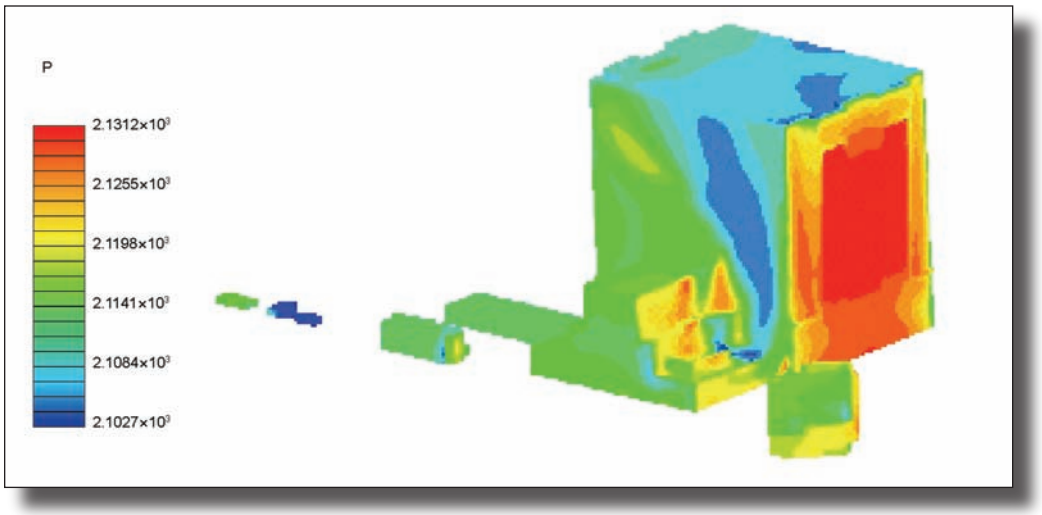

Figure 3. Pressure distribution from Category 1 simulation (74-mph east wind).

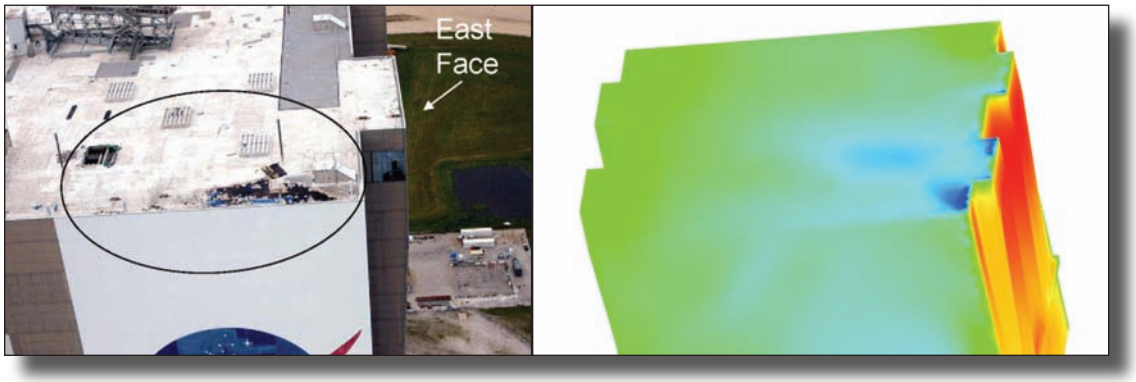

Figure 4. Roof damage (Category 1, 74-mph east wind).

failure mechanisms because it helps facility engineers plan their repair and reinforcement strategies to migrate future damage to complex structures.

Key accomplishments:

- Developed facility model.
- Established CFD boundary conditions.
- Performed multiple CFD analyses.
- Documented results in the *KSC Hurricane Recovery Report 2004*.

Key milestones:

- Compared actual damage to CFD analyes.
- Presented study at the ASME Fluid Engineering Summer Conference.
- Began the Large Eddy Simulation turbulence modeling.

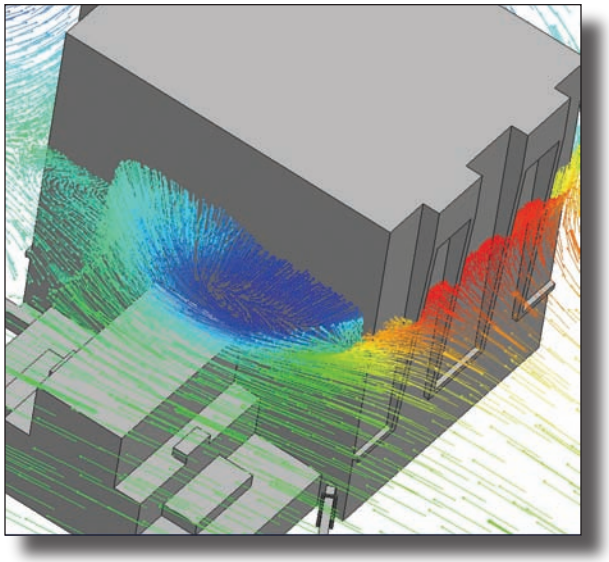

Figure 5. Wind vectors around the south face of the VAB (velocity ≥115 mph).

Contacts: Dr. Bruce T. Vu <Bruce.T.Vu@nasa.gov>, NASA DX-F3, (321) 867-2376; and Jan A. Zysko <Jan.A.Zysko @nasa.gov>, NASA KT-D2, (321) 867-8774

High-Temperature Acoustic Liners

Large-Material and Equipment Handling

This study has demonstrated that production of a sound absorption coating is possible in the extreme environment of rocket exhaust gas impingement. Based on the combination of screening through acoustical wave tube and plasma jet (above 3,000 °F) torch work, a coating formula was developed to satisfy the requirements of survival at extraordinarily high heat flux and acoustical damping of approximately 25 percent.

Acoustical absorbers are applied either as liners or as discrete cavities, and both act as a series of Helmholtz resonators that remove energy from the vibratory system. The typical treatment is to consider one resonator element as the mass of gas in the orifice, using the volume of gas behind it to form a traditional oscillatory system. To arrive at a successful coating in the areas of acoustical performance, high-temperature survival, and coating stability, formulations involving families of materials (homogenous and composite) aimed at absorption through either bulk-material properties or control of porosity and internal reflective/destructive interference were developed and tested. Acoustical testing was performed in the University of Missouri-Rolla standing wave tube to determine the absorptive characteristics of each material at 63, 125, 250, 500, and 1,000 Hz (Figure 1).

Shown in Figure 2 is one of the first sodium-based samples to demonstrate any successful impedance. Later changes in porosity in the sodium-based system produced acoustic absorption near 25 percent. The other more traditionally formulated acoustical absorption coating was an elastomeric-based system. These architectural-grade material samples had holes drilled in the sheetrock substrate. This significantly increased the absorption as frequency increased. The effect of changing particle size on absorption was also investigated. A clear trend of increasing absorption with decreasing particle size was noted. The best organic material outperformed the inorganic sample with the smallest tested particle size.

High-temperature testing was carried out at the Plasma Jet Facility at Marshall Space Flight Center (MSFC) (Figure 3). The plasma jet provides 130 Btu/ft^2/s with 500 m/s hot gas flow of argon/nitrogen.

Figure 1. Acoustical wave tube setup.

This testing has provided an excellent initial screening process for the high-temperature ducting applications. The heat profile is much more aggressive, both from a time and a heat flux standpoint, than launch hardware is expected to experience. The plasma torch feedback controls provide a defined heat flux rather than a predetermined temperature. This is actually the most practical way of obtaining reliable data around the expected use conditions because the kinetics of material emissivity and combustion are complex enough to make instantaneous temperature measurement unlikely. Approximate

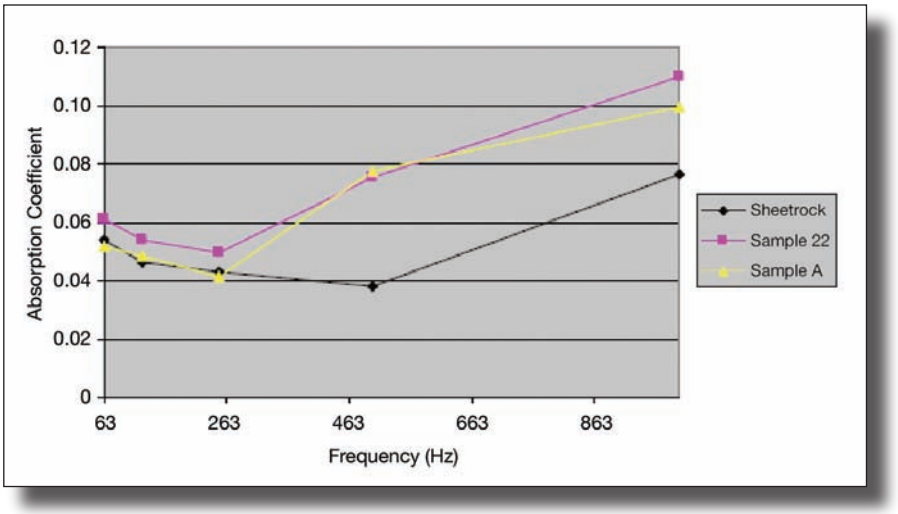

Figure 2. Absorptive properties of sodium-based samples.

front-surface temperature measurements are made using an optical pyrometer. The estimates provided for the samples based on the pyrometer laser measurements are surface temperatures in the range of 2,750 to 3,600 °F.

Key accomplishments:

- Demonstrated experimentally a high-temperature (tested to 3,500 °F at the MSFC Plasma Jet Facility) acoustical absorption (25 percent in normal-incidence acoustical wave tube testing) coating for ducted acoustics.
- Demonstrated that production of a sound absorption coating is possible in the extreme environment of rocket exhaust gas impingement.
- Completed Small Business Technlogy Transfer (STTR) Phase I contract.
- Presented the study at the 2005 Thermal-Fluid Analysis Workshop (TFAWS), NASA KSC.

Key milestone:

- Begin STTR Phase II contract.

Contact: Dr. Bruce T. Vu <Bruce.T.Vu@nasa.gov>, NASA DX-F3, (321) 867-2376

Participating Organizations: Mabel's Prototyping (Floyd Roberts and Gerry Arner) and University of Missouri-Rolla (Dr. Walter Eversman and David Burd)

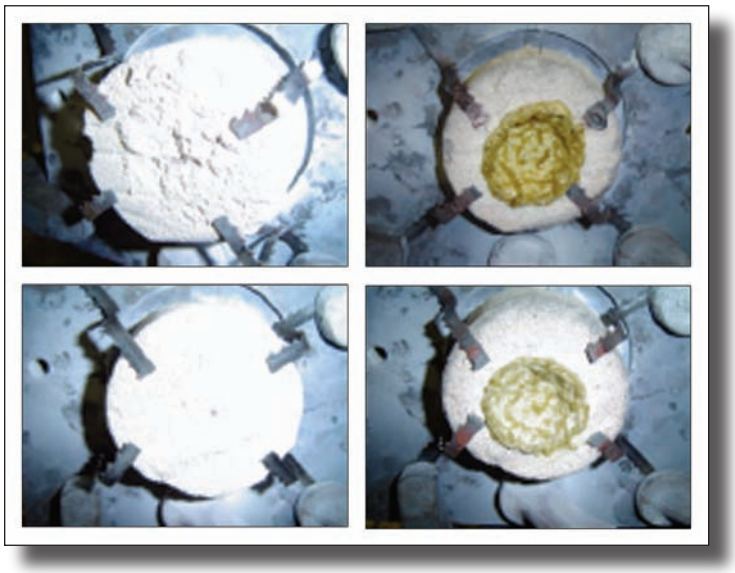

Figure 3. Plasma torch testing.

Distribution of Forces in Granular Materials

Large-Material and Equipment Handling

Although granular materials are very common in engineering applications (cryogenic insulation material, lunar soil as an engineering resource, etc.), their mechanical behaviors are poorly understood and there is no straightforward way to predict their stress-strain response. However, recent advances in computing technology have enabled dramatic progress.

One example of the challenges is to understand how forces spread out through a granular packing. Rather than spreading out evenly, the forces self-organize into long-range "force chains" that travel through narrow chains of grains, while the surrounding grains bear little of the load. The probability curve for finding a particular value of force on a particular grain contact, $P(f)$, is shaped somewhat like the Maxwell-Boltzmann distribution of thermodynamics, although $P(f)$ has unique features that (until now) had not been explained. A theory to explain this curve will help predict the stress-strain response of granular materials and will predict what fraction of the grains will be crushed.

Research was performed to explain the physics behind $P(f)$ and to create a software algorithm that predicts it rapidly. The first insight enabling this research is that there are three conservation laws in a granular material, each consisting of a conserved layer of force orthogonal to the other two spatial directions, whereas in thermodynamics, all conservation laws are taken with respect to the single direction of time. This implies that granular statistical mechanics may be viewed as a generalization of thermodynamics to permit the analogy of multiple, orthogonal "time" dimensions.

$$\tilde{\rho}^{(3)}\{f_{\alpha\beta},\theta_{\alpha\beta}\,|\,W_x,W_y,P_{4\theta}\}=\left\{\sum_{i=1}^{N!}\prod_{C_i}\delta\left(\vec{f}_{\gamma\delta}+\vec{f}_{\kappa\lambda}\right)\right\}\prod_{\alpha=1}^{N}\delta\left(\sum_{\beta=1}^{4}\vec{f}_{\alpha\beta}\right)$$
$$\times\sum_{\beta=1}^{4}\Theta\left(f_{\alpha\beta}\right)\delta\left[P_{4\theta}-Q_{4\theta}\left\{\theta_{\alpha\beta}\right\}\right]\delta\left(\sum_{\alpha}w_{x\alpha}-W_x\right)\delta\left(\sum_{\alpha}w_{y\alpha}-W_y\right) \tag{1}$$

The second insight is that by summing the density of states for granular packings over all particle exchanges, the equations become equivalent to a generalized form of quantum-mechanical Bose Einstein statistics. Then, we may count states just as we do with bosons while enforcing the orthogonal conservation laws through the method of Lagrange multipliers.

$$\frac{\partial}{\partial v_{p\ldots u}}\left[\ln\Omega\{v_{i\ldots n}\}-\lambda_x\left(\sum_i\ldots\sum_n v_{i\ldots n}w_{xi}\right)-\lambda_y\left(\sum_i\ldots\sum_n v_{i\ldots n}w_{yi}\right)-\sum_k\ldots\sum_n\gamma k\ldots n\left(\sum_i\sum_j v_{i\ldots n}\right)\right]=0 \tag{2}$$

This obtains a closed-loop "transport" equation analogous to Boltzmann's transport equation.

$$\rho_g\left(w_x,w_y,\theta_1,\ldots,\theta_4\right)=\prod_{\beta=1}^{4}\Theta\left[f_\beta(\cdot)\right]G\left(\theta_\beta\right)e^{-\lambda_x w_x-\lambda_y w_y}$$
$$\times\iiint_o^\infty d^4f\prod_{\gamma=1}^{4}\left[P_{f\theta}\left(f_\gamma,\theta_\gamma\,|\,\rho_g\right)\right]^{1/2}$$
$$\times\ \delta\left(w_x-w_x^{right}(\cdot)\right)\delta\left(w_x-w_x^{left}(\cdot)\right)$$
$$\times\ \delta\left(w_y-w_y^{top}(\cdot)\right)\delta\left(w_y-w_y^{bottom}(\cdot)\right) \tag{3}$$

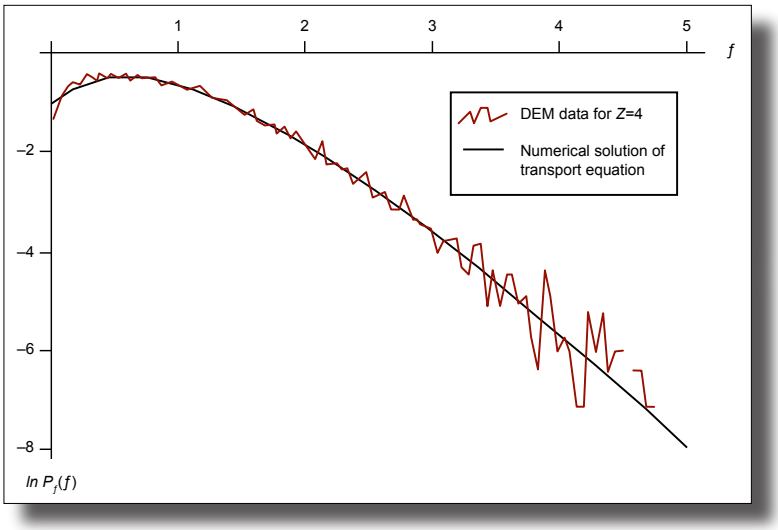

Figure 1. Probability distribution function (semilogarithmic) for the magnitudes of forces among grains inside a granular material, comparing theory (black) with dynamic simulation data (red). The excellent comparison of the theory to the data demonstrates that the theory is correct.

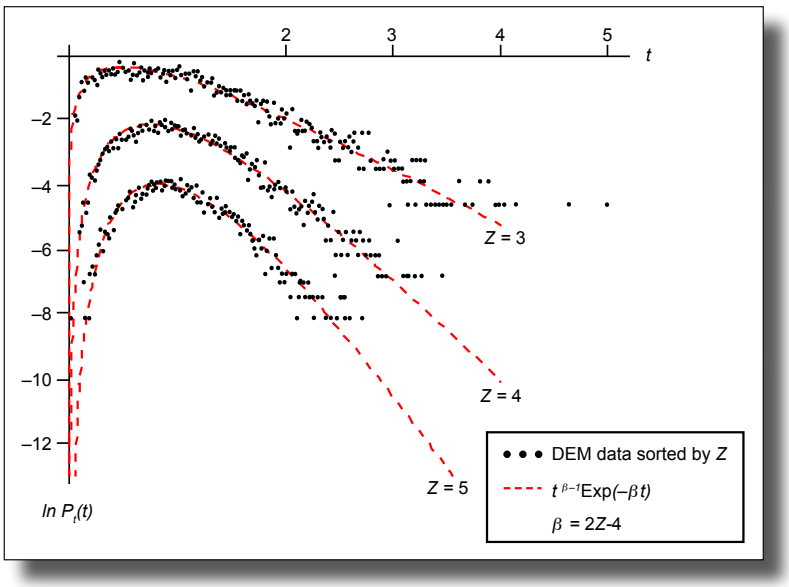

Figure 2. Probability distribution function (semilogarithmic) for the total pressure on individual grains inside a granular material (a packing of random disks), comparing theory (black) with dynamic simulation data (red). The data are segregated into three curves depending on the number of contacts that a grain has with its neighbors. The three sets if curves have been shifted vertically for clarity.

An algorithm was developed to solve this equation. This algorithm is vastly more efficient than performing a full computer simulation based on Newton's laws. The algorithm solves the data for 1 million grains in 1 minute on a desktop computer, whereas the prior methods would take several days of computing time. The results of the algorithm were then compared to the data from the full computer simulations and this demonstrates that the theory is correct.

Contact: Dr. Philip T. Metzger <Philip.T .Metzger@nasa.gov>, NASA KT-D1, (321) 867-6052

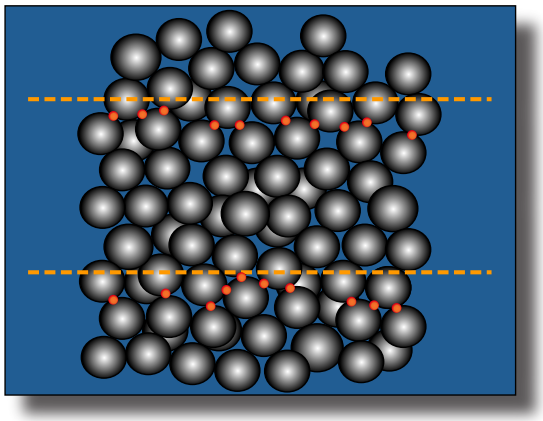

Figure 3. Neglecting gravity, the total weight borne by the grain contacts (red dots) in the top layer of grains must equal the total weight borne by the grain contacts in the bottom layer of grains. This is analogous to the conservation of energy in thermodynamics, so a space dimension inside a granular material is analogous to the time dimension in thermodynamics. This analogy leads to a successful theory explaining how stresses spread out in a granular material.

Physics of Rocket Exhaust Cratering

2005 Center Director's Discretionary Fund Project

Large-Material and Equipment Handling

During the Apollo and Viking programs there was considerable research into the blast effects of launching and landing on planetary regoliths. That work ensured the success of those missions but also demonstrated that cratering will be a significant challenge for other mission scenarios. For example, high-velocity spray of eroded soil will challenge attempts to land multiple spacecraft within short distances of one another on the Moon. The first spacecraft to land may be scoured and contaminated by the spray from the second. We observed a relevant example when the Apollo 12 Lunar Module landed 155 meters from the deactivated Surveyor 3 spacecraft. Portions of Surveyor 3 were returned by the Apollo astronauts to Earth for analysis, where it was found that the surfaces had been sandblasted and pitted and that every opening and joint was injected with grit from the high-speed spray.

Simply building a berm to block the spray around the landing site will not provide a complete solution. While the majority of soil particles are ejected into low elevation angles and stopped by the berm, some fraction may be ejected over the berm because of local surface roughness. Also, after engine cutoff there is a central core eruption of soil in the vertical direction as gases beneath the plume's stagnation region are suddenly released from the soil. This eruption entrains dust and will contaminate the engine combustion chambers, creating dangerous hot spots during the next engine firing. Furthermore, repeated landings on the same site will eventually loosen the compacted surface and produce the chance of localized soil fluidization or pressure cratering beneath the plume on subsequent launches or landings.

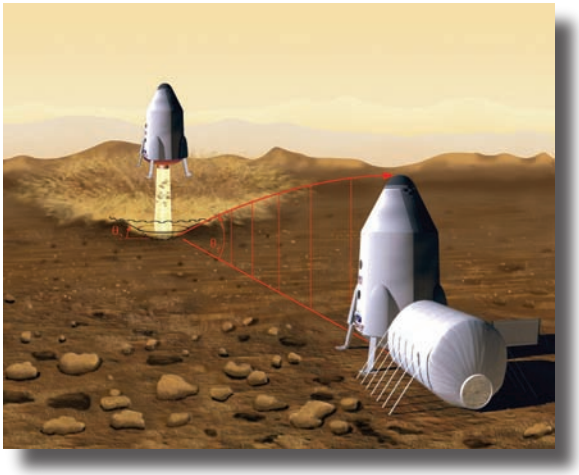

Conceptual model of a surface environment for the purpose of rocket cratering research.

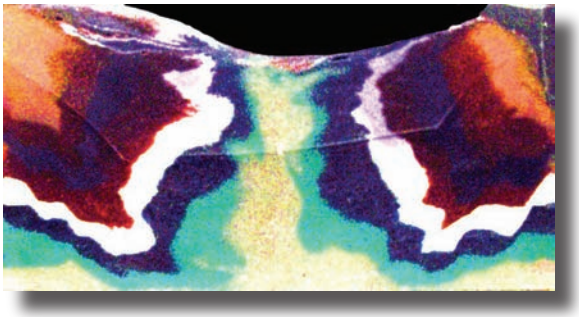

Cross section of a jet-induced crater. The layers of colored sand were originally horizontal, but the downwardly impinging jet forced the deepest layers to drive upward beneath the center of the crater.

Despite its shortcomings, the use of berms is the leading strategy to mitigate lunar soil erosion. Berm effectiveness must therefore be quantified to provide the environmental design requirements for hardware outside the berm. Prior studies of soil erosion and cratering were performed before modern instrumentation was available. Hence, there has never been an adequate description of the physical scaling that occurs inside a jet-induced erosion event. Also, the prior theory was based on the erosion of desert dunes and has been superseded in published literature as new computer simulation data have become available. Therefore, this project began with a series of tests to observe and describe the physics and obtain the scaling laws. Phase II of this research will use these physical insights to begin computer modeling of the physics and adapting the model to lunar conditions to evaluate berm effectiveness and other mitigation technologies.

So far, tests have been performed with subsonic jets of different gases (nitrogen, carbon dioxide, argon, and helium) at different exit velocities, different nozzle heights above the soil, and different sand grain sizes. The tests have used a sharp-edged plexiglass sheet as the

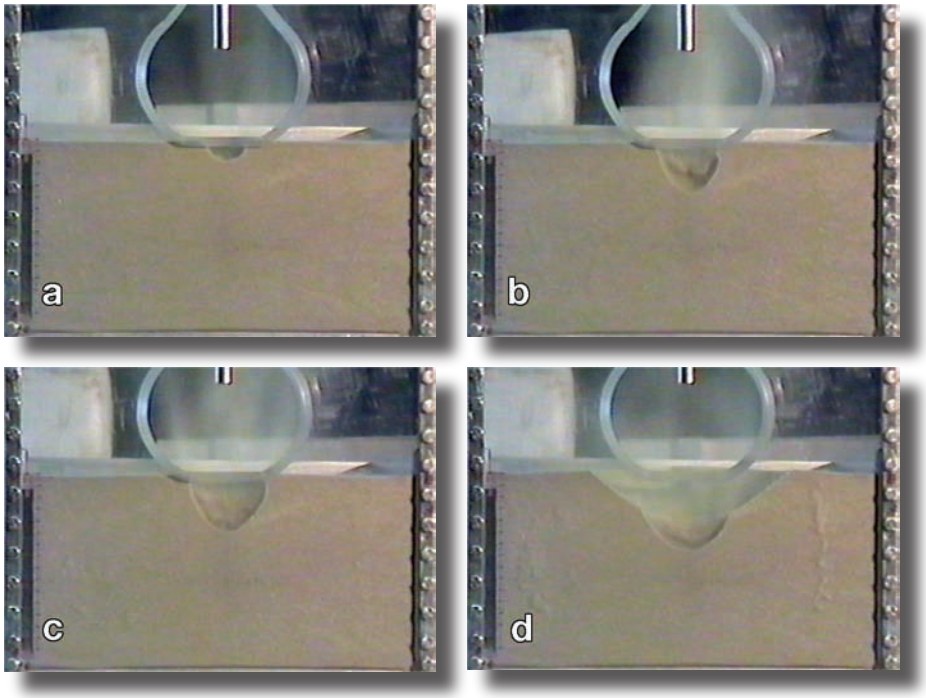

Sequence of crater growth: (a) Erosion/fluidization forms a cup. (b) Toroidal recirulation cell consisting of airborne grains forms inside the cup. (c) Crater widens until traction along inner surfaces is insufficient to maintain steep sides. (d) Sides collapse to the angle of repose, producing a recirculating surface layer of rolling grains that return to the inner crater.

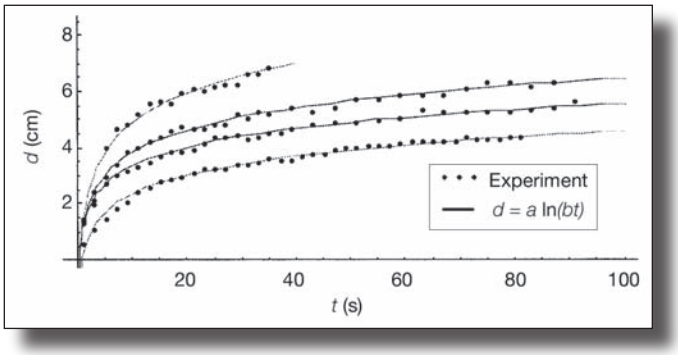

Crater depth versus time. All cratering events are governed by a simple differential equation that universally produces a logarithmic growth in crater depth.

front wall of a box of sand, splitting the jet in half so the cratering effects beneath the surface can be observed inside the box. The jets have been applied both suddenly and gradually, with high-speed videography to capture the transient and quasistatic effects. Surprisingly, sudden application of the jet resulted in the deepest soil flowing upward, instead of downward beneath the center of the crater. Also, the crater was observed to evolve into a complex structure consisting of (1) an inner crater that provides the excavation surface, (2) an outer crater at the angle of repose that creates a rolling layer of grains that flow back to the inner crater, (3) a mass of airborne grains recirculating toroidally inside the hollow, and (4) transient dunes of locally deposited material around the inner and outer lips. The depth of the crater over time universally follows a logarithmic growth curve with only two scaling parameters, regardless of the physical conditions of the test. Ongoing research is concentrated on explaining the differential equation that produces this universal form and on identifying the physical dependencies for the two scaling parameters.

Contact: Dr. Philip T. Metzger <Philip.T.Metzger@nasa.gov>, NASA KT-D1, (321) 867-6052

Participating Organizations: Berry College (Carly M. Donahue) and ASRC Aerospace (Robert B. Cox, Alex R. Taylor, and Brian D. Larson)

Nonpyrotechnic Latch and Release System for Aerospace and Other Applications

Defect/Damage Location and Spacecraft Handling Systems

This research began investigations of the operation and performance of a new class of latching and release mechanism based on a wire basket latch with an initial pinch force. The stated goals of the research were to develop mathematical models or equations describing the operation of the nonpyro latch device and construct and test prototypes. American Remote Vision Company (ARVC) found that the general class of the mechanism is vastly larger than initially anticipated; and they invented a new type of force-multiplying rotational latch and release system. ARVC investigated the force-multiplying behavior of the basket latch version experimentally, started investigating (theoretically and experimentally) optimal basket configuration, built and tested two-dimensional photoelastic models of the basket version (to show that the basic physics of the model was correct or at least plausible), and conceptually designed a controlled-release mechanism based on these grabbers.

Release system choices that are fast-acting and do not use pyrotechnics are limited today. Testing and future development of umbilical, robotic, and support systems are expected to require release and latch mechanisms that are safer, reusable, controllable, and reliable. Present methods for providing instantaneous separation or separation under large loads typically include the use of pyrotechnic-initiated systems. Although systems containing pyrotechnic devices do their job well, they typically have significant drawbacks, such as handling and storage hazards, contamination concerns, high shock and vibration induction, and debris generation, that warrant development of nonpyrotechnic release systems. Pyrotechnic systems cannot generally be reset and reused, which leads to extra costs.

ARVC researched and developed a novel new class of nonpyrotechnic latch and release mechanism for use in servicing umbilical applications. This class of mechanism was found to be robust, reliable, reusable, and scaleable and had antifouling characteristics. This mechanism can replace explosive fasteners, function as a work holder or collet, and serve as a robotic gripper. The significance of this innovation is the creation of a class of mechanisms that are simple in nature, are scaleable over a large load range, can be controlled, and can work in a hostile environment.

Contact: Paul A. Schwindt <Paul.A.Schwindt@nasa.gov>, NASA DX-F3, (321) 867-9294

Participating Organization: American Remote Vision Company (Stuart Gleman and Steve Thayer)

Two-thousand-pound test. Left: air pressure cuff for the initial pinch; left center: one nylon tie wrap for initial pinch; right center: two tie wraps; right: a hose clamp provided adequate initial pinch.

The 1-ft ruler is parallel to the air cylinder actuator, which pushes or pulls the scissor mechanism to stretch or compress the basket, which is at a right angle to the ruler and cylinder.

Extraction of Lead Compounds for Remediation of Lead-Based Paints

2005 Center Director's Discretionary Fund Project

Though lead paint was banned in 1978, the presence of lead in painted surfaces and elsewhere still poses serious concerns for human health and our environment today. The removal of lead-containing paint remains a costly and hazardous process, and even the foremost removal method, dry abrasive blasting, releases large amounts of contaminated particulate matter—hardly an effective solution.

Small particles of lead compounds are dispersed in the pigment of lead paint and are suspended by the paint's binding agent. By design, these compounds are very stable, and the particles are difficult to extract from the binder. However, it may be possible to chemically swell the binder and leech the pigment out of the paint matrix without having to physically remove all the paint on a surface. If successful, such a technique could dramatically reduce the cost, labor, and hazards associated with traditional lead paint remediation.

Chelating agents—chemical compounds with the ability to form multiple bonds to a single metal atom—were evaluated as a means of increasing the mobility of the lead-containing pigment particles. These agents can not only chelate metal ions already in solution but can dissolve compounds containing metal atoms that are otherwise considered insoluble. Making lead compounds more soluble could make them easier to leech out of the paint.

Experiments with several common chelating agents identified the best candidate for treating lead oxide: Mercaptosuccinic acid (MSA) dissolved the lead oxide quickly with minor agitation, in part because its sulfur content allows it to bind easily with the lead oxide.Two types of lead paint chips and scrapings were then placed in a solution of 5 percent MSA in water at pH=7. Type I consisted of lead pigment and linseed oil as the binder. In addition to lead oxide, Type II contained a small amount of iron oxide for color and other additives to extend paint life and hasten drying. The MSA solution dissolved as much as 75 percent of the lead oxide in both paints in under 48 hours. As a follow-up, glass slides covered in the same two paint types were soaked in the MSA solution for 24 or 144 hours. Some of the painted slides were pretreated with d-limonene to make the paint more permeable. The table shows the results for Type II paint. Pretreating with d-limonene allowed as much lead to be dissolved in 1 day as was dissolved in 6 days.

Multiple extraction experiments showed that the same sample of MSA solution continued to dissolve lead pigment but in smaller quantities, leading to the conclusion that the chelating solution eventually becomes saturated and ineffective. However after two to three MSA extractions, the paint loses adhesion to the glass slide and strips from the surface. Results from experiments on old painted steel panels from launch umbilical towers at KSC were inconclusive because of nonuniform lead concentrations resulting from weathering effects. The combination of chelation and swelling the binder shows promise for a safer method of lead paint remediation and will be examined further.

Contact: Dr. Jacqueline W. Quinn <Jacqueline.W.Quinn@nasa.gov>, NASA KT-D2, (321) 867-8410

Participating Organization: University of Central Florida (James G. Captain)

Results of applying MSA solution to Type II paint..

Type II Paint on Glass Slides	Lead Concentration in AA Aliquot (ppm)	Paint Mass (g)	Calculated Concentration of Removed Lead (ppm)	Lead Removed (%)
Nitric acid digest (control)	382	0.2502	152,478	100
24-hour MSA treatment	74	0.4986	21,513	14
144-hour MSA treatment	74	0.4991	59,286	39
Pretreatment w/d-limonene + 24-hour MSA treatment	353	0.4233	64,740	42
Pretreatment w/d-limonene + 144-hour MSA treatment	251	0.5571	62,266	41

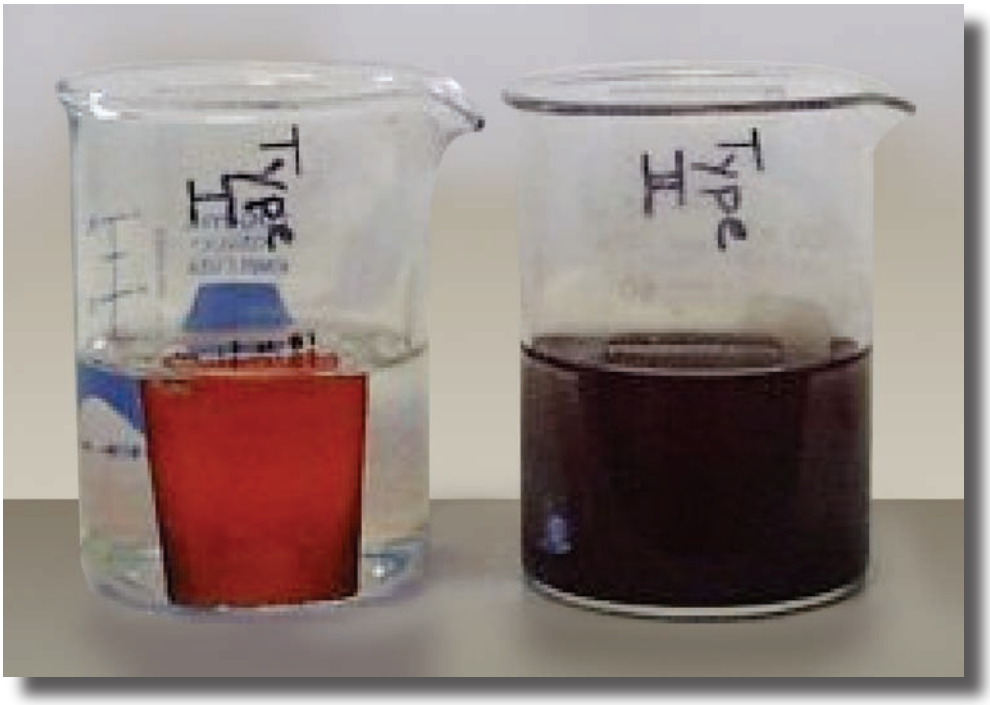

Treatment of Type I and Type II paint samples in MSA solution. The MSA solution changes color to purple in response to the iron oxide found in the Type II paint.

Range Technologies

Range Technologies consist of unique facilities and equipment technologies that provide the control and measurement data necessary to ensure the safety of launch and test operations for the range/spaceport. Examples of these technologies include (1) data processing equipment for range safety analysis, communications systems for telemetry processing, reception, and destruct command systems; (2) sensor and instrumentation systems for vehicle tracking, such as radar systems and optical tracking displays; and (3) data communications management, distribution, and recording systems. Significant capital investment is required to build and maintain this capability and as a result, these assets have traditionally been slow to modernize or have limited flexibility to accommodate new requirements and vehicles. In addition, the cost associated with range system infrastructure is difficult to quantify.

Future range operations will require flexible range technologies that can incorporate the latest technological advances. It is expected to be largely space-based and will be seamlessly augmented with mobile, deployable, and/or ground-based assets. Minimal ground infrastructure will be required and will primarily be located at the launch head, reducing the operational cost. Self-healing autonomous ground and flight systems will become the norm. Range systems will have situational awareness and be intelligent enough to reconfigure autonomously when individual systems "drop out" or are unavailable. A National/Global Range Network with regional hubs is envisioned, which provides 24/7 coverage, is scalable to user requirements, and is seamlessly integrated into the national and global air space. The modernization activities will also ensure that future technology improvements will be able to adapt to different space flight hardware designs, and the degree of customization or reconfiguration for specific launch vehicles operations will be minimized. Multiple simultaneous test and launch operations by multiple vehicles from multiple spaceports are also envisioned.

With the goals and objectives of improving safety, improving range responsiveness (support more launches, reduce lead and turnaround time, and reduce delays), reducing variable launch and range costs, reducing cost of fixed infrastructure, and improving capacity and flexibility, the KSC team has joined with the Air Force Space Command to lead a national coalition called Advanced Range Technologies Working Group (ARTWG), which is identifying the range technology roadmaps for the next 25 years.

The seven range technology focus areas are

- weather measurement and forecasting,
- tracking and surveillance,
- telemetry,
- decisionmaking support,
- planning, scheduling, and coordination of assets,
- range command and control systems, and
- communication architecture.

For more information regarding Range Technologies, please contact Richard A. Nelson <Richard.A.Nelson@nasa.gov>, NASA KT-C, (321) 867-3332.

Multistation Sonic Location of Lightning Strikes

Localized Weather Forecasting and Measurement

The objective of this project was to deploy and evaluate the performance of multiple Sonic Lightning Locator (SOLLO) units in a configuration to allow the strike location to be computed using more than one system. The SOLLO units are designed to locate lightning strikes, using acoustic information within a 1-km radius of the individual station. In a typical multistation SOLLO scenario, two or more units are required to cover the area of interest. SOLLO is considered a short-range system (less than 1 km) and is designed to locate lightning strikes with an accuracy of within a few meters. Lightning does not have to strike electronic equipment or systems directly to cause damage. The location information produced by SOLLO can be used independently or in conjunction with other systems such as existing cameras and monitoring equipment. Obtaining information on nearby lightning is important when determining which structures, equipment, or systems are candidates for investigation and testing following a period of lightning. In the past, other systems, most notably cameras, were used to determine the vicinity of a strike; however, heavy downpours and limited camera coverage reduced their effectiveness.

A SOLLO unit is triggered by the electromagnetic energy produced by the fast-varying electric currents associated with a lightning strike. The electromagnetic field propagates through space and triggers the unit through a small antenna located on the electronics cabinet. SOLLO then records approximately 3.2 s of acoustic information from four microphones. The acoustic data is stored in onboard flash memory for later retrieval. The time of arrival of the electromagnetic trigger is used as the starting point, time zero, for each acoustic event. The information recorded is used to estimate the location of the strike. The difference in the time of arrival of the acoustic waves is used to calculate the direction and distance to the strike, and the first arrival of the acoustic energy can be used as an estimate of the maximum distance. SOLLO microphones can be set up in various geometries; however, the system is easiest to set up with one microphone at the origin and the remaining three along the axes of a Cartesian coordinate system so that each baseline from the origin is perpendicular to all others. The baseline for each leg is typically 4 to 7 m and provides good direction resolution and reasonable range information using a short baseline calculation based on the times of arrival of the acoustic waves. The differences in times of arrival are calculated by the cross correlation of the three microphone waveforms on the axes with the waveform at the origin. The resulting calculation yields an azimuth and elevation (direction) to the strike and a range. Because of the short baselines and the signal resolution (sampling rate), the range has a large uncertainty, but the direction information is reasonably good. By using a multistation approach, the intersection of the two directions provides a location with a low positional error. Additional units and channels provide redundancy and reduce uncertainty.

SOLLO installation at Space Launch Complex 20.

Key accomplishments:

- Deployed multistation evaluation SOLLO units at Cape Canaveral Air Force Station Space Launch Complex 20.
- Obtained data on the multistation system.
- Identified additional requirements and enhancements for permanent systems.

Key milestones:

- First deployment of a SOLLO unit in a typical pad environment.
- First-time use of multiple SOLLO units for strike solutions.

Contacts: Michele R. Taylor <Michele.R.Taylor@nasa.gov>, NASA DX-E3, (321) 867-3402; and Bob A. Ferrell <Bob.A.Ferrell@nasa.gov>, NASA KT-C, (321) 867-6678

Participating Organization: ASRC Aerospace (Stephen M. Simmons, Temel Erdogan, and Michael A. Bertucci)

NASA Hail Monitor Development Progress

Localized Weather Forecasting and Measurement

Kennedy Space Center is located in an area characterized by very dynamic meteorological conditions. On May 13, 1999, the Space Shuttle Discovery sustained significant hail damage while on the launch pad. The damage, caused by pea-size hail, required a rollback of STS-96 to the Vehicle Assembly Building for repair of the External Tank (ET) foam. As a result of ET foam loss on STS-114, there is renewed interest in accurately monitoring and measuring crushed-foam damage on the ET, as well as other sources of damage that may occur during launch preparations at KSC. However, hail in the vicinity of the launch pads is often difficult to detect and measure since it tends to be localized and is often embedded in and obscured by intense rainfall. Before the rainfall subsides, any hail quickly melts in the hot Florida climate, erasing all signs that possible hail damage may have occurred.

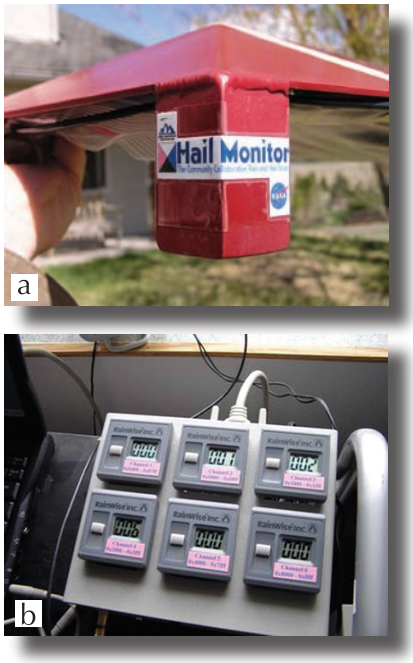

Figure 1. The monitor ([a] sensor and [b] DSP) uses acoustics to count the number of hailstones. It also breaks down their size into six categories.

The total energy dissipated by hydrometeor collisions with the ET surface is a function of many parameters, including horizontal wind velocity, hydrometeor state (liquid, solid, and mixed ratio), size and shape, velocity angle, and point of impact. The ability to map the ET surface and assess damage inflicted by energetic hydrometeors in 3-D would contribute significantly to safety and operation of the Space Shuttle and future launch vehicles. To address concerns about the damaging effects of hail on the Space Shuttle and its fuel tanks, hail monitors were developed (see "A Study of Hail Monitoring Strategies for Shuttle Launch Safety," *Kennedy Space Center Research and Technology 2003 Annual Report*) to detect hail at the launch site, as shown in Figure 1. These monitors would be installed close to the Shuttle launch pad, as shown in Figure 2.

In spring 2005, three NASA hail monitor calibration sites were selected and set up in the high plains of eastern Colorado, with the help of Colorado State University and the Community Collaborative Rain, Hail, and Snow Network (CoCoRaHS, <*http://www.cocorahs.org/*>). The frequency of hail at any location in this region averages 7 days per year. Figure 3 shows that the occurrence of hail in this area is second only to an area just to its north, at the junction of Colorado, Wyoming, and Nebraska, which averages 9 hail days per year. Note that the vicinity of the Shuttle launch pads averages less than 1 hail day per year.

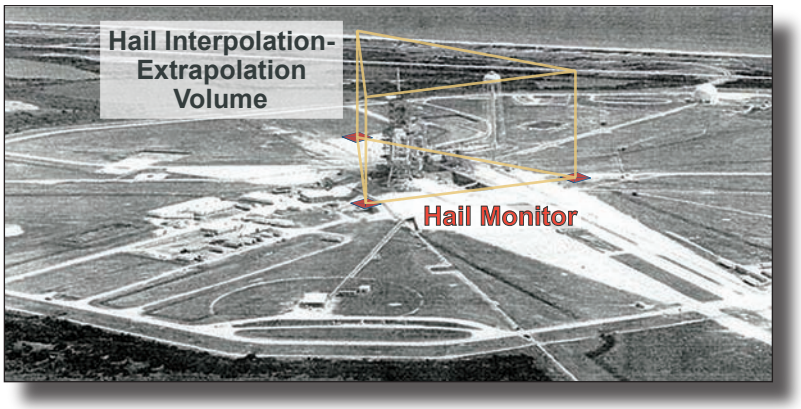

Figure 2. Shuttle pad placement strategy using three hail monitors.

CoCoRaHS volunteer observers measure rainfall daily (snowfall in winter) and record the amounts in an online database. During major storms, they post readings more frequently so forecasters and emergency managers can update storm alerts with data from places where there are no weather stations.

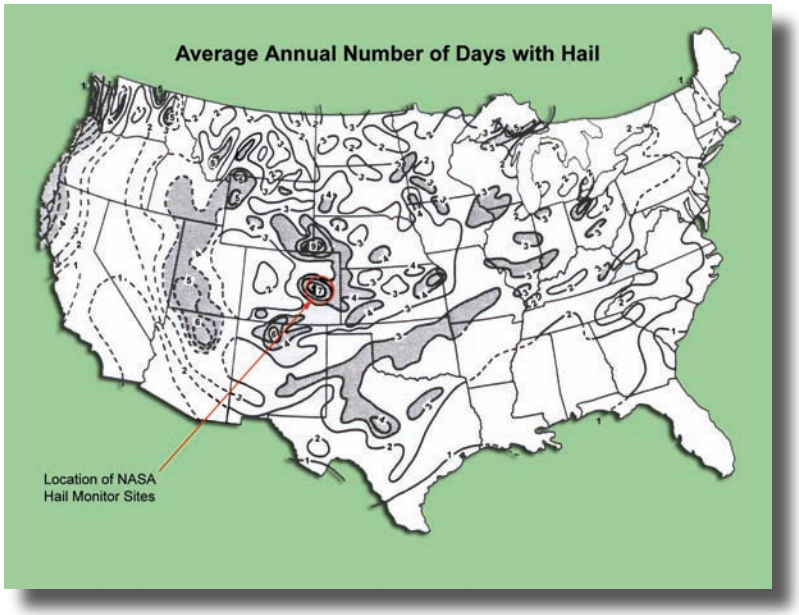

Figure 3. Map showing average annual frequency of hail days over the continental United States. The numbers correspond to the average number of days per year that hail has fallen at any given site.

In spring and summer, the CoCoRaHS volunteers set out hail pads made of Styrofoam wrapped in aluminum foil to record hailstorms. Hailstones leave dents on the 12-inch squares, which can be used to determine the size and density of the hail, as well as the direction it fell. Three of the nearly 3,000 CoCoRaHS sites now also include a NASA hail monitor. The CoCoRaHS volunteers at Parker, Bennett, and Elizabeth, Colorado (Figure 4), record the hail monitor readings from the six digital-signal processor (DSP) displays corresponding to six hail size categories, photograph dents in the colocated hail pads, and log any other relevant data. By collecting and analyzing this kind of data, the NASA hail monitor processing electronics and software can be fine-tuned to yield the best possible measurement of hail counts and size.

Key accomplishments:

- Set up three hail monitor calibration sites in eastern Colorado.
- Refined the hail pad–to–hail monitor calibration procedure, based on probability matching.
- Designed and fabricated stand-alone DSPs.
- Collected data to provide necessary input for the development of a lighting impulse suppression filter.

Figure 4. (a) CoCoRaHS hail pad (right) and NASA hail monitor (left) at Bennett, Colorado, site; (b) hail monitor awaiting hail at Parker, Colorado, site. A cable runs indoors from the hail monitor to the DSP.

Contact: Dr. Robert C. Youngquist <Robert.C.Youngquist@nasa.gov>, NASA KT-D1, (321) 867-1829

Participating Organizations: ASRC Aerospace (William D. Haskell, Robert B. Cox, Jeffrey A. Rees, and Dr. John E. Lane), Colorado State University (Howard W. Reges and Nolan J. Doesken), and CoCoRaHS (Robert J. Burkhart, Jay Brigham, and Bud Barber)

Spectral Analysis Using a Second-Order Response Function

Localized Weather Forecasting and Measurement

Elemental analysis involves the study of a spectrum generated from a sample of unknown composition to identify the sample's trace elements and relative quantities. For example, proton-induced x-ray emission (PIXE) spectroscopy generates a spectrum of x-ray energies. A silicon/lithium (SiLi) detector counts x-ray photons over a range of energies, corresponding to L- to K-shell electron decay. This decay occurs because of an external high-energy projectile proton or alpha particle knocking the K-shell electron from the atom. The vacancy is then filled by an electron from a higher shell number, thus producing an x-ray photon. The number of photons counted in all channels (energy bins) generates the target PIXE spectrum. The process of spectral analysis involves interpreting the spectrum and identifying characteristic peaks (Figure 1). These peaks can be thought of as delta functions with zero width, which are spread out over many energy bins as a result of the detector response. The measured spectrum $F_y(x)$ can be described by the convolution of the characteristic peaks $h_x(x)$ with the detector response $f_s(x)$, over all energies x within the range of measurement.

$$F_y(x) = \sum_{k=1}^{N} \int f_s(x - x')h_x(x')dx' \qquad (1)$$

or expressed in discrete form, where Δx is the width of the energy bin:

$$F_y(k\Delta x) = \Delta x \sum_{j=1}^{N} \{f_s(k\Delta x - j\Delta x) \cdot h_x(j\Delta x)\} \qquad (2)$$

The PIXE detector response is usually modeled as a Gaussian function:

$$f_s(x) = \frac{1}{\sigma\sqrt{2\pi}} e^{-(x-\mu)^2/(2\sigma^2)} \qquad (3)$$

The goal of PIXE spectral analysis is to numerically remove the detector response from the measured spectra, yielding a usable estimate of the elemental characteristic peak's position and amplitude. A typical numerical procedure usually involves fitting a prototype spectrum, convolved with the detector response, to the actual spectrum.

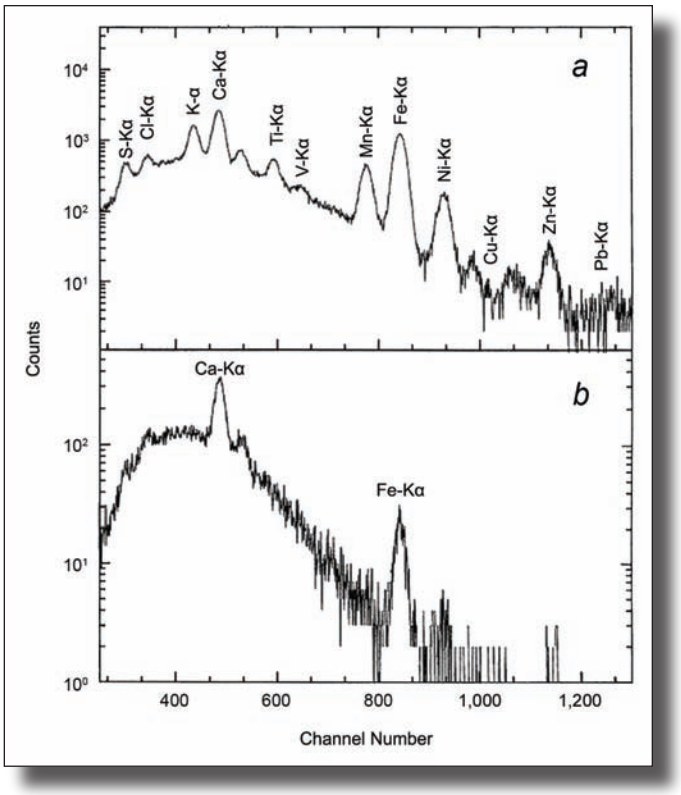

Figure 1. PIXE spectrum of a geological sample.

In the case of an electromechanical transducer, such as the hail monitor, which is based on converting the mechanical impulse of a hailstone striking a metal plate to an electrical signal using a piezoelectric element, a proposed response function is based on the second-order spring-mass system (Figures 2 and 3). The equivalent of the SiLi x-ray detector response given by (3), for the electromechanical transducer, is

$$(f_s)_{ij} = \frac{x_i x_j / Q}{\sqrt{(x_i^2 - x_j^2)^2 + (x_i x_j / Q)^2}} \Bigg/ \sum_k \frac{x_k x_j / Q}{\sqrt{(x_k^2 - x_j^2)^2 + (x_k x_j / Q)^2}} \qquad (4)$$

where x now corresponds to hail diameter (in the case of the hail monitor) and the denominator is a scaling factor.

Figure 4 shows the result of deconvolving the hail spectrum for various values of Q. Note that as Q becomes large, the deconvolved spectrum equals the convolved spectrum. This checks the validity of the transformation since for very large Q, the sensor response should be a delta function. To determine the correct value of Q for the transducer, calibration spectra need to be generated corresponding to single particle types (same size hail for example). The NASA hail monitor, based on qualitative analysis, has a Q in the range of 2.

Key accomplishments:

- Developed a deconvolution method for spectral analysis of electromechanical transducers.
- Applied this method to the NASA hail monitor.

Contact: Dr. Robert C. Youngquist <Robert.C.Youngquist @nasa.gov>, NASA KT-D1, (321) 867-1829

Participating Organization: ASRC Aerospace (Dr. John E. Lane)

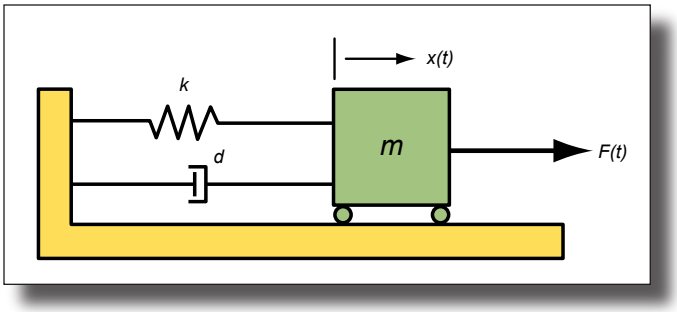

Figure 2. Second-order vibration system.

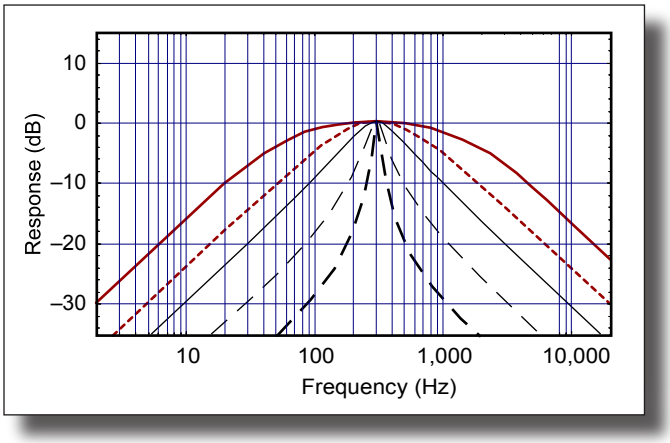

Figure 3. Gain response for second-order band pass function with f_0 = 300, Q = 0.2; dotted line, Q = 0.5; thin solid line, Q = 1; thin dashed line, Q = 3; and dashed line, Q + 10.

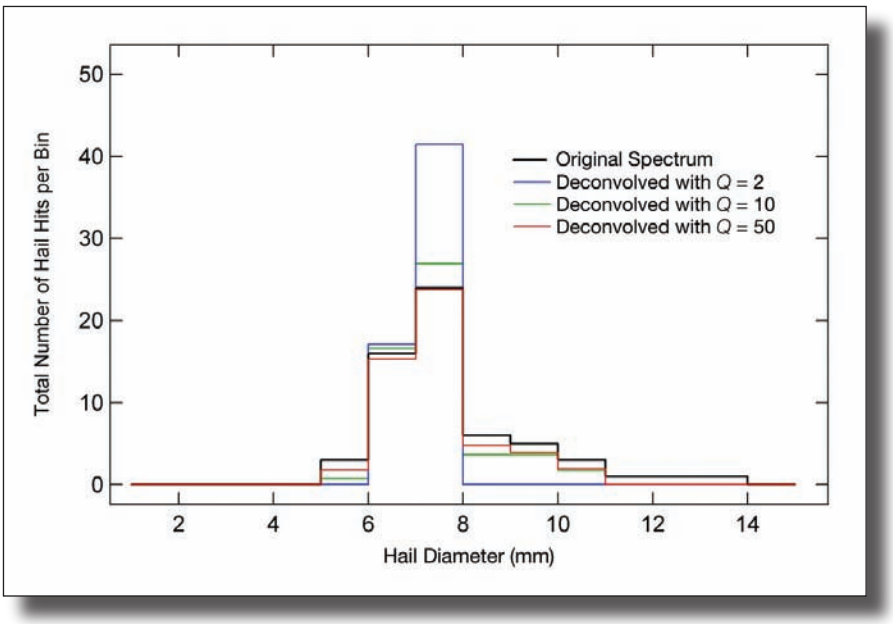

Figure 4. Deconvolution of hail spectrum, using a second-order band pass function.

Reconfigurable Wideband Digital Receiver and Transmitter Architecture for the Tracking and Data Relay Satellite System (TDRSS)

TDRSS-Compatible Transceiver

A high-speed command communication system is critical for the long-term exploration of space. It must be adaptable, easily reconfigurable, flexible, and applicable to a variety of launch, landing, and general command communications actions. The system must be reliable and self-maintained.

The heart of the system is the Software-Defined Radio (SDR), which is a collection of hardware and software technologies that enable reconfigurable system architectures for radio networks and user terminals. An SDR provides an efficient and cost-effective solution for building multimode, multiband, multifunctional radio devices that can be adapted or enhanced by software upgrades while in flight. The results are advanced capabilities and significant life cycle cost reduction.

A real-time hardware and software simulator was built to simulate the communications infrastructures expected during space exploration (e.g., satellites or lunar/terrestrial ground stations, spacecraft travel to the Moon and Mars). This simulator models a high-data-rate communications system through an SDR.

The communication system is modeled in MATLAB Simulink using both the Communications Toolbox and the Signal Processing Toolbox for high-level algorithm development (Figure 1). Simulink is a powerful graphical modeling system that allows complex systems to be designed using a block diagram methodology. After the algorithm is developed, the specific code is generated using Simulink for both the digital-signal processor (DSP) and the field-programmable gate array (FPGA), using Texas Instruments Code Composer Studio and Xilinx System Generator, respectively.

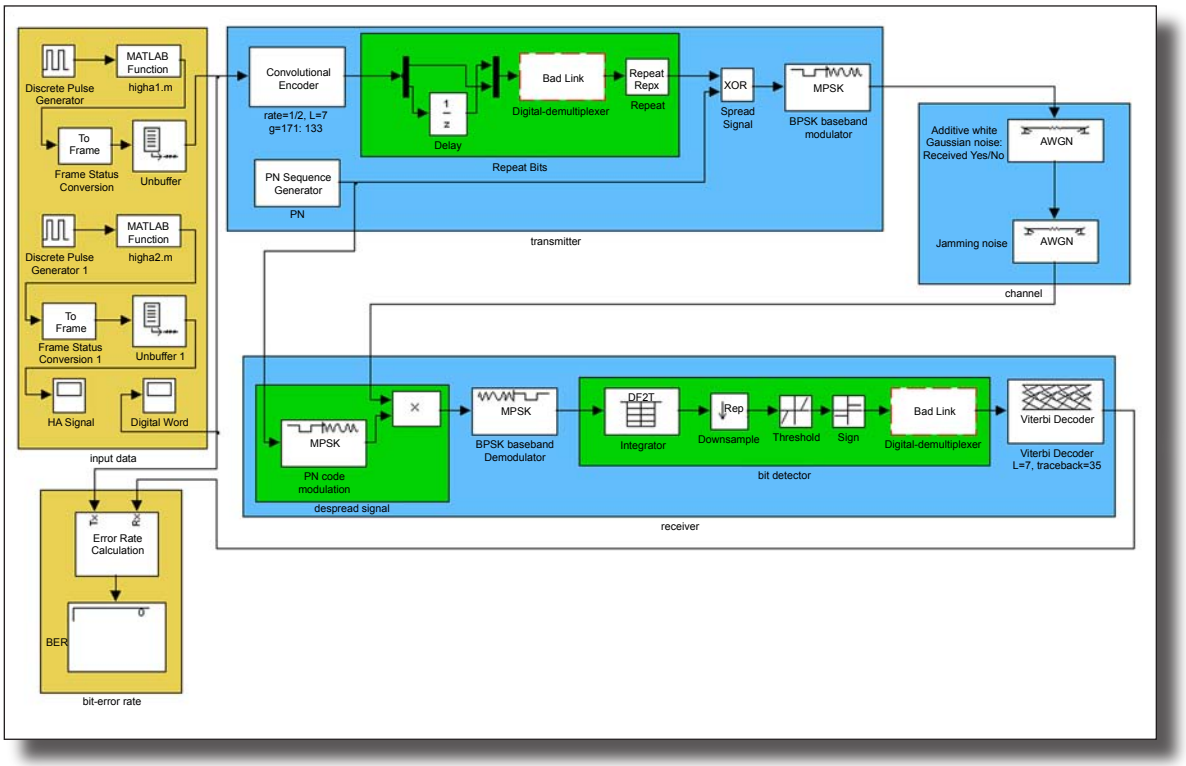

Figure 1. Simulink simulation of the TDRSS communication channel.

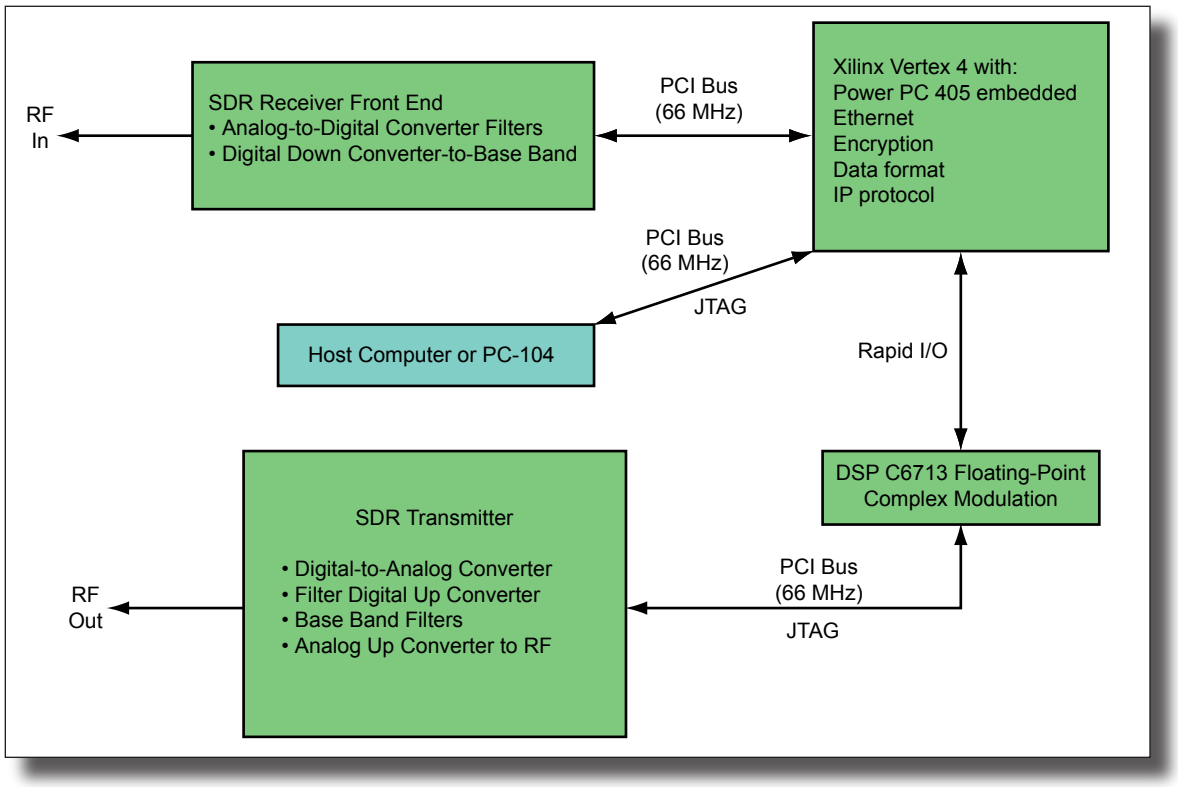

Figure 2. SDR block diagram.

The hardware portion of the SDR consists of the DSP and FPGA (Figures 2 and 3), as well as high-speed analog-to-digital converters and digital-to-analog converters. The Xilinx FPGA uses a protocol control information (PCI) bus to communicate with the personal computer (PC) and rapid I/O to communicate with the DSP. The FPGA will be used to implement an embedded Power PC, Ethernet, data formatting (such as Internet Protocol [IP]), and encryption. The Texas Instruments C6713 DSP will be used to generate the complex modulation. The rest of the architecture will consist of radio frequency (RF) up and down converters.

Key milestones:

- Simulated the TDRSS RF channel in Simulink.
- Procured and stacked the hardware.
- Programmed the SDR boards.
- Interfaced the DSP with the SDR boards.

Contact: Chris Forney <Christopher .S.Forney@nasa.gov>, NASA KT-C, (321) 867-6672

Participating Organization: ASRC Aerospace (Richard B. Birr)

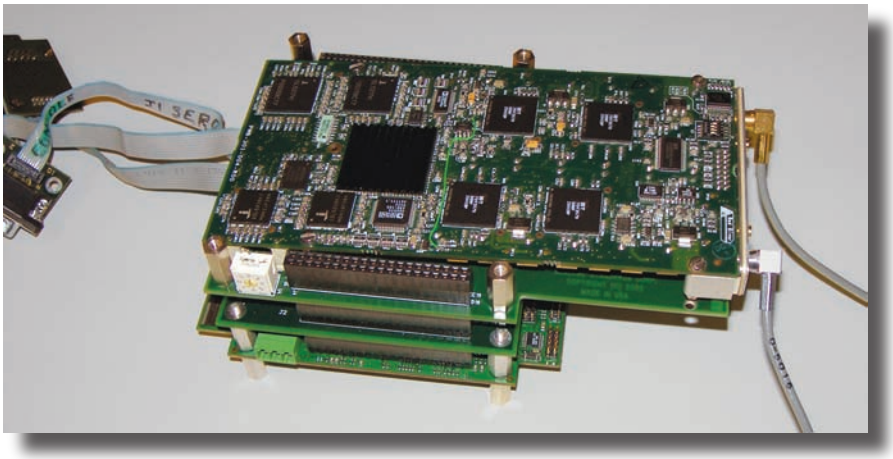

Figure 3. SDR hardware.

Space-Based Telemetry and Range Safety Experiment on a Sounding

TDRSS-Compatible Transceiver

The objective of this experiment was to prove the feasibility of using over-the-horizon communications assets to send Range Safety commands and to receive status back from the flight vehicle.

Sounding rockets are suborbital rocket vehicles that are used for upper-atmospheric and space research. The term comes from the old nautical term "sound," which in this usage means remote measurement. Sailors measured the depth of the ocean by lowering a rope with regularly spaced knots to the ocean floor. They then "sounded off" the number of knots as they hauled the rope back aboard. Likewise, sounding rockets take remote measurements of the upper atmosphere and space and send, or sound off, the measurements back to the ground via telemetry radio links.

The Space-Based Telemetry and Range Safety (STARS) study demonstrated the capability of a space-based platform to provide Range User (telemetry) and Range Safety support to supplement remote ground-based assets. NASA's Tracking and Data Relay Satellite System (TDRSS) was used for the space communications link.

This experiment tested only the Range Safety portion of the overall STARS experiment. The STARS Range Safety experiment is composed of three major subsystems: a low-power transceiver (LPT) with multichannel capabilities, a custom-built command and data handler (C&DH) flight processor, and a commercial Global Positioning System (GPS) receiver (Javad JNS 100 C/A code). Two TDRSS satellites were used simultaneously for both the forward flight termination commands and the return telemetry. Each satellite was in a different position and was used for diversity (to increase the odds that the LPT would receive a good signal). The LPT is configured to receive Range Safety data from the two TDRSS satellites at a rate of 840 bps. This was accomplished by means of a spread-spectrum technique using two unique pseudorandom codes for each satellite. Telemetry data was sent back to the ground control station at 10 kbps via the two satellites, containing tracking data and health and status indicators for the Range Safety system.

The location of the STARS antennas on the sounding rocket is shown in Figure 1. The Range Safety system uses three wraparound antennas: transmit at 2,287.5 MHz, receive at 2,106.4 MHz, and GPS at 1,575 MHz. The experiment was launched from Wallops Island, Virginia, and flew over 200 km in height and 150 km downrange in less than 5 minutes. The speed exceeded 1,500 m/s. The payload splashed down in the Atlantic Ocean and was recovered by ship. Special care was taken to ensure that the payload section remained sealed from the ocean water. Figure 2 shows the sealed section with the STARS experiment, and Figure 3 shows the functional block diagram of the experiment.

Key milestones:

- Configure the STARS experiment for a sounding rocket flight.
- Conduct preflight testing.
- Coordinate all preflight interfaces with the sounding rocket contractor, NSROC.

Contacts: Chris Forney <Christopher.S.Forney@nasa.gov>, NASA KT-C, (321) 867-6672; and Steve N. Bundick <Steve.N.Bundick@nasa.gov>, NASA GSFC/WFF Code 569, (757) 824-1424

Participating Organizations: ASRC Aerospace (Richard B. Birr)

Figure 1. Terrier Mark 70-Improved Orion sounding rocket carrying STARS experiment recovery section.

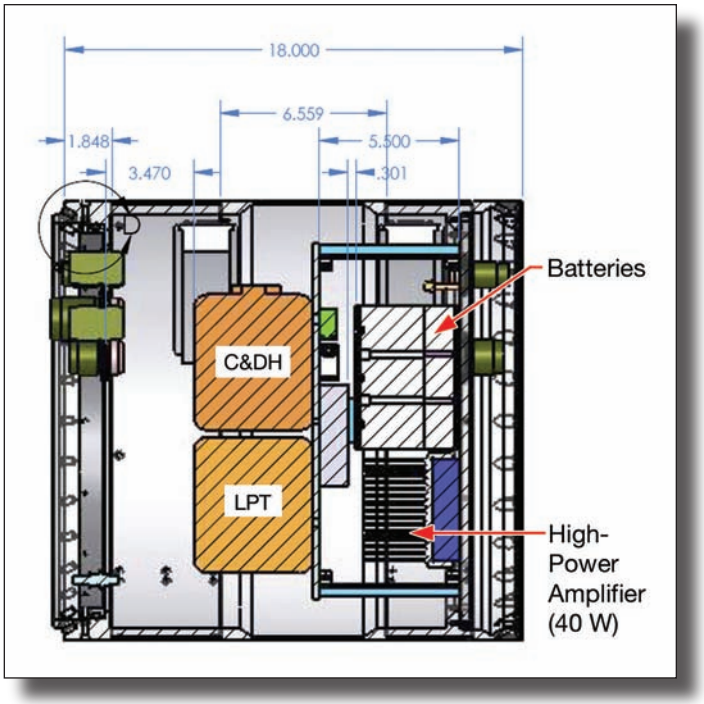

Figure 2. STARS experiment recovery section.

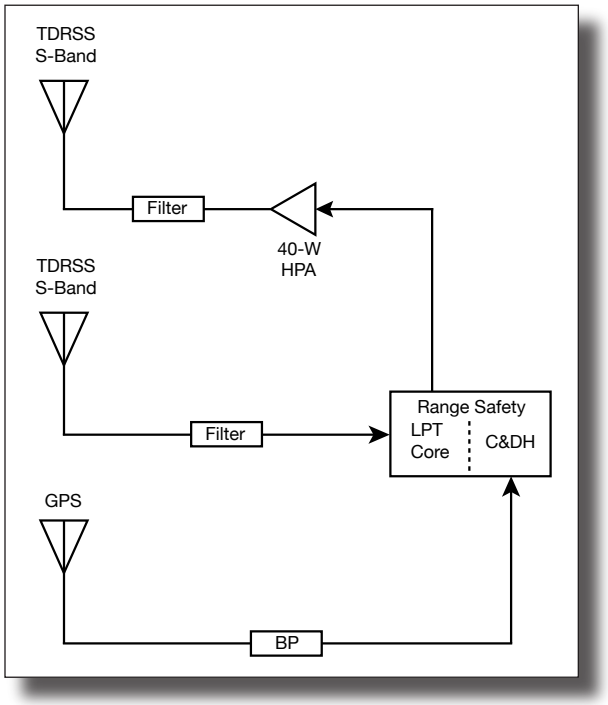

Figure 3. Block diagram of the STARS experiment.

NASA Support of the March 2005 GlobalFlyer Mission

Seamless Command and Control Coordination

GlobalFlyer is a uniquely designed and built, lightweight aircraft from Scaled Composites that Steve Fossett piloted for the first solo, around-the-world, nonrefueled, powered-aircraft flight. GlobalFlyer took off from the Municipal Airport at Salina, Kansas, on March 1, 2005, at 0047 GMT and returned on March 3, 2005, at 1948 GMT. The flight also set the record for the longest nonrefueled flight by a jet-powered aircraft.

NASA supplied the satellite communications system for low-rate, real-time video (about one to two frames per second) from the GlobalFlyer cockpit to the Mission Control Center at Salina, Kansas. The Space-Based Telemetry and Range Safety (STARS) project provided the transmitter, antenna, and video encoder/decoder. NASA's Tracking and Data Relay Satellite System (TDRSS) was the satellite link. NASA also provided a pocket-sized personal cabin pressure monitor that immediately emits an alert should the cabin begin to depressurize to dangerous levels, which thankfully never occurred.

The GlobalFlyer mission support provided by NASA was an intensive 2-month cooperative effort among Scaled Composites, Virgin Atlantic Airways, Kansas State University at Salina, and several NASA Centers and their contractors, including NASA Headquarters, Kennedy Space Center, Dryden Flight Research Center, Goddard Space Flight Center, Wallops Flight Facility, and White Sands Complex.

TDRSS resources were scheduled only on an as-available basis. It was therefore considered successful that TDRSS resources were available 65 percent of the time during the GlobalFlyer mission. The STARS system transmitted real-time video 50 percent of the total time—during the remaining time there were occasional dropouts or the system was turned off. TDRSS resources were also successfully scheduled for ground and flight testing.

GlobalFlyer.

The NASA/KSC Telescience Lab converted, recorded, and routed the downlinked video to the Mission Control Center. The video was combined with the audio at KSC to produce a synchronized video-audio record of the mission, which was then placed into Internet Protocol (IP) packets and routed to different locations, including the Mission Control Center and various public and private servers. The video was also recorded for use in a documentary of the mission.

During the flight, Mr. Fossett carried a KSC-developed personal cabin pressure monitor in a specially designed breast pocket of his flight suit to alert him if the cabin depressurized to dangerous levels without requiring him to constantly monitor gauges. The warnings included audio, vibration, and flashing-light alarms. Because of the exceedingly loud cockpit noise and vibration present in the GlobalFlyer, the monitor was modified to emit a much louder alarm and a much more forceful vibration than is standard. Mr. Fossett was also instructed on how to best use this monitor for GlobalFlyer conditions. The result was a small effective sentinel that added a margin of safety that otherwise would not have been available.

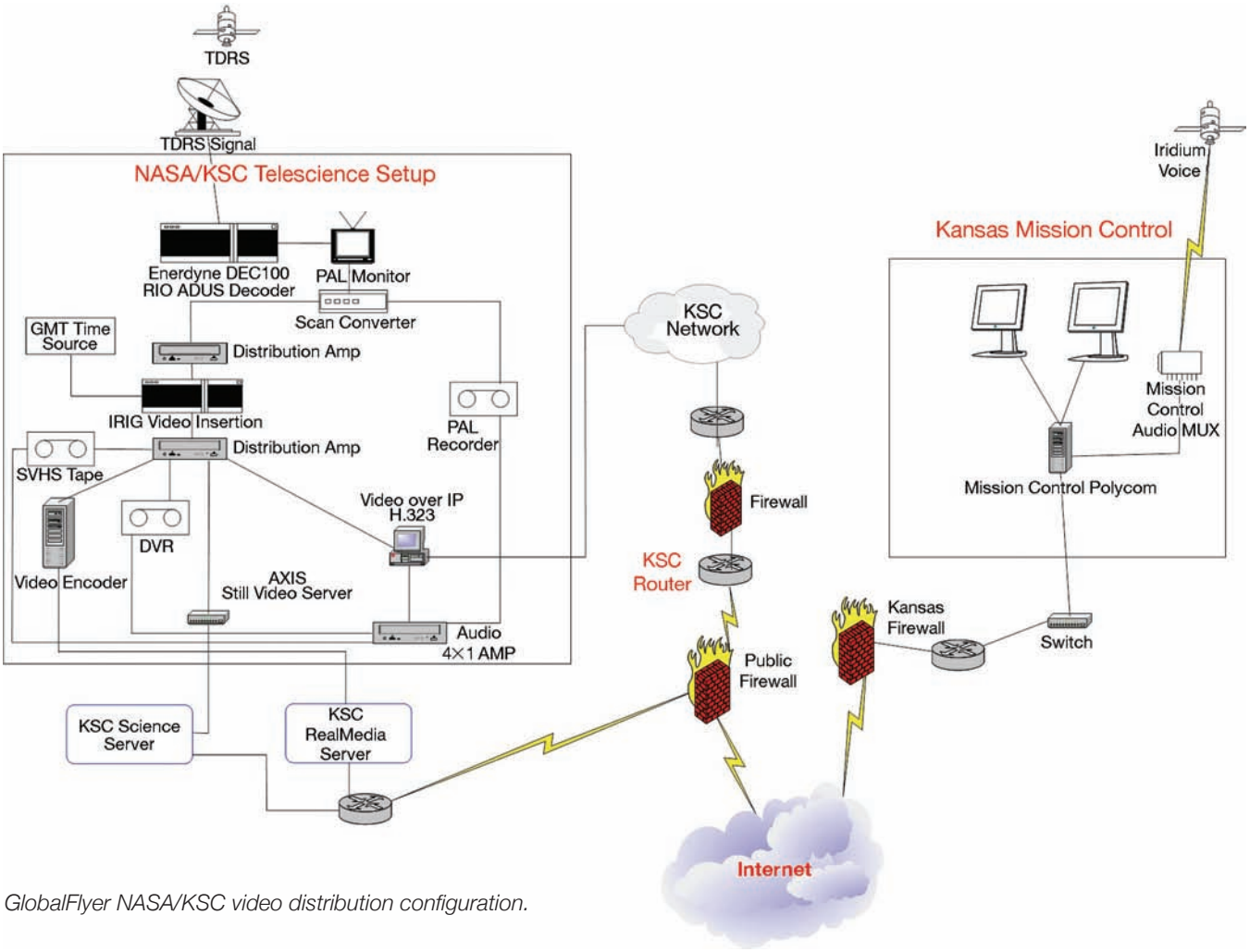

GlobalFlyer NASA/KSC video distribution configuration.

Key accomplishments:

- December 10, 2005: NASA support requested by Virgin Atlantic Airways.
- February 16, 2005: Test flight of STARS on GlobalFlyer.
- March 1–3, 2005: STARS provided real-time video during GlobalFlyer mission.
- August 3, 2005: GlobalFlyer final report with postflight analysis results.

Contacts: Lisa M. Valencia <Lisa.M.Valencia@nasa.gov>, NASA KT-C, (321) 861-7682; Steve N. Bundick, Wallops Flight Facility, (757) 824-1424; Jan A. Zysko, NASA KT-D2, (321) 867-8774; and Richard A. Nelson, NASA KT-C, (321) 867-3332

Participating Organizations: NASA KT-C (Chris Forney and Dr. James C. Simpson), NASA DX-E4 (Erik C. Denson), NASA IT-C1 (Michael T. Downs and James M. Dumoulin), Dryden Flight Research Center (Donald E. Whiteman), ASRC Aerospace (Richard B. Birr), ITT (David L. Wampler), Virgin Atlantic Airways (Richard Branson), Scaled Composites (Burt Rutan), and Hammer (Johnny D. Jones)

Personal Cabin Pressure Monitor.

Space-Based Telemetry and Range Safety (STARS)

Seamless Command and Control Coordination

2005 was another busy and productive year for STARS—a multicenter NASA project to demonstrate the performance, flexibility, and cost savings of using space-based communications assets during vehicle launches and landings. After the initial series of F-15 flights at Dryden Flight Research Center (DFRC) in 2003, the Range Safety low-power transceiver, Command and Data Handler, and Global Positioning System (GPS) receiver components were combined into a single unit called the Range Safety Unit (RSU). The forward (command) flight termination signal link rate was increased from 400 to 840 bps and Triple DES encryption was added. Reed-Solomon encoding was implemented on both the forward and return (telemetry) links, and the Range User System was upgraded to a higher-data-rate Ku-band system with a steerable phased-array antenna.

STARS provided the communications system for real-time cockpit video during the historic GlobalFlyer mission in March 2005. The RSU was modified and installed in the aircraft in less than 4 weeks and provided low-rate video (57 or 114 kbps, corresponding to about one to two frames per second). The RSU inside the GlobalFlyer cockpit is shown in Figure 1. A video data compressor converted phased-alternation-by-line (PAL) video to compressed digital video, which was then relayed via the Tracking and Data Relay Satellite System (TDRSS) to the White Sands Complex (the TDRSS ground terminal) and sent over land lines to the GlobalFlyer control room at Kansas State University at Salina, Kansas, for display and distribution over the Internet. This video was used in conjunction with an Iridium voice link during pilot interviews throughout the mission. The RSU performed well during the 3-day flight. GlobalFlyer presented an excellent opportunity to compare predicted and actual link margins for many hours during mostly straight and level flight using a simple one-antenna configuration on a nonconductive airframe. There were no environmental problems and the measured link margins generally exceeded the predicted by about 3 dB. No attitude information was available, so the predicted models assumed a straight and level profile. This was a reasonable assumption since GlobalFlyer was not designed for dynamic flight and flew nearly straight and level with only very gradual and careful flight maneuvers. This flight experience and data will be useful for future STARS test flights.

The STARS Range Safety System flew on a Terrier Mark 70-Improved Orion sounding rocket at Wallops Flight Facility on December 20, 2005. This flight tested the Range Safety System

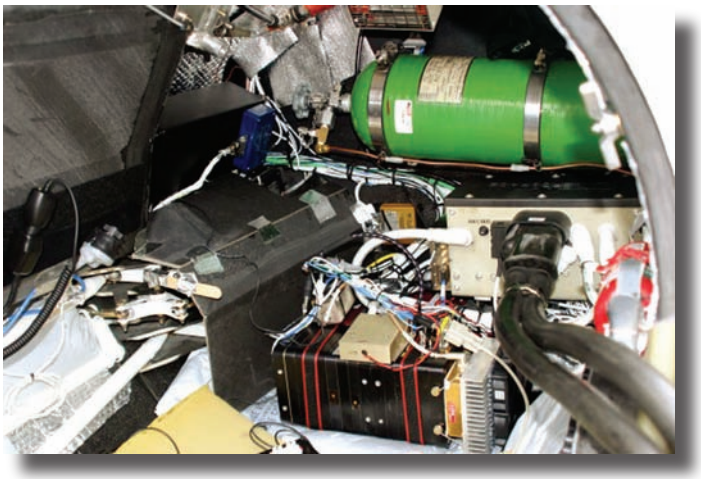

Figure 1. STARS box inside GlobalFlyer.

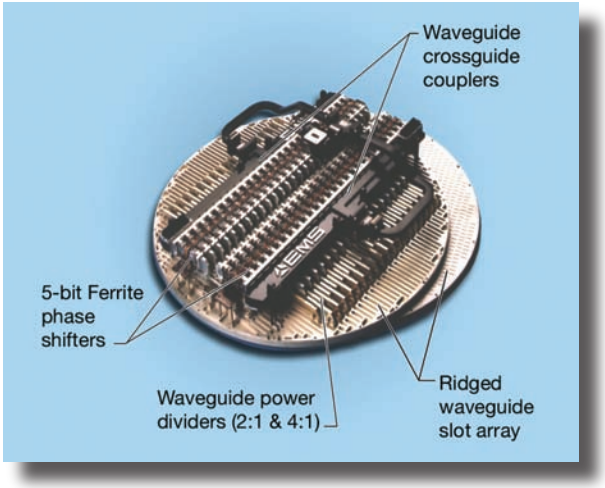

Figure 2. Ku-band phased-array antenna.

at Mach 5 speeds and altitudes up to 200 km on a rocket spinning at 4 to 5 Hz with wrap-around S-band antennas. Two TDRSSs were used simultaneously for the forward flight termination commands and the return telemetry streams. The hardware was successfully recovered. Preliminary analysis indicates that the system performed well, with minimal dropouts and large link margins.

There were also preparations for another set of F-15 flights at DFRC in mid 2006 to test a Ku-band Range User System with the phased-array antenna from EMS Technologies shown in Figure 2. The goal is to achieve a data rate of 5 Mbps. The antenna is electronically steerable in elevation and mechanically steerable in azimuth and will be mounted on top of the F-15 behind the cockpit. The test configuration is shown in Figure 3.

Key accomplishments:

- STARS provided real-time video during the 67-hour GlobalFlyer mission.
- Extensive postflight analysis and GlobalFlyer final report.
- Sounding rocket flight test of the upgraded Range Safety System.
- Planning for F-15 flights to test the Ku-band Range User and upgraded Range Safety systems.

Key milestone:

- Summer 2006: Flight tests on an F-15 at DFRC.

Contacts: Daniel G. Baize <Daniel.G.Baize@nasa.gov>, NASA KT-A, (321) 861-3639; Lisa M. Valencia, NASA KT-C, (321) 861-7682; Steve N. Bundick, Wallops Flight Facility, (757) 824-1424; and Robert D. Sakahara, Dryden Flight Research Center, (661) 276-2566

Participating Organizations: NASA KT-C (Chris Forney, Richard A. Nelson, and Dr. James C. Simpson), NASA DX-E4 (Erik C. Denson), Goddard Space Flight Center (Donald E. Whiteman), White Sands Complex (David O. Glasscock), ITT (David L. Wampler), ASRC Aerospace (Richard B. Birr), and Hammer (Johnny D. Jones)

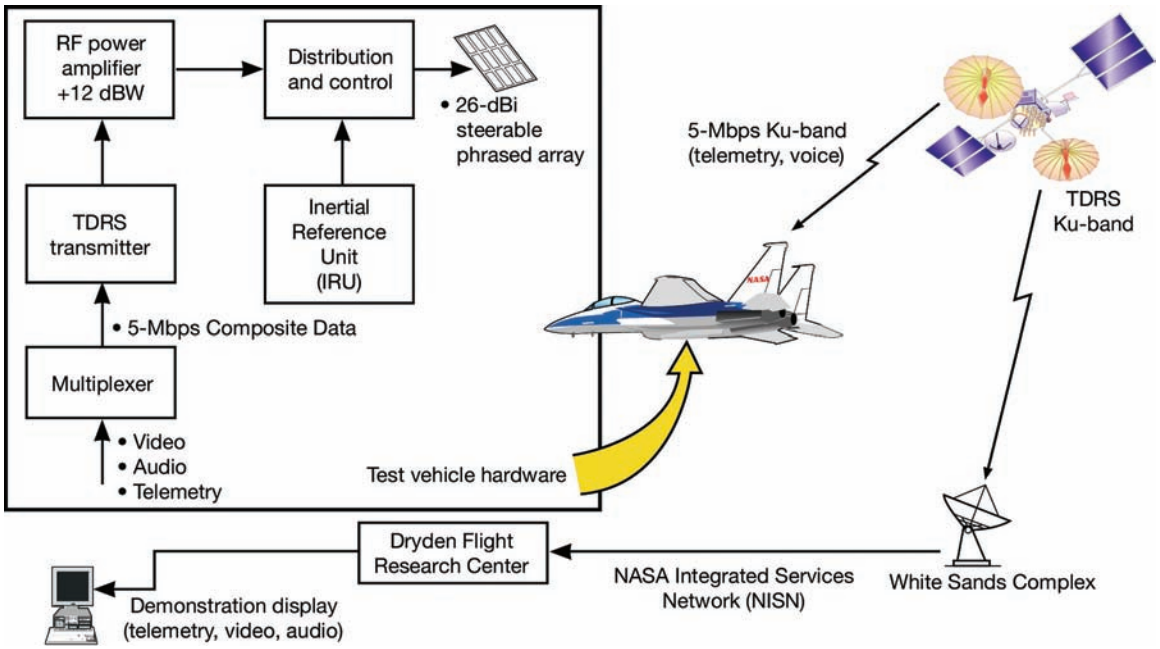

Figure 3. Test configuration for upcoming F-15 flights.

Autonomous Flight Safety System (AFSS): Phase III

Decision/Data Models and Analysis

AFSS, a joint project between KSC and Wallops Flight Facility (WFF) in its third phase of development, is an independent and autonomous flight termination subsystem intended for Expendable Launch Vehicles. It uses tracking and attitude data from onboard Global Positioning System (GPS) and Inertial Measurement Unit (IMU) sensors and configurable rule-based algorithms to make flight termination decisions. The objectives of AFSS are to increase launch capabilities by allowing launches from locations that do not have Range Safety infrastructure, reduce costs by eliminating some downrange tracking and communications assets, and increase safety by reducing reaction time for flight termination decisions.

A full AFSS unit consists of redundant chassis, each containing two independent flight processors, one internal GPS sensor, connections to an external IMU sensor, and a Command and Switching Logic Interlock Circuit (CSLIC) responsible for initiating the firing sequence (Figure 1). Each processor receives all input sensor data and is loaded with the mission rules. During the flight, the data from each GPS/IMU sensor is available to each flight processor, and the rocket's current trajectory is continually checked against the mission flight rules. Each CSLIC simultaneously monitors the state (MONITOR/ARM/FIRE) of all flight processors and initiates a destruct based on the majority vote.

Work in 2005 included

- improved efficiency and accuracy of mission rule algorithms;
- an expanded set of mission rule algorithms;
- a PC-based data monitor to display telemetry in real time and archived data for postflight analysis (Figure 2);
- baseline design for multiple input sensors, multiple flight processors, and a redundant CSLIC;
- extensive simulation testing, ground vehicle testing, and aircraft testing;
- environmental testing and preparation of the AFSS chassis to fly on the Terrier Mark 70-Improved Orion sounding rocket; and
- successful testing of the following mission rule algorithms: Parameter Threshold Violation, Physical-Boundary Violation, and Two-Point Gate rules.

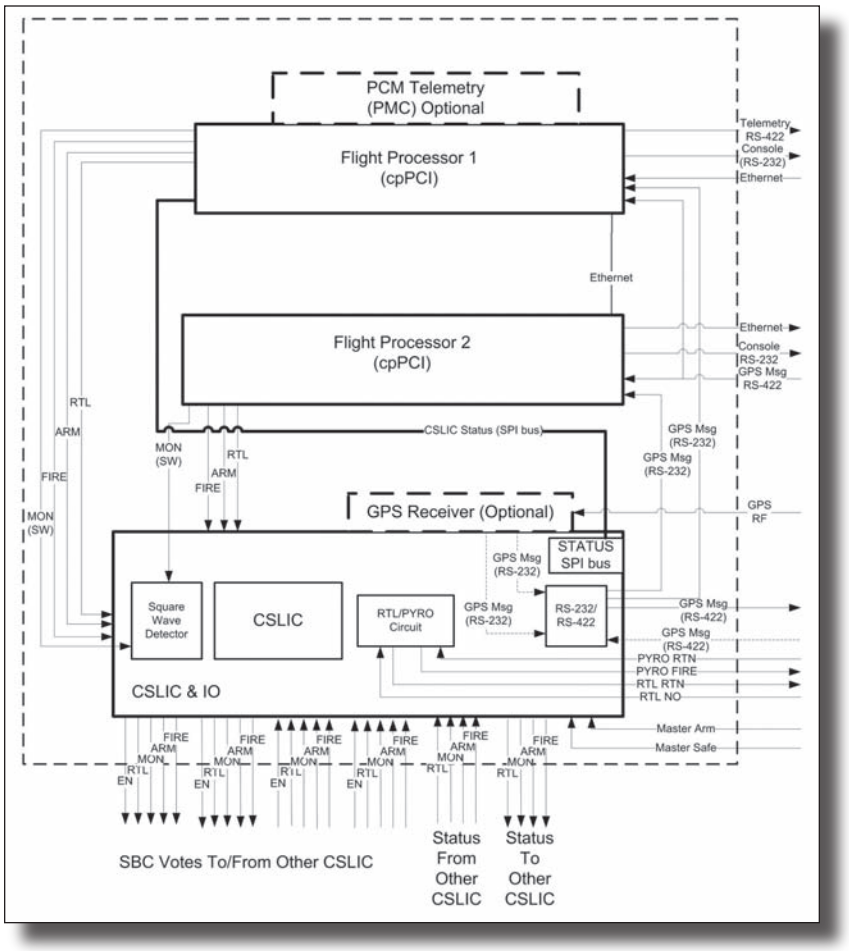

Figure 1. AFSS unit functional diagram.

The first test on a moving vehicle using live data was also conducted. A minivan with a GPS antenna on the roof was driven around the KSC Industrial Area in a corridor that was surveyed prior to testing. The Parameter Threshold Violation rule, Physical-Boundary Violation rule, and Two-Point Gate rule were tested successfully.

An aircraft flight took place in September 2005 on a Cherokee 235 over the St. Johns River, west of KSC, to test instantaneous impact point limits and 3-D static and moving gates. All the tests were successful and the algorithms and hardware performed as expected.

A prototype AFSS unit flew on a Terrier Mark 70-Improved Orion sounding rocket at White Sands Missile Range on April 5, 2006. This was only a test and AFSS was not connected to the flight termination system. The chassis contained two processors running simultaneously but independently. Both processors received inputs from two different GPS receivers. One of the processors was configured so the nominal trajectory would not violate any safety rules. The other processor was configured so the nominal trajectory would generate multiple destruct conditions. The status and tracking data was sent to the ground using the rocket's telemetry system. The system behaved as expected, although one of the GPS receivers provided very little data because of the rocket's high dynamics. The flight hardware was recovered and the data is currently under analysis.

The AFSS team remains in close contact with members of the range community for their input in shaping the final requirements, design, and testing of the AFSS concept. The goal is to have a flight-qualifiable unit by mid 2006 built around a ruggedized, compact PCI processor. More flights are planned as vehicles become available

Key accomplishments:

- 2000: Phase I, Lockheed Martin Space Systems Company Feasibility Demonstration.
- 2002: Phase II, Lockheed Martin Space Systems Company/KSC/WFF Bench Prototype.
- 2003: Phase III, new software development; simulation regression testing of Phase III algorithms against Phase II launch scenarios with various failure modes.
- 2004: Phase III, Preliminary Design Review.
- 2005: Phase III, first moving ground test; first aircraft test; production of two ruggedized flight prototype units.
- 2006: First sounding rocket test.

Key milestones:

- 2006: Additional sounding rocket flight tests and integration of CSLIC.
- 2006/2007: Additional flight and simulation testing.

Contacts: Dr. James C. Simpson <James.C.Simpson@nasa.gov>, NASA KT-C, (321) 867-6937; Chris Forney, NASA KT-C, (321) 867-6672; David P. Kotsifakis, NASA/WFF, (757) 824-1364; and Raymond J. Lanzi, NASA/WFF, (757) 824-2492

Participating Organizations: ASRC Aerospace (Roger D. Zoerner), LJT & Associates, Inc. (Hubert C. Chang), Summer High School Apprentice Research Program (SHARP) (A.K. Cowan), and USAF 30th and 45th Range Safety Offices

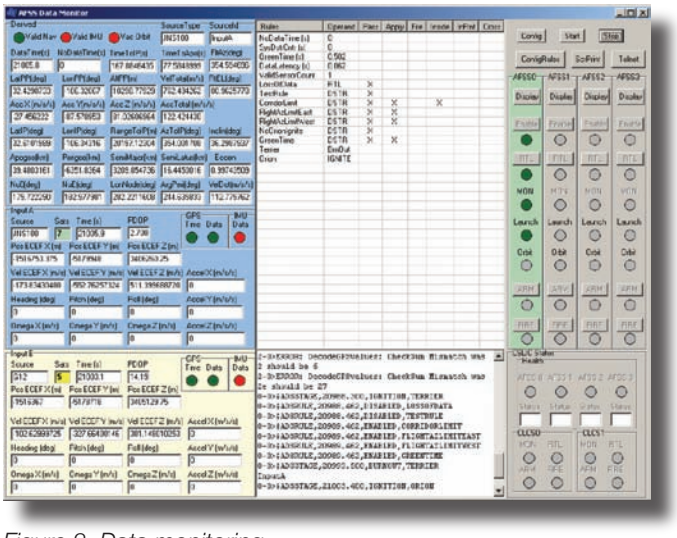

Figure 2. Data monitoring.

Emerging Communication Technology (ECT)

Communications Technology Upgrades

Range technology systems currently rely heavily on expensive networks of unique and costly ground-based legacy communication assets to interconnect tracking, communications, and flight termination functions. Much of this aging infrastructure is interconnected through legacy-installed, nonmovable cables. A future vision of a more flexible spaceport and range is emerging based on modern high-speed first mile/last mile cable-free communication technologies. Such technologies can seamlessly extend existing legacy range infrastructure without wires and cables and hold great promise for preserving the utility of existing range infrastructures while achieving life cycle cost savings and increased operational flexibilities for meeting new range communication needs.

The most promising technologies to date are free-space optics (FSO), Wireless Ethernet (Wi-Fi), and ultra-wideband (UWB). Together, these technologies enable flexible communication at high data rates over the short distances needed for implementing first-mile/last-mile range communication connectivity.

In support of continuing work investigating these key technologies, investigations into methods for mitigating optical scintillation for wide-beam, non-autotracking FSO equipment were continued this year. Likewise, limitations caused by Fresnel Zone degradation that preclude extending operational communication ranges for extended-range Wi-Fi equipment operating in the newly authorized 24-GHz Industrial, Scientific, Medical band were also explored.

These activities were accomplished for FSO-related research through integration of wide-beam FSO equipment procured previously with optical test equipment and atmospheric measuring equipment supplied by Harris Corporation and the University of Central Florida. The resulting researched efforts extended the theoretical accuracies in predicting a priori FSO Bit Error Rate (BER) link performance in the presence of optical scintillation.

Free-space optical testing of scintillation effects on BER at the Shuttle Landing

The unique assets of the KSC Shuttle Landing Facility (SLF) were used for FSO field testing. Fortunately, the SLF is a nearly ideal laser communication test range. Its large expanse of precisely grooved and flat-milled concrete, spanning 15,000 ft by 300 ft, was used to create and validate new optical scintillation theories to permit the prediction of FSO system link performance.

For extended-range Wi-Fi research, a newly released product operating at 24 GHz was identified, procured, tested, and evaluated. Limitations of Fresnel Zone degradation were explored, also using the SLF runway, but as a millimeter wavelength test range instead of as an optical range as for FSO testing.

Together, these emerging communication technology research topics are helping to implement flexible, high-speed extensions to the existing legacy range communications infrastructure. A clearer view of the future is developing—a view that increased communication reliability at lower cost can be achieved relative to the legacy communications technologies historically used on the range.

Plans for FY 2006 are to continue investigations into networking FSO and Wi-Fi systems and to install operational FSO and extended-range Wi-Fi links.

The ultimate goal of introducing operational systems that use new communication technologies to augment future range capabilities while increasing range safety and lowering life cycle costs appears feasible.

Key accomplishments:

- Successfully identified, procured, and tested an extended-range, Wi-Fi, 24-GHz Ethernet wireless link over distances up to 5 km.
- Characterized receiver aperture averaging effects of optical scintillation on BER for FSO systems operating over 1 km.
- Wrote, presented, and published a technical conference paper at SPIE 2005 Optics and Photonics Conference in San Diego, California, on aperture averaging effects on BER for FSO systems.

Key milestones:

- September 2003: Submitted ECT Phase II final report detailing testing results for Wi-Fi, UWB, and narrow-beam autotracking FSO communication equipment.
- September 2004: Submitted ECT Phase III final report detailing testing results for wide-beam, nontracking FSO communication equipment.
- September 2005: Submitted ECT Phase IV final report detailing aperture averaging mitigation of optical scintillation for overcoming limitations on BER common for FSO communication equipment operating in hot climates, such as that found at KSC.

Contact: Richard A. Nelson <Richard.A.Nelson@nasa.gov>, NASA KT-C, (321) 867-3332

Participating Organization: ASRC Aerospace (Dr. Gary L. Bastin, William G. Harris, José A. Marin, and Temel Erdogan)

Radio Frequency Health Node

Integrated System Health Management Technologies

Current instrumentation systems are based on wired communications between the controlling system and the sensors. These systems are vulnerable to safety problems because of the aging of the wires and are costly to augment with additional sensors after production. Spacecraft and aircraft wiring has caused numerous anomalies and failures, including a wiring short 5 seconds after the launch of STS-9, which disrupted the primary computers on two of the three main engines. Also, wiring adds significant weight at approximately 30 pounds (24 AWG wire) per mile (230 miles of wire in every Shuttle, 300 miles in every DC-9 airplane). Therefore, reducing or eliminating wires results in less expensive and more reliable air and space travel.

Advances in technology have provided the means to miniaturize sensors while adding more capability. One major new capability for sensors is to receive commands and send data out through a wireless link. In response to the new capability, NASA KSC, with support from ASRC Aerospace, built and tested the Radio Frequency Health Node (RFHN) prototype to interface with these wireless sensors. The RFHN sends commands and receives data from the sensors wirelessly. The user controls the RFHN through an Ethernet interface, and sensor data collected by the RFHN can be sent out in a pulse code modulation (PCM) format or through the Ethernet interface. One of the main features of the RFHN, in addition to the wireless interface, is its ability to perform such onboard processing sensor data functions as data preprocessing, data fusion, and trending and to pass along the information. The passing of information rather than raw sensor data provides the means to distribute the processing load for instrumentation systems that use Integrated Systems Health Management (ISHM) technologies. Also, the RFHN serves as a centralized node that can support many sensors of different types.

The design of the RFHN is based on a modular architecture that can accommodate interfaces for future wireless sensors with minimal effect. The RFHN was designed to be lightweight, use low power, and withstand the launch environment. The hardware consists of both custom and commercial off-the-shelf (COTS) boards based on the PC 104+ standard. VxWorks is used as the real-time operating system, and the software is written in the C programming language. The system uses the unlicensed Instrumentation Scientific Medical frequency of 916.5 MHz for communications with a baud rate of 50 kbps. The prototype was implemented for flight applications; however, the RFHN could be implemented for ground applications with many of the same advantages.

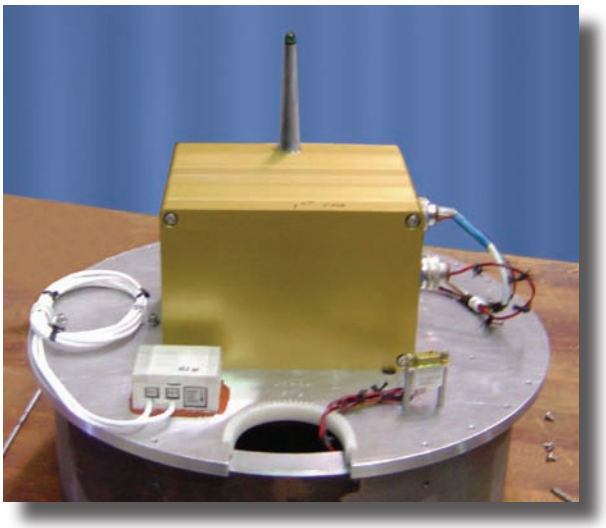

RFHN mounted on the sounding rocket's deck plate.

Advantages of a wireless instrumentation system such as the RFHN include low-cost solutions for after-market instrumentation, rapid response to changing instrumentation needs, and a reduction in the amount of wiring, which is key to spacecraft and aircraft applications. Also, the RFHN can be constituted as a building block within the framework of the ISHM technologies with the potential for many applications. KSC identified ISHM as a crosscutting technology and ranked it third among 28 high-priority needs.

On September 23, 2004, the RFHN was successfully launched on a suborbital flight test onboard a sounding rocket from the White Sands Missile Range. The flight was managed by Wallops Flight Facility (WFF) using the NASA Sounding Rocket Operations Contract (NSROC) with support from U.S. Army, Navy, and NASA KSC personnel. This flight of opportunity evaluated the reliability of the wireless link and demonstrated that a wireless system is viable for future instrumentation systems. The COTS sensors from Invocon, Inc., wirelessly transmitted thousands of packets of data to the RFHN during flight. The postflight data analysis showed the reliability of the wireless link during flight was equal to, and in some instances better than, the reliability experienced during integration and preflight testing. No packets were lost and the success criteria were met; however, the system's deterministic response needs more work before the technology can be used operationally. Consequently, the next step is to develop the interface for the RFHN for the next generation of wireless sensors (SensorNet) to support instrumentation systems with real-time, deterministic requirements.

Key accomplishments:

- Built and tested RFHN.
- Flight-tested RFHN onboard a sounding rocket (September 2004).

Key milestone:

- Develop next-generation SensorNet wireless interface for the RFHN.

Contacts: Emilio Valencia <J.Emilio.Valencia@nasa.gov>, NASA KT-C, (321) 861-9074; and Paul J. Mackey <Paul.J.Mackey@nasa.gov>, NASA DX-E3, (321) 867-6682

Participating Organizations: NASA DX-E3 (Priscilla C. Stanley), NASA DX-E4 (Robert L. Morrison and Hong My Le), NASA DX-E2 (Jeffery S. Vickers), and ASRC Aerospace (Anthony J. Eckhoff, Norman N. Blalock, Drew P. Schmidt, and Theresa G. Overcash)

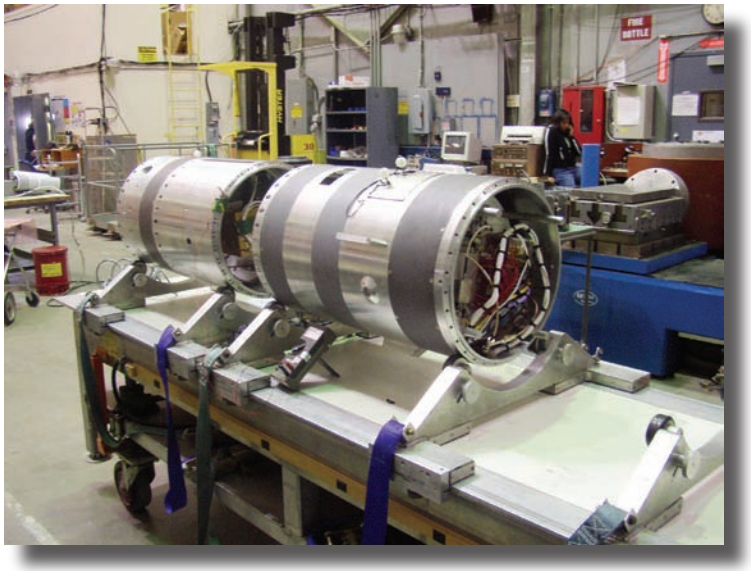

RFHN mounted on inside the sounding rocket's payload section.

Sounding rocket mounted on the rail.

High-Fidelity Aerothermal and Material-Response Analyses for Application to Engineering-Level Debris Survivability Tools

Risk Assessment Tool

This project seeks to determine whether computational fluid dynamics (CFD) and high-fidelity material-response modeling can reasonably improve the accuracy of existing engineering-level debris survivability tools. As more objects go into space, the potential for significant injury or damage resulting from reentering debris falling onto populated areas increases. Because some of these debris objects might contain radioactive material, recovering them rapidly is essential. Thus, the ability to accurately predict whether a debris object will survive atmospheric reentry and, if so, where and with how much energy it will strike Earth is very desirable. These predictions must also be rapid since initial conditions for an uncontrolled or unplanned reentry are not known a priori. This calls for an engineering-level analysis tool (i.e., based on empirical correlations and approximations) rather than a more time-consuming, high-fidelity approach, such as CFD. However, the latter can be employed to greatly improve the accuracy of the correlations and approximations in the former.

The four primary debris survivability codes currently in use are the Object Reentry Survival Analysis Tool (ORSAT) developed by NASA-Johnson Space Center, Aerospace Corporation's Atmospheric Heating and Breakup (AHaB) code, the ANSP-3DOF program used by the Aerospace Nuclear Safety Program, and the European Space Agency's Spacecraft Atmospheric Reentry Aerothermal Breakup (SCARAB) code. To predict surface heat flux, all four codes employ a blunt-body stagnation point, convective heat-flux relation, such as that by Fay and Riddell [1].

NASA Ames Research Center (ARC) specializes in the design of thermal protection systems for atmospheric entry vehicles through the application and coupling of trajectory, CFD, and material-response analyses, supported by experiments. ARC has used these tools to develop high-fidelity aerothermodynamic databases [2,3] and aerodynamics models [4] to enhance engineering-level trajectory predictions. It is plausible that the same can be done for reentry debris survivability tools. To help assess the value of such an effort, two CFD-based sample debris simulations were conducted and the results compared to those obtained with at least one of the four debris codes.

The first simulation, the atmospheric entry of a hollow aluminum sphere, was calculated previously with AHaB; key parameters are given in the table. The simulation started with a Mach number (M) of 22.4 and ended at t = 184.0 s, with M = 5, when the heat flux had fallen near zero. The final, uniform wall thickness was 0.0202 m, a 25.7-percent reduction.

Key parameters for AHaB debris simulation.

Aluminum (2024-T8) Sphere Atmospheric Entry		
Body Parameters	Radius	0.6096 m
	Wall Thickness	0.02718 m
	Mass	340.19 kg
	Ballistic Coefficient	316.74 kg/m^2
Initial Conditions	Relative Speed	6400 m/s
	Relative Flight Path Angle	–0.5 deg
	Altitude	77.784 km
	Wall Temperature	856 K

A trajectory for the aluminum sphere is generated with the ARC 3-DOF trajectory code Traj, using the same parameters used in AHaB. Figure 1 shows the relative-velocity history predicted by the two codes. In Figure 2, the average convective heat flux is plotted versus time. The AHaB heat flux is calculated using the formulation of Detra, Kemp, and

Riddell [5]. In Traj, two separate but similar heat-flux relationships can be used, one by Fay and Riddell [1] and the other by Tauber [6] (Figure 2).

The ARC codes Data Parallel Line Relaxation (DPLR) (for compressible, real-gas CFD) and Fully Implicit Ablation and Thermal (FIAT) response (for material response [including ablation]) are used to predict the aeroheating environments and the surface recession and mass loss, based on the Traj trajectory, for the aluminum sphere and one other sample debris case. The predicted mass loss iscompared with AHaB, for the sphere, and the corresponding engineering-level tool for the second case.

Key accomplishment:

- Obtained sample debris AHaB trajectory for aluminum sphere from the Aerospace Corp.

Key milestones:

- Completed literature survey to determine the state of the art in debris survivability predictions.
- Designed the first sample debris simulation.
- Calculated trajectory and began CFD analysis for the first sample debris case: an aluminum sphere.

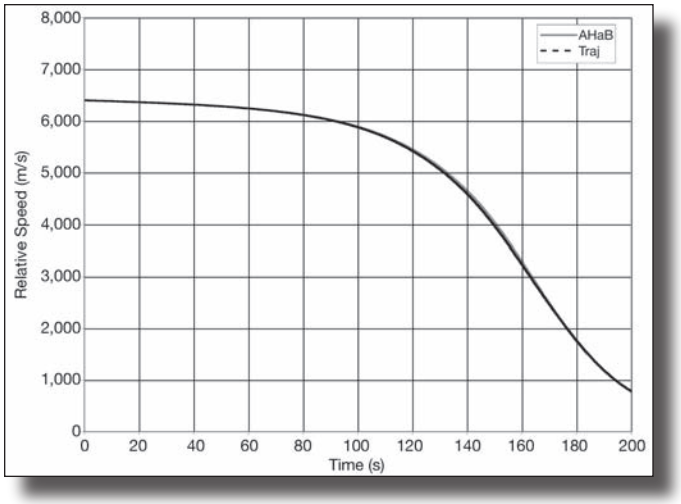

Figure 1. Relative speed versus time for AHaB and Traj.

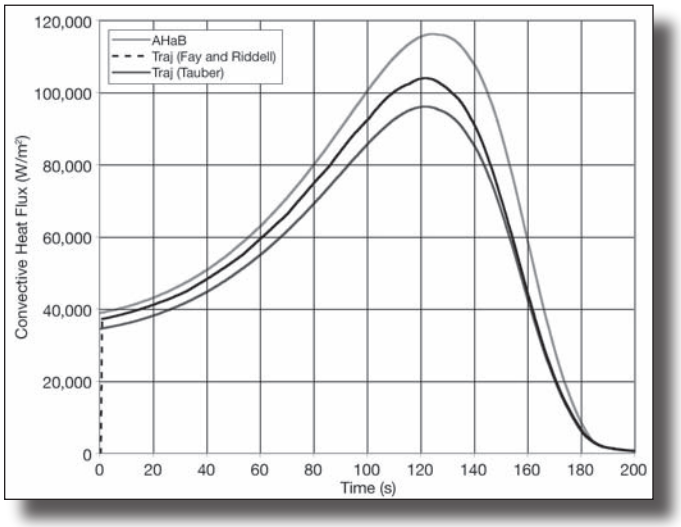

Figure 2. Heat flux versus time for AHaB and Traj.

References

[1] J.A. Fay and F.R. Riddell, "Theory of Stagnation Point Heat Transfer in Dissociated Air," *Journal of the Aeronatutical Sciences,* Vol. 24, No. 2, February 1958, pp. 73–85, 121.
[2] D. Prabhu et al., "X-33 Aerothermal Environment Simulations and Aerothermodynamic Design," AIAA Paper No. 98-0868, January, 1998.
[3] J. Bowles et al., "Development of an Aerothermodynamic Environments Database for the Integrated Design of the X-33 Prototype Flight Test Vehicle," AIAA Paper No. 98-0870, January 1998.
[4] S. Murman, M. Aftosmis, and S. Rogers, "Characterization of Space Shuttle Ascent Debris Aerodynamics Using CFD Methods," AIAA Paper No. 05-1223, January 2005.
[5] R.W. Detra, N.H. Kemp, and F.R. Riddell, "Addendum to 'Heat Transfer to Satellite Vehicles Re-entering the Atmosphere'," *Jet Propulsion,* Vol. 27, December 1957, pp. 1256–1257.
[6] M.E. Tauber, "A Review of High-Speed Convective Heat Transfer Computation Methods," NASA TP 2914, July 1989.

Contacts: George F. Haddad <George.F.Haddad@nasa.gov>, NASA VA-F4, (321) 861-7387; and Jeff Brown <jbrown3@mail.arc.nasa.gov>, NASA ARC 230-2, (650) 604-6192

Participating Organization: NASA ARC (Nagi Mansour)

Fluid System Technologies

Fluid System Technologies help reduce the cost of access to space and increase safety by reducing the human oversight of servicing, reducing the waste streams, and reducing the number of hazardous operations and vehicle interfaces. Fluid System Technologies will support developing a better understanding of the fluid environment in all areas of spaceport activity through analysis and simulation. In addition, Fluid System Technologies will seek to develop the means to reduce thermal losses associated with cryogenic fuels, minimize maintenance and process monitoring costs, and provide for safe operation of the spaceport. A major goal of this technology product line is to create efficient technologies that can be quickly adapted to the changing fluid needs of future space vehicle elements and systems residing at the spaceport. The focus areas that drive Fluid System Technologies development are

- storage, distribution, and servicing systems,
- production, recovery, and disposal management systems,
- vehicle interface systems,
- fluid safety systems, and
- Expendable Launch Vehicle/Reuseable Launch Vehicle thermal/fluids environments and management.

For more information regarding Fluid System Technologies, please contact Robert G. Johnson <Robert.G.Johnson@nasa.gov>, NASA KT-E, (321) 867-7373.

Parameter Estimation of Spacecraft Fuel Slosh

Spacecraft Nutation Models

Liquid slosh in the fuel tanks of an attached spacecraft has been a long-standing concern for space missions with a spinning upper stage. The resulting loss of rotational kinetic energy affects the gyroscopic stability of the combined spacecraft and upper stage and causes an ever-increasing wobble or nutation, which can grow to cause severe control problems. The nutation angle—the angular displacement between the spacecraft's principal axis of rotation and its angular momentum vector—is a measurement of the magnitude of nutation. Nutation Time Constant (NTC) is defined as the time it takes the nutation angle to increase by a factor of e and is a key parameter in assessing the stability of the spinning spacecraft during the upper-stage burn. The NTC can sometimes be very difficult to calculate accurately during the early stages of spacecraft design.

The current research is directed toward modeling fuel slosh on spinning spacecraft, using simple one-degree-of-freedom (1-DOF) pendulum analogs that model a spherical tank, as in Figure 1. An electric motor induces the motion of the pendulum to simulate free-surface slosh. Parameters describing the simple pendulum models characterize the modal frequency of the free-surface sloshing motion. The 1-DOF model helps explain fuel sloshing and serves as a stepping stone for more complex future simulations to predict the NTC accurately with less time and effort. Various simulation parameters are estimated by matching the pendulum/rotor model response to the experimental response of full-sized test tanks in NASA's Spinning Slosh Test Rig (SSTR). The SSTR can subject a test tank to a realistic nutation motion, in which the spin rate and the nutation frequency can be varied independently. The spin rate is chosen to create enough centrifugal acceleration to simulate a zero-gravity configuration of the bladder and liquid in the tank. The propellant motion is simulated using models with various parameters (inertia, springs, dampers, etc.), and the problem reduces to parameter estimation to match the experimental results obtained from the SSTR. The data from the tests is used to derive model parameters that are then used in the slosh blocks of a MATLAB/SimMechanics-based spacecraft and upper-stage simulation.

The current research is an effort to automate the laborious, trail-and-error process of slosh model parameter identification, using a MATLAB/SimMechanics-based computer simulation of the experimental SSTR setup of two different parameter estimation and optimization approaches. The first approach uses Newton's method for nonlinear least squares, or the MATLAB LSQNONLIN algorithm. The second is a "black box" approach using MATLAB's Parameter Estimatation Toolbox. To evaluate each approach, a simple 1-DOF pendulum experiment was constructed and motion was induced by an electric motor. By applying each estimation approach to a simple system with known characteristics, its effectiveness and accuracy can be evaluated. The same experimental setup can then be used with fluid-filled tanks to further evaluate the effectiveness of the process. This parameter estimation procedure is illustrated in Figure 2.

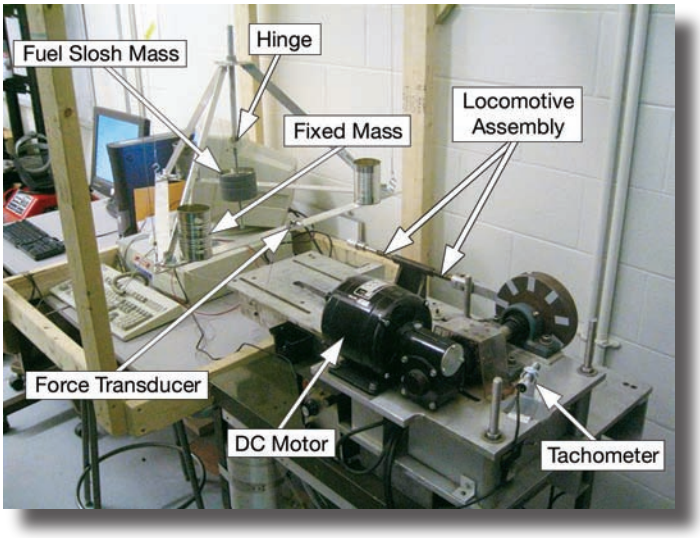

Figure 1. One-DOF pendulum experiment.

Ultimately, the proven process can be applied to the full-sized SSTR setup to quickly and accurately determine the slosh model parameters for a particular spacecraft mission. A spherical tank undergoing free-surface slosh is the simplified model for determining the pendulum parameters. Free-surface slosh has a well-defined resonant frequency. The only sloshing motion assumed to be taking place in this simplified model is a surface wave that is simulated by the pendulum. The rest of the liquid is essentially at rest and can be treated as a fixed mass.

The experiment and the simulation are being calibrated using fixed masses. This is to verify that the model is accurately representing the experiment's way of oscillating the pendulum frame using a flywheel and locomotive arm. Examples comparing the simulation and experimental data are shown in Figures 3 and 4. The main problem in comparing the two data sets is the noise in the experimental data. Currently, several methods of filtering the data are being considered so that it closely matches the simulation data. As a proof of concept, the experimental calibration data was used in the nonlinear least squares algorithm to achieve a simulation response matching very closely with the experimental response.

Key accomplishments:

- Built a 1-DOF pendulum experiment to provide accurate and reliable data sets for use in the parameter identification process.
- Illustrated the parameter identification concept.
- Validated least-squares approach to match the simulation data to the experimental data.

Key milestones:

- Validate the Parameter Estimation Toolbox parameter identification method.
- Gather pendulum experimental data.
- Build a tank experiment to verify the pendulum analog's accuracy.
- Incorporate parameter identification method into SSTR MATLAB simulation.

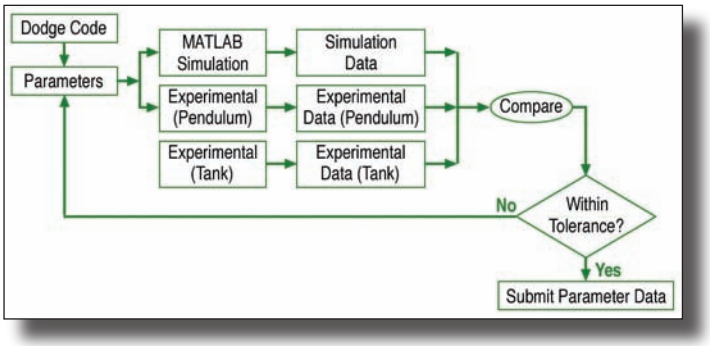

Figure 2. Parameter identification process.

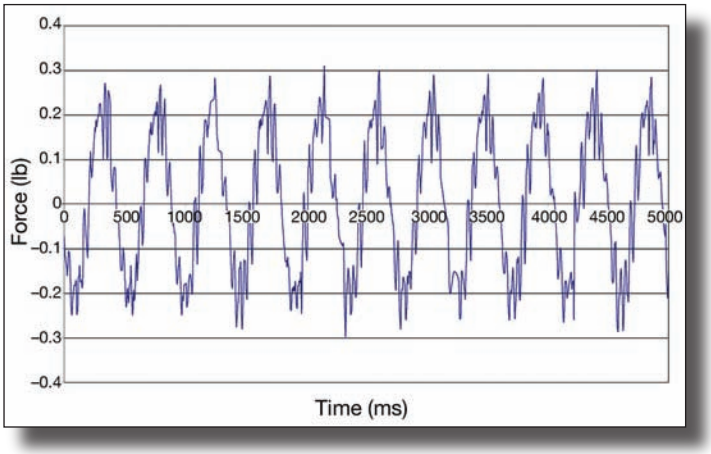

Figure 3. Example of experimental nonsloshing data for 8-in sphere at 2.0 Hz at 80-percent fill level; mass = 6.54 lb; length = 0.155 in.

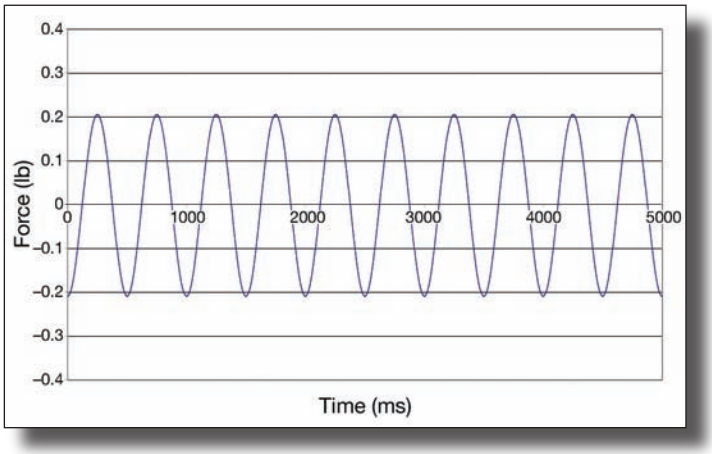

Figure 4. Example of simulation nonsloshing data for 8-in sphere at 2.0 Hz at 80-percent fill level; mass = 6.54 lb; length = 0.155 in.

Contact: James E. Sudermann <James.E.Sudermann @nasa.gov>, NASA VA-F3, (321) 867-8447

Participating Organizations: Embry-Riddle Aeronautical University (Dr. Sathya Gangadharan, Keith Schlee, and James Ristow), Hubert Astronautics, Inc. (Dr. Carl Hubert), and The Mathworks, Inc. (Dr. Bora Eryilmaz)

Evaluation of 3-D Thermal Boundary Layer Correction Factors for Circular Heat Flux Gauges Mounted in a Flat Plate With Surface Temperature Discontinuity

Flight Environment Measurement

Cylindrical flush-mounted Schmidt-Boelter-type heat flux gauges are frequently installed on launch vehicles for measuring convective heat flux during ascent. When flush-mounted in ablators or insulators of relatively low thermal conductivity that form the vehicle surface, these gauges (normally metallic, such as aluminum, stainless steel, or copper) are subjected to wall temperatures several hundred degrees lower than that of the surrounding vehicle skin material. Consequently, the measured heat flux is in error by factors as great as 2 to 4. Correction factors have been proposed in the past to account for the difference of the measured heat flux from the true heat flux. A major deficiency of these integral solutions is connected with the assumption of constant thermal properties, which can lead to significant errors when the difference between the plate and gauge surface temperatures becomes large, such as occurs at high Mach numbers encountered in flight conditions.

The principal objective of this task is to carry out a 3-D Navier-Stokes simulation of the thermal boundary for the plate-gauge system subjected to a stepwise surface temperature discontinuity. Comparisons of the 3-D analysis with 2-D computational fluid dynamics (CFD) results and integral solutions have been performed. The effect of the property variations and three-dimensionality of the thermal boundary layer on the convective heat flux corrections for the gauges has been investigated.

The flow solution (for density, velocity, and temperature distribution) was obtained by the OVERFLOW Navier-Stokes CFD code. A zonal two-equation $k-\omega$ Shear Stress Transport (SST) turbulence model was considered, where k and ω, respectively, represent the turbulent kinetic energy and rate of dissipation of turbulent kinetic energy. Results were obtained for a freestream Mach number of 4, and a freestream Reynolds number of 1 million. The ratio of the gauge radius (R) to the length (L) from the plate leading edge to the gauge is taken as $R/L = 0.01$. The gauge surface temperature T_{w2} is held at 600 °R, while the flat-plate temperature T_{w1} is varied from 600 to 3,000 °R. The freestream temperature T_{∞} is taken as 519 °R. At these freestream conditions, the adiabatic wall temperature (or the recovery temperature) T_{aw} becomes about 2,000 °R.

Figure 1 highlights the dimensionless heat transfer coefficient (Stanton number) distribution on the gauge surface. The extent of the three-dimensionality of the thermal boundary layer is evident near the leading edge and the trailing edge of the gauge.

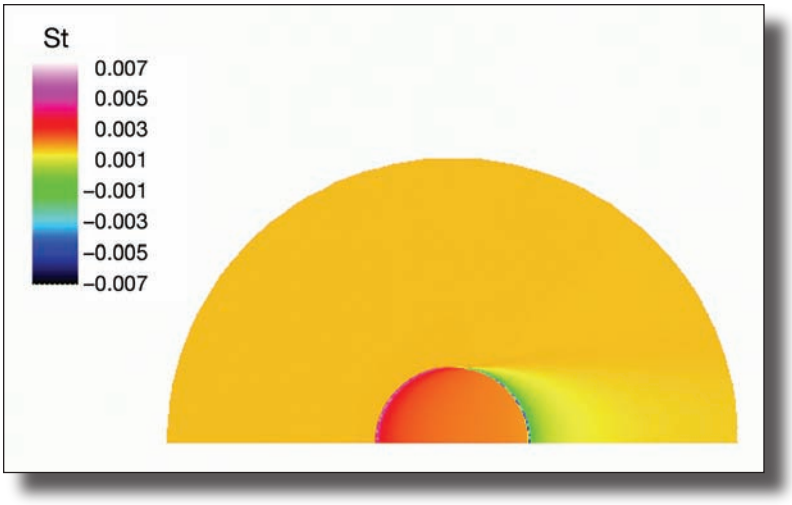

Figure 1. Stanton number distribution on the gauge surface.

The variation of the heat flux correction factor q_2 / q_1 with the flat-plate temperature is presented in Figure 2. Here q_1 stands for the true heat flux, and q_2 stands for the heat flux measured by the gauge. The results reveal that the deviation between 2-D and 3-D CFD increases as the plate wall temperature increases, indicating the importance of the 3-D thermal boundary layer. At the highest wall temperature, the heat flux

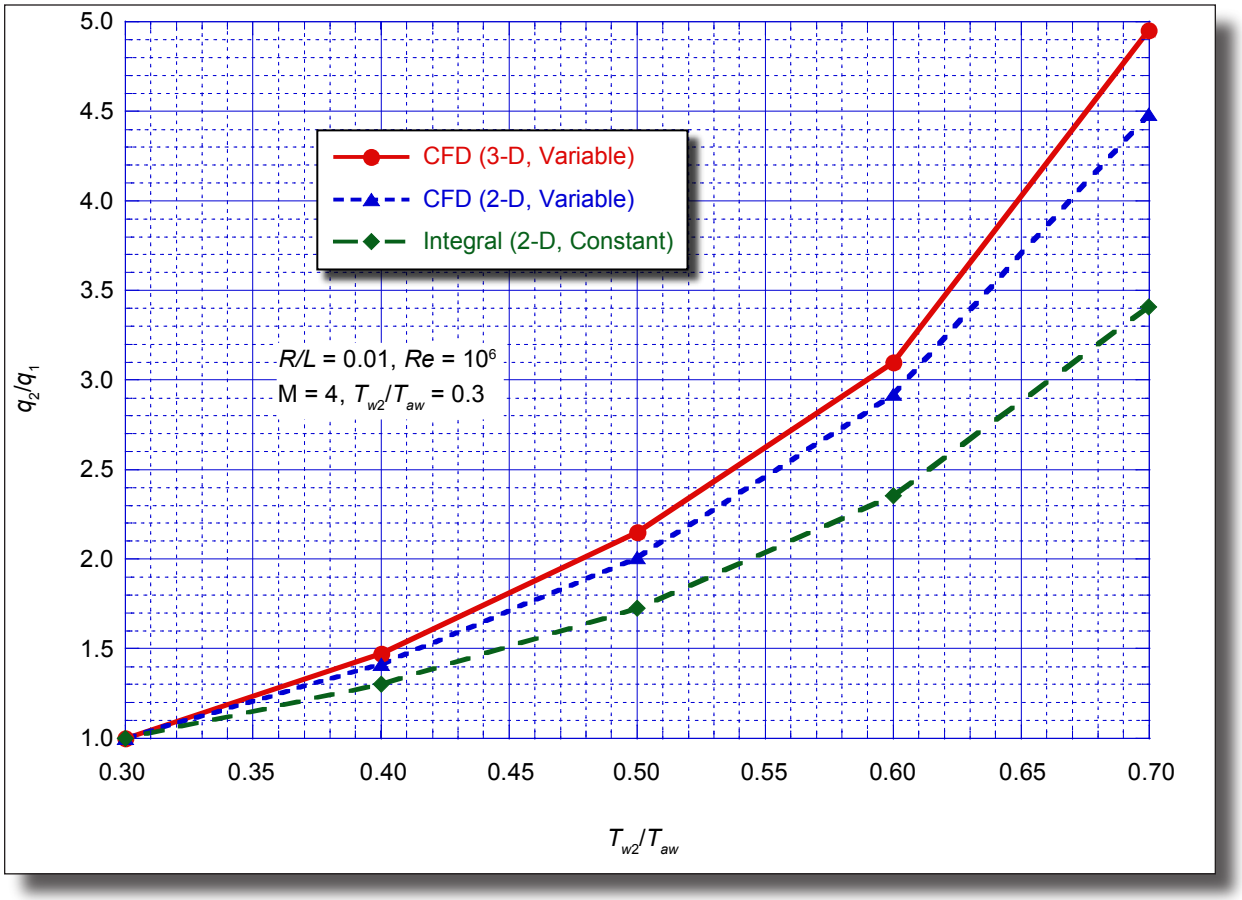

Figure 2. Comparison of heat flux correction factor at Mach 4.

correction factors of various predictions range from 3.5 to 5.0, while the difference caused by three-dimensionality is about 30 percent of that attributable to property variation.

Future plans include comparison of the 3-D correction factors with available experimental data so that CFD predictions can be validated.

Key accomplishments:

- Obtained 3-D baseline CFD solution for the heat flux correction.
- Investigated the effects of property variation and parametric effects.

Key milestones:

- March 2005: Completed 3-D grid system.
- May 2005: Completed baseline CFD solution.
- July 2005: Completed parametric study.

Contact: George F. Haddad <George.F.Haddad@nasa.gov>, NASA VA-F4, (321) 861-7387

Participating Organization: Sierra Lobo, Inc. (Dr. Max Kandula)

Assessing the Mechanics of Granular Materials Undergoing Narrow-Cavity Shear in Gravity

Propellant Loading/ Servicing/Storage

Currently, the liquid-hydrogen and liquid-oxygen tanks at the Space Shuttle launch pads are insulated with perlite, a powder made from crushed volcanic rock. This material occupies the relatively narrow space between the inner and outer spherical shells of the tanks. One problem with perlite is that over time as the tank undergoes repeated thermal cycles, the expansion and contraction of the inner tank compacts the perlite very densely so that it becomes a poor insulator.

It is difficult to analyze the mechanical behavior of a granular material in such a situation. Janssen's law predicts that the overlying weight of granular material contained between narrow walls is not proportional to the amount of overlying material because microscopic granular arches form between the walls and partially support the load. However, because the material is biaxially sheared inside the tank, not driven as a plug flow as Janssen's law presumes, there was no way to predict the actual stress state at various locations in the tank prior to this work. The traditional methods of analysis were insufficient because (1) the physics of granular materials has never been solved and so the behavior of these materials cannot be predicted adequately using traditional finite-element modeling (FEM), (2) there are too many particles in such a large tank to simulate their behavior individually using discrete-element modeling (DEM), and (3) the behavior of the material in a small-scale experiment will not be the same as in the large-scale tank because of the unpredictable competition of shearing versus Janssen's effect.

Liquid-oxygen tank.

To solve this problem, a team of researchers at KSC invented a new paradigm called the "compressing slot" to analyze the mechanical properties of granular materials in such difficult, large-scale situations. This work was applied to perlite replacement powders, but it can be applied to any other type of granular material as well. Through the combination of mechanical theory, computer modeling (both FEM and DEM), and small-scale experiments, the compressing slot assesses the properties of granular materials as they undergo shear inside a narrow space under the effects of gravity. One wall of the slot compresses the material, forcing it to slide upward against gravity while the stresses are measured along the side walls and floor. As the material slides, the upside-down version of Janssen's effect causes an exponential growth of stress toward the bottom of the slot, while the formation of shear bands simultaneously breaks up Janssen's effect just as it would during the thermal cycling of a cryogenic tank. Wherever Janssen's scaling is sufficiently reduced, the material slides frictionally as in a direct-shear test. Wherever Janssen's scaling becomes too severe, the material cannot slide and simply compresses in bulk. This method is more appropriate than triaxial testing, direct-shear testing, or other traditional tests of granular materials because it combines the competing aspects of the physics into a realistic test. The mechanical response is scalable from the small-scale experiments because it directly calibrates the material parameters for a large-scale computer simulation using traditional

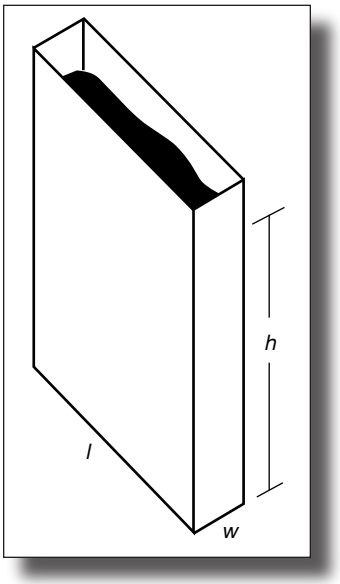

Schematic showing the geometry of the slot experiment.

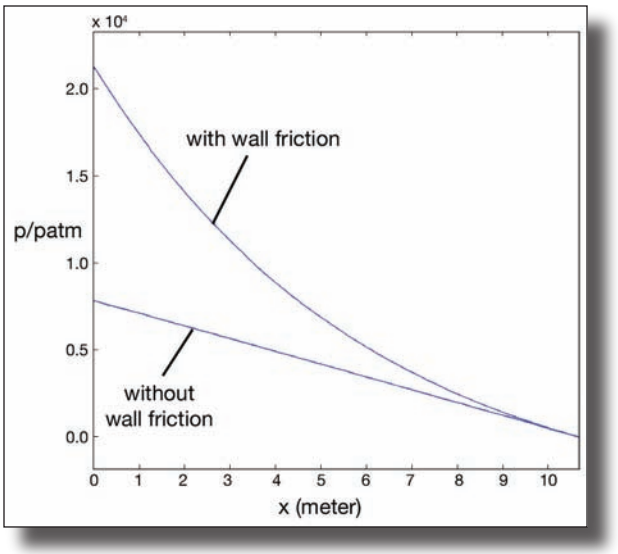

Results for the compressing slot.

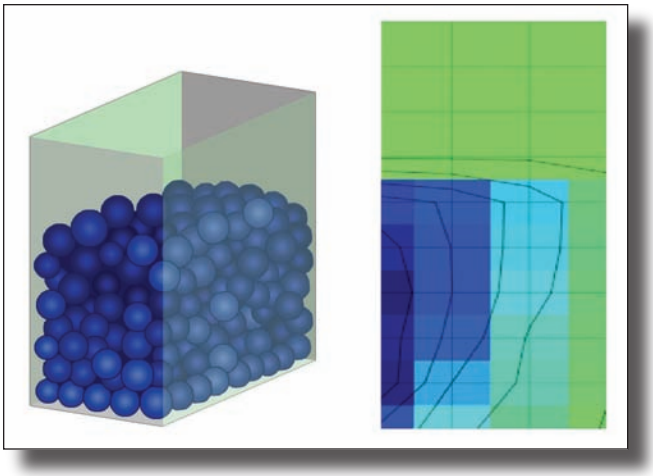

DEM of the sliding slot under compression and the velocity contours.

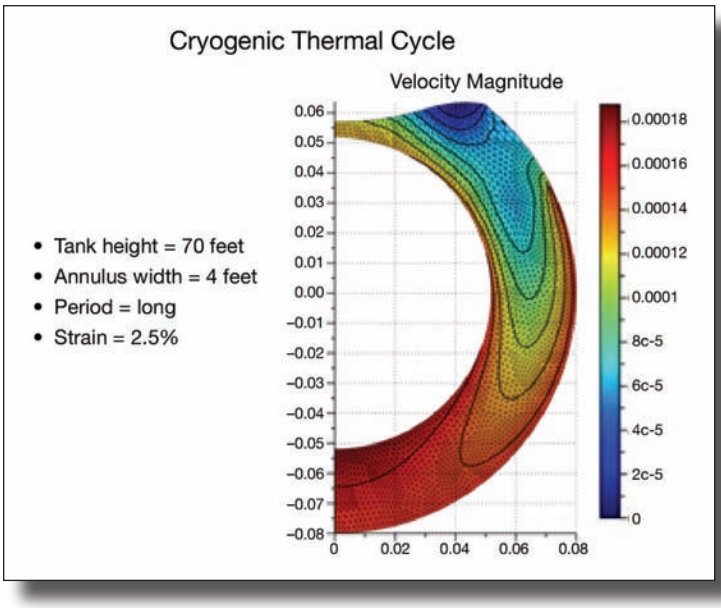

Cross section of annular space in a cryogenic tank during a thermal cycle. Color indicates shearing velocity of the insulation material.

continuum codes. The analytical, computational, and experimental tools developed through this work will allow investigators to perform simple laboratory tests that will inform practical design decisions for large-scale applications.

Contacts: Dr. Philip T. Metzger <Philip.T.Metzger@nasa.gov>, NASA KT-D1, (321) 867-6052; and James E. Fesmire <James.E.Fesmire@nasa.gov>, NASA KT-E, (321) 867-7557

Participating Organizations: Clarkson University (Dr. Brian T. Helenbrook, Dr. Hayley H. Shen, Paul Ashman, and Mike Powers), Sierra Lobo, Inc. (Douglas A. Rewinkel and Stephen J. Sojourner), and ASRC Aerospace (Ivan I. Townsend)

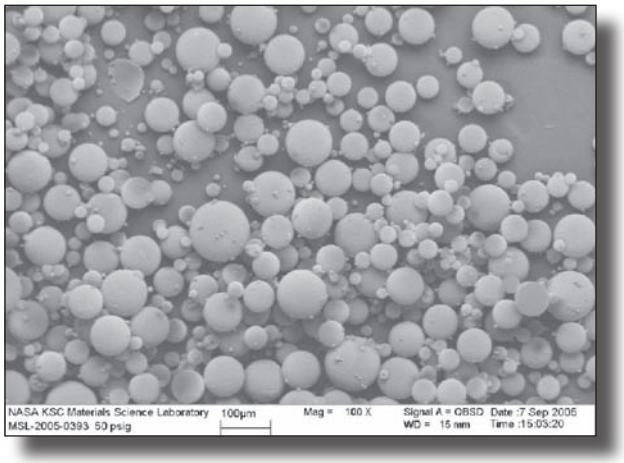

Picture of possible perlite replacement (granular insulation material) magnified 100 times.

Highly Reliable Liquid-Oxygen Pump

Propellant Loading/ Servicing/Storage

Barber-Nichols, Inc., (BNI) has developed a new liquid-oxygen (LOX) pump with Small Business Innovative Research (SBIR) funding. The pump is intended for propellant transfer applications for Space Shuttle, other launch vehicles, and propulsion system test stands. This new pump's innovative sealing method uses a noncontacting dynamic seal in combination with a purged labyrinth seal. This highly reliable sealing arrangement will replace the typical bellows-type face seal, which is prone to cracking, fatigue, and premature wear caused by freezing damage and misalignment of the mating rings.

Phase I focused on reliability problems surrounding the primary sealing arrangement in the LOX pumps and demonstrated the feasibility of a noncontacting combination of a dynamic seal and a purged labyrinth seal set as the primary seal in LOX transfer pumps. This arrangement eliminates the present configuration wherein the face seal is a wearing component. In addition, Phase I efforts proposed a new LOX pumping system for vehicle loading operations, where two pumps could operate in parallel (1,800 gpm total), providing an increase in Space Shuttle LOX transfer of up to 50 percent. Each pump satisfies the current Space Shuttle propellant transfer rates. In the event of a mechanical failure, this redundant pump system would minimize launch delays. The pump design also uses a single integrated drive shaft to maximize rotor-dynamic stability and minimize vibration effects in the sealing area for increased reliability.

Thus far during Phase II, BNI has completed detailed design and manufacture and has started testing two prototype pumps. The noncontacting seal design has been refined to address operational concerns. BNI finished fabricating and assembling the complete pump and support stand at its facility in July 2005 and then evaluated the pump and seal performance by means of a closed-loop water test. The pumps and seals performed

Liquid-oxygen pump retracted to maintenance position.

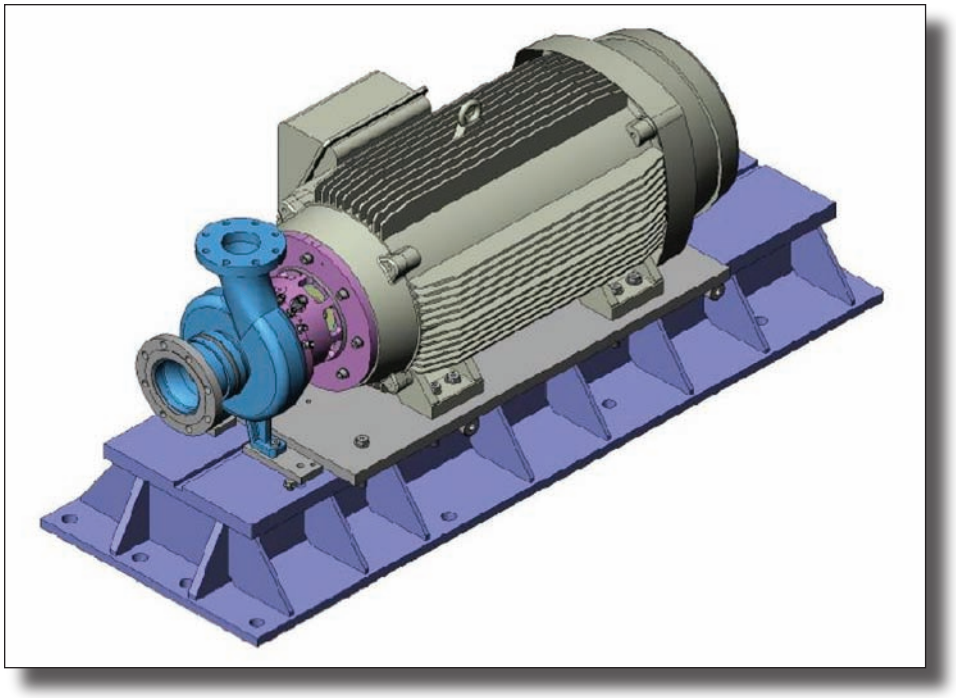

Liquid-oxygen pump solid model (operational position).

as expected: the pumps met the desired head and flow requirements, and the seals were leakproof during operation. Cryogenic testing began in December 2005 at KSC.

The proposed pumping system (incorporating the new seal arrangement) could be applied to retrofit the existing Shuttle LOX loading pumps at KSC. The system was designed to have minimal impact on existing mechanical, piping, and electrical infrastructures used for vehicle loading at launch pads. Furthermore, there are a great number of LOX transfer pumps currently employed by NASA (e.g., Stennis Space Center, White Sands Test Facility) and the Department of Defense that could be replaced by this more reliable pump. With some modifications, NASA could use the pump to transfer liquid hydrogen as well as other propellants.

Technology developed in the Phase II effort can be applied to any low-viscosity, hazardous, fluid pumping application. Potential markets include the chemical and petrochemical industry, where nearly all pumped fluids meet these criteria. This high-capacity pump would offer an attractive alternative to submersible pumps and would be cost-competitive in this growing market. A market that perhaps should be counted in long-term plans is commercial space vehicles. As more private space vehicle firms achieve success, this pump could be marketed to support the ground test and launch facilities of private and commercial space industries. A large market for this pump technology also exists in liquefied natural-gas transfer and ship off-loading, wherein this pump would be more efficient and have a lower life cycle cost. This pump also has potential use for future launch systems in support of the Vision for Space Exploration.

Contact: Donald M. Pittman <Donald.M.Pittman@nasa.gov>, NASA LX-D, (321) 867-6894

Participating Organization: Barber-Nichols, Inc. (Matthew E. Rottmund)

Cryo-Tracker Mass Gauging System Testing in a Launch Vehicle Simulation

Propellant Loading/ Servicing/Storage

Improvements in launch vehicle propellant management for prelaunch operations and flight have been under continuing investigation across the spectrum of launch and space flight vehicles. Existing capabilities would be significantly enhanced by more reliable sensor systems and higher-fidelity data defining the quantities and thermodynamic states of cryogenic propellants. In pursuit of this objective, Sierra Lobo, Inc., has developed the Cryo-Tracker Mass Gauging System.

The heart of the Cryo-Tracker Mass Gauging System is a patented, ultra-lightweight, one-piece, mechanically flexible probe with multiple integral silicon diode sensing elements. The unique features of the Cryo-Tracker probe include dual temperature and liquid-level sensing capability, mechanical flexibility that allows the probe to conform to any tank geometry, ultralow weight, low thermal mass for quick thermal response, and one-piece construction that increases reliability and simplifies handling and installation. In addition to the probe, the system includes an electronics package and software, providing real-time propellant mass calculations and continuous data recording.

The objective of this test series was to demonstrate the ability of the Cryo-Tracker to provide lab-quality thermodynamic and mass-gauging data in a large-scale system made for an Expendable Launch Vehicle (ELV). The test, utilizing liquid nitrogen (LN_2), was designed as a risk reduction precursor to planned liquid-oxygen (LOX) testing in a flightlike Atlas launch vehicle test tank. The LN_2 test series was performed at the Cryogenics Test Laboratory at KSC.

The test rig consisted of an insulated vertical 20.32-cm (8-in) pipe, 9.14 m (30 ft) tall, representing the LOX tank, plumbed to an LN_2 supply dewar, drain line, and gaseous-nitrogen (GN_2) pressurant supply. Test rig instrumentation was designed to promote test rig control and validate the liquid-level measurements taken by the Cryo-Tracker System.

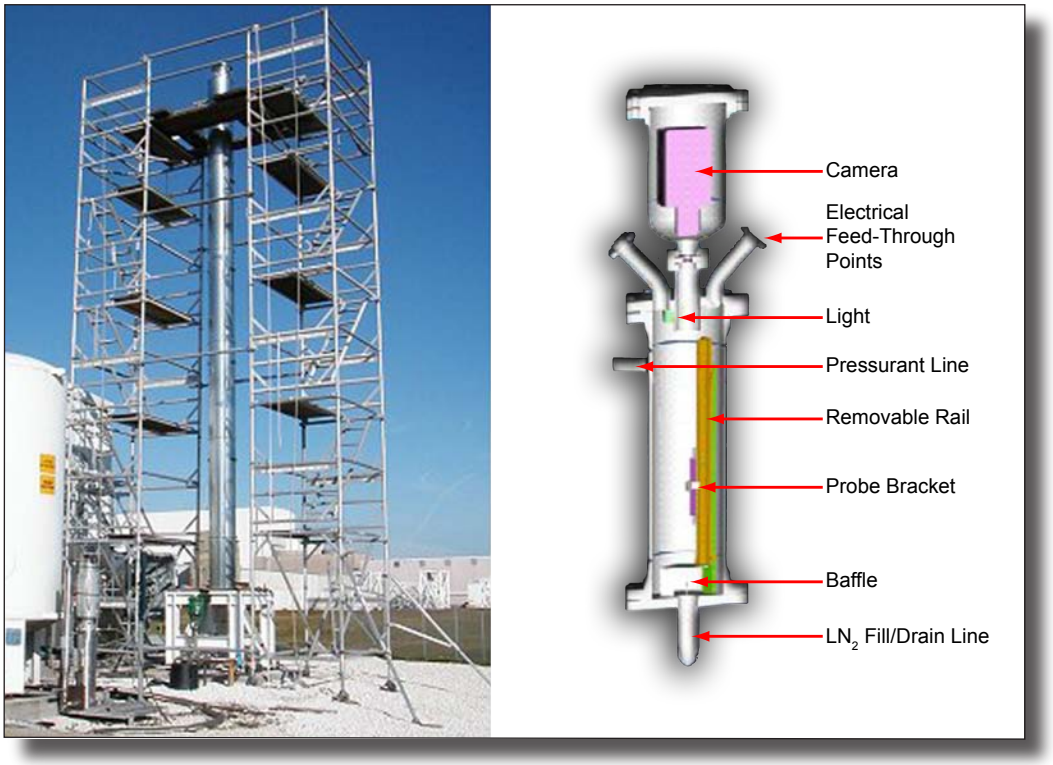

Photograph and solid model of the LN2 test rig at the Cryogenics Test Laboratory at KSC.

The nominal test profile was designed to meet the following operational parameters:

- simulate LOX fill rate (in terms of rate of change of the liquid level),
- stop fill at LOX tank nominal fill level,
- maintain fill level for some significant duration to simulate pad hold time,
- drain at a rate to simulate LOX expulsion during launch (in terms of rate of change of liquid level), and
- stop expulsion when the liquid level is near the bottom of the tank.

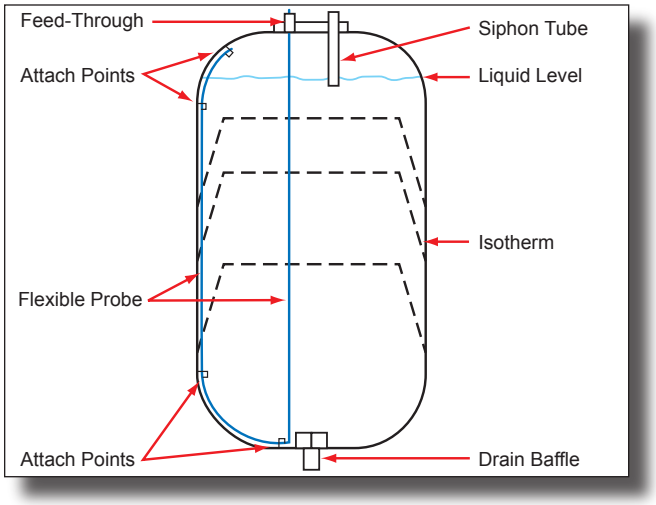

Line drawing of a Cryo-Tracker probe installed in a densified cryogen propellant.

Throughout each test, the Cryo-Tracker Mass Gauging System continuously monitored, recorded, and displayed the liquid level. In addition to determining liquid level, the system calculated and recorded fluid mass, demonstrated the ability to serve as an engine cutoff sensor, and measured and recorded tank temperature profiles simultaneously with the liquid-level and mass-gauging calculations.

The system successfully demonstrated all of its intended functions in the simulated LOX tank environment. A series of prelaunch and launch simulations with the large-scale prototype ELV system was accomplished, providing further confirmation of the mass-gauging system's potential for future use in launch vehicle applications.

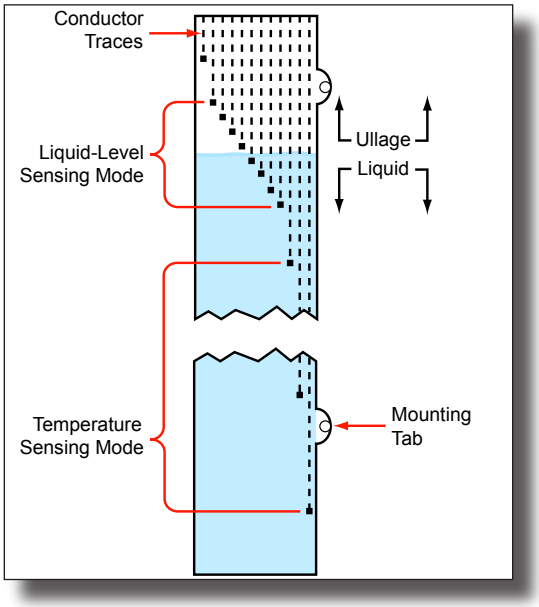

Line drawing of a Cryo-Tracker probe illustrating a customized diode configuration.

Key accomplishments:

- Fabrication of the longest Cryo-Tracker probe to date.
- Installation technique proven with only two attachment points at top and bottom of tank.
- Probe survival in a harsh environment and repeated thermal cycles with no loss of signal or structural integrity.
- Probe's successful measurement of liquid levels and temperatures under all conditions and successful demonstration of its feasibility as an engine cutoff signal.

Key milestones:

- Completion of facility, test hardware, and instrumentation setup in preparation for LOX testing.
- Completion of LOX testing in Lockheed Martin's tank simulation facility.

Contact: Laurie K. Walls <Laurie.K.Walls@nasa.gov>, NASA VA-F3, (321) 867-1968

Participating Organization: Sierra Lobo, Inc. (Daniel J. Schieb)

Ray Trace Math Model and Windows Software Implementation for a Focused Infrared Lamp Projection System

Propellant Loading/ Servicing/Storage

A ray trace math model was developed to predict the intensity of infrared (IR) heat energy that could be projected from a halogen lamp, or cluster of lamps, to heat a target. The target in this particular case is the Space Shuttle External Tank (ET). The mathematical ray trace model developed for this special application can easily be extended to accommodate other optical, as well as acoustic, ray-tracing applications, where the approximation of ideal reflecting surfaces and incoherent waves is appropriate.

When the Shuttle's ET is filled or in the process of being filled with the cryogenic fuel components (liquid oxygen and liquid hydrogen), moisture from the atmosphere forms water ice on the external surface and possibly under the ET's sprayed-on foam insulation (SOFI). This ice formation can lead to several potential problems: (1) integrity of the SOFI can be threatened, leading to the possibility of a foam chunk falling onto critical Shuttle components at high velocity during the first few minutes of launch, (2) falling pellets of ice may become projectiles during launch, and (3) foam chunks with embedded hard ice pellets may become projectiles.

Two solutions to the problem have been considered: blowing hot dry air over the surface to prevent ice formation, and projecting electromagnetic energy (light) to heat the ET surface. This project concerns projecting focused IR light onto the surface using halogen lamps and focusing reflectors. In this case, the light hardware must be located far from the launch pad (435 ft). A big challenge is to select design parameters that will lead to an efficient projection system where a large percentage of the lamp wattage is projected to the ET surface area of interest.

Parabolic projector proof of concept.

Many software packages are available for ray tracing (ray tracing is a technique that has been practiced for centuries). However, only in recent years has the numerical computing power of PCs made it possible to combine Monte Carlo integration techniques with ray-tracing geometry. Even though commercial off-the-shelf software may be available to solve this problem, it was decided that developing the capability from scratch would provide a better solution and one that could be customized to this specific problem.

The current version of the model and software assumes ideal parabolic surfaces and ideal reflectors. This limitation could be improved with more work. However, for the current application, this limitation is not considered a major disadvantage.

Key accomplishments:

- Developed a generalized ray-tracing math model, incorporating a cylindrical source, a parabolic reflector, and a semispherical forward reflector.
- Implemented the math model in FORTRAN 90.
- Implemented the math model in C, with a graphics output section, using dynamic link libraries compiled from FORTRAN.
- Compared model predictions to measured data.

Contacts: Dr. Robert C. Youngquist <Robert.C.Youngquist@nasa.gov>, NASA KT-D1, (321) 867-1829; and Dr. John E. Lane <John.Lane-1@ksc.nasa.gov>, ASRC Aerospace, ASRC-20, (321) 867-6939

Participating Organization: ASRC Aerospace (Steven J. Klinko)

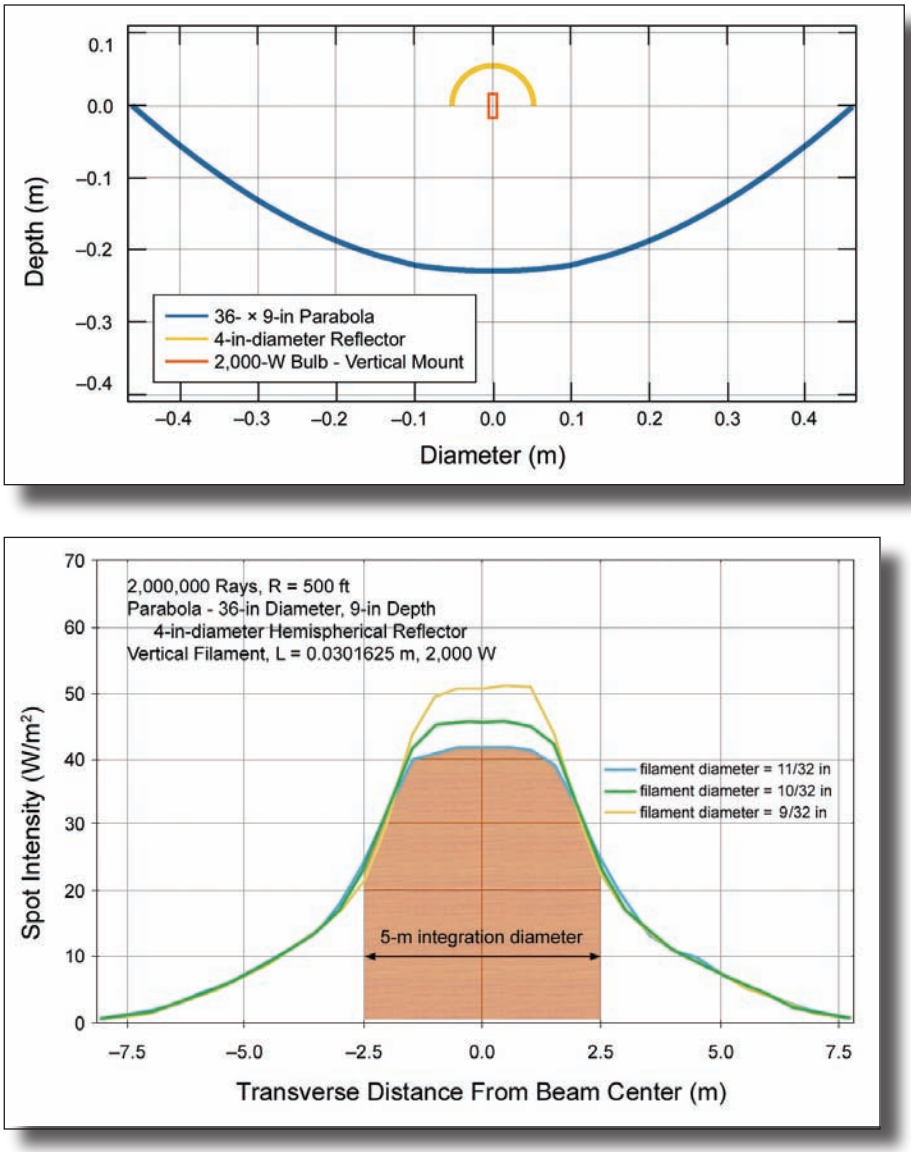

Output of Ray Tracer software for a typical configuration. Top: Beam intensity profile; Bottom: Reflector geometry, including filament, bulb, and front reflector.

Remote Infrared Heating of the External Tank

Propellant Loading/ Servicing/Storage

One of the Space Shuttle Program return-to-flight objectives was to develop ice mitigation techniques that could be performed on launch day to reduce or eliminate ice on the Space External Tank (ET). In response, ASRC Aerospace was asked to design a system employing an array of infrared projection assemblies (IPAs), consisting of halogen light bulbs, parabolas, and bulb reflectors, to heat the surface of the ET. The intent was to raise the surface temperature of a local specific area of the tank as closely as possible to the ambient air temperature to prevent condensation, which may result in frost or ice.

Figure 1 shows a potential location of the skid containing the 12 IPAs. The skid is designed to withstand the launch environment and to minimize potential foreign-object debris (FOD) projectiles that could damage surrounding facilities and ground support equipment.

The IPA (Figure 2) was designed to allow 20 degrees of adjustment in the vertical direction and 360 degrees of adjustment about the horizontal. It was intended to provide the adjustability to point the IPAs at their final target in the field manually. There are self-containment features in the design to minimize the chance of creating FOD. The bulb, parabola, and reflector work together to direct the infrared (IR) radiation onto the designated ET target. The bulb adjustment mechanism controls the focus to achieve uniform light intensity over a specific diameter. The respective alignment of the bulb, reflector, and parabola is critical to determining the amount of IR radiation that can be projected.

The IR projection system can deliver heat by means of light and/or IR radiation to mitigate the formation of condensation on the ET foam at the ET liquid-oxygen feed

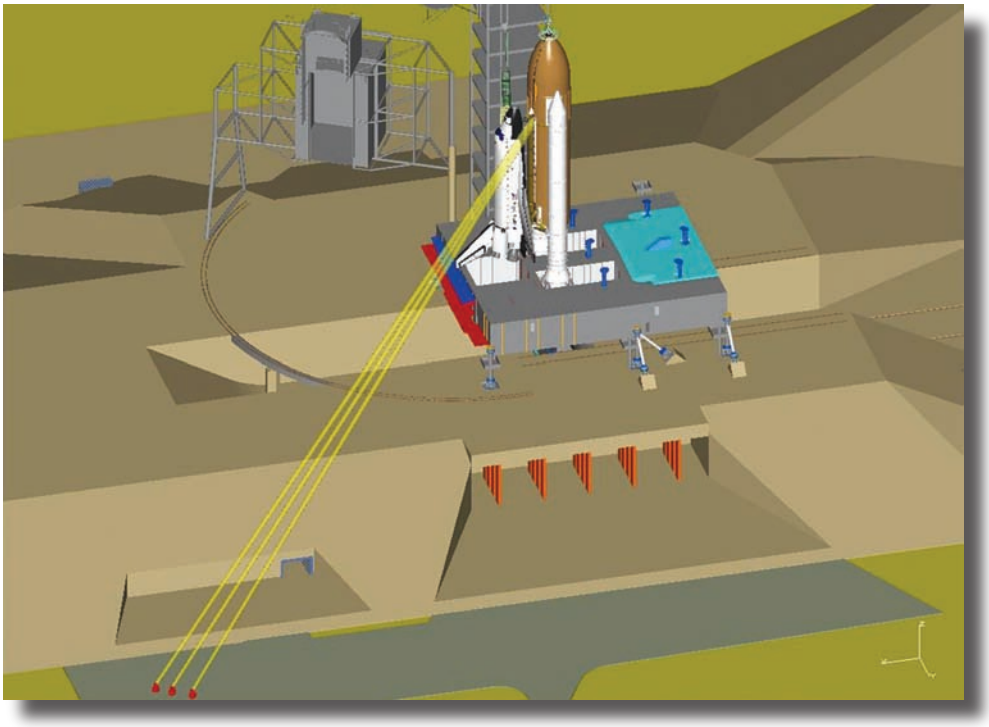

Figure 1. Proposed installation of infrared projector system at Space Shuttle launch pad.

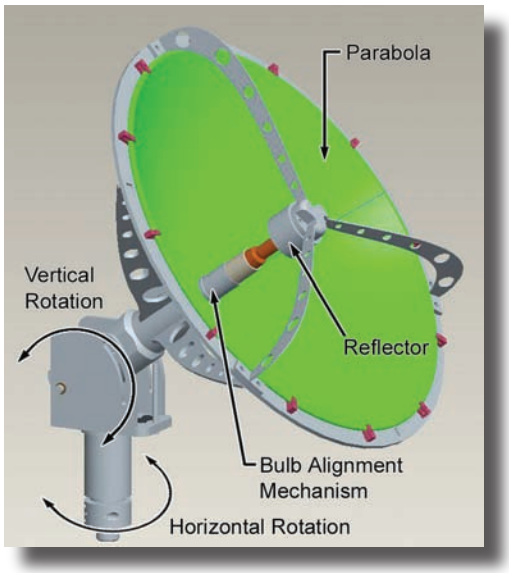

Figure 2. Details of a single projector.

Figure 3. Complete system ready for delivery to launch pad.

line bellows and bracket area. The system provides ice mitigation service to within 15 minutes of T-0. The system delivers 330 W/m^2 (approximately 1/3 solar) of evenly distributed IR energy in a minimum 10-ft-diameter circle at a distance of 380 ft during normal operation. The system does not exceed 550 W/m^2 (approximately 1/2 solar) of evenly distributed IR energy in a minimum 10-ft-diameter circle at a distance of 380 ft during normal operation. This sacrificial system is required to operate only once in the launch environment (permanent damage acceptable).

Key accomplishments:

- A prototype halogen-light parabola/reflector system was designed using software programs (see "Ray Trace Math Model and Windows Software Implementation for a Focused Infrared Lamp Projection System," p. 90) to optimize the amount of IR radiation that can be generated from off-the-shelf components.
- The light filament and parabola of each operational IPA was aligned and tested at 380 ft to obtain the maximum IR radiation from each unit (Figure 2).
- The final configuration (Figure 3) consisted of 12 custom 3-ft parabolas mounted on a skid with a power supply system. Persistent polishing of the parabola reflecting surface was required to meet focusing specifications. The complete system was delivered to United Space Alliance.

Contact: Dr. Robert C. Youngquist <Robert.C.Youngquist@nasa.gov>, NASA KT-D1, (321) 867-1829

Participating Organizations: ASRC Aerospace (Robert B. Cox, John K. Trautwein, Mark C. Minich, and Joseph N. Dean) and NASA KT-D1 (Douglas E. Willard)

Biological Sciences

The difference between manned and unmanned space missions is the presence of life support systems. Biological processes are present within all life support systems. Some of these processes represent highly robust, low-mass/low-energy alternatives to systems that rely solely on high temperature and pressure or that require large amounts of expendable materials.

The KSC Biological Sciences program conducts research and develops technology in four basic life sciences areas:

- systems for regenerating life support consumables, including removal of carbon dioxide, and regeneration of clean water and oxygen in long-term space missions;
- ecology and application of microorganisms to water recovery and solid-waste reduction in space;
- flight hardware development, design, construction, and validation for biological science experiments; and
- application of results from this research and technology development to managing ecosystems on Earth.

For 20 years, research in bioregenerative life support systems at KSC has focused on crop growth and development, with primary emphasis on biomass production under closed conditions. In recent years, the focus has shifted to include the potential use of biology in recycling solid and liquid waste to generate clean water and the reuse of constituent elements of the waste as an *in situ* resource, rather than transporting heavy materials or equipment from Earth.

The Biological Sciences program initiated significant efforts to understand photosynthetic processes under space flight conditions. A series of studies was carried out to determine the response of higher plants to microgravity and to determine if they would remain viable and useful components of a life support system. These experiments required adding new plant flight hardware and refurbishing older flight hardware that had been used for previous science experiments. Flight hardware development efforts include studying highly efficient specific-wavelength light-emitting diodes, using porous-tube systems to deliver water and nutrients, and developing physical and biological sensors that could give a more complete understanding of the hardware operation during space flight.

Another goal of these studies was to determine the stability of microbial communities associated with the closed life support systems. Studies to determine the stability and effectiveness of microbial communities with physiological profiling and molecular approaches continued during the past year. In addition, a metabolite-profiling capability was added to evaluate biological responses. The ultimate goal is to develop reactors in which microorganisms recycle elements from solid and liquid wastes, including urine, graywater, inedible residues, and trash, to produce nutrients and clean water. The development of life support technologies and the ability to evaluate them in the space flight environment will permit NASA to estimate the resources needed to design, construct, and test life support systems for future missions. Understanding and optimizing life support systems, along with their associated reliabilities and costs, will help those systems sustain the autonomous human colonies essential for exploration of space.

In support of the near term needs of the Exploration Program, KSC is now focusing its biological technology development activities on water and waste processing, air monitoring, and habitat support systems. Efforts are also focusing on understanding the microbial community in closed space flight systems.

For more information regarding Biological Sciences, please contact Charles D. Quincy <Charles.D.Quincy@nasa.gov>, NASA KT-B, (321) 867-8383.

Water Offset Nutrient Delivery Experiment (WONDER): Feedback Moisture Control for Porous-Tube and Substrate Nutrient Delivery Systems for Plant Growth in Space

Bioregenerative Life Support System Operation/ Validation/Control

The development of a space-flight-rated Porous-Tube Insert Module (PTIM) nutrient delivery tray has enabled a series of studies evaluating various aspects of water and nutrient delivery to plants as they would be cultivated in space. There is a need for microgravity-based plant culture nutrient delivery systems (NDSs) for both bioregenerative Advanced Life Support and Exploration crew vehicle systems. Providing adequate water (without causing waterlogging) and oxygen to the root zone are the most crucial components deterring major advancements in this area.

The WONDER space flight experiment was designed to compare a porous-tube NDS and a substrate-based NDS while evaluating three different wetness-level treatments for each of these approaches. It was anticipated that preset wetness levels different than those used on Earth will be required to support optimal plant growth in space. The PTIM (Figure 1) was specifically designed to fulfill the requirements of this project.

PTIM provides a feedback moisture sensor control strategy for maintaining root zone wetness level set points. Wheat seedlings were inserted into each of three substrate NDS (SNDS) modules prepacked with 0.25- to 1-mm substrate and maintained at root zone relative water content levels of 70, 80 and 90 percent (see the table). The SNDS contained a bottom-situated porous tube around which a capillary mat was wrapped. Three porous-tube NDS (PTNDS) modules were planted using similar protocols (but without the substrate) and also maintained at these three moisture-level set points.

The PTIM incorporates moisture sensors to monitor and control the wetness levels both on the three porous tubes and within the three substrate compartments contained within the PTIM. The capillary mat wicking material used with the PTNDS modules holds less water, and thus, less water is required to maintain root zone wetness levels (Figure 2).

Figure 1. The PTIM design with alternating porous-tube and substrate-based NDSs visible in a photograph taken at the end (harvest) of an experiment.

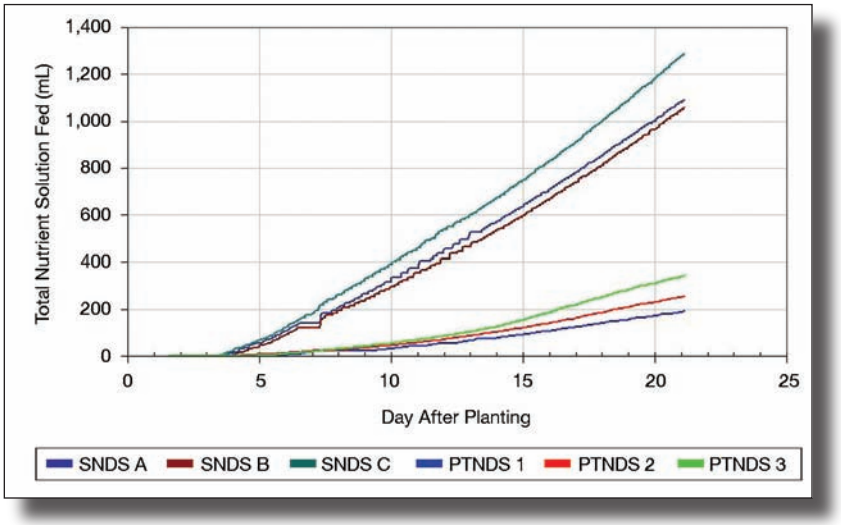

Figure 2. Cumulative nutrient solution volume fed for the different treatments. The irrigation rates for the SNDS modules were substantially higher than those for the PTNDS modules partly due to work-holding capacity of particulate media and higher rates of evaporative losses from the SNDS; (which have gas-permeable membranes on all sides).

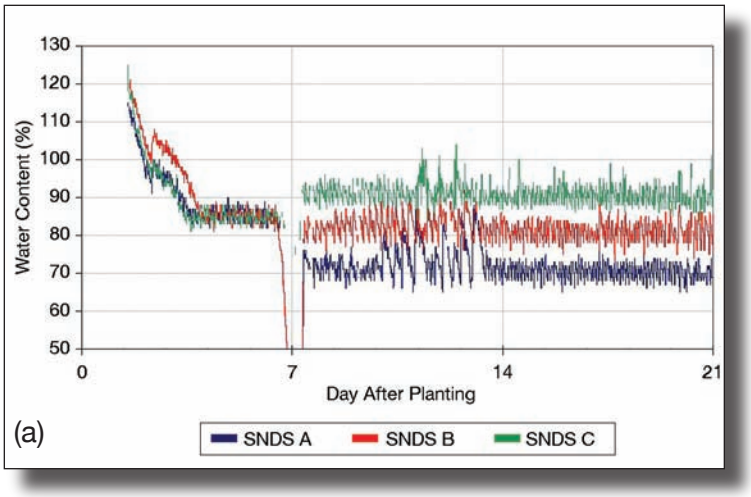

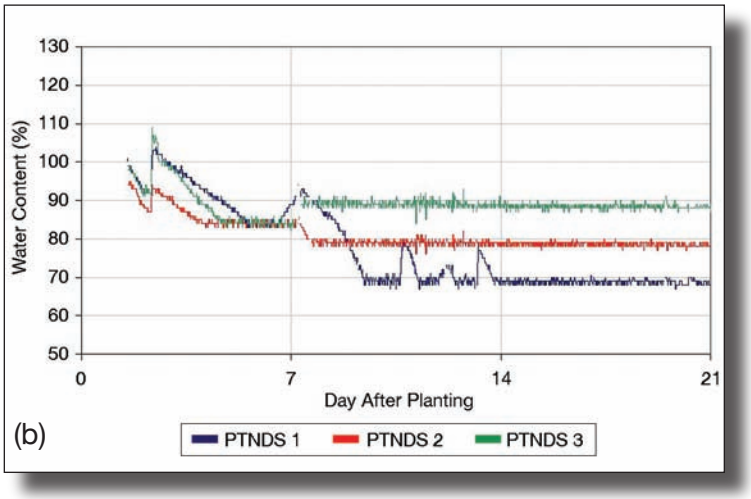

Figure 3. The average RWC measured in the (a) SNDS and (b) PTNDS modules during the experiment. An initial set point of 85% was used for all modules. On DAP 7, the treatments indicated in the table were initiated. Greater variability for the SNDS modules was partially due to longer delay time between irrigation and sensor response.

Root zone moisture content set points for both the SNDS and PTNDS modules and mean (+ SD) measured RWC values in the modules for DAP 14 to 21. RWC levels represent the volume of water in the media relative to the total volume of water the media holds.

	Target RWC (%)	Mean RWC (%)	Standard Deviations
PT 1	70	68.8	0.63
PT 2	80	78.6	0.57
PT 3	90	88.4	0.71
SC A	70	70.5	2.10
SC B	80	81.1	2.60
SC C	90	90.4	2.60
PT: porous tube; SC: substrate compartment			

The control system operated such that irrigation pumps activated when the relative water content (RWC) levels fell below a lower limit and deactivated when the RWC levels reached an upper limit. The target RWC was 85 percent for all modules during the "ground operations" portion of the experiment from day after planting (DAP) 1 (based upon initiation of imbibition) to DAP 7. Target RWC levels and those achieved during the experiment are shown in the table. Figure 3 illustrates the water content levels in the NDS modules during the course of the experiment.

Ongoing ground-based experiments are investigating the operations of this automated plant growth hardware and the attributes of crops grown in the PTIM system.

Key accomplishments:

- Conducted PTIM/Plant Generic Bioprocessing Apparatus (flight growth chamber) integration testing (2004).
- Conducted high-fidelity moisture treatment experiment with feedback irrigation control using flight hardware (2004).
- Completed moisture sensor characterization using both substrate media and wicking material media.

Key milestones:

- Conduct high-fidelity experiments in the PTIM hardware in a ground-based growth chamber (2005).
- Collect tissue for gene expression characterization of water status differences in the crop.

Contacts: Dr. Howard G. Levine <Howard.G.Levine@nasa.gov>, NASA KT-B1, (321) 861-3502; Daniel C. Shultz <Daniel.C.Schultz@nasa.gov>, NASA DX-B1, (321) 861-2896; and Dr. John C. Sager <John.C.Sager@nasa.gov>, NASA KT-B1, (321) 861-2949

Participating Organizations: Dynamac Corporation (Jessica J. Prenger and Donna T. Rouzan-Wheeldon) and Bionetics Corporation (Kevin A. Burtness, Trevor Murdoch, April C. Spinale, and Howard W. Wells)

Passive Observatories for Experimental Microbial Systems (POEMS): Novel Payload Hardware for Microbial Growth in Space

Bioregenerative Life Support System Operation/ Validation/Control

For long-duration exploration missions where resupply is not a viable alternative for human crews, sustainable strategies based on integrated bioprocesses and physical-chemical systems are required. Bioregenerative life support elements enabling human exploration systems require microbial communities that are physiologically diverse, functionally stable, and nonvirulent. Given the potential for rapid change in microbial populations through processes that may be accelerated in space (i.e., mutation, recombination, and natural selection), multigeneration experiments are required to understand the pattern and process of microbial evolution and community assembly in the space environment. One requirement for these studies is a cell cultivation unit with low mass, volume, energy, and crew-time requirements for the multigeneration growth of microbial populations in the space environment. POEMS is an integrated flight-ready unit to support multigeneration microbiological studies. The POEMS cultivation unit integrates the OptiCell (P/N 1100), a small sterile growth chamber sealed between optically clear gas-permeable growth surfaces, with a new generation of Biological Research in a Canister (BRIC) flight hardware developed entirely at KSC. Each BRIC-Opti canister provides mechanical support for four replicate OptiCell chambers, a captured volume of atmosphere for microbial metabolism, gas-sampling capability, and autonomous temperature and relative-humidity data logging during the mission. The first POEMS experiment will enable analyses of bacterial growth and evolution in a microgravity environment on STS-121 during ULF1.1 and on the International Space Station during Increments 12 and 13.

Either monocultures or mixed populations of cells will propagate passively in the OptiCell without crew intervention for multiple generations of growth. Two self-sealing septa permit introduction of media and inoculum into the interstitial space between the optical membranes (Figure 1). The investigator may choose the cell inoculum, growth medium, and support matrix (liquid, solid, or semisolid). As cells respire, gas exchange between the growth chamber and the ambient atmosphere across the gas-permeable membranes enables maintenance of pH and optimum levels of oxygen and carbon dioxide in the cultivation matrix. In addition, the optically clear membranes permit direct microscopic observation and imaging of cell morphology and behavior at high resolution.

In the space flight configuration, OptiCells are contained within the BRIC-Opti canister, which is designed to meet multiple engineering and science objectives:

- provide a closed environment with an atmosphere of known initial composition for microbial growth;
- provide a support structure for four self-contained OptiCell culture chambers;
- provide two redundant levels of containment for potentially hazardous materials or organisms; and
- provide autonomous temperature data logging at three physical locations within each canister.

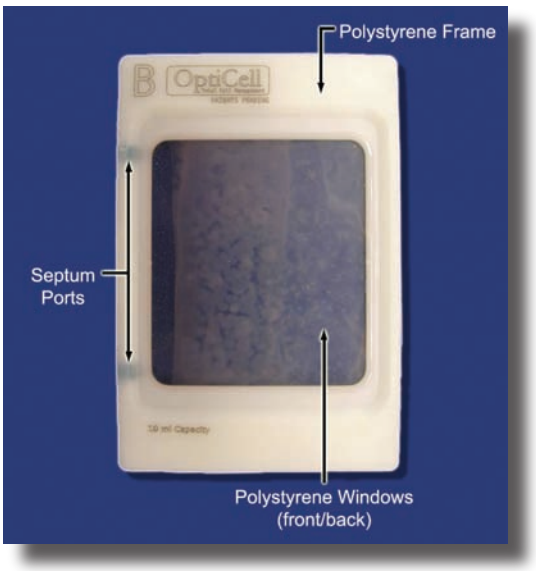

Figure 1. OptiCell culture chamber.

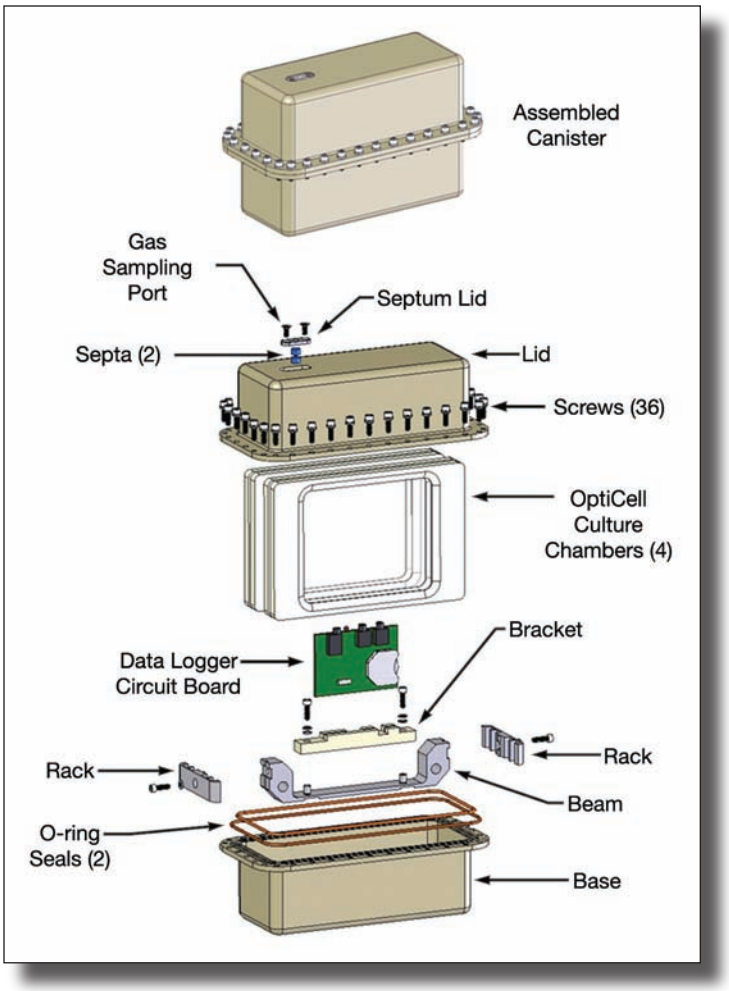

Figure 2. Integrated POEMS.

Figure 3. Partially integrated POEMS canister.

The BRIC-Opti (Figures 2 and 3) is an environmentally sealed aluminum container providing two levels of biological and atmospheric containment during all phases of operation. Each BRIC-Opti is a sealed environment with no active thermal control and no gas, liquid, or material exchange between the interior BRIC-Opti atmosphere and the spacecraft cabin. Biological specimens should be specifically selected to be tolerant of both the ambient thermal environment onboard the spacecraft and the physical atmosphere within the BRIC-Opti at launch. A gas-sampling septum is embedded in the lid of the BRIC-Opti to accommodate pre- and postflight gas sampling for atmospheric gas composition analysis. Each BRIC-Opti accommodates four independent OptiCell subelements and a single autonomous multichannel data logger made by Onset Corporation. The HOBO data logger (P/N H08-007-IS) provides sensors for relative humidity and up to three channels of temperature via T-type sensors attached by short cables (not shown). The data loggers are activated prior to payload integration and read out postflight.

Contacts: David R. Cox <David.R.Cox@nasa.gov>, NASA KT-B, (321) 867-6051; and Dr. Howard G. Levine <Howard.G.Levine@nasa.gov>, NASA KT-B1, (321) 861-3502

Participating Organizations: Bionetics Corporation (David W. Reed and Todd E. Mortenson) and Dynamac Corporation (Dr. Cheryl M. Frazier and Dr. Michael S. Roberts)

Development and Coupling of Metabolomics Capability With Transcriptomics To Dissect Cellular and Molecular Processes of Living Organisms

2005 Center Director's Discretionary Fund Project

Bioregenerative Life Support System Operation/ Validation/Control

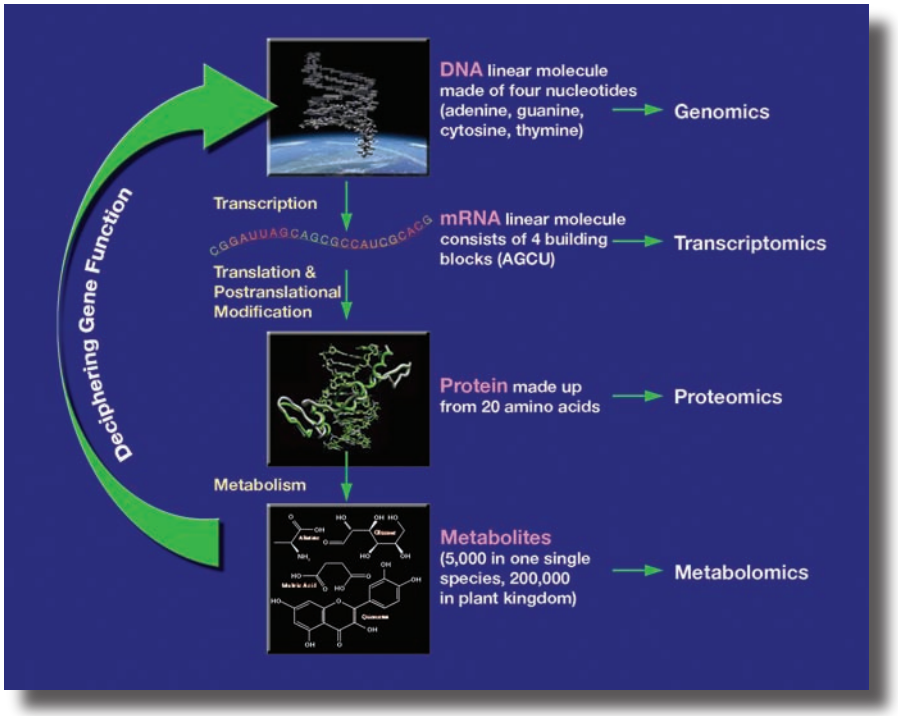

Figure 1. Central dogma of biology and "omics" revolution.

Regulatory control in biological systems is exerted at all levels within the central dogma of biology: DNA→messenger RNA (mRNA)→Enzymeinactive→ Enzymeactive→Metabolites (Figure 1). Metabolites are the end products of all cellular regulatory processes and reflect the ultimate outcome of potential changes suggested by genomics and proteomics caused by an environmental stimulus or genetic modification. Following on the heels of genomics, transcriptomics, and proteomics, metabolomics has become an inevitable part of complete systems biology because none of the lower "-omics" alone provides direct information about how changes in mRNA or protein are coupled to changes in biological function. Analogous to the precedent "-omics," metabolomics is the systematic study of collections of small molecules (i.e., metabolites) in a biological system (a cell, organ, or organism). In contrast to the traditional biochemistry approach in which target metabolites and enzymes are studied, metabolomics takes a holistic view of the entire suite of metabolites (the metabolome) in an organism to capture the coordinated regulation of biological systems. Thus, metabolomics, coupled with other "-omics" such as transcriptomics and proteomics, holds great promise for deciphering the functions of genes, predicting novel metabolic pathways, and providing insights to the regulation of a biological event, as well as directing metabolic engineering of plants for human benefit. However, the challenge is much greater than that met by genomics because of the greater number of metabolites and greater structural, and thus property, diversity. Developmental work is needed in areas such as (1) methodologies for unbiased extraction of metabolites and subsequent quantification, (2) algorithms for systematic identification of metabolites, (3) expertise and competency in handling a large amount of information (data set), and (4) integration of metabolomics with other "-omics" and data mining (implication of the information).

Preliminary study of the consequences of superelevated CO_2 by the metabolomics approach has demonstrated clear CO_2 phenotypes (Figure 2). The metabolites strongly influenced by CO_2 are not limited to carbohydrates (photosynthetic products) but also trickle down to other primary and secondary compounds such as amino acids, organic acids, and the precursors of the phenylpropanoid and flavonoid pathways.

CO_2 is an abundant molecule in the Martian atmosphere and in enclosed habitats that can easily reach a concentration up to 4,000 parts per million (ppm). However, plants evolved on Earth and have become acclimated and evolved to flourish at levels below 400 ppm. In numerous studies, plants experience enhanced productivity when exposed to elevated CO_2 levels no more than 1,200 ppm. Further increase in CO_2 leads to deceased yield and other peculiar physiological effects. A key long-term objective centers

on harnessing the plant photosynthetic machinery to remove overabundant CO_2 that would otherwise be potentially harmful to human inhabitants. The best option would be to recycle CO_2 into photosynthesis, converting it into food to benefit the crew. Ultimately, we must identify the factors that limit plant yield when no resource (water, light, CO_2, and nutrient) is limiting to growth. Currently, an experiment using a model plant, *Arabidoposis*, exposed to 400-, 1,200- and 4,000-ppm CO_2 is under way. Plant samples are being collected for parallel analysis of the metabolome and transcriptome at two growth stages (Figure 3) to address this question.

There are many more questions (e.g., effects of artificial lighting, reduced gravity and pressure, and increased ultraviolet and cosmic radiation) that are critical to the development of a robust bioregenerative system for space exploration that could be better answered by the marriage of metabolomics and transcriptomics. Metabolomics is not limited to plant biology, but can be extended to (1) evaluate the biofluids of astronauts in space biomedical research and occupational health, (2) unambiguously evaluate the result of genetic and metabolic engineering of crops for specific quality traits, (3) study the health effects of food products on apparently healthy people, (4) measure the physiological response to either the toxicity or efficacy of a compound, or find specific markers indicating known diseases that are curable by early diagnosis, and (5) better understand microbial and biotic ecology of closed-system environments.

Key accomplishments:

- Built a team with expertise in biochemistry, genomics, analytical chemistry, and statistics.
- Acquired essential equipment for extensive metabolite profiling.
- Implemented and optimized procedures for metabolite extraction, derivatization, and gas chromatography/mass specterometry (GC/MS) analysis.
- Greatly expanded mass spectra library and hence capability for metabolite identification.
- Constructed a preliminary automated program for processing raw GC/MS data files.
- Designed and started a superelevated CO_2 experiment to address such questions as what limits photosynthetic potential and the functions of genes involved in CO_2 regulation.
- Generated great interest of academic partners.
- Secured second-year funding and submitted proposals to the National Science Foundation to partially fund these investigative efforts.

Contact: Dr. Raymond M. Wheeler <Raymond.M.Wheeler@nasa.gov>, NASA KT-B1, (321) 861-2950

Participating Organizations: Dynamac Corporation (Dr. Lanfang H. Levine), University of Florida (Dr. Charles Guy and Dr. Fatma Kaplan), and Max Planck Institute for Molecular Plant Physiology (Dr. Joachim Kopka)

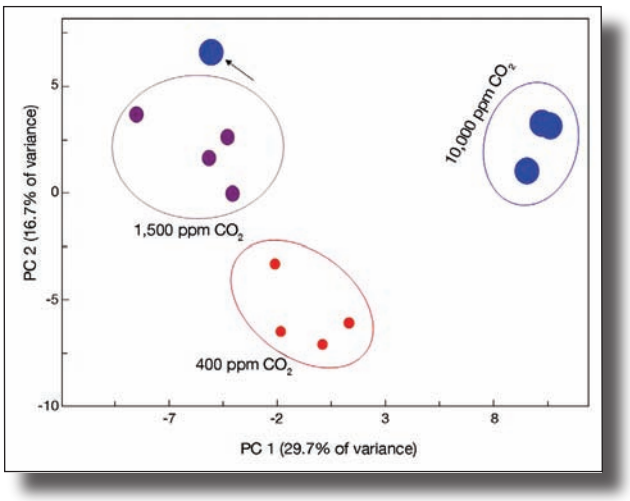

Figure 2. PCA Log 10 of metabolite response to CO_2 treatments.

Figure 3. Drs. Charles Guy and Fatma Kaplan take and preserve samples for metabolite and mRNA profiling.

Generation One Bioregenerative (GOBIO) Subsystem Interfacing Test Module: Project Background and Infrastructure

Bioregenerative Life Support System Operation/ Validation/Control

Bioregenerative life support systems have been developed and studied for 20 years by the researchers at KSC. These systems use plants to grow food, recycle water, and revitalize the air for the crew. In addition, the plants provide a psychological benefit for the crew. The promise of bioregenerative systems is that they could be self-sustaining such that human outputs (wastes) could be processed and fed back into the plant production area, with the plants then extracting the resources they require to continue to provide life support to the crew. The Vision for Space Exploration requires that bioregenerative systems development take the next step and start to integrate plant and resource recovery operations, subsystems that are typically developed and tested individually. The GOBIO Subsystem Interfacing Testbed is being developed to allow the subsystems to interconnect so operational protocols can be developed and system optimization studies can be conducted (Figure 1). A test facility is being proposed to support the metabolic mass flows (edible biomass, oxygen, carbon dioxide, waste water) for one crew member, but this facility would not be human-rated (i.e., not used for human testing). The scope of this project is broad, and the planning and systems analysis have initially focused on the water loop for a bioregenerative system. Anticipated water production estimates from plant transpiration do not correlate well with water consumption rates by plants. This was partly due to the wide range of literature values on crop water use. In addition, water use by plants fluctuates greatly over the course of a growing period (Figure 2). Initial estimates suggest that an area of only about 5 m^2 of crop plant would be sufficient to evaporate and purify the water needed by one human. The need to manage crops for food and water production emphasizes the need for an interfacing test module.

Key accomplishments:

- Completed assessment of critical mass flows for biomass production subsystem.
- Initiated quantification of water requirements and outputs.

Key milestone:

- Submitted summer faculty report on findings to date.

Contacts: Dr. Raymond M. Wheeler <Raymond.M.Wheeler@nasa.gov>, NASA KT-B1, (321) 861-2950; and Dr. John C. Sager <John.C.Sager@nasa.gov>, NASA KT-B1, (321) 861-2949

Participating Organizations: Dynamac Corporation (Neil C. Yorio, Gary W. Stutte, and Dr. Jay L. Garland), Bionetics Corporation (Todd E. Mortenson), National Research Council (Dr. Hyeon-Hye Kim), and University of Kentucky (Dr. Joey H. Norikane)

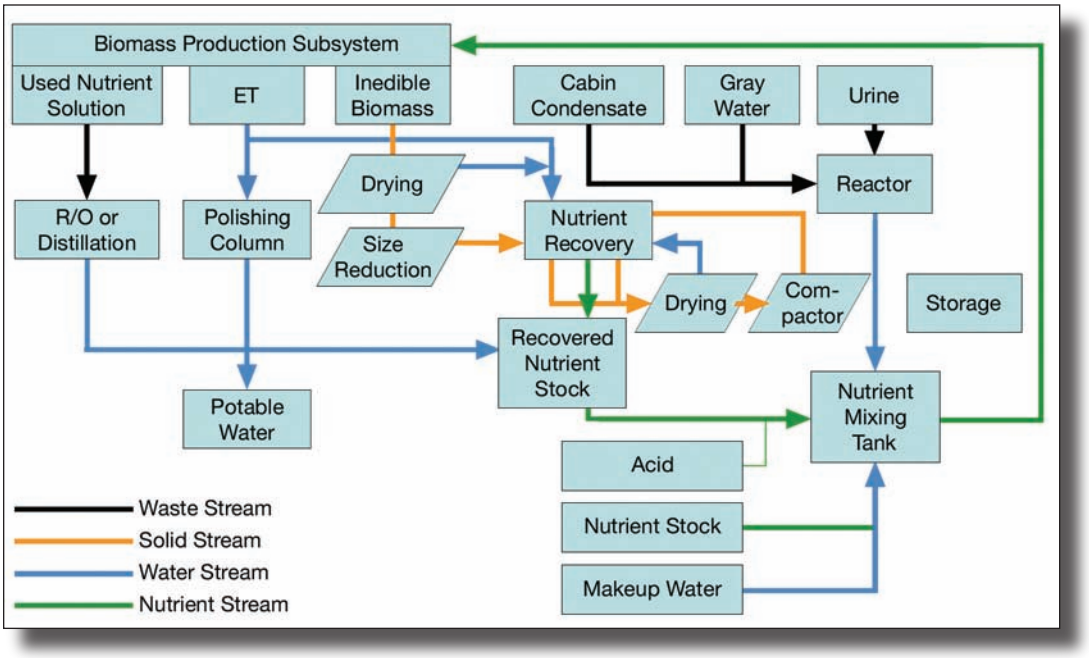

Figure 1. Mass flow for a biomass (crop) production system, where recycled water and nutrients are used to sustain the crops. The crops are then used to generate food and potable water.

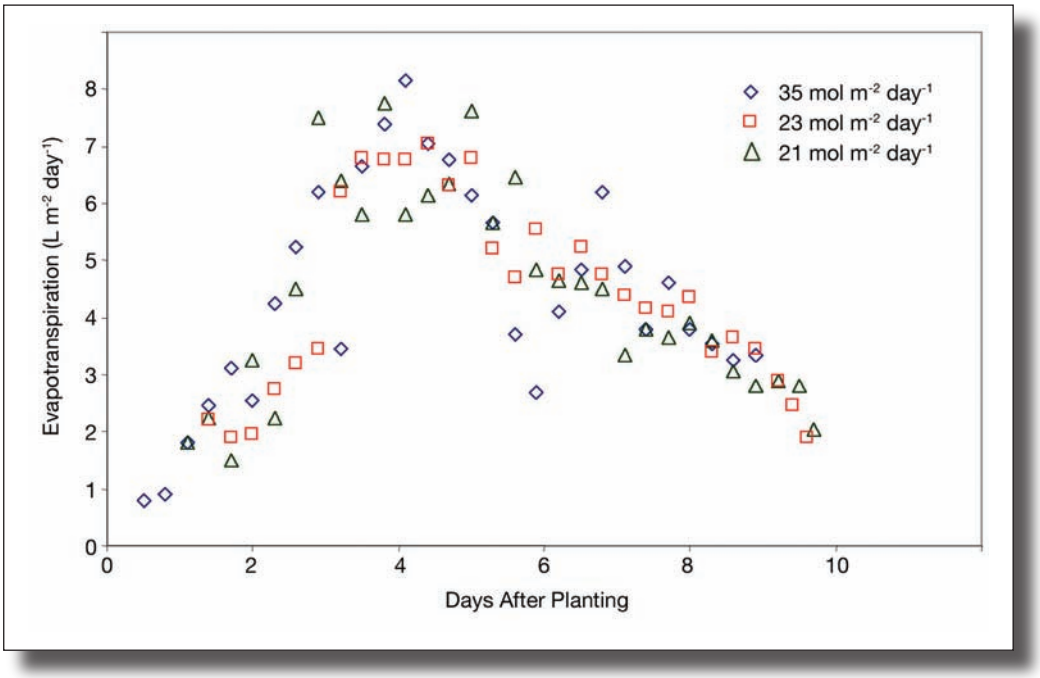

Figure 2. Water production (evapotranspiration) rates of soybean stands grown at three different light intensities.

Advanced Life Support (ALS) Project: Growth of Salad Crops for Long-Duration Space Exploration

Bioregenerative Life Support System Operation/ Validation/Control

Early plant growing systems onboard planetary transit vehicles or in planetary modules will be limited in size and power to reduce equivalent system mass and minimize costs. These systems will need to operate under atmospheric conditions controlled by an Environmental Control and Life Support System, which may not be optimal for plant growth but would be useful in producing perishable salad-type crops to supplement foods supplied from Earth. Fresh produce could be of significant psychological benefit to the crew and could provide essential vitamins, minerals, and antioxidants in a more natural, bio-stable form, to aid in the reduction of inherent reactive oxygen species (e.g., oxidative stress) associated with long-duration space flight. Furthermore, depending on size, minor atmospheric regeneration through photosynthesis and water purification through collection of transpired water are possible.

Over the last year, several projects have been underway in growth chambers located at the Controlled Environment Laboratory in the Space Life Sciences Laboratory, investigating the growth of these crops under potential spacecraft lighting and atmospheric conditions. Tests include three variations in light intensity (daily light integral), temperature, and carbon dioxide concentration to generate environmental response surfaces of plant growth under potential spacecraft growing conditions.

Radish, Onion, and Lettuce Spacecraft Baseline Studies

Radish, onion, and lettuce cultivars were grown in monoculture and mixed culture at spacecraft baseline conditions of 22, 25, and 28 °C under 8.6, 17.2, or 25.8 mol m^{-2} d^{-1} daily light integral and 400 (ambient), 1,200, or 4,000 ppm CO_2 (Figure 1). Baseline environmental testing of these salad crops is near completion.

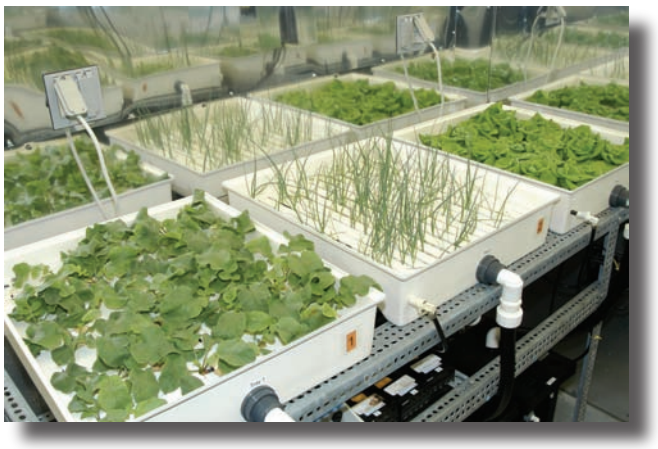

Figure 1. Twenty-one day old radish, onion. and lettuce grown as a monoculture and under spacecraft environmental conditions in the Controlled Environment Laboratory.

Tomato and Pepper Spacecraft Baseline Studies

Following a cultivar selection process, one dwarf tomato (*Lycopersicon esculentum L.* cv. Red Robin) and one dwarf pepper (*Capsicum annum L.* cv. Hanging Basket) variety were selected and tested for their growth characteristics under baseline spacecraft conditions (Figure 2). Both tomato and pepper plants showed three- to five-fold increases in edible yields in response to increased light.

Strawberry Cultivar Trials

A strawberry cultivar screening process for inclusion in an ALS crop system recently identified three cultivars (Everest, Tribute, and Whitney) that were able to grow hydroponically and produce fruit under spacecraft environmental

Figure 2. Dwarf tomato (left) and pepper (right) grown hydroponically under spacecraft environmental conditions at the Controlled Environment Laboratory.

conditions (Figure 3). The psychological benefit of the colorful, aromatic, and tasty fruit to the crew is supported by anecdotal comments from astronauts and others living in isolated, confined environments (such as Antarctica). However, further testing is needed to quantify these effects.

Figure 3. Evaluating strawberry cultivars grown under spacecraft environmental conditions at the Controlled Environment Laboratory.

Low-Atmospheric-Pressure Plant Growth

A low-pressure cooperative study was initiated with the University of Guelph's (Ontario) Controlled Environmental Systems Research Facility (Figure 4). Atmospheric-pressure treatments were selected to approximate the conditions that could be anticipated for a human-rated plant growth facility. They include total pressures of 95 kPa, 66 kPa (or two-thirds of Earth-normal pressure), and 33 kPa (or one-third of Earth-normal pressure). These pressures were selected because crews have worked under these conditions for sustained periods during Skylab, Mir, and STS missions.

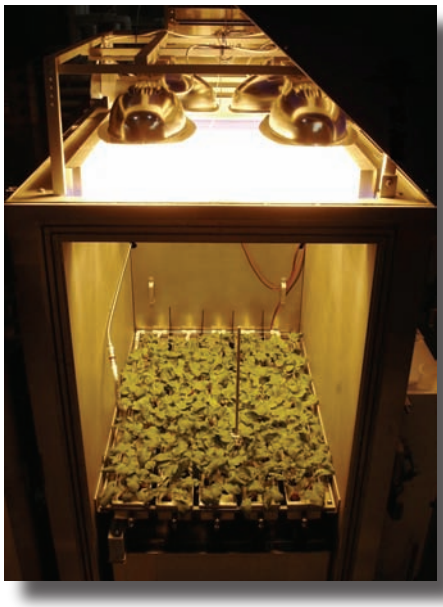

Figure 4. An inside view of the hypobaric plant growth chambers located in the University of Guelph's Controlled Environmental Systems Research Facility. Inside are radish plants ready for harvest following 21 days' growth at one-third Earth-normal atmospheric pressure (33 kPa).

Key accomplishments:

- Completed all environmental baseline studies and mixed-crop studies under the 28 and 25 °C temperature regime (incorporating the matrix of light and CO_2 interactions), with two more experiments required to complete the remaining 22 °C study.
- Completed the dwarf tomato and pepper cultivar evaluation, resulting in the selection of one cultivar of each species for further investigations.
- Selected six cultivars for a strawberry cultivar evaluation with assistance from several key scientists at the USDA, University of Florida, and University of Maryland.
- Selected three strawberry cultivars for further nutrient studies.
- Completed initial series of low-atmospheric-pressure plant growth experiments in cooperation with the University of Guelph's Controlled Environmental Systems Research Facility.

Key milestones:

- Complete the 22 °C regime for both spacecraft environmental baseline and mixed-crop studies.
- Continue a strawberry evaluation study under hydroponic nutrient film technique conditions.
- Continue dwarf tomato and pepper spacecraft environmental baseline tests.
- Continue a cooperative research project investigating low-atmospheric-pressure plant growth experiments with the University of Guelph's Controlled Environmental Systems Research Facility.

Contacts: Jeffrey T. Richards <richajt@kscems.ksc.nasa.gov>, Dynamac Corporation, DYN-3, (321) 861-2929; Dr. Raymond M. Wheeler <Raymond.M.Wheeler@nasa.gov>, NASA KT-B1, (321) 861-2950; and Dr. John C. Sager <John.C.Sager@nasa.gov>, NASA KT-B1, (321) 861-2949

Participating Organization: Dynamac Corporation (Gary W. Stutte and Neil C. Yorio)

Capacitance-Based Moisture Sensing

2005 Center Director's Discretionary Fund Project

Bioregenerative Life Support System Operation/ Validation/Control

Measurement and feedback control of moisture in plant root zones is critical to the development of healthy plants in reduced gravity. Adequate moisture content and distribution in media of space-borne nutrient delivery systems (NDS) is required for optimal growth in plant-based life support systems. Current moisture sensor technologies suffer from interferences such as air bubbles, contact area of media, and root growth. Because most are point sensors, the measurements are localized over a small volume at the point of insertion. This makes it difficult to get an accurate representation of true moisture content and distribution in the bulk media. In addition, a network of point sensors is required, increasing the cabling, data acquisition, and calibration requirements.

The first of two sensors developed under this project was a bulk moisture sensor for terrestrial-based applications. A test fixture was designed to precisely control the amount of nutrient solution within the sensor. A cylindrical-based capacitor configuration was implemented for the prototype sensor because it adapted best to the test fixture and is easily modeled electrically. The sensor in the test stand, with the moisture control plumbing removed, is shown in Figure 1. The sensor was tested to determine its frequency response of the sensor to different media (glass beads and Turface, a claylike medium) and with different nutrient solutions. Literature suggests that at certain frequencies, capacitance values will be mostly independent of the ion content (salinity) of the nutrient solution. This frequency was found to be about 300 kHz for both 1-mm and 2-mm glass bead substrates with different Hoagland's nutrient solutions. A plot of the capacitance versus volumetric water content is shown in Figure 2 for the 2-mm glass bead substrate for the different solutions.

Figure 1. The bulk moisture sensor is shown in its test fixture without the moisture control plumbing attached.

An empirical relationship was found for determining volumetric water content from a capacitance measurement. However, testing in porous media shows that salinity still has a small effect on the capacitance reading. So, an empirical relationship was also found to give more accurate volumetric water content readings as a function of both capacitance and conductivity measurements. This second method has the added benefit of obtaining the salinity, which is important in feeding plants. The work is continuing to further characterize sensor performance with porous media and the presence of root mass.

In space-borne applications, the microgravity substrate environment operates in a force balance between surface tension and capillary forces, making it difficult to measure and understand the distribution and availability of nutrients in plant growth experiments. Over the past few years, KSC has been exploring a new area in the development of a system to provide 3-D imaging of dielectric objects using an array of capacitors, referred to as electrical capacitance tomography (ECT). This is a relatively undeveloped area in the United States (prior work has been done in England) and the hope is that it will lead to a new method for imaging

objects, such as moisture in soil, using safe low-frequency electromagnetic radiation and a very inexpensive sensing system. The primary reason this has not been accomplished previously is that a very large amount of processor power is required, which has not been available until recently. Algorithmic development and electronic performance are critical and key to determining the capability of this new imaging system.

The second sensor developed under this project is an ECT system to further our understanding of soil moisture distribution in microgravity environments, thus promoting improvements to the NDS. Two 4 by 4 sets of electrodes were used to construct a 3-D ECT system with rectangular geometry rather than the typical 2-D system with 8 to 12 electrodes. Figure 3 shows a front view for one of the two electrode arrays and a side view of both arrays and the surrounding guard. The measurement electronics were designed around a new capacitance-to-digital converter integrated circuit produced by Analog Devices, Inc., the AD7746. A number of algorithms have been created to reconstruct the image with varying degrees of success. They have been tested with idealized synthetic data, synthetic data with controlled amounts of noise added, and real data to determine the most suitable methods.

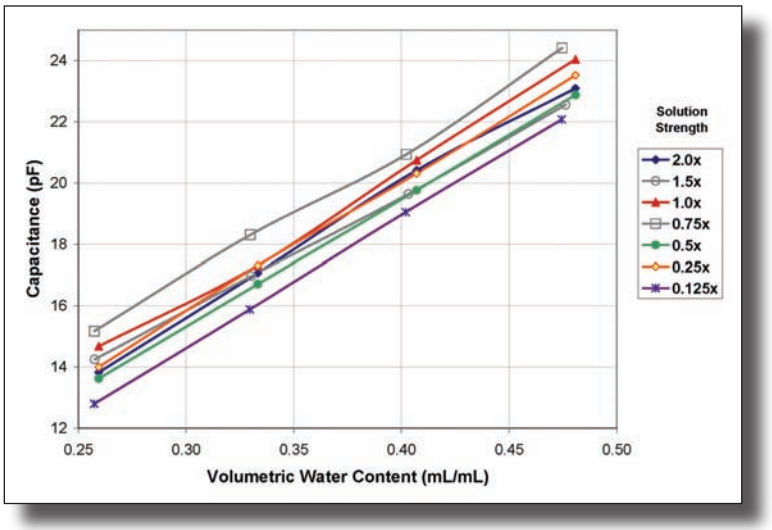

Figure 2. Graph showing the bulk moisture sensor capacitance output vs. volumetric water content for 2-mm glass bead substrate with different salinity solutions.

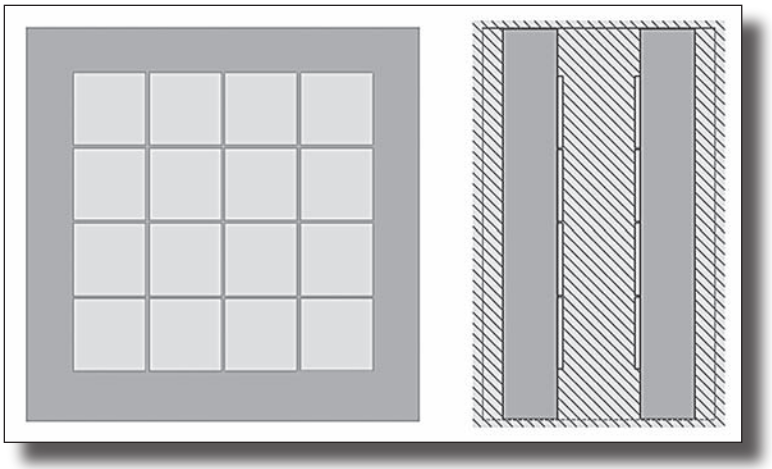

Figure 3. Front (left) and side views (right) of the electrode geometry used for the 3-D Electrical Capacitance Tomography (ECT) system. The side view shows the position of both electrode arrays and the surrounding guard.

Work is progressing on reconstructing images from data taken with the ECT system described above. To get the best fidelity image, the measured capacitance readings must be accurate to about 0.3 fF for the chosen geometry. The circuitry used provides this accuracy, but the technique requires that data be taken both with and without the sample present. The reconstructed image is then based on the difference between the two sets of capacitance readings. A number of improvements have been made to reduce drift and noise. A reference capacitor and temperature measurement were implemented to compensate for drift caused by temperature and humidity variations. Also, a new enclosure was constructed for the switching electronics to rigidly mount the circuit boards and to shorten cable paths. The images have improved but are now limited by alignment errors created by the hand-built construction of the electrodes and their enclosure.

Contacts: Mark A. Nurge <Mark.A.Nurge@nasa.gov>, NASA KT-D1, (321) 861-9068

Participating Organizations: Dynamac Corporation (Dr. Oscar A. Monje, John A. Catechis, and Jessica J. Prenger)

Using Noninvasive Techniques To Quantify the Effects of Mild Water Stress on Plants

Remote Plant/ Microorganism Health Sensing

Such fields as agriculture, fire modeling, and space exploration would benefit from the ability to use remote sensing technology to detect plant water status and health. Water stress causes plants to show a decrease in photosynthesis, accompanied by a corresponding increase in reflectance and fluorescence, which may be measured remotely. The objective of this study was to determine whether changes in the physiology and morphology of plants grown under differing water availabilities could be detected, and whether spectral data (reflectance) could be correlated to factors of plant growth, such as photosynthesis, moisture content, and chlorophyll pigment concentration.

This study used a hydroponics system, the Porous-Tube Plant Nutrient Delivery System (PTPNDS), to control the amount of water supplied to wheat plants. The PTPNDS was developed to grow plants in the microgravity environment of space. The system delivers a nutrient solution to roots under slightly negative pressures by capillary action. A PTPNDS consisting of eight ceramic tubes was placed on each of three laboratory trays (see the Kennedy Space Center Research and Technology 2003 Annual Report for details on PTPNDS setup). Thirty seeds of wheat (*Triticum aestivum*, cv. Perigee) were placed on each tube, with a wet strip of lab wipe placed on the seeds to promote germination. The standpipes of each PTPNDS were then adjusted to three different levels 7 days after planting (tray A: –0.098 kPa, tray B: –1.96 kPa, tray C: –3.92 kPa). Tray A began to show signs of yellowing and stunted growth during the third week, so the standpipe was lowered 5 cm to a pressure of –0.49 kPa 16 days after planting.

Routine measurements were taken on height, water, temperature, humidity, and light intensity. On 21 and 22 days after planting, a combination of physiological and

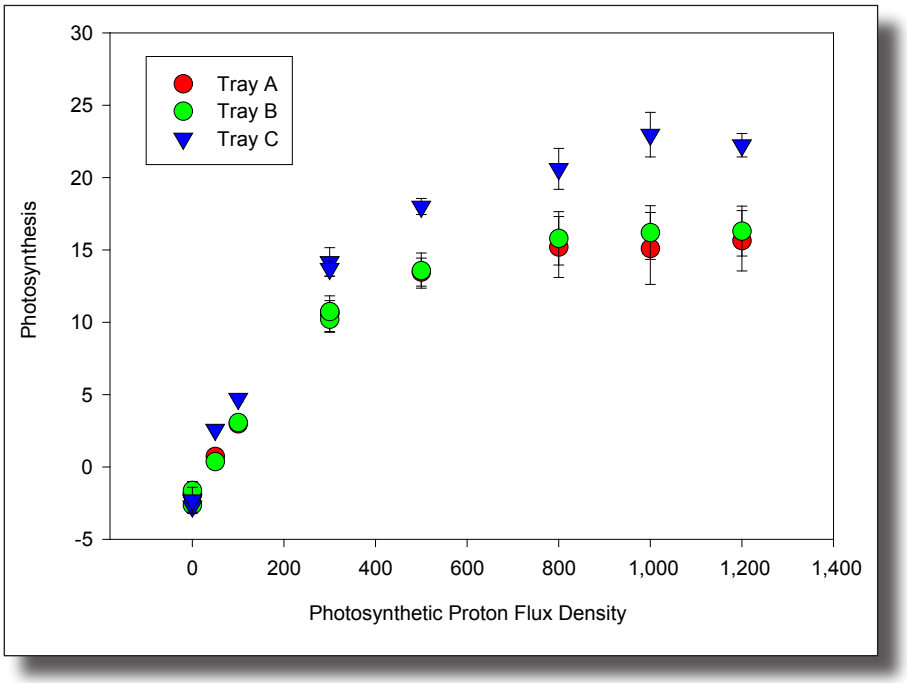

Figure 1. Rate of photosynthesis for wheat plants grown at three water availabilities.

morphological measurements was taken on representative plants from each treatment. Photosynthesis, fluorescence, and conductance measurements were taken on three leaves from each tray, using a LiCor 6400 portable photosynthesis system. An ASD Field Spec Pro was used to make reflectance measurements on each of the 12 leaves taken from each tray for the above set of measurements. Pigment extractions were analyzed using a spectrophotometer (Beckman DU 640) to determine the pigment concentration.

No differences in chlorophyll concentrations were found among the three water availabilities. Although differences were found in height growth, photosynthesis, and percentage moisture, reflectance was found to be correlated only to photosynthesis.

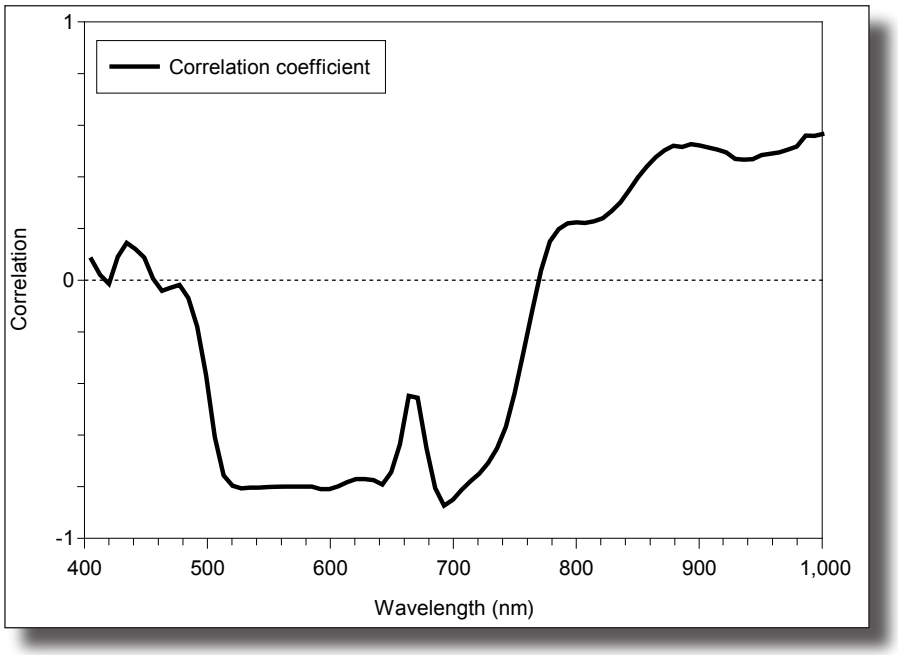

Figure 2. Correlation between photosynthesis and reflectance.

Using noninvasive techniques, we were able to detect small differences in physiology and morphology among plants grown at differing water availabilities. Plants grown with the most available water showed more signs of being water-stressed than plants grown with less water, likely because of waterlogging. They showed lower photosynthetic rates (Figure 1) and higher fluorescence and reflectance but still had the highest percentage moisture and exhibited greater height growth than plants grown with the least amount of available water.

The treatments with more available water had higher levels of reflectance. Significant negative correlations between reflectance and photosynthesis were found in two sections of the spectra (Figure 2): a section associated with red, green, and yellow light, as well as a section associated with fluoresced light (approximately 715 nm). Lower reflectance is generally a sign of higher photosynthesis rates as the plant uses more light energy. As the rate of photosynthesis increases, the reflectance of the plants decreased. These differences could be seen in the negative correlation between rate of photosynthesis and reflectance. The data collected indicated that the green-yellow and red wavelength regions, as well as the region near 700 nm (fluoresced light), may be used for remotely determining the status of plants.

Contacts: Dr. Raymond M. Wheeler <Raymond.M.Wheeler@nasa.gov>, NASA KT-B1, (321) 861-2950; and Carlton R. Hall <Carlton.Hall-1@ksc.nasa.gov>, Dynamac Corporation, DYN-2, (321) 476-4101

Participating Organization: Dynamac Corporation (Tammy E. Foster)

Bioluminescent Monitoring System for Opportunistic Pathogens in the Spacecraft Environment

Remote Plant/ Microorganism Health Sensing

The subject luminescent biosensor systems use a bacterial bioreporter that responds to a specific chemical in the environment, the autoinducer acyl-homoserine lactone (AHL), with the response manifested by the production of visible light at a wavelength of 490 nm. Genetic construction of the bacterial bioreporter consists of the *lux* operon, derived from the marine bacterium *Vibrio fischeri*. The *lux* operon contains five genes, *luxA, B, C, D,* and *E*, where *luxAB* produce luciferase and *luxCDE* produce an aldehyde substrate. Inclusion of the entire operon within the bioreporter bacterial strain allows for intrinsic whole-cell bioluminescence without the addition of any exogenous chemicals or cofactors. This project focuses on the development of a suite of four bacteriophage-based luminescent biosensor systems for detecting and identifying opportunistic pathogens, with an end goal of deploying the bacterial bioreporters on small, disposable, microelectronic chips that will enable online real-time monitoring within the spacecraft environment.

Bacteriophages, also known as phages, are viruses that infect bacteria. Some of these viruses will only infect a certain species of bacteria, and it is this trait that is exploited for the purposes of this project. Bacteriophage-based luminescent bioreporters use the pathogen-specific phage infection as a means of inducing bioluminescence through a modified quorum-sensing signal. The *luxI* gene, which also originates from *V. fischeri*, is inserted into the genome of the phage, resulting in the production of AHL molecules upon host infection. In these bioreporter systems, the AHL molecules will diffuse into the bioreporter cells containing the *luxRCDABE* operon. These AHL molecules bind to the *LuxR* protein which is the product of the *luxR* gene, and promote transcription of the *lux* operon, thus creating bioluminescence.

The four bioreporters being developed and tested are for the detection of the following bacteria: *Staphylococcus aureus*, which causes nasal and skin infections; *Pseudomonas aeruginosa*, which proved to be the causative agent of a urinary tract infection of the Apollo 13 Lunar Module pilot and was also implicated in material degradation in the Russian Space Station; *Escherichia coli*, which has been recovered numerous times from crew members during Apollo-Soyuz missions; and *Salmonella* spp., a leading cause of food-related illnesses, which has not yet been recovered from the space flight environment but whose existence on longer manned missions is a very strong possibility. Only one strain of bacterial bioreporter is required for all four systems. This requires only the identification and genetic modification of a bacteriophage for each of the target pathogens.

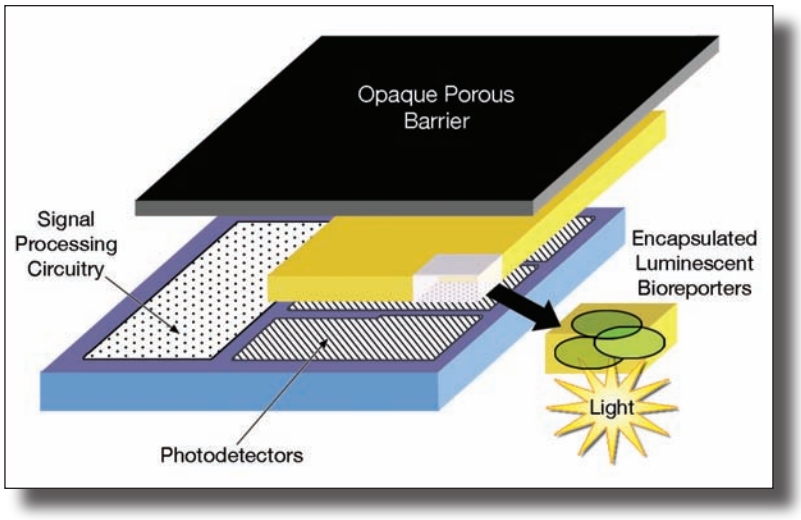

Schematic of the BBIC.

The University of Tennessee Center for Environmental Biotechnology (CEB) is responsible for the construction of the four bioreporter systems and for preliminary baseline testing. Scientists on the Life Sciences Services Contract

at KSC are responsible for the system's environmental stress testing (the majority of testing). Microbial samples have been collected both from the Orbiter 10 to 14 days preflight and from the astronaut crew quarters so the bioreporters can be exposed to pathogens from the environments in which they will be used. Oak Ridge National Laboratory is developing and evaluating the integrated-circuit optical transducer (the "microchip") on which the bioreporter system will be placed.

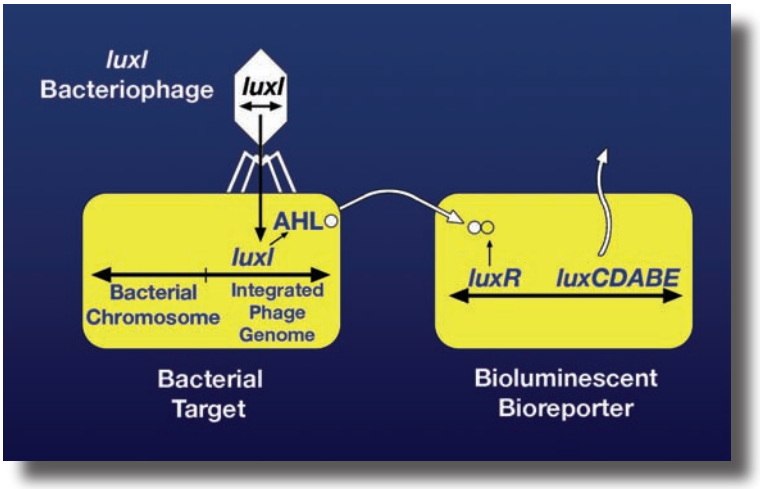

Schematic of the biosensor microbial activity.

The bioreporter system for detection of *E. coli* has been fully developed and has undergone preliminary testing at the CEB for the single *luxI* phage. Extensive environmental testing has been completed at KSC. To boost the visible light output for the *E. coli* system, a multiple *luxI* phage was created and initial testing has been completed at KSC. The bioreporter system for the detection of *Salmonella* spp. is nearly complete, and baseline studies have been carried out that indicate its success. The bioreporter system construction for the detection of *P. aeruginosa* has been completed and initial validation testing has been completed at KSC. The bioreporter system for the detection of *S. aureus* is being developed and provides a few unique challenges because the organism is Gram-positive and AHL-resistant. The development of the microchip is continuing; however, the bacterial cells are not needed to design and test the electronic components of the chip.

Key accomplishments:

- Validated the *E. coli* single *luxI* Lambda phage bioreporter system.
- Constructed the bioreporter for the *E. coli* multiple *luxI* Lambda phage system and began the validation process.
- Constructed the bioreporter for the *P. aeruginosa* system and began the validation process.

Key milestone:

- Encapsulate respective bioluminescent bioreporter systems on an integrated-circuit optical transducer (termed a bioluminescent bioreporter integrated circuit [BBIC]) that will be capable of real-time online monitoring of pathogens within the spacecraft environment.

Contact: Dr. John C. Sager <John.C.Sager@nasa.gov>, NASA KT-B1, (321) 861-2949

Participating Organizations: Center for Environmental Biotechnology (Dr. Gary S. Sayler and Dr. Steven Ripp), Oak Ridge National Laboratory (Dr. Michael L. Simpson), Dynamac Corporation (Dr. Jay L. Garland and Michele N. Birmele), and University of Tennessee (Kathleen A. Daumer)

Bioluminescent Biosensors for Monitoring Volatile Organic Compound Contaminants in the Spacecraft Environment

Remote Plant/ Microorganism Health Sensing

Air contamination within a closed spacecraft environment presents a credible health hazard to the astronaut crew during long-duration space flight. Volatile organic compound (VOC) contaminants are a vital concern since prolonged and excessive exposure could lead to critical physiological problems for the crew.

Effective air quality monitoring of the spacecraft habitat is necessary to properly manage the risks of VOC exposure to crew health and safety. Current technologies for monitoring VOC contaminants in the International Space Station have had limited success because of the constraints of available on-orbit power, stowage space, and crew time. In addition, the need for postflight ground analysis of samples collected during flight inhibits real-time analysis and response to mitigate the on-orbit exposure risks.

In response to these concerns, a suite of whole-cell bioluminescent biosensors, or bioreporters, is being developed for the specific detection and identification of VOC contaminants within spacecraft habitats. To create the bioluminescent biosensor, genetically engineered bacterial strains are inserted with the lux cassette, derived from the marine bacterium *Vibrio fischeri*. The lux cassette contains five genes: *luxA, B, C, D,* and *E*. By including the entire gene cassette, whole-cell bioluminescence can be achieved without the addition of any exogenous substrate. For VOC-specific detection, bioreporters containing the *luxCDABE* cassette are also inserted with an inducible regulatory system that has been chosen for its specificity for the target compounds to be tested.

These biosensors, with the capability for a self-generated, VOC-specific bioluminescent signal, are mated directly to a microluminometer chip, yielding a Bioluminescent Bioreporter Integrated Circuit (BBIC). The bacterial bioreporter will generate a luminescent signal when exposed to a specific VOC contaminant. The signal is detected, quantified, and recorded by the microluminometer chip, allowing for rapid notification of a specific exposure event. The microelectronic technology employed in these biosensors will enable autonomous, low-power, real-time environmental monitoring and control of target VOCs during space flight.

To accomplish this research, a collaborative team of scientists and engineers has been assembled from the University of Tennessee (UT) Center for Environmental Biotechnology (CEB) and Electrical and Computer Engineering Departments, Dynamac Corporation at KSC, NASA Jet Propulsion Laboratory, and Micro Systems Technologies. The objective of this research is to enhance current biochip technology to support NASA's need for autonomous, deployable environmental monitoring and control devices that are conducive to the low-mass, low-power applications of space flight. Ultimately, this collaborative science and engineering effort will provide a real-time VOC contaminant monitoring and control device for prospective application

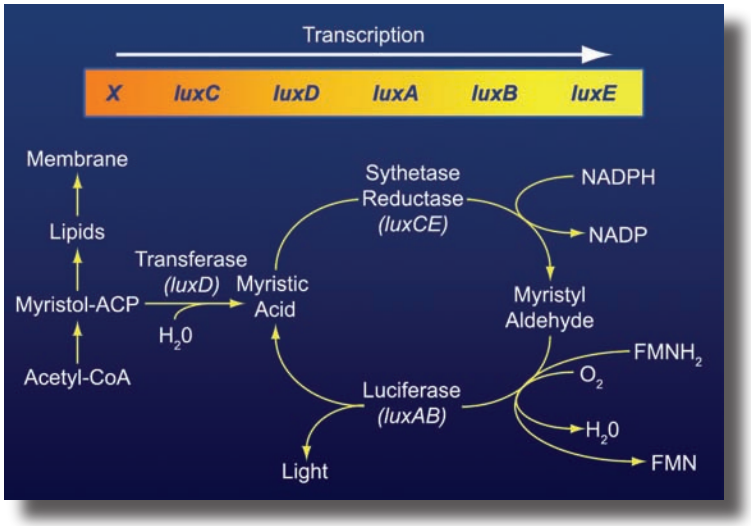

Bioluminescent response of bacterial bioreporter. Bioreporter contains an inducible regulatory system (x) that is sensitive to VOCs.

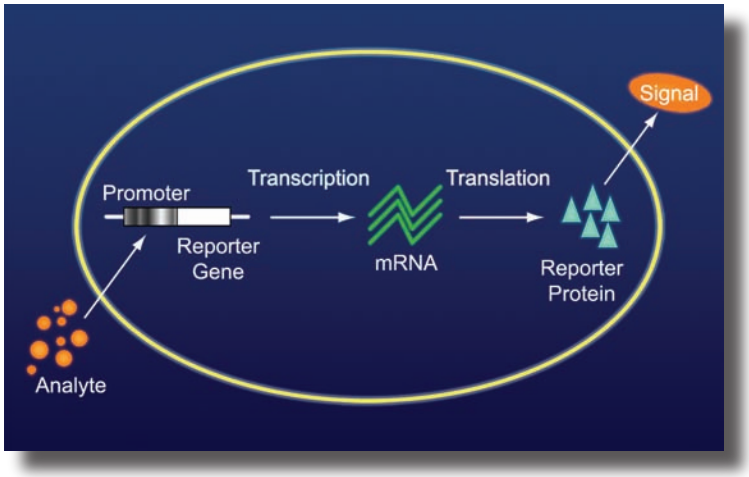

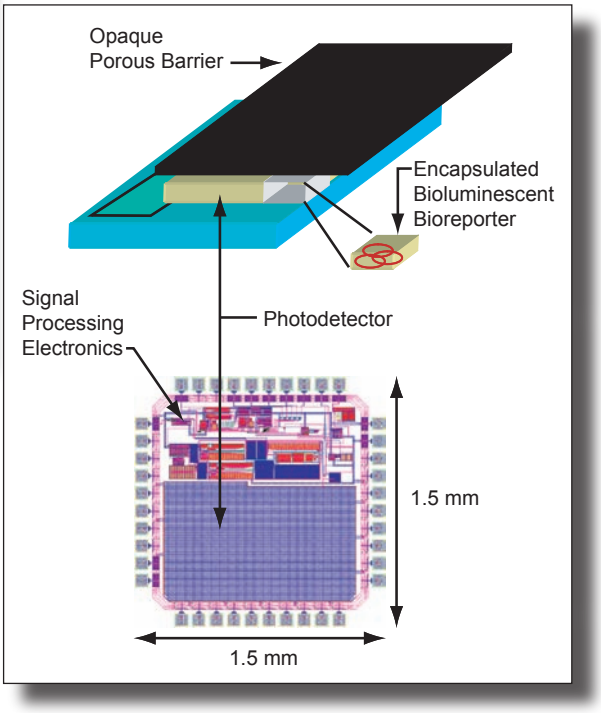

Bioluminescent Bioreporter Integrated Circuit (BBIC).

toward Technology Readiness Level 7 (system prototype demonstration in a space environment).

The CEB is responsible for the genetic construction of the bioluminescent biosensors for specific sensing of two target chemicals: formaldehyde and dichloromethane. In addition, the CEB will provide a well-characterized biosensor for toluene, to be used for initial testing purposes. These chemicals are among the high-priority contaminants that NASA wants to monitor, detect, and control in the spacecraft environment. UT's Electrical and Computer Engineering Department and Micro Systems Technologies will integrate and optimize the CEB's bioreporter systems with the microluminometer chip to create the BBIC.

The scientists with Dynamac Corporation at KSC are responsible for developing and operating novel test facilities that will be used to validate overall BBIC performance. Research at KSC will include extensive testing to quantify biosensor response characteristics of the BBIC when exposed to specific, high-priority VOC contaminants in a simulated spacecraft environment. This test facility, termed the BBIC Test Apparatus, uses a toxic-vapor generator and mass flow controllers to provide and control calibrated gas concentrations to the biosensor environment in the part-per-billion range.

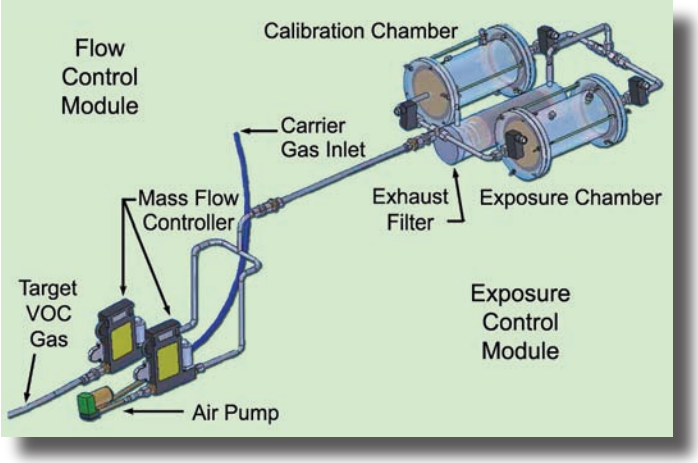

BBIC test apparatus.

Key accomplishments:

- Designed and constructed BBIC Test Apparatus.

Contacts: William T. McLamb <William.McLamb-1@nasa.gov>, Dynamac Corporation, DYN-3, (321) 861-2984; and Daniel C. Shultz <Daniel.C.Shultz@nasa.gov>, NASA DX-B1, (321) 861-2896

Participating Organizations: Dynamac Corporation (Dr. Jay L. Garland) and Center for Environmental Biotechnology (Dr. Gary S. Sayler and Dr. Steven Ripp)

Volatile-Organic-Compound Filter Cartridge for Biological Experiments in Space

2005 Center Director's Discretionary Fund Project

Remote Plant/ Microorganism Health Sensing

The accumulation of volatile organic compounds (VOCs) in spacecraft cabin air can contribute to poor air quality and threaten the health of the crew during long-term missions in space. In addition, removal of these VOCs represents an additional load on the air purification systems of the spacecraft. Furthermore, air quality also affects the quality of the science that can be carried out in spacecraft (e.g., the spacecraft maximum allowable concentration [SMAC] for ethylene is 294 ppm, but plants respond to concentrations of ethylene as low as 25 ppb). These concerns are important to NASA's goal of exploration, whereby humans and biological systems share an air supply.

Biological (plant/animal/insect) experiments in space are potential sources of VOCs that can introduce trace contaminants into the cabin air of spacecraft. Science in these biological payloads may also suffer from effects of VOCs found in spacecraft cabin air.

The project objective is to develop a VOC filter cartridge that is passive (multiple passes over absorbent) and able to reversibly bind the VOCs after long-term storage. The filter cartridge should permit identification and quantification of VOCs and meet flight safety guidelines. Project activities have spanned 2 years.

- Filter Media Characterization – Selection of a mixed-bed, multifunction absorbent and determination of the filter size and chemical specificity required to meet scrubbing limits required by plant payloads. The challenge was to find a suitable filtering medium to meet the scrubbing requirements of biological payloads in the available volume (FY 2004).
- Filter Cartridge Design – Mechanical design and sizing of the filter cartridge suited for controlling VOCs in a large plant chamber (FY 2005).
- Efficacy Testing – Performance testing of a prototype reusable VOC filter in ground-based plant experiments (FY 2005).

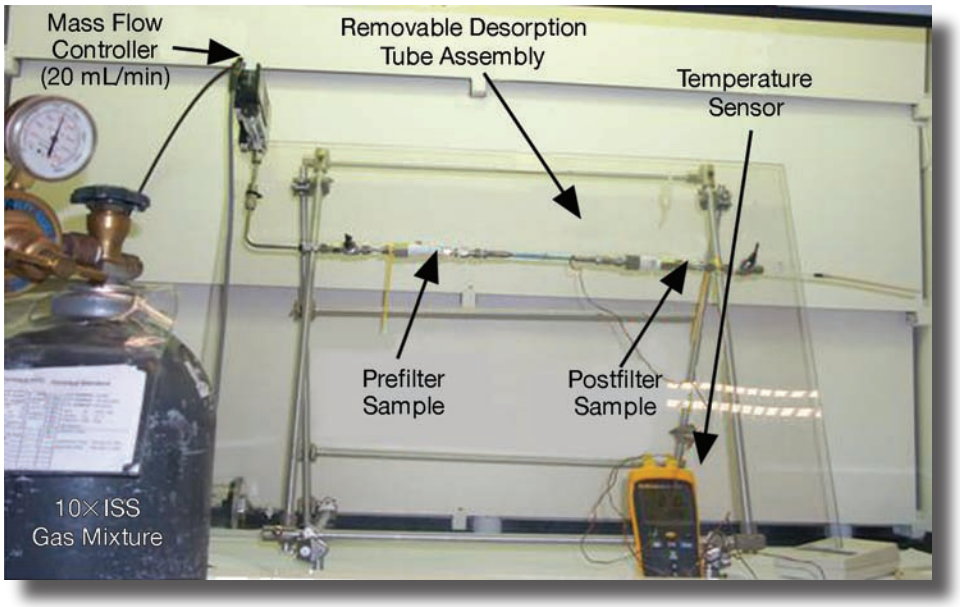

Benchtop system for VOC filter media characterization.

Key accomplishments:

- Characterized the adsorption properties of five thermally desorbing compounds, using seven major VOCs found in International Space Station air.
- Developed the techniques to measure rates of emission of plant-produced VOCs in 0.25-m^2 plant growth chambers.
- Used the emission rates and the adsorptive properties of plant-produced VOCs to select and size a suitable filter to control VOC concentrations in plant growth chambers.
- Designed, constructed, and tested the performance (via thermal desorption) of a prototype reusable ethylene filter. Ethylene is the primary VOC to be controlled in plant payloads because of its ability to elicit biological responses at very low concentrations (approximately 25 ppb).
- Conducted a test of the reusable ethylene filter in an actual 21-day plant production experiment (0.25-m^2 radish crop).
- Developed sampling methods for monitoring atmospheric concentrations in open-top chambers deployed in natural ecosystems. The same methods and analysis (expanded TO-15 EPA Method) were used to sample VOCs in the Multi-Purpose Logistics Module spacecraft.

Key milestones:

- Completed the design of a reusable VOC filter for use in biological payloads.
- Conducted an integrated method to test the efficacy of the reusable filter for controlling VOCs in an actual plant growth production setting.
- Published results of the findings and disseminated the information learned via presentations at national and international conferences.
- Supported the training of two students during the 2005 Space Life Sciences Training Program.

Contact: Dr. John C. Sager <John.C.Sager@nasa.gov>, NASA KT-B1, (321) 861-2949

Participating Organizations: Dynamac Corporation (Dr. Oscar A. Monje, Jeffrey T. Richards, and Ignacio Eraso) and NASA TA-H2-C (Dr. Timothy P. Griffin)

Plant Lighting Systems

Efficient Lighting Systems

Plants will likely be an integral part of any long-term future space mission. As part of the Advanced Life Support (ALS) program, the Biological Sciences research group is investigating the feasibility of using plants to produce food, regenerate oxygen, remove carbon dioxide, purify water, and recycle wastes to support space inhabitants. A major challenge to growing plants in space will be controlling and supplying sufficient quantity and quality of light. Conventional broad-spectrum light sources, such as metal halide and fluorescent lamps, provide an adequate spectrum for normal plant growth and morphology. However, they are not as photosynthetically efficient as low-pressure sodium lamps, high-pressure sodium lamps, or high-output red light-emitting diodes (LEDs). LEDs are a promising electric-light source for space-based plant growth chambers and bioregenerative life support because of their small mass and volume, solid-state construction, superior safety, and longevity. In addition, LEDs can illuminate near the peak light absorption regions of chlorophyll while producing virtually no near-infrared radiation (which is not used in photosynthesis).

At the Space Life Sciences Laboratory, experiments using LEDs were performed with ALS candidate salad-type crops. Salad-type crops could potentially provide a portion of fresh food as well as psychological benefits to the crews aboard future space transportation vehicles. Experimental data generated with salad-type crops in the presence of light sources with various spectral qualities will provide important data for modeling and developing future missions.

A combination of red and blue LEDs has proven to be an effective and efficient lighting source for producing salad-type crops (spinach, radish, and lettuce) in controlled environments. However, plant leaves readily absorb red and blue light, so absorptance is high and reflectance is low. Therefore, even healthy plants grown under red and blue LEDs alone appear purplish gray to humans. Hence, the addition of green LEDs to red and blue LED arrays would make plants appear normal (green) to the crew. Green light may also promote plant growth since green light penetrates the plant canopy better than red or blue light. Leaves in the lower canopy could use the transmitted green light in photosynthesis. For a space mission, highly optimized lighting systems are necessary to conserve power and maximize plant growth, so supplemental green light needs to be evaluated. Research was begun to evaluate the beneficial aspects of supplemental green light on salad crops in terms of enhancing the aesthetic appeal of plants grown under LEDs and increasing light penetration in the canopy.

Work has been completed with lettuce plants grown under or exposed to different light sources to examine the effects on the stomatal conductance, a measure of the plant's ability to assimilate carbon; on dry-matter production of lettuce plants grown under a day/night cycle with different spectra; and on stomatal conductance of short-term exposure to different spectra. Lettuce plants were grown with 18-hour light and 6-hour dark periods under four different spectra: (1) red and blue LEDs (RB), (2) red and blue LEDs with green fluorescent lamps (RGB), (3) green fluorescent lamps (GF), and (4) cool white fluorescent lamps (CWF) that provided 0, 24, 86, and 51 percent of the total photosynthetic photon flux in the green region of the spectrum, respectively (Figure 1). Conductance of plants

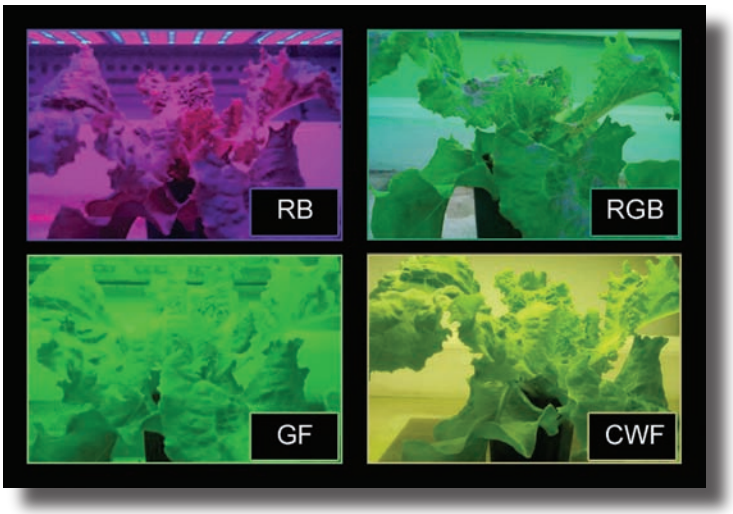

Figure 1. Appearance of a lettuce plant under different light sources: RB, red and blue LEDs; RGB, red and blue LEDs with green fluorescent lamps; GF, green fluorescent lamps; and CWF, cool white fluorescent lamps.

grown for 23 days under CWF rose rapidly on illumination to a maximum in the middle of the light period, and then decreased again before the dark period when it was minimal. However, the maximum was lower in plants grown under RB, RGB, and GF. This demonstrates that spectral quality during growth affects the diurnal pattern of stomatal conductance (Figure 2). Although stomatal conductance was smaller in plants grown under RGB than CWF, dry-matter accumulation was greater, suggesting that stomatal conductance did not limit carbon assimilation under these spectral conditions. Temporarily changing the spectral quality of the plants grown for 23 days under CWF affected stomatal responses reversibly. This study provides new information showing that stomatal conductance is responsive to spectral quality during growth and, in the short-term, is not directly coupled to dry-matter accumulation. Further studies are needed to determine required levels of green light for optimal plant growth, and more tests with different green peak wavelengths (using green LEDs) and red and blue LEDs would be useful in determining a green-light response spectrum. These findings could then be used to design spectrally balanced LED systems for supporting optimal plant growth in space while enhancing the aesthetic appeal of the plants.

Figure 2. Measurement of stomatal conductance with a lettuce plant using a steady-state porometer.

Key accomplishments:

- 1999: Began experiments growing salad-type plants with LEDs and microwave lamps.
- 2000: Completed initial salad-type plant growth studies with LEDs and microwave lamps. NASA Research Announcement Solicitation 98-HEDS-01 grant to Dynamac Corporation (Dr. Gregory D. Goins) was extended through 2001.
- 2001: Began experiments with mixtures of salad-type plant species to compare the growth of multiple crops in a common environment/hydroponics system. Testing included characterization of photosynthetic reaction center stoichiometry (photosystem I versus II) in response to light quality.
- 2002: Began experiments to evaluate the beneficial aspects of supplemental green light on salad crops in terms of increasing light penetration in the canopy and enhancing the aesthetic appeal of plants grown under LEDs.
- 2003: Completed initial plant growth and development studies with supplemental green light.
- 2004: Completed the stomatal conductance study of lettuce plants with supplemental green light at different levels.
- 2005: Continued to evaluate supplemental green light at different levels to determine the photobiological effects on salad crops.

Contacts: Dr. John C. Sager <John.C.Sager@nasa.gov>, NASA KT-B1, (321) 861-2949; and Dr. Raymond M. Wheeler <Raymond.M.Wheeler@nasa.gov>, NASA KT-B1, (321) 861-2950

Participating Organizations: National Research Council (Dr. Hyeon-Hye Kim), Dynamac Corporation (Neil C. Yorio and Stacy N. Gordon), and North Carolina A&T State University (Dr. Gregory D. Goins)

Membrane Filtration for Water Recovery and Recycling

Water recovery and recycling is an important consideration for reducing payload during long-term space missions. One of the processes currently being evaluated for closed-loop water recovery and recycling incorporates the Aerobic Rotational Membrane System (ARMS). ARMS is a novel compact membrane bioreactor that converts ammonia to nitrates. The rotating hollow-fiber membrane module provides mixing to maintain high mass-transfer rates between the bulk liquid and the biofilm. Membrane filtration processes can be used for downstream treatment of the bioreactor effluent. Interfacing a membrane filtration system with a bioreactor requires both treatability and operational compatibility assessment to ensure that the final effluent meets the required water quality standards with minimum or no significant membrane fouling within the anticipated operating conditions. Previous experimental studies focused on the performance of membrane filtration systems from effluent quality perspectives. The filtration experiments conducted with different membranes showed that microfiltration did not provide significant quality improvement and it is necessary to use nanofiltration or reverse-osmosis systems for downstream treatment of the bioreactor effluent.

Extracellular polymeric substances (EPS) are large-molecular-weight compounds that are excreted by bacteria. Because of their flexible molecular structure (similar to gel) and strong adhesive characteristics, EPS play an important role in biofilm development and behavior, especially for attachment, detachment, and protection against environmental stress factors. Since EPS exhibit self-assembly characteristics, they can initiate and develop a highly hydrated gel matrix on surfaces where the microbial cells can attach and establish a stable consortium.

Design and operational aspects of interfacing membrane filtration systems with the aerobic bioreactor are currently being investigated. Although the membrane systems can significantly improve the water quality of the ARMS effluent, the EPS may cause fouling, especially during intermittent filtration conditions. Preliminary experiments were completed to assess the fouling potential of the ARMS effluent. Microtopographical images of the membrane surfaces were captured by an atomic-force microscope (AFM) to assess the rate of membrane fouling and flux recovery during intermittent filtration conditions.

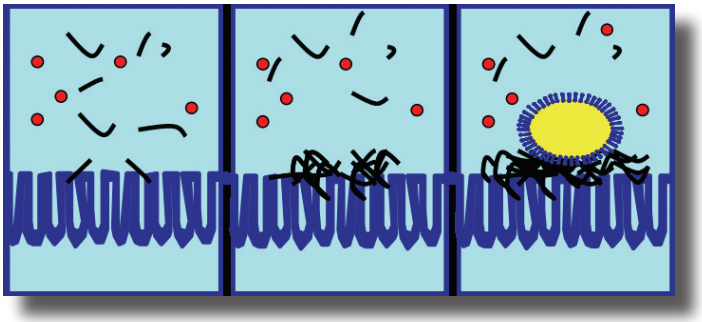

Role of EPS in biofouling.

Crossflow filtration test cell.

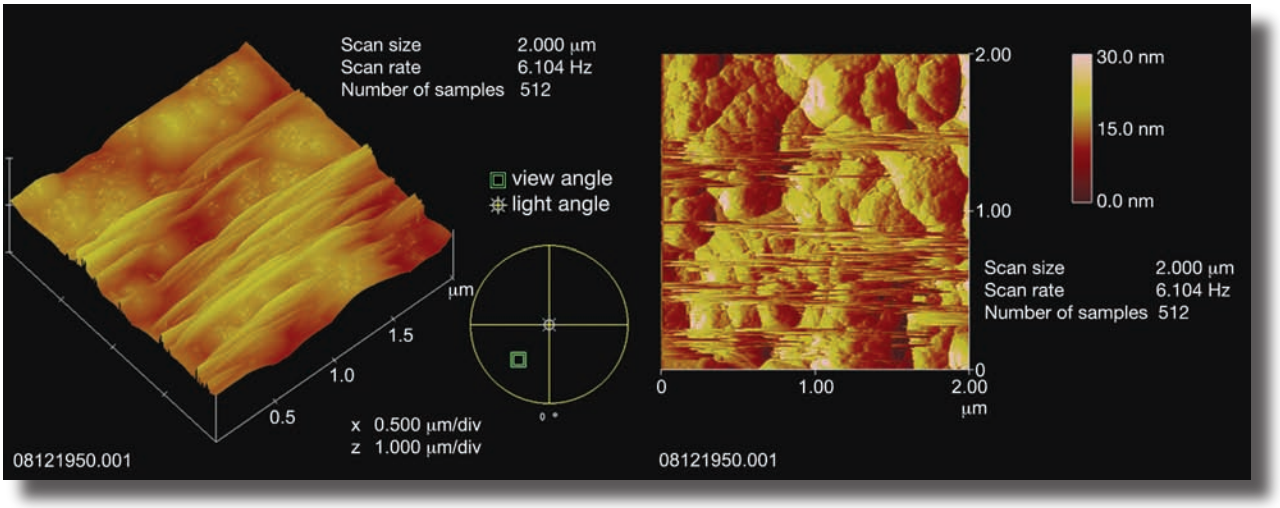

Visualization of membrane fouling by AFM.

Analyses of the microtopographical images indicate that contamination of the membrane surface begins immediately during the filtration process. However, crossflow filtration conditions limit the formation of a stable film on the membrane surface. A significant and rapid flux recovery was observed after each intermission during the test runs.

Key accomplishments:

- 2004: Evaluated performance of different membranes for improving the quality of ARMS effluent.
- 2005: Conducted intermittent filtration tests for microtopographical evaluation of membrane fouling.

Key milestones:

- Complete preliminary membrane screening and evaluation for effluent quality improvement.
- Collect microtopographic data to assess membrane fouling during different operating conditions.
- Correlate analytical water quality parameters with membrane-fouling characteristics.

Contacts: Dr. John C. Sager <John.C.Sager@nasa.gov>, NASA KT-B1, (321) 861-2949; and Dr. Raymond M. Wheeler <Raymond.M.Wheeler@nasa.gov>, NASA KT-B1, (321) 861-2950

Participating Organizations: Florida International University (Dr. Berrin Tansel) and Dynamac Corporation (Dr. Jay L. Garland)

Mapping Fire Scars in Fire-Adapted Vegetation at KSC

After NASA acquired the land on Merritt Island, Florida, in 1962, fire suppression remained in effect on KSC until 1981. This altered structure and landscape pattern and also damaged habitat for many plant and animal species. The population of Florida scrub-jay, an endangered indicator species, has experienced a dramatic decline. Restoration of the native vegetation became a major task for KSC natural-resource managers.

Since 1981, vegetation at KSC has been frequently burned by prescribed fires. Mapping when and where fires occurred in the past is critical for improved understanding of the relationships between landscape structure and fires. This updated knowledge can be applied for adaptive management of natural resources at KSC. The objective of this study is to develop a reliable remote sensing approach to accurately map burned areas in the vegetation at KSC.

The computer experiment includes feature selections and image data classifications. The best features to use with the Landsat Thematic Mapper (TM) data acquired in April 1987 are Principal Component (PC) 3, TM band 4, Tasseled Cap (TC) 2, and Normalized Difference Vegetation Index (NDVI). Stacking all four features into one image data set significantly increased classification accuracy and allowed comparison to the 7 original TM features, NDVI alone, 4 PCs, 3 TCs, and all 15 features.

Fire scars are mapped with an integration of image data classification and filtering with geographic information systems. A standard classification protocol was designed, and clean and accurate fire scars were mapped.

Key accomplishments:

- Completed classification experiments.
- Designed a classification protocol.
- Completed a peer-reviewed manuscript for the *International Journal of Remote Sensing*.

Contacts: Dr. Guofan Shao <Shao@purdue.edu>, Purdue University, (765) 494-3630; and Lori N. Jones <Lori.N.Jones@nasa.gov>, NASA DX-B2, (321) 861-2916

Participating Organization: Dynamac Corporation (Brean W. Duncan)

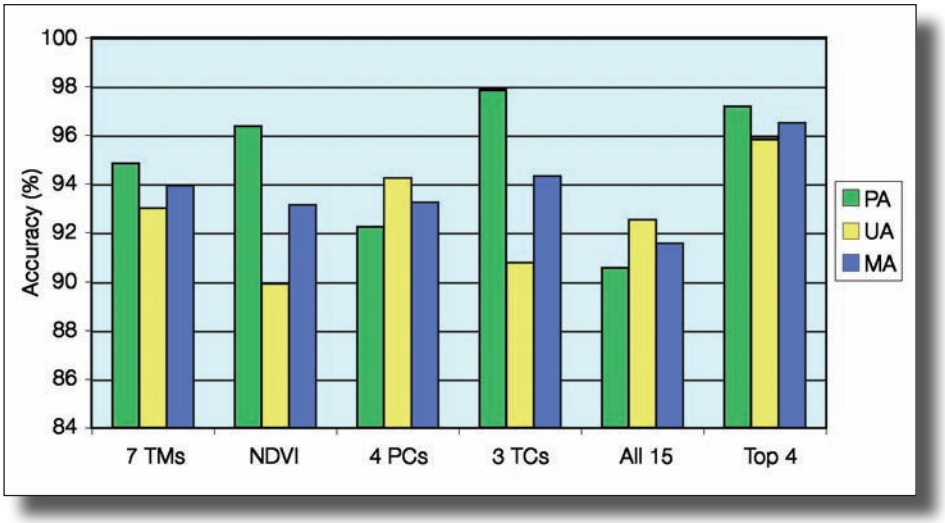

A comparison in classification accuracy (percentage) among different combinations derived from the KSC TM data set. PA is producer's accuracy, UA is user's accuracy, and MA is the mean of PA and UA.

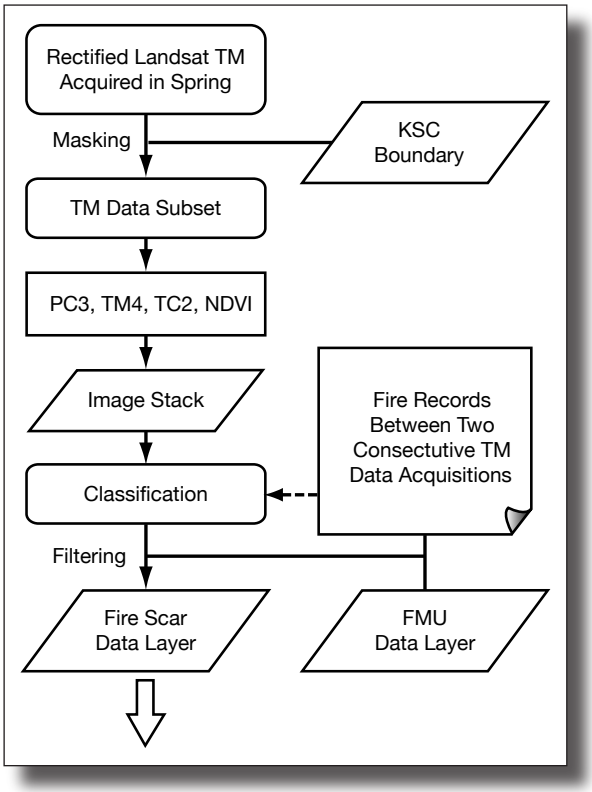

A flow chart of mapping fire-scar time series at KSC with TM data.

Fire scars (in black) mapped after filtering initial classification map with the burned fire management units (FMUs) data layer.

Micro-Electro-Mechanical-System-Based *In Silico* Cell Physiology System for Measuring Real-Time Gravity Responses in Single Cells

During early development in fern spores (*Ceratopteris richardii*), the single-haploid cells sense and respond to gravity through a mechanism that involves a transcellular calcium (Ca) ion current that opposes the gravity vector [1]. This irreversible process drives polar-axis development within the cell and was discovered using the self-referencing Ca microelectrode to measure transmembrane Ca^{2+} flux during this period of gravimorphogenesis. The self-referencing technique allows for the measurement of dynamic flux from individual cells based on computer-controlled micropositional translation and data acquisition of a single ion-selective microprobe [2]. While this technique is useful for studying electrophysiology in cells, its usefulness in researching these ion-current-signaling events is inherently limited. Specifically, we need to continually measure Ca^{2+} fluxes from multiple positions around each cell and monitor multiple cells at the same time. The ultimate goal of this work is to create new technology to advance our basic understanding of cell sensing mechanisms and electrophysiology in future NASA microgravity flight experiments.

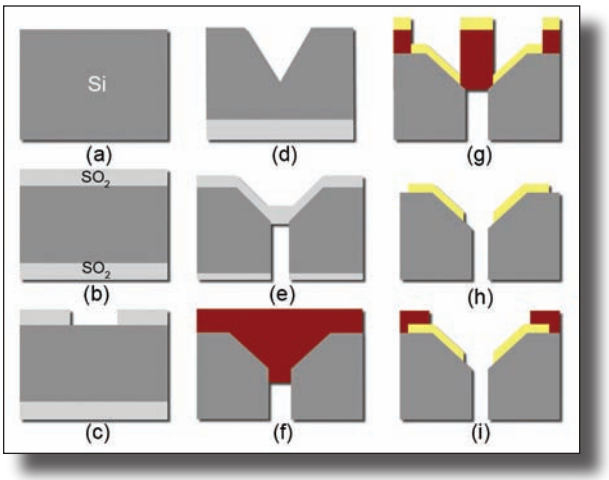

Figure 1. Fabrication process flow of the MISA chip.

With the use of current microfabrication techniques [3,4], the Microfluidic Ion Sensor Array (MISA) chip is now being fabricated (Figure 1). This chip uses the concept of self-referencing Ca^{2+} ion detection probe technology [2], but with the added robustness of solid-state sensors. It allows for real-time measurements of multidimensional Ca flux, using four separate electrodes for each of 16 individual fern spores. The chip consists of 16 pyramidal cells (150 μm^2) formed by a self-terminating potassium hydroxide etch. Each cell has four silver electrodes that have their surfaces modified (from silver [Ag] to silver chloride [AgCl]) by treatment in 1M hydrochloric acid for 1 hour. The electrodes are also coated with an ionophore (ETH-5234)-based, Ca^{2+}-selective membrane to impart ion selectivity. These electrodes are positioned at the four poles of the cell, ensuring that the electrodes come within 10 to 15 μm of the poles of the fern spore. Every cell has a microfluidic port to control fluid flow. The solid-state sensor array was tested and calibrated against an external Ag/AgCl reference electrode inserted into the cell (Figure 2).

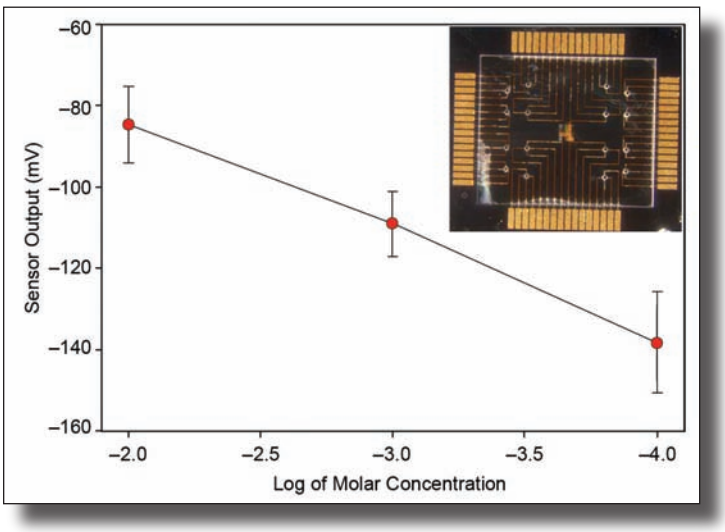

Figure 2. Circuit diagram of a noninverting amplifier that will be used to measure the output of each of the 64 electrodes on the MISA chip.

The MISA chip will be mounted on a printed circuit board that will perform onboard amplification and have an interface with a 32-channel, 18-bit data acquisition unit. The amplification unit consists of 64 precision operational amplifiers with very low noise and drift. The operational

amplifiers are arranged in noninverting configuration (Figure 3) with a gain of 20 and placed close to the chip to reduce noise susceptibility. A stable external power supply of ±10 V provides sufficient resolution for accurate measurement. The data acquisition unit uses a 512-cross-point matrix in a dual, 8×32, one-wire configuration that reads 16 sensors at a time in differential mode. This approach measures the concentration gradient between any eight pairs of electrodes at once and is referred to as the dual-electrode differential coupling. This technique is unique in that the working electrode is referenced against another working electrode, allowing for relative concentration measurements. This permits direct monitoring of transcellular flux by pairing electrodes at opposite poles of the cell.

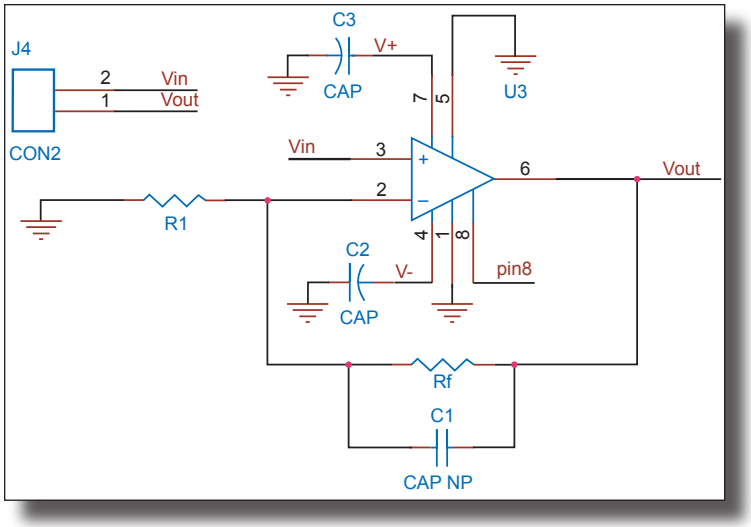

Figure 3. Calibration curve of solid-state calcium electrode array.

The data acquisition system (Figure 4) is accessed by software written in LabVIEW. The software can display any one differential (e.g., top-bottom, left-right) for all cells, all six differentials for two cells, and the Ca flux at the top, right, bottom, and left for two cells. The Ca flux in each position for each cell can also be displayed graphically using a color scale to indicate the magnitude and direction of the flux. A custom scan list can be created that displays eight user-defined differentials. While this project is focused on developing unique technology for basic research, we anticipate that this type of cell physiology lab-on-a-chip can be modified for any number of applications in biomedical and pharmacological research.

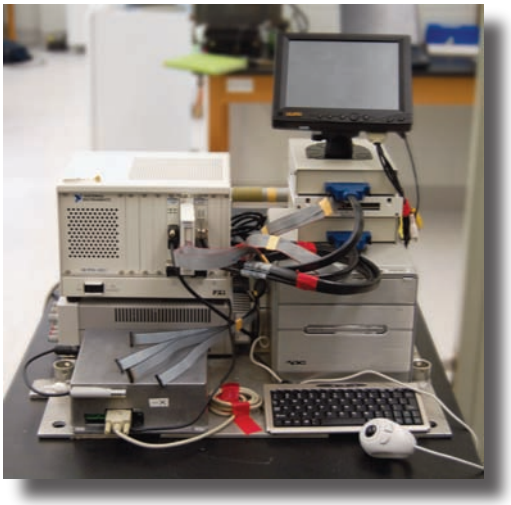

Figure 4. Assembly of the data acquisition system components for microgravity experiments. The system also includes an accelerometer and sensors for temperature and atmospheric pressure.

References

[1] A. Chatterjee et al., (2000), *Planta*, 210: 607–610.
[2] D.M. Porterfield, (2002), "The use of microsensors for studying the physiological activity of plant roots," in Y. Waisel, A. Eshel, and U. Kafkafi (eds.), *Plant Roots: The Hidden Half*, 3rd ed., Marcel Decker, New York, 333–347.
[3] A. Hierlemann et al., (2003), "Microfabrication techniques for chemical/biosensors," *Proc. IEEE*, 91: 839–863.
[4] O.T. Guenat, (2005), "Microfabrication and characterization of an ion-selective micro electrode array platform," *Sensors and Actuators B*, 105: 65–73.

Contacts: William T. McLamb <William.McLamb-1@ksc.nasa.gov>, Dynamac Corporation, DYN-3, (321) 861-2984; and Daniel C. Shultz <Daniel.C.Shultz@nasa.gov>, NASA DX-B1, (321) 861-2896

Participating Organizations: Purdue University (Aeraj ul Haque, Andrew R. De Carlo, Dr. Steven T. Wereley, and Dr. D. Marshall Porterfield), Bionetics Corporation (Howard W. Wells), and University of Texas at Austin (Dr. Stanley J. Roux)

Process and Human Factors Engineering Technologies

Process and Human Factors Engineering Technologies include research and development of innovative tools and technologies to improve manufacturing and launch site operations safety, efficiency, and effectiveness. Spaceport and range systems have many unique aspects that require development of advanced process, human factors, and industrial engineering technologies. Process and Human Factors Engineering emphasizes the interfaces among people, processes, and hardware/software systems in specific work environments. Process and Human Factors Engineering focuses on the science of process improvement and optimization of the operational phases of complex systems, including current and future space transportation systems. The overall goal of Process and Human Factors Engineering is to develop and apply technologies for designing, implementing, improving, and managing safe and efficient processes, tasks, systems, and work environments that can be quickly adapted to the changing needs of our spaceport and range customers.

The following are the fundamental principles of Process and Human Factors Engineering:

- All work activities can be represented as processes.
- All processes involve humans.
- All processes can be improved.
- Processes must be measured to be managed and improved.

Process and Human Factors Engineering Technologies directly support NASA's goals of safe, reliable, and affordable space access and exploration. Technology projects develop new concepts, methodologies, processes, and/or systems that advance the state of the art in one or any combination of the following technology focus areas:

- modeling and simulation,
- human factors and ergonomics,
- task analysis technologies,
- process and operations analysis,
- life cycle systems engineering tools,
- scheduling and risk assessment technologies, and
- management support system technologies.

For more information regarding Process and Human Factors Engineering Technologies, please contact Dr. Gena Henderson <Gena.M.Henderson@nasa.gov>, NASA EA-C, (321) 867-4261, or Tim Barth <Tim.Barth@nasa.gov>, NASA KT-A, (321) 867-6230.

Power Simulation Testbed: Launch Complex 39 Safety-Critical Power Systems Interactive Digital Maps

Task/Process Modeling and Simulation

The Power Simulation Testbed project relies on a series of events and human decisions to plan and support missions, configure electrical systems, conduct studies, and perform spaceport operations analysis. The objective is to develop a unique suite of simulation models running on the Virtual Testbed (VTB) platform to help electrical-system planners assess the dynamic electrical system and its operational impact. This suite of simulations can help analyze the KSC electrical infrastructure by feeder, by substation, or by the entire network and show its connections to critical systems.

This VTB collaborative computing environment may be used to deal with such scenarios as

- evaluating contingencies to avoid launch delays and hazards,
- generating and validating cost estimates and potential designs,
- accessing information directly from the Supervisory Control and Data Acquisition System (SCADA) or the KSC Geographic Information System (GIS),
- identifying and scheduling electrical maintenance and safety activities to support launches, and
- finding and assessing the impact of damage to electrical infrastructure, improved facility design, and security.

The Power Simulation Testbed will use the following modeling and simulation technologies and developments:

- parallel and distributed Web-based simulation,
- complexity and system-of-systems theories,
- network simulation and analysis,
- GIS,
- 3-D mapping technologies based on laser, such as polarimetric imaging laser radar, and
- information technology security.

For the past year, a team from NASA, the University of Central Florida, and Space Gateway Support (SGS) has focused on electrical-system issues and feasibility studies required to conceptualize and design electrical system architectures capable of handling the different demands. The planned system prototype of the KSC launch pads, using a high-level architecture, has the following objectives and deliverables:

- demonstrate the capabilities of a future electrical system by providing a basic tool for engineers,
- provide a software platform using GIS, and
- provide an operational model of a mission-critical system located at Launch Pad 39 that uses the VTB as the integration and synchronization mechanism.

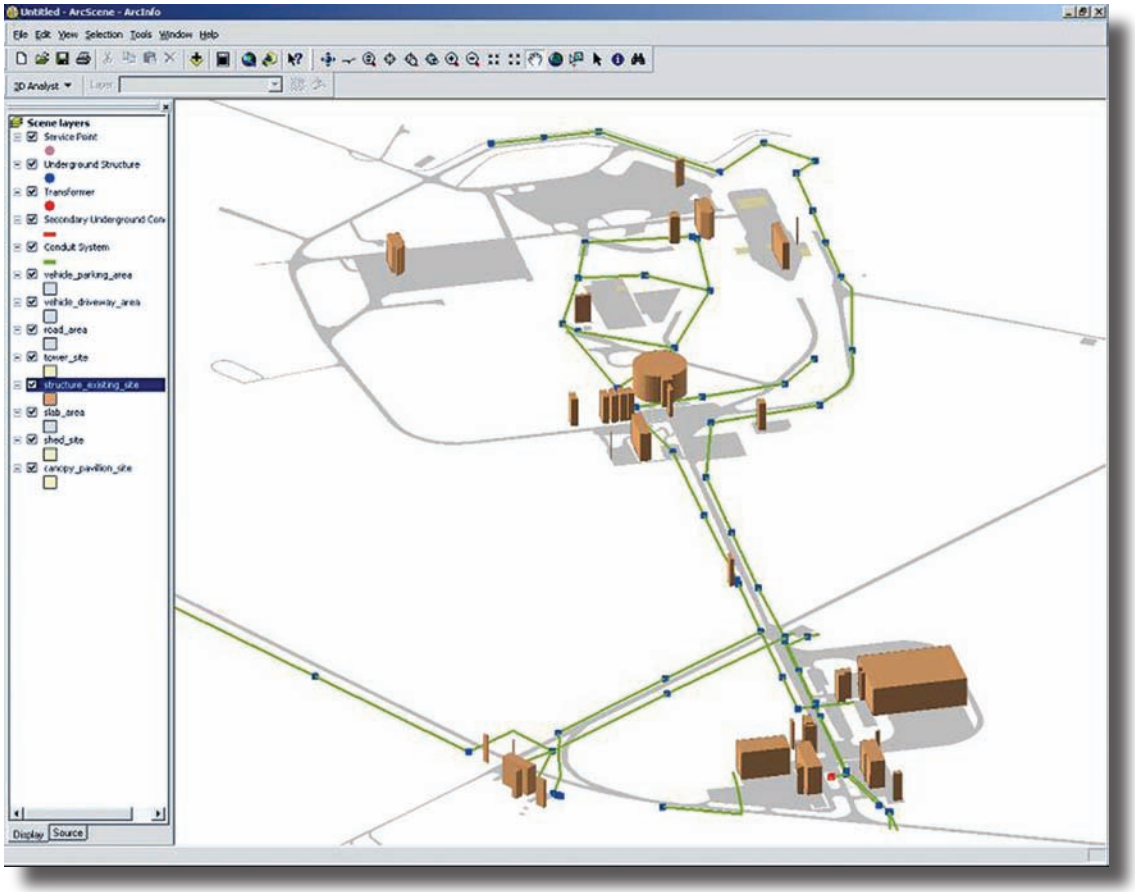

3-D map (Launch Pad 37) developed by SGS (using ArcFM) that shows the typical facilities associated with a launch complex.

The following specific tasks are envisioned:

- acquire software and resources,
- map the primary electrical system to GIS,
- map the secondary electrical system for one mission-critical system (e.g., Environmental Control System) from Launch Pad 39B,
- complete 3-D modeling,
- develop a preliminary discrete-event simulation (DES) model,
- develop a VTB interface for DES and ArcFM, and
- complete verification and validation report, training, security, and lessons learned.

Key accomplishments:

- FY 2005: Built coalition and completed initial assessment report.

Contact: Robert Turner <Robert.Turner@nasa.gov>, NASA SA-E, (321) 867-6388

Participating Organizations: University of Central Florida (Dr. Luis C. Rabelo), NASA SA-B1 (Lawrence W. Salberg), NASA SA-E3 (Jeppie R. Compton), and Space Gateway Support (David A. VanAuken)

Analyzing Exploration Operations With System Dynamics

Task/Process Modeling and Simulation

NASA plans to retire the Shuttle fleet in 2010. The Crew Exploration Vehicle Launch System (CEVLS) may use some Shuttle components, but there could be a considerable interruption in component orders between Shuttle retirement and inauguration of the new program. NASA wants to analyze the effects of this interval before it happens, to improve its decisionmaking process and mitigate any disruptions in availability of critical components and skills.

The structure of a business enterprise guides its behavior, and behavior determines results. The organizational structure of NASA's Exploration Initiative—its financial procedures and supply chain—will strongly influence the interaction and behavior of multiple tiers of contractors, subcontractors, suppliers, etc. Ultimately, these interactions determine business growth, productivity, inventory oscillations, and employment levels, including possible instances of depleted stock, excess inventory, and layoffs. Cost performance and enterprise success will be determined by decisions made early in the Exploration design phase. In fact, by the time the Exploration vehicles are designed, there will be little that can be done to influence ultimate results. Statistical modeling is inadequate to project future results because it merely extrapolates historical process data into trends. It does not project well when the future is significantly different from the past or when unexpected events occur. By contrast, structural modeling projects future results by simulating the activities or operations. It does not depend on data to create the model because the flow of activities is independent of data. Data is used to tailor, calibrate, and validate model results.

System dynamics (SD) was used to model the structure of the NASA CEVLS organization and interactions among organizational components at the highest level. The models enabled scalable, quick, and risk-free analysis of options to improve management decisions.

Historically, operation of the supply chain for Shuttle components is fairly stable since it has reached steady state with nearly constant demand for product. For example, a plot of production activity and inventory levels for Shuttle component suppliers is fairly flat over the last several years. To investigate future operations, researchers used a hierarchy of SD models (Figure 1) to simulate the transition between Shuttle operations and Exploration missions using Shuttle-derived components.

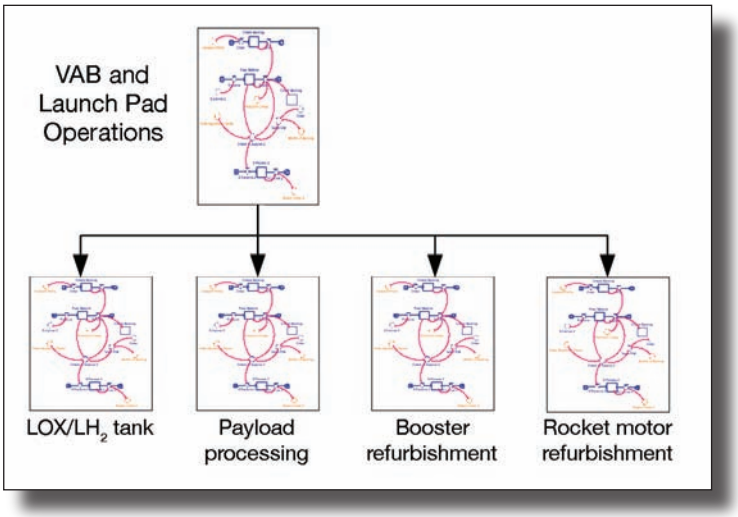

Figure 1. Hierachical system dynamics model of Shuttle/Exploration supply chain transition.

The research results quantified what may happen if there is a gap in demand between the last Shuttle launch in 2010 and the first Exploration launch. For example, Figure 2 shows how long it might take for raw-material inventory (plot 3) and element shipments (plot 5) to return to normal at the liquid-oxygen (LOX)/liquid-hydrogen (LH_2) tank vendor if demand for tanks stops for 1 year. The SD model generated graphs with wider swings in critical parameters for the 2-year interruption. Graphs for suppliers with a higher demand level also showed more volatility. In the course of the study, researchers made the following assumptions.

- Demand is constant at six launches per year.
- Any dynamics observed in the simulation are entirely due to internal activities and adjustments made to demand.
- After 2 years, demand for Shuttle operations stops for 1 or 2 years.
- The following values hold for all the entities in the model:
  - Delay for adding/removing capacity is 2 years.
  - Normal production lead time is 2 months.
  - Desired backlog for finished goods is also 2 months.
- Target raw-material inventories and finished-goods inventories are limited to eight times normal demand.

Key accomplishments:

- Studied Shuttle element usage and production dynamics.
- Developed hierarchical model of Shuttle/Exploration supply chain.
- Developed methodologies for assessment of interruptions in element demand.

Contact: Charles H. Goodrich <Charles.Goodrich-1@ksc.nasa.gov>, ASRC Aerospace, ASRC-17, (321) 867-6956

Participating Organizations: NASA DX-C1 (Edgar Z. Zapata) and ViaSim (Chris White)

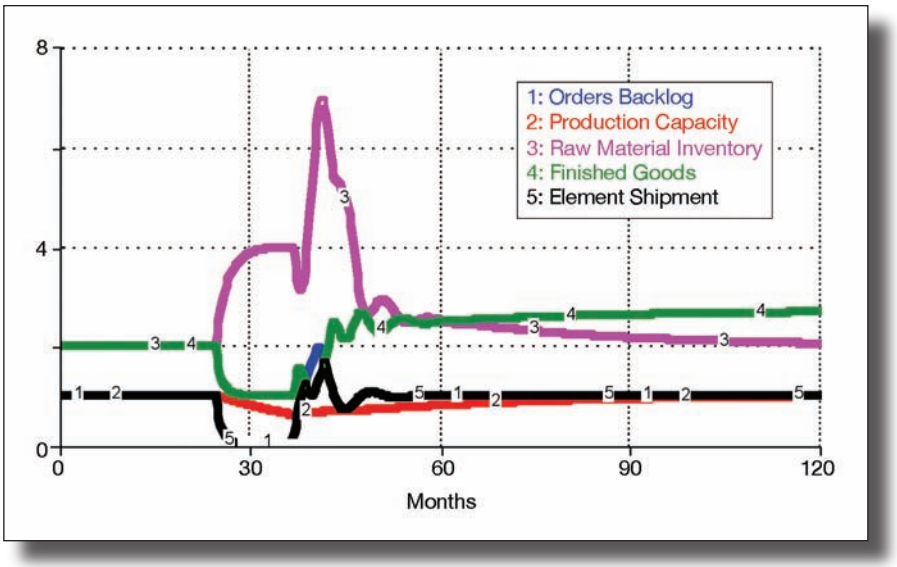

Figure 2. SD plot of LOX/LH_2 tank vendor operations with 1-year demand interruption.

Orbiter–External Tank (ET) Mate Simulation

Task/Process Modeling and Simulation

The scope of this project was to complete a simulation (kinematic) of the Space Shuttle Orbiter-ET mate. This simulation represents a horizontal and vertical transfer of the Orbiter through the Vehicle Assembly Building (VAB) and movement of major, auxiliary, and extensible working platforms. The technical challenge was to animate the models in Pro/ENGINEER (a hybrid parametric solid-modeling software) and then produce a movie using Windows Movie Maker.

The simulations were created, as mechanisms, using the Design Mechanism module of Pro/ENGINEER. These mechanisms were completed by converting static constraints to dynamic connections and placing servomotors to control degrees of freedom. A number of parts and assemblies were completed to make the simulation more realistic. An assembly model of the Orbiter Transporter System (OTS) was completed. Assemblies of the OTS Orbiter forward and aft attach fixtures, Orbiter sling, and High Bay 3 platforms were built. The following Orbiter sling parts were modeled: slide link, forward adapter, slide shoe, jack arm, cross beams, and hand wheels. Steel structure was added to the VAB model. Emphasis was placed upon completing parts and assemblies that would enhance the virtual representation of the VAB environment. Computer file size was managed by using "simplified reps and shrinkwrap." The Orbiter-ET mate mechanism assembly was then used to compare and analyze the Orbiter-to-platform critical clearance distances using different Orbiter hang angles. It was found that a 15-minute arc angle change in Orbiter hang angle affected distance at the platform critical spots as much as .550 inch.

Using Windows Movie Maker, a Moving Picture Experts Group (MPEG) film clip of the Orbiter-ET mate, which can be viewed using Windows Media Player, was developed as a training aid. This simulation may be used by ground support equipment personnel to emulate scenes and scenarios commonplace to the Orbiter-ET mate. These parts, assemblies, and mechanisms may be viewed using Product View Express (a part, assembly, and drawing viewer), Pro/ENGINEER, or Pro/INTRALINK (an engineering part and assembly management system). The movie clip, parts, assemblies, and mechanisms may be used by engineers as decisionmaking tools.

Orbiter and Orbiter sling assembly.

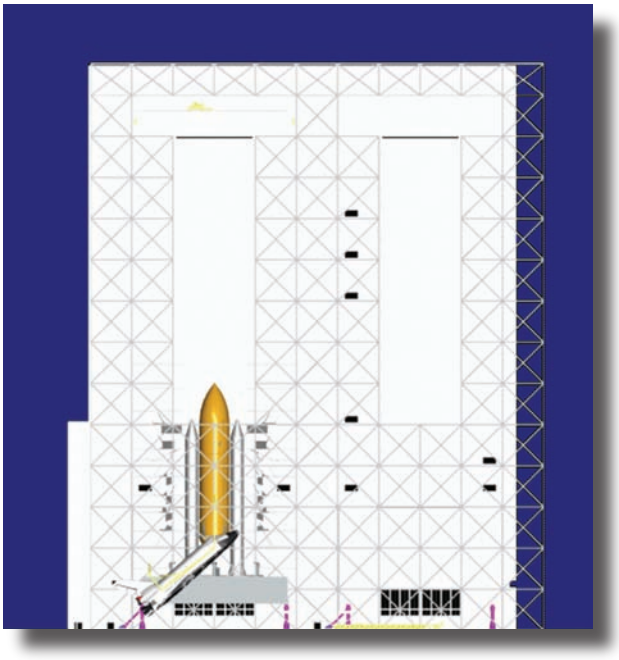

Orbiter being rotated to a vertical position.

Orbiter moved into High Bay 3.

The simulation yielded the following conclusions:

- Translation of solid models is best attempted by exporting and importing a STEP file. An IGES file may be used to export and import surfaces. These surfaces may be converted into protrusions, but some boundaries and edges may need to be fixed. These file formats represent the ISO and ANSI 3-D solid-model data exchange standards.
- Pro/INTRALINK, to which access has been established, will let engineers access a "master model" library. Parts, assemblies, and drawings may be viewed and manipulated using Pro/INTRALINK.
- A single reference or survey benchmark should be established in the VAB. All measurements should be made from this single reference point. A single reference point would allow for more accurate interpretation of data.

Contact: Jeffrey S. Brink <Jeffrey.S.Brink@nasa.gov>, NASA PH-I1, (321) 861-3619

Participating Organizations: University of Wisconsin-Stout (Dr. Gary S. Godfrey), Vaughn College of Aeronautics and Technology (Dr. Donald P. O'Keefe), Purdue University (Dr. Danny B. Wittenborn), West Virginia University (Curtis E. Groves) and NASA PH-I (Frank J. Kapr)

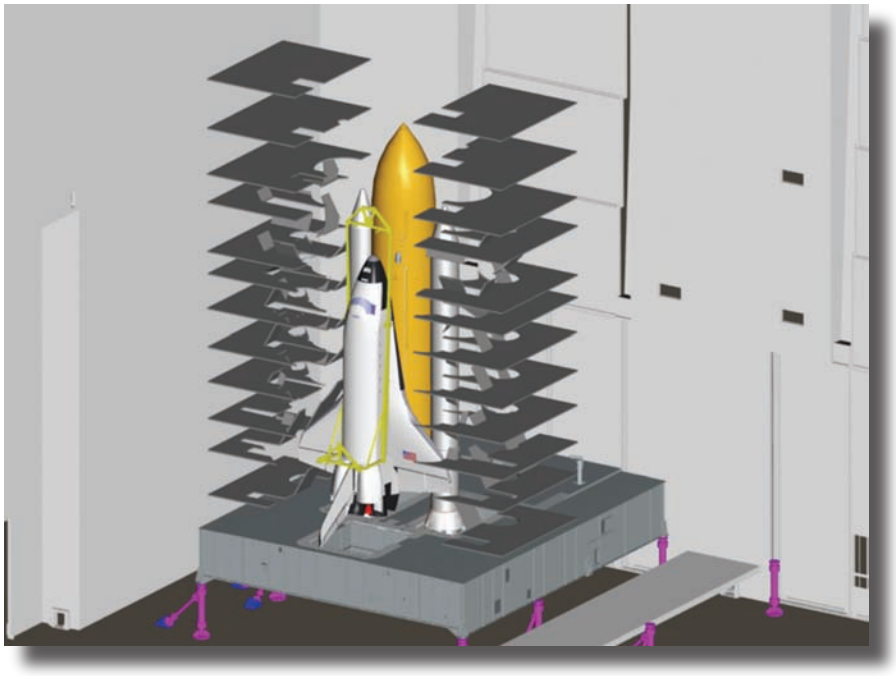

Depiction of extensible-platform clearance and crane rotation concerns.

Supply Chain Simulation: First-Ever Application of 21st Century Supply Chain Modeling, Simulation, and Analysis to Earth-to-Orbit Systems

Task/Process Modeling and Simulation

This project supports the Exploration Program challenge to grasp supply chain infrastructure issues relating to technology both credibly and early in the decisionmaking process and develops a supply chain modeling, simulation, and analysis tool. Focus in the first year is on Earth-to-orbit systems and will extend in later years to lunar and Mars applications.

As exploration operations expand farther into space, NASA must enhance its understanding of the increasingly complex supply chain movement of materials, people, and information from sources (somewhere on Earth) to destinations (somewhere in space [low Earth orbit, geostationary Earth orbit, the Moon, Mars, etc.]). Without the ability to understand, estimate, project, and affect decisionmaking relevant to the supply chain, NASA will find it increasingly difficult to work as an informed collaborator with suppliers and contractors in the development of new concepts. The cost of operating and sustaining the resulting systems will continue to grow, exceeding designated budgets. Operability and sustainability are optimized by considering the entire supply chain.

The 4-year project consists of multiple tasks that will be integrated into a capability enhancing supply chain decisionmaking. In 2005, Phase 1 of the project, the tasks included creating a graphical user interface, developing functional diagrams, developing and populating an ontology for the Exploration supply chain (a combination of the many views on diverse supply chain data), developing automation within the interface, and ultimately integrating the supply chain tool within a simulation of Earth-to-orbit launch operations ground processing.

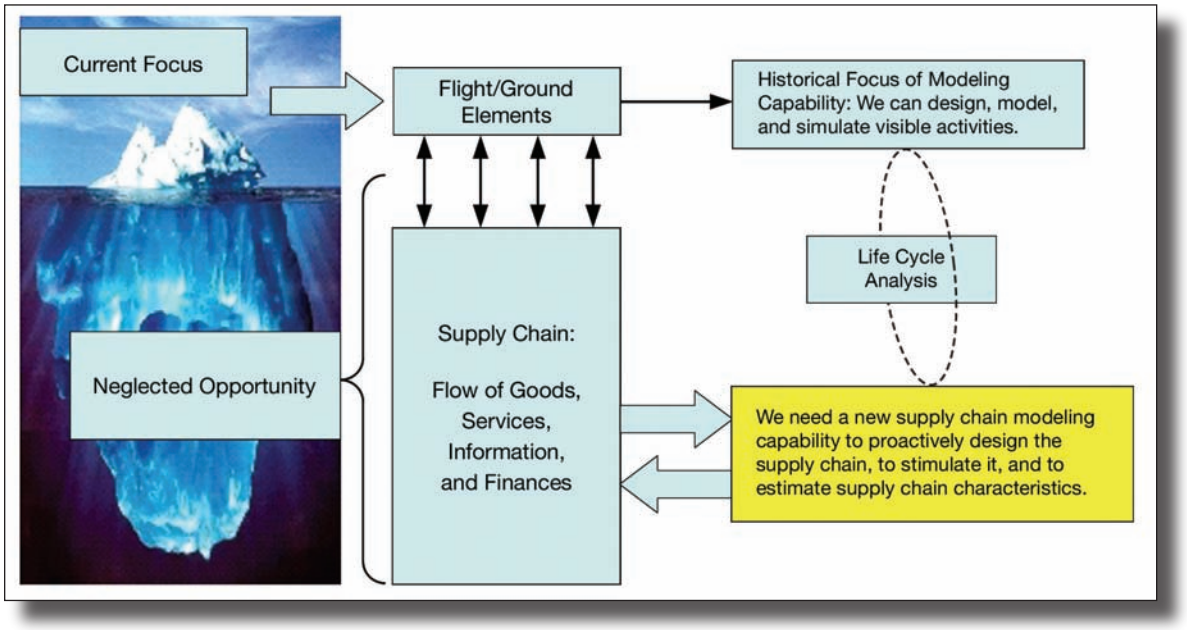

Supply chain as encompassing business process and flows—more than just integrated logistics systems implemented correctly.

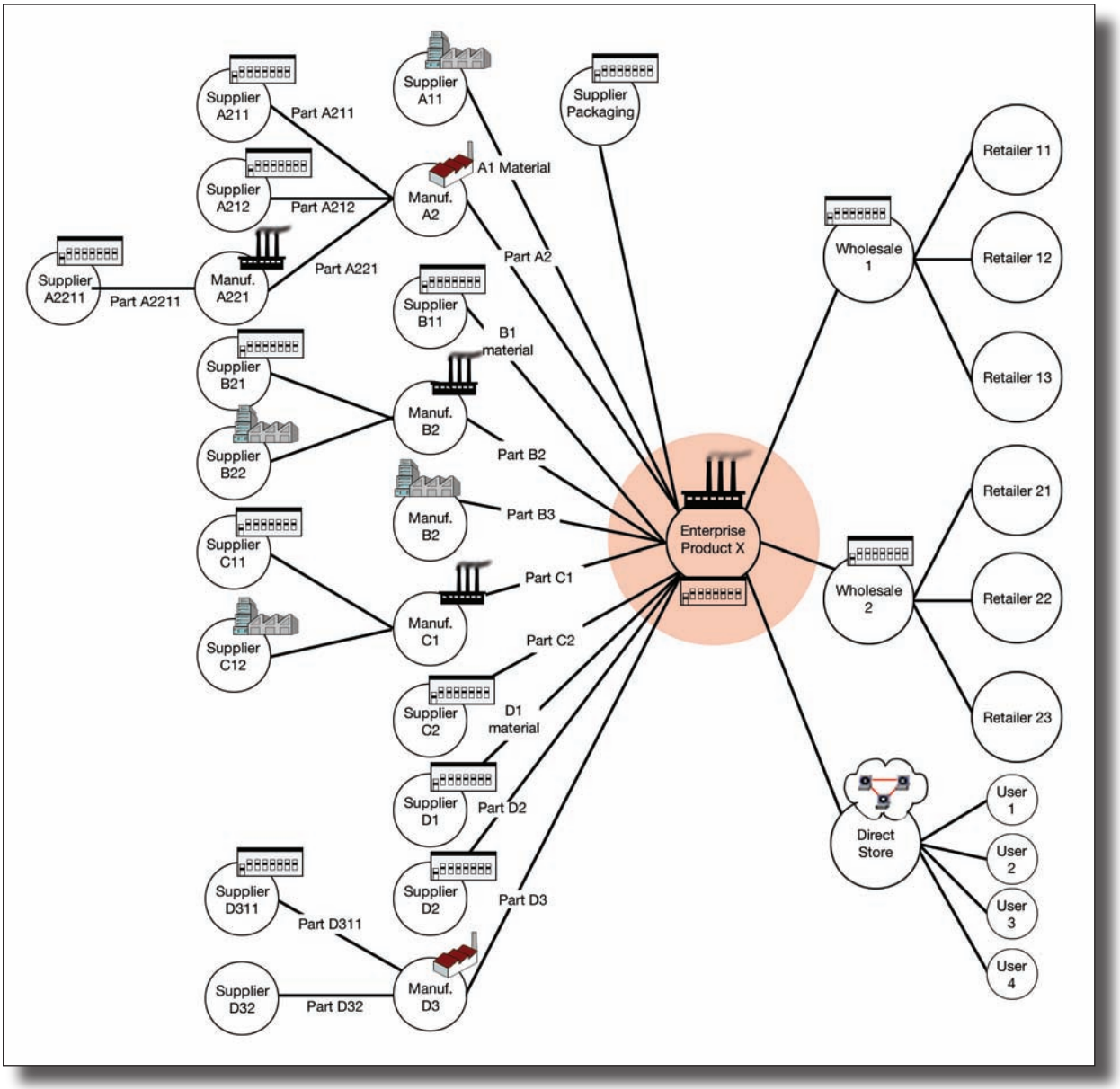

The NASA supply chain is a collection of several independent Centers, manufacturing sites, enterprises, or business units. Each supply chain entity consists of several elements that partner together to achieve specific goals by complementing one another.

This project supports KSC high-priority technology needs in process models, in this instance for analysis of ground operations enabling infrastructure processes, needs, and scope for future space transportation systems.

Contacts: Edgar Z. Zapata <Edgar.Zapata@nasa.gov>, DX-C1, (321) 867-6234; and Steve Kyramarios <Steve.N.Kyramarios@nasa.gov>, DX-B1-1, (321) 861-9172

Participating Organizations: Productivity Apex, Inc. (Dr. Mansooreh Mollaghasemi and Dr. Mohamed S. Fayez) and Marshall Space Flight Center (Dr. Michael B. Nix)

Software Quality Diagnosis and Prognosis Model

2005 Center Director's Discretionary Fund Project

Decision/Data Models and Analysis

The development of software systems will be a key component to implementing the Vision for Space Exploration. The next generation of space vehicles will rely on software to provide not only an interface for command and control, but also more intelligent applications such as autonomous operations, failure analysis/recovery, and decision support. To ensure the safety and reliability of such complex software systems, it is necessary to more precisely define, understand, and manage the quality of NASA's software development products.

A software quality model has been developed to provide a consistent representation of the various software product quality attributes and the factors that affect those attributes. This model quantifies drivers of software quality over the course of a development life cycle and produces a set of quality metrics for software products in terms of the characteristics recommended in ISO/IEC 9126: Software engineering-product quality standard. The software quality model

- diagnoses the quality of a delivered software product,
- provides a reliable prognosis (forecast) of the quality of a software product under development,
- identifies high-risk areas within a developed software product, and
- identifies the elements of the software development effort that have the most significant impact on the quality of the software product.

The software quality model uses Bayesian Belief Networks, a machine learning method, to depict the cause-effect relationships in the software development life cycle. The model's structure captures problem complexity, process maturity, and team skill/experience as drivers of software product quality. The figure is a cause-effect diagram that details the model structure used to predict specific software product quality metrics.

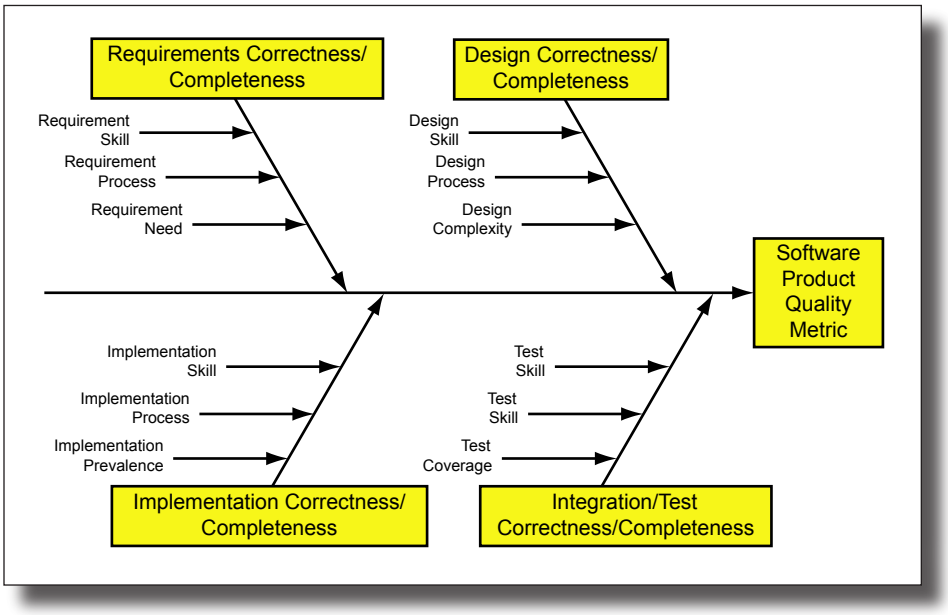

The approach to modeling a quality attribute.

Product quality metrics are affected by the correctness and completeness of the activities and artifacts at each phase of the development life cycle, which are driven by team skill/experience level, process maturity, and problem complexity at each phase.

The developed software quality model performed well in predicting 16 of the ISO/IEC 9126 software product quality metrics. The table lists the metrics used to assess the product quality of 27 software projects and validate the accuracy of the model.

The Average Relative Error (ARE) is a measure of deviation of predicted values versus actual values for the listed quality metrics. ARE values of 0.1 or less are desirable because they indicate that the values predicted by the model are within 10 percent of the actual values. In validating the developed software quality model, the ARE values in the table represent the model's predictive accuracy using software engineering data available at the conclusion of the design phase.

Modeled software quality metrics.

ISO/IEC 9126 Quality Metric	Metric Description	ARE
Access Auditability	Extent to which access logins are audited as required.	0.08
Access Controllability	Extent to which system access is controlled as required.	0.09
Data Encryption	Implementation of required encryption of data items.	0.03
Activity Recording	Extent to which data items are logged/recorded as required.	0.10
Efficiency Compliance	Compliance of system with applicable performance standards.	0.04
Failure Avoidance	Extent to which system failures were avoided as required.	0.11
Functional Adequacy	Proportion of the requirements suitably implemented.	0.05
Functional Completeness	Proportion of the requirements verified to be implemented.	0.06
Functional Coverage	Proportion of the requirements correctly implemented.	0.05
Time Behavior	Extent to which time-critical performance was met.	0.04
Input/Output Utilization	Extent to which input/output utilization budgets are met.	0.03
Reliability Compliance	Compliance of system with applicable reliability standards.	0.04
Restorability	Extent to which the system may be restored as required.	0.07
Status Monitoring	Extent to which system status is monitored as required.	0.06
Usability Compliance	Compliance of system with applicable usability standards.	0.04
User Operation Cancellability	Extent to which required user operations could be cancelled.	0.03

Key accomplishments:

- Developed a model for assessing and predicting product quality in a software development effort.
- Collected software quality data for 27 different software engineering projects.
- Verified the predictive validity of the developed software quality model for 16 of the ISO/IEC 9126 quality metrics.

Key milestone:

- Potential follow-on efforts to institutionalize the model for broader use.

Contact: Justin M. Beaver <Justin.M.Beaver@nasa.gov>, NASA DX-E1, (321) 861-2443

Participating Organization: University of Central Florida (Dr. Guy A. Schiavone)

Dual-Role Taxonomy for Categorizing Factors Contributing to Adverse Safety Events

Intelligent Work Instruction/Work Control Systems

Safety reporting systems include multiple taxonomies. A taxonomy is a structure that provides a way of classifying items into a series of hierarchical groups to make them easier to identify and evaluate. Contributing-factor taxonomies are tools used to classify the factors that contribute to an adverse safety event, including a mishap, accident, or close call. Contributing factors are selected by reporters, investigators, or independent analysts, depending on the safety reporting system being used.

Contributing-factor taxonomies have two purposes: to enable identification of all relevant factors contributing to a particular safety event, and to enable building a database of contributing-factor categories over many events to help identify and prioritize systemic problems.

A common current practice for taxonomy design is to select an existing taxonomy that appears to be a reasonable fit for a specific organization and then modify it. The lack of defined methods for systematically designing contributing-factor taxonomies has several effects. Some taxonomies are incomplete, which results in contributing factors being missed during safety reporting and incident analysis. For example, the contributing-factor taxonomy used at KSC for many years focused on individual, procedural, and training factors. Information was not collected on such contributing factors as team communication and schedule pressure. A taxonomy with a poor structure provides limited diagnostic ability to prioritize systemic problems with the database of contributing factors.

A dual-role taxonomy of contributing factors was successfully developed and tested with Shuttle Processing data. The dual-role taxonomy, when combined with an influence chain approach to identifying relationships among contributing factors, is a powerful tool to evaluate systemic safety issues and corrective/preventive actions.

Key accomplishments:

- 2002: Completed comparative analysis of key contributing-factor taxonomies.
- 2003: Developed dual-role taxonomy.
- 2004: Developed influence chain methodology.
- 2005: Completed prototype mishap analysis tool with applications to Shuttle Processing. Applied results to Exploration Systems through NASA Taxonomy Working Group.

Key milestones:

- 2006: Test and further refine the mishap analysis tool.
- 2007: Apply the tool to significant historical NASA events and other organizations.

Contact: Tim Barth <Tim.Barth@nasa.gov>, NASA KT-A, (321) 867-6230

Participating Organizations: University of Central Florida (Dr. Julia J. Pet-Armacost and Dr. Robert L. Armacost) and NASA Ames Research Center (Dr. Barbara G. Kanki)

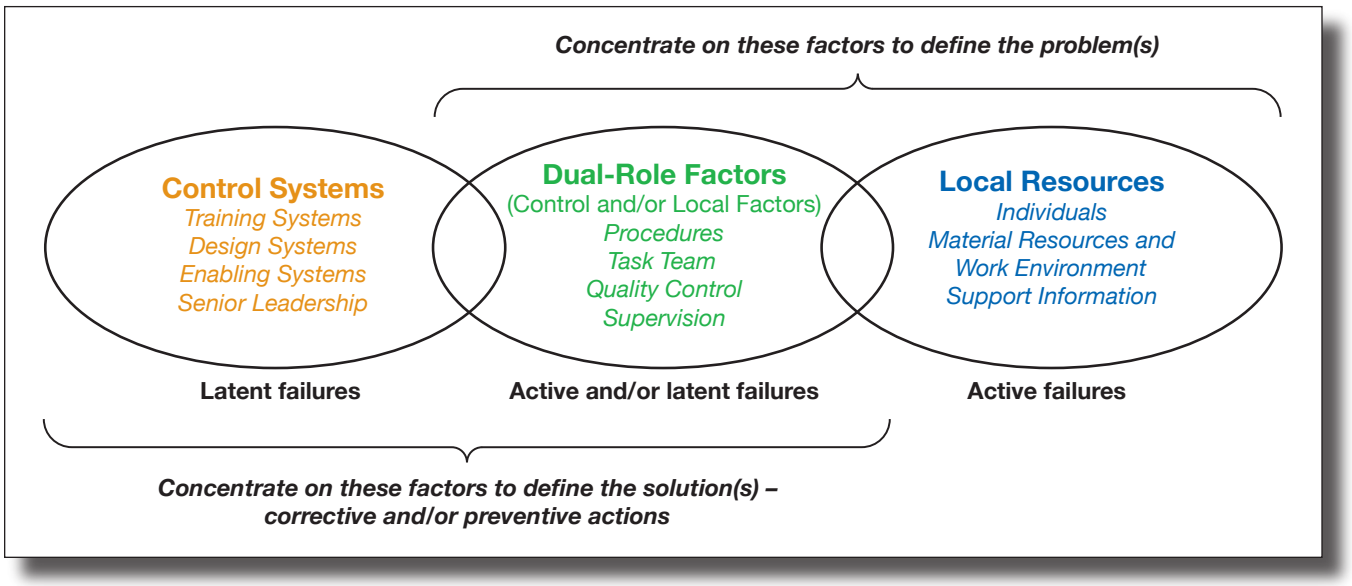

Dual-role model of organizational systems.

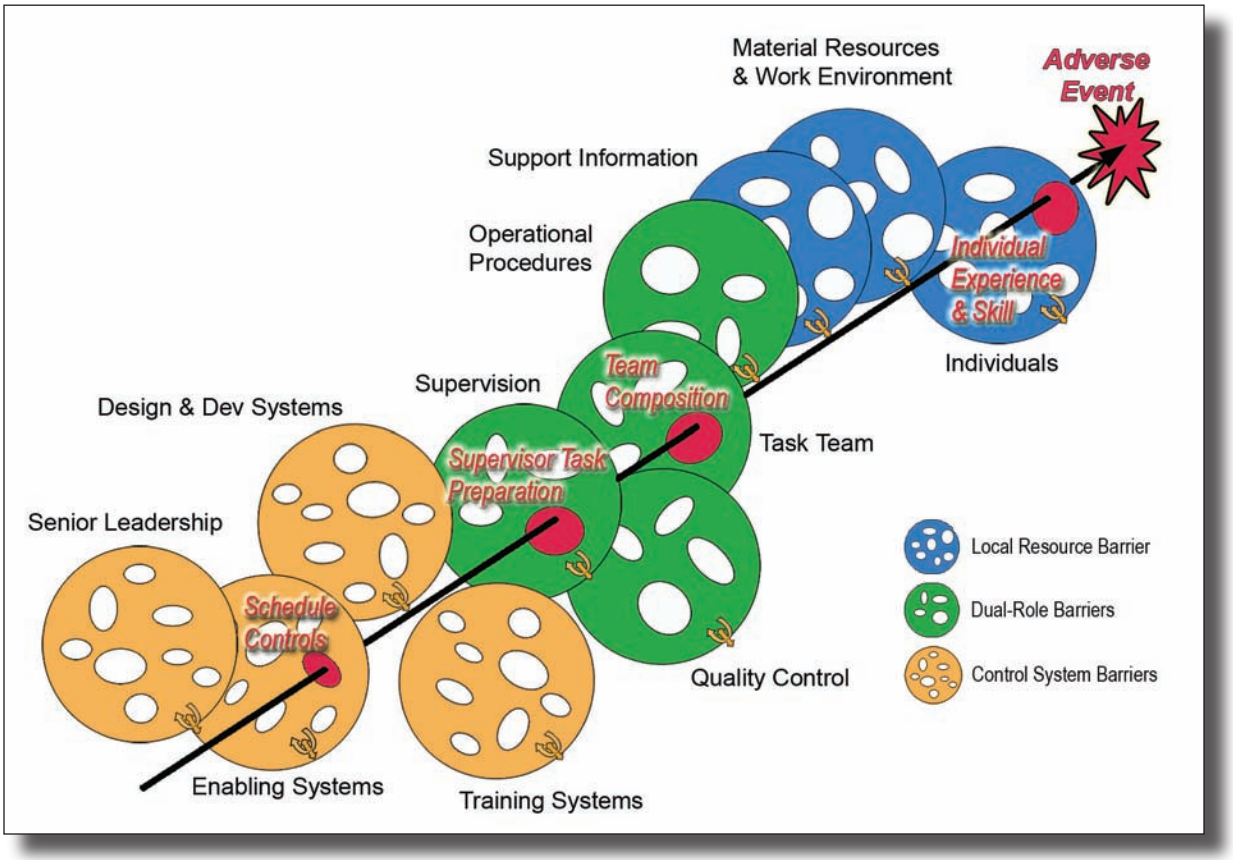

Example error trajectory through primary organizational barriers.

Command, Control, and Monitoring Technologies

Command, Control, and Monitoring (CCM) Technologies help enable future affordable, responsive, and safe spaceports. These spaceports can be Government-owned or commercial, orbital or nonterrestrial. The goal is to reduce the cost of access to space while increasing safety. CCM Technologies can help in this role by reducing or eliminating unique interface and infrastructure requirements. As we move away from a one-for-one cardinality between launch vehicle and ground infrastructure toward a truly many-to-many paradigm, we must shift our thinking about how we process and launch spacecraft. Spacecraft will have to become smarter and be in control of their spaceport processing, requesting needed services from the spaceport, as opposed to the smart spaceport telling the vehicle that it is now OK to fly. We must strive to remove complexity not only in the design but also in how information is presented to humans, wherever they may be in the loop, and provide decision support. Increases in processing requirements throughout the spaceport will drive advancements in the communication infrastructure, capability, and security. Finally, when dealing with human space flight, we need to support robust, fault-tolerate designs in both the software and hardware systems. The CCM Technology focus areas that drive toward this ultimate vision are

- sensors and data acquisition,
- spaceport processing and health maintenance,
- advanced software and computing architectures, and
- simulation and situational awareness.

For more information regarding Command, Control, and Monitoring Technologies, please contact Jim Shaver <Jim.Shaver@nasa.gov>, NASA DX-E1, (321) 867-9883, or José M. Perotti <Jose.M.Perotti@nasa.gov>, NASA DX-E3, (321) 867-6746.

Leak Detection Clip for Hypergolic Fuel and Oxidizer

Hazardous-Leak Detection and Isolation

Hypergols are especially useful rocket propellants on the Space Shuttle Auxiliary Power Unit (APU) and on the Orbital Maneuvering System/Reaction Control System (OMS/RCS). Not only is the combination of hypergolic fuel with hypergolic oxidizer self-igniting, but the reaction also produces high-energy thrust. Hydrazines (hypergolic fuel) and dinitrogen tetroxide (hypergolic oxidizer) are the components of the hypergolic propellants currently being used on the Shuttle's APU and the OMS/RCS. In addition to being extremely reactive, these compounds are highly toxic and corrosive. Because they are so reactive and toxic, leaks of hypergolic-propellant components are potentially disastrous. Consequently, leak detection in any hypergol-loaded system is of the utmost importance for equipment and personnel safety.

The hypergolic fuel and oxidizer clip is a semiquantitative point source leak detector designed to be fastened onto potentially leaking fittings and to give a visual indication of the presence of a leak. The clip contains a pad treated with chemical indicators that change color dramatically when exposed to either hypergolic fuel or hypergolic oxidizer. The intensity of the color that develops is proportional to the concentration of the leaking vapors, so a color wheel was developed to estimate the concentration of the leaking vapors. This new technology enables personnel to quickly identify, locate, and estimate the severity of a hypergol leak. Determining the source point of the leak enables personnel to take corrective actions with minimal exposure to hypergolic vapors.

Because of the reactive and corrosive nature of hypergols, all the materials used in the leak detection clip were originally selected based on their compatibility with hydrazines and dinitrogen tetroxide. The final selections were tested for compatibility and determined to be nonreactive. In addition, these materials maintain their structural integrity even when exposed to pure hypergolic fluids.

Key accomplishments:

- Developed and optimized chemical indicator formulations.
- Tested and selected compatible materials.
- Developed a prototype clip-on device.

Key milestones:

- Developed a color wheel concentration estimator.
- Delivered prototypes.

Contacts: Dr. Timothy P. Griffin <Timothy.P.Griffin@nasa.gov>, NASA TA-H2-C, (321) 867-6755; and Dr. Kathleen B. Brooks <Kathleen.B.Brooks@nasa.gov>, NASA TA-H2-C, (321) 867-7637

Participating Organization: University of Central Florida (Christina M. Berger)

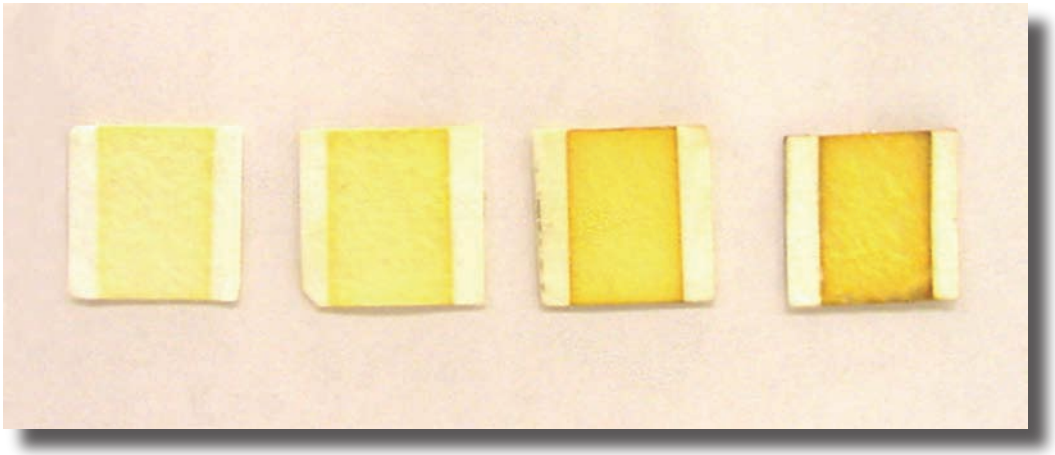

Left to right, indicator pads exposed to nitrogen dioxide vapors at 1, 5, 16, and 30 parts per million.

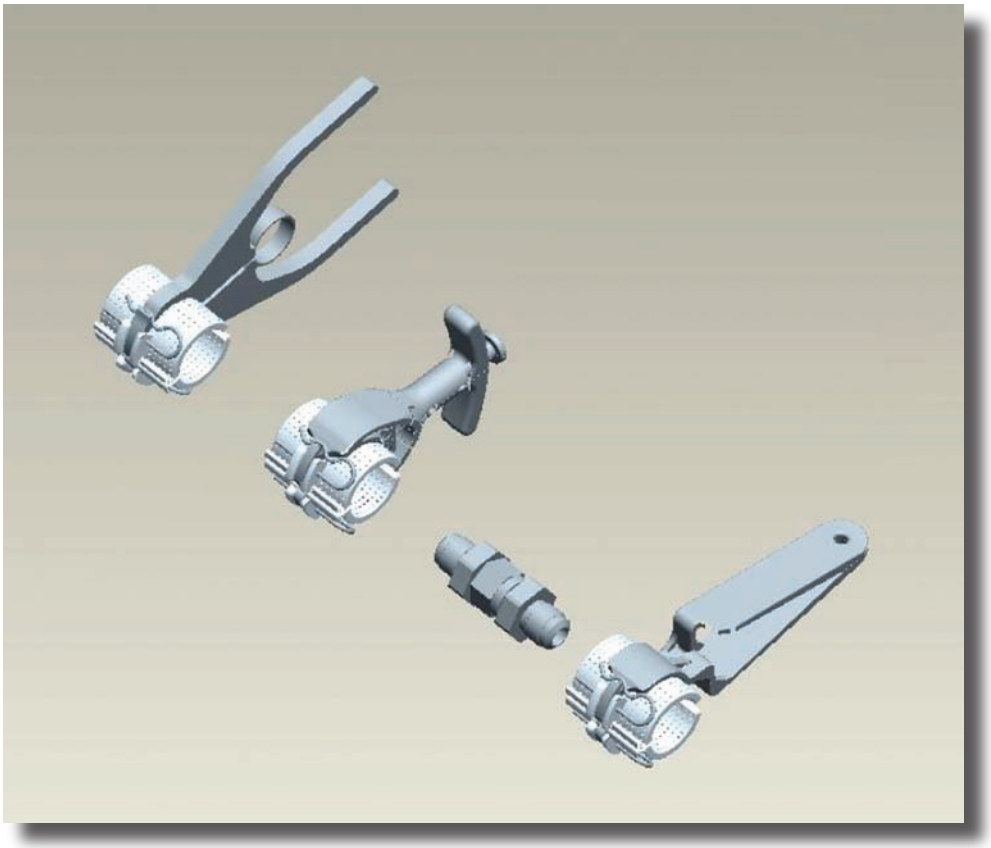

Clip hardware designs. Additional testing was performed to confirm that false positives would not occur with exposure to other compounds typically found at the sampling site. These common interferences include isopropyl alcohol, methyl ethyl ketone, toluene, acetone, and humid air. Several clip prototype designs were manufactured to ensure compatibility in a variety of fixtures.

Small Gas Analyzer for NASA, Environmental, and Commercial Applications

Hazardous-Leak Detection and Isolation

Mass spectrometers are capable of not only quantifying compounds, but identifying unknowns—even in a mixture. These analyzers can be very specific in component identification. This, coupled with a wide dynamic range, makes these analyzers very desirable. These qualities make field-portable mass spectrometers important to NASA and industry. Unfortunately, mass spectrometers are generally very large and heavy, and developing field-portable units presents quite a challenge. It is important to NASA that the environment around personnel and vehicles remain free of hazardous chemicals. Thus, there is a need to develop small portable systems capable of quantifying a vast number of airborne chemicals.

NASA has developed a transportable system for monitoring air quality around different locations. The system was designed for aircraft applications but has proven very useful as a portable gas analyzer. The system has been used to monitor air quality around volcanoes, in cities, and in the surrounding areas. The system has been transported by aircraft, cars, and people.

The system used has a total weight of 85 lb and a volume of 92,000 cm^3, requires 350 W of power at steady state, and can operate between 25 °C and –65 °C and within a pressure range of 760 to 50 torr. The system can operate in aircraft flying at altitudes up to 41,000 ft above sea level. The system is capable of monitoring and quantifying 16 gases simultaneously. Common components monitored include helium, carbon dioxide, sulfur dioxide, hydrogen sulfide, nitrogen, oxygen, argon, and acetone.

The Aircraft-Based Volcanic Emissions Mass Spectrometer (AVEMS) has demonstrated its usefulness in different applications (Figure 1), including aerial plume analysis at volcanoes (Figure 2) and ground fumarole emission analysis. Also, the concentration of carbon dioxide around urban areas (Figure 3) was measured spatially multiple times to provide temporal information. In this application, the AVEMS system was placed inside

Figure 1. Left: AVEMS system with two battery packs located in the middle row of the Cessna airplane for aerial gas analysis. Right: intake port for the AVEMS instrument along with the GPS.

a car, where an operator controlled the system via laptop. Figure 3 shows results for carbon dioxide concentrations around San Jośe, Costa Rica. High values are mainly found on the main highway.

Important characteristics of the AVEMS system are that it is transportable and measures directly at the sampling point, so it can monitor air in urban zones at every location of interest.

Work is under way to improve the control software and user interface to optimize system operation and reduce user interaction time. This will in turn reduce the labor costs associated with operating the system and reduce human-factors errors. This technology benefits NASA in terms of leak detection and air quality monitoring. Commercial applications across a wide variety of industries include quality control and regulatory-compliance monitoring.

Key accomplishments:

- Integrated a Global Positioning System into the AVEMS system.
- Modified circuit boards for increased altitude.
- Reduced weight from 104 to 85 lb.
- Developed new software for rapid data analysis.

Key milestones:

- Improve helium detection.
- Improve software upgrade.

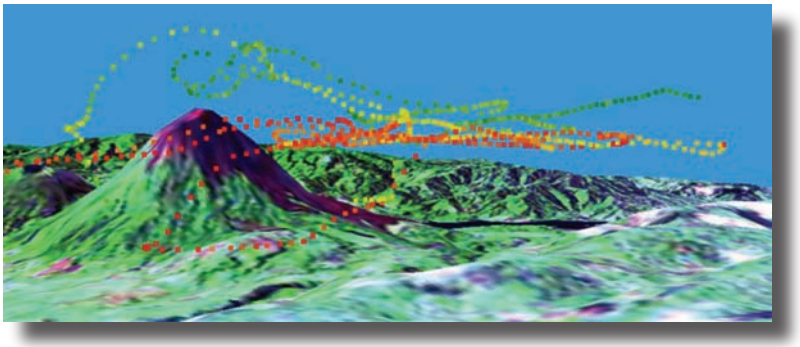

Figure 2. Carbon dioxide concentrations around Arenal Volcano.

Figure 3. Carbon dioxide concentrations around San José, Costa

Contact: Dr. Timothy P. Griffin <Timothy.P.Griffin@nasa.gov>, NASA TA-H2-C, (321) 867-6755

Participating Organizations: ASRC Aerospace (Dr. C Richard Arkin, Charles H. Curley, David P. Floyd, Guy R. Naylor, and William D. Haskell) and Universidad de Costa Rica (Dr. J. Andres Diaz, Elian Conejo, Carlomagno Soto, Laura Bogantes, Kristel Heinrich, and Oliver Gomez)

Chemical Analysis in Nonair Atmospheres

Hazardous-Leak Detection and Isolation

Chemical analysis of bulk and trace components in air is well understood and fairly common. This technology is vital in ensuring safety and quality control. However, the traditional instruments that detect and analyze components of atmospheric air do not always perform well in purged areas, common settings for space applications.

Common commercial hydrogen detectors are often based on a reaction between hydrogen and the oxygen in the air. If there is no oxygen present or the amount of oxygen present is insufficient, the detector does not function properly. Most instruments work on the assumption that the unit will operate in atmospheric air and, as a result, may not detect or accurately quantify components in the helium- or nitrogen-purged applications common in aerospace processes.

The Hazardous Gas Detection System 2000 was created to analyze purged areas. The system works well in a nitrogen background. Unfortunately, the system has a dynamic-range limitation in a helium background. Helium-purged areas are common in space vehicle processing, so improving the dynamic range in helium backgrounds would expand the capability of the systems used to process the Space Shuttle and other vehicles.

The primary problem lies with the high ionization energy of helium. This changes ion dynamics in a way that interferes with the instrument's usable range. The figure illustrates how the usable portion of the response curve (its linear dynamic range) is much smaller in a helium background than in a nitrogen background. This means that the instrument cannot detect as wide a concentration range when the sample is present in helium.

Reducing the number of helium ions and excited helium neutrals reaching the detector should help alleviate the problem. This could be accomplished in several ways: simply adjusting the ionization energy, or current; adjusting the conductance limit leading to the gas chamber; or selectively reducing the relative amount of helium entering the analyzer. Research to investigate such parameters is ongoing.

Such research will not only allow existing systems to detect a wider range of trace element concentrations in helium for Space Shuttle processing but provide knowledge useful to a host of other space applications. The atmosphere of Mars consists of 95 percent carbon dioxide, which presents challenges similar to helium. Knowledge gained is also directly applicable to monitoring for impurities in critical, high-purity gases, such as hydrogen and oxygen produced for use in fuel cells for aerospace and eventually commercial applications. In addition, this knowledge is relevant for Expendable Launch Vehicles, the Crew Exploration Vehicle, and commercial space applications.

Key accomplishments:

- Developed concepts to increase instrument dynamic range to support Space Shuttle processing and future programs requiring analysis in nonair atmospheres.
- Developed a procedure to test the effects of ionization parameters on linear dynamic range.

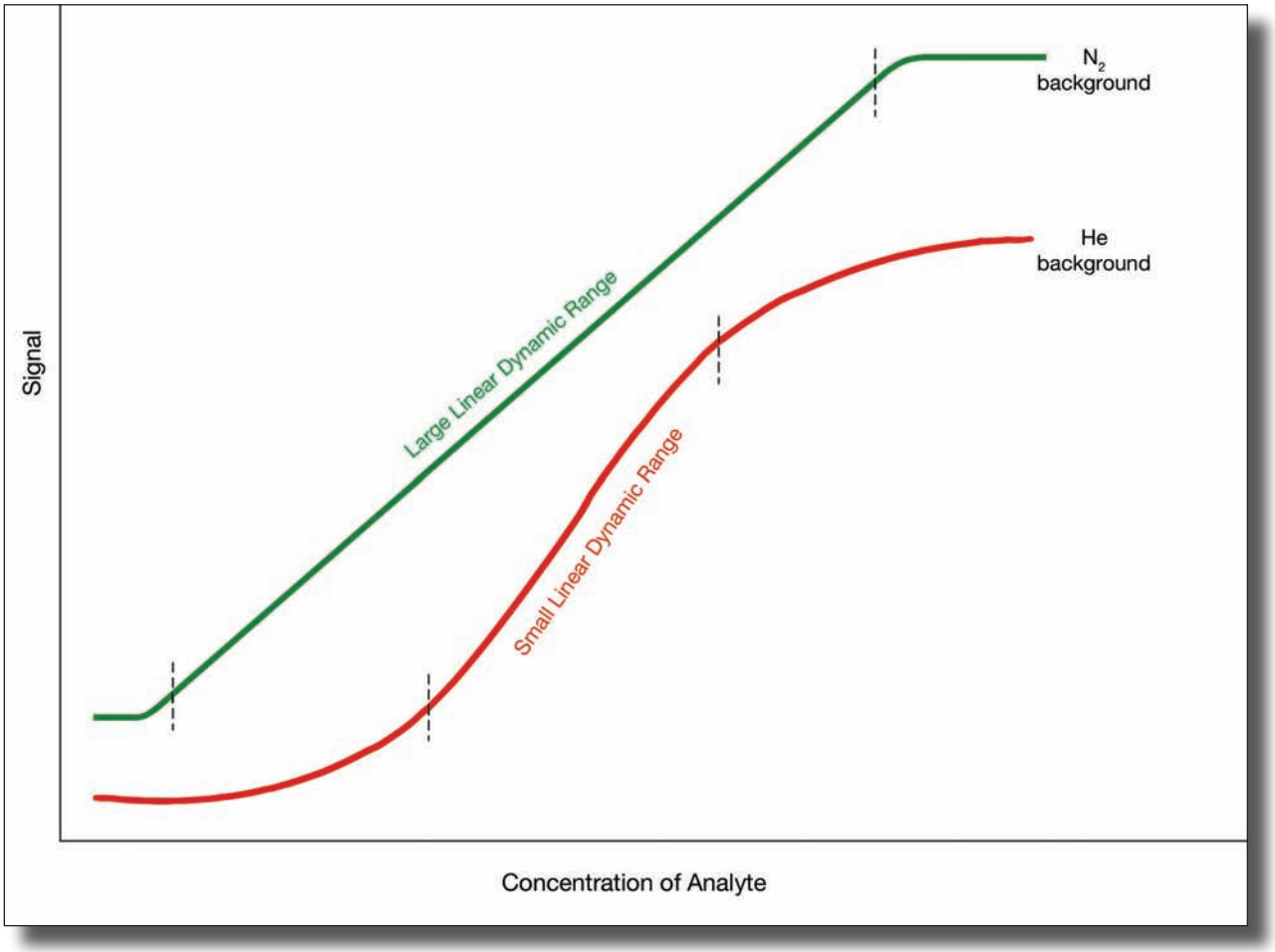

Signal versus analyte concentration illusrates the difficulty in measuring a wide range of concentrations when using helium backgrounds. Response curves generally vary substantially with background gas.

Contacts: Eric J. Gore <Eric.J.Gore@nasa.gov>, NASA PH-F2, (321) 861-4333; and Timothy O. Fish <Timothy.O.Fish@nasa.gov>, NASA PH-F2, (321) 861-7975

Participating Organization: ASRC Aerospace (Brian M. Hunter and Dr. C Richard Arkin)

Reaction Rate Calibration Techniques

2005 Center Director's Discretionary Fund Project

Hazardous-Leak Detection and Isolation

Analytical instruments used for measuring gases need to be calibrated. Existing calibration techniques involve generating a calibration curve by measuring instrument signal response to a variety of gas standards over a range of concentrations. This concentration range is produced by using several (usually two to five) stock bottles containing calibrated standards (external calibration commodities). Gas samples of unknown concentration are quantified by comparison to the calibration curve.

Calibration curve techniques have many disadvantages. For example, the gas bottles used to generate the calibration curve are generally large and heavy. Often these calibration bottles need to be placed near the instrument, which frequently means in the field at the sampling site. Moving large gas cylinders to a sample site is not feasible. In addition, these pressurized tanks pose safety hazards and must be handled by trained personnel. Often the primary reason an analysis must be performed is concern about the presence of a particular chemical. Taking additional amounts of that chemical, often at toxic concentrations, to the sample site is a further safety hazard. Moreover, the accuracy of using these gas standards for calibration is typically only 2 percent because it relies not only on the instrument and method, but also on the accuracy of the stock bottle commodity concentrations. Calibration is a lengthy process resulting in downtime when the instrument is not available to monitor the sample.

These problems can be mitigated through the use of calibration via reaction. The reaction rate calibration technique monitors the rate at which the subject gas reacts to other compounds to determine concentration.

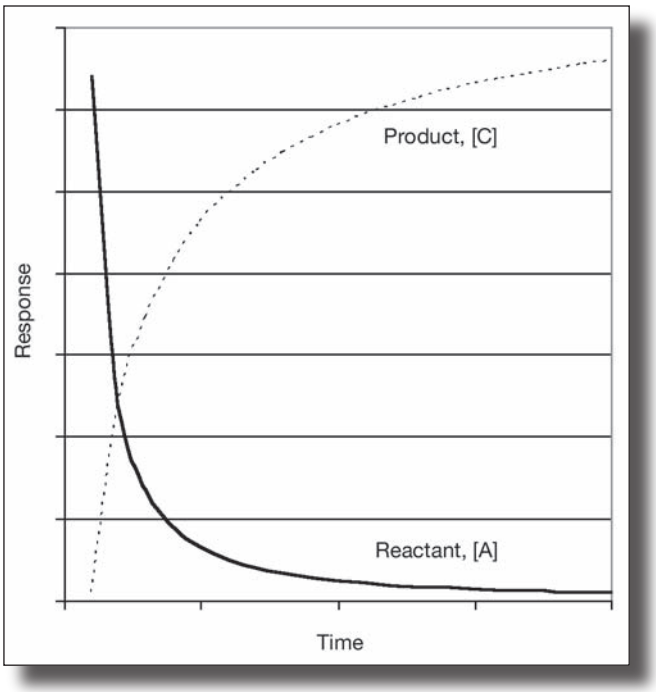

Figure 1. Relation of reaction rate to a specific experimentally determined rate constant.

Consider the reaction: A + B → C + D. The general rate equation for this reaction is $r = k\,[A]^m\,[B]^n$, where $[A]$ and $[B]$ are reactant concentrations, m and n represent the order of the reaction with respect to the reactant, r is the reaction rate, and k is a rate constant specific to that reaction. A reaction rate equation relates concentration and reaction rate for any given reaction to a specific, experimentally determined rate constant. This reaction is shown in Figure 1. Established techniques exist for empirically determining the variables r, k, A, B, m, and n. It follows from inspection of the rate equation that if the reaction rate constant k is known, concentration can be determined from an experimental reaction rate. Herein lies the basis for reaction rate calibration. Specifically, reaction rates are monitored and unknown concentrations are calculated using the observed reaction rates in conjunction with previously determined rate constants.

By eliminating the need for external calibration gas bottles, many problems associated with the calibration curve method are eliminated.

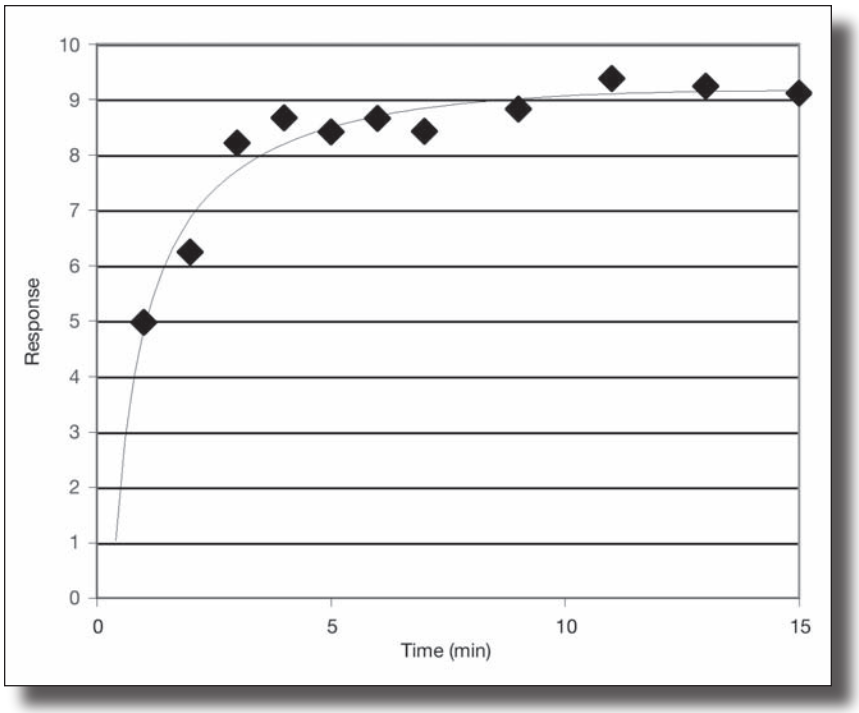

Figure 2. Rate of formation of the colored complex created by the reaction of nitrogen tetroxide with another compound.

For example, the reactant compound is not the same compound being monitored, thus reducing the risk of any toxic exposures and the false positive rate. The accuracy is shifted to the instrument and method alone, no longer limited by the manufacturer of the calibration standard. The calibration and the monitoring occur simultaneously, allowing the instrument to operate with reduced downtime.

One method used for proof of concept is to monitor the reaction of nitrogen tetroxide (hypergolic oxidizer) with another compound to form a colored complex. The rate of formation of the colored complex is monitored spectrophotometrically. Figure 2 shows the data from this experiment. From this data, the initial concentration of the nitrogen tetroxide gas can be calculated. This reaction is specific to nitrogen tetroxide gas, so it provides a means to measure (even in mixtures).

Other proof-of-concept methods have been investigatged to monitor such items as permanent gases, volatile organic compounds, and hydrazines.

Further research will focus on elucidating reaction methods for quantifying various other compounds, particularly those presently on the Spacecraft Maximum Allowable Concentrations list. Additional research will focus on applying this technology to the detection and quantification of leaks.

Key accomplishments:

- Examined three methods for proof of concept.
- Built two experimental systems.

Key milestones:

- Examine various possible applications and techniques.
- Examine factors influencing various techniques.
- Examine different substrates for volatile organic compounds and air components.

Contact: Dr. Timothy P. Griffin <Timothy.P.Griffin@nasa.gov>, NASA TA-H2-C, (321) 867-6755

Participating Organizations: ASRC Aerospace (Dr. C Richard Arkin, Guy R. Naylor, and Brian M. Hunter) and University of Central Florida (Christina M. Berger)

Chemochromic Hydrogen Detection

Hazardous-Leak Detection and Isolation

Hydrogen, a primary energy source for space exploration missions, is a main component in Space Shuttle rocket propellant. A dependable sensor is critical for hydrogen leak detection at the Shuttle launch pad, storage facilities, and other usage sites because of low explosive limits.

The Florida Solar Energy Center (FSEC), a division of the University of Central Florida, has developed a chemochromic hydrogen detection film with an irreversible response to hydrogen. This is a durable, functional material that changes color from beige to gray in the presence of hydrogen. This tape is designed to detect leaks in connection ports where hydrogen is transferred or used. It can be applied as an area monitor or integrated with personal protective equipment as an additional safeguard.

A flexible tape serves as a sensor with a platinum metal group oxide (titanium dioxide [TiO_2]) pigment produced according to the FSEC provisional patent application titled "Gas Permeable Chemochromic Composition of Hydrogen Sensing." Formulations were compared to find the most effective pigment. Several TiO_2 substrates were investigated with regard to their catalytic role. This affects the response time to hydrogen and overall color change.

Each pigment formulation was exposed to hydrogen in a glass chamber and analyzed at specific intervals. Samples were analyzed with a colorimeter to obtain the ΔE value for analytical analysis of overall color change. Samples are shown in Figures 1 and 2. The original color and final color change can be adjusted with the different formulations.

Degussa TiO_2 pigment responds within 15 seconds to hydrogen exposure but is less stable with time. Aldrich and Fisher TiO_2 formulations respond intensely to hydrogen. DuPont R103 has a unique alumina surface treatment intended to prevent discoloration that adversely affects the color change of the tape.

One of the objectives was to optimize the elasticity and ruggedness of the chemochromic tape without sacrificing the sensitivity and integrity of the film. Environmental testing was required to examine the effect of the harsh outdoor conditions in which this tape will be used. The conditions were designed to mimic application of the tape onto the KSC's cross-country hydrogen lines (Figures 3 through 5). Samples were placed at KSC's Corrosion Technology Testbed for exposure to temperature and sunlight cycling, sea spray, and rain (Figure 6). After 1 week of beachsite exposure, the samples responded faster to hydrogen than samples stored in a more controlled laboratory environment. To date, the laboratory studies include submersion in water and salt water, and exposure to an inert nitrogen atmosphere, 95 °F heat, and ultraviolet light.

These factors influence the rate of a positive color change. Continuing investigations are under way to fully elucidate the environmental effects on the hydrogen tape. FSEC found improved selectivity

Figure 1. Pigment films exposed to hydrogen.

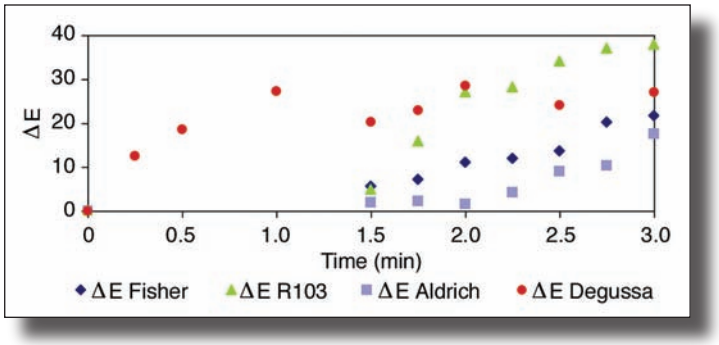

Figure 2. Comparison of pigment formulatioins with exposure to hydrogen.

Figure 3. Cross-country hydrogen lines.

Figure 4. Overhead hydrogen lines and Fixed Service Structure at KSC launch pads.

with carbon monoxide exposure. Behavior at cryogenic temperatures and other possible interferences will also be examined.

This sensor presents numerous advantages over current qualitative leak detection technology. In addition to being easy to use, the sensor does not require personnel to remain present at potentially hazardous sampling sites. The sensor can be discarded without the cost of hazardous-waste disposal. Preliminary information from the Material Test for Flight Hazards indicates that the film components have been approved for Shuttle flight (MAPTIS-II database at Marshall Space Flight Center); however, further certification will be necessary before approval is granted for use on the Shuttle.

Key accomplishment:

- Demonstrated production of nonreversible pigments and applications (2005).

Key milestone:

- Demonstrate production of reversible pigments and applications (2006).

Contact: Dr. Janine E. Captain <Janine.E.Captain@nasa.gov>, NASA KT-D2, (321) 867-6970

Participating Organizations: NASA KT-D1 (Dr. Robert C. Youngquist), FSEC (Dr. Gary Bokerman, Jessica H. Macpherson, Dr. Nahid Mohajeri, Dr. Nazim Muradov, and Dr. Ali T-Raissi), ASRC Aerospace (Barbara V. Peterson), NASA Space Life Sciences Training Program (Michelle M. Michalenko, Rensselaer Polytechnic Institute, New York), and University of Central Florida (Christina M. Berger and Dr. Mary C. Whitten)

Figure 5. Checking the width of a fitting for leak-testing material on the Fixed Service Structure.

Figure 6. Michelle Michalenko places film at the Corrosion Technology Testbed for environmental exposure.

Self-Validating Thermocouple (SVT)

The concept of SVT sensors and specifically of thermocouples has been investigated for many years. There is a great advantage to industry, particularly to process monitoring and control, in continuously monitoring and validating sensor measurements and in determining their health. The most common causes for thermocouple measurements to fail are related to the physical bonding between the thermocouple sensor element and the surface it is attached to. The SVT can detect thermocouple probe open circuits, short circuits, and unnoticeable faults such as probe debonding and probe degradation. This validation will work on the most common types of thermocouples, such as T, K, J, and E.

The SVT uses an integrated approach by combining real-time measurement/analysis, statistical tools, advanced circuit design, and the "Novel Thermocouple Junction With Built-in Heater Design and Bonding/Debonding Detection Capabilities" (NTJ) to effectively determine the measurement's health and control the pulse-width-modulated (PWM) signal to excite the NTJ.

The instrumentation is composed of a cold-junction compensator, signal conditioner circuitry, thermocouple excitation, PWM signal, analog-to-digital converter (ADC), processor, power section, and a Universal Serial Bus (USB) interface. It operates as follows.

Temperature Measurement: The ADC is measuring the voltage of the thermocouple and the cold-junction compensations. Since the output voltage of the thermocouple is very small (microvolts to millivolts), it is necessary to use the internal gain of the ADC. The ADC also monitors the output of the cold-junction compensator, so depending on the type of thermocouple used, the processor compensates the thermocouple output to obtain an accurate reading. The temperature is then calculated by using (1).

$$T_{tip} = A_0 + A_1 V_{out} + A_2 V_{out}^{\ 2} + \ldots + A_n V_{out}^{\ n} \quad (1)$$

Note that the coefficients of the equation (A_0, A_1, etc.) are different for each type of thermocouple.

Thermocouple Validation: To determine if the thermocouple is short or open, each differential line of the thermocouple is measured as single-ended to estimate the common mode. The leakage resistance of the capacitors (used to AC-couple the PWM signal) will either pull high or low any lead in case of an open circuit. This is detected by the processor, which flags the condition as one of the failure modes. The thermocouple is biased slightly to have a common-mode offset, which will change in the case of a short circuit. This is also detected by the processor and flagged as another failure mode.

Bonding/Debonding Detection: The processor sends a PWM excitation signal for a certain period to heat up the NTJ. The increase in temperature and the time required to return to the original temperature (Δ temperature/Δ time) will indicate the health of the thermocouple and if it is bonded or debonded. The AC stimulation signal does not affect the thermocouple cold junction because the inductors will act as an open circuit. In a similar manner, the DC voltage generated by the thermocouple will not affect the resistor voltage since the capacitor will act as an open circuit.

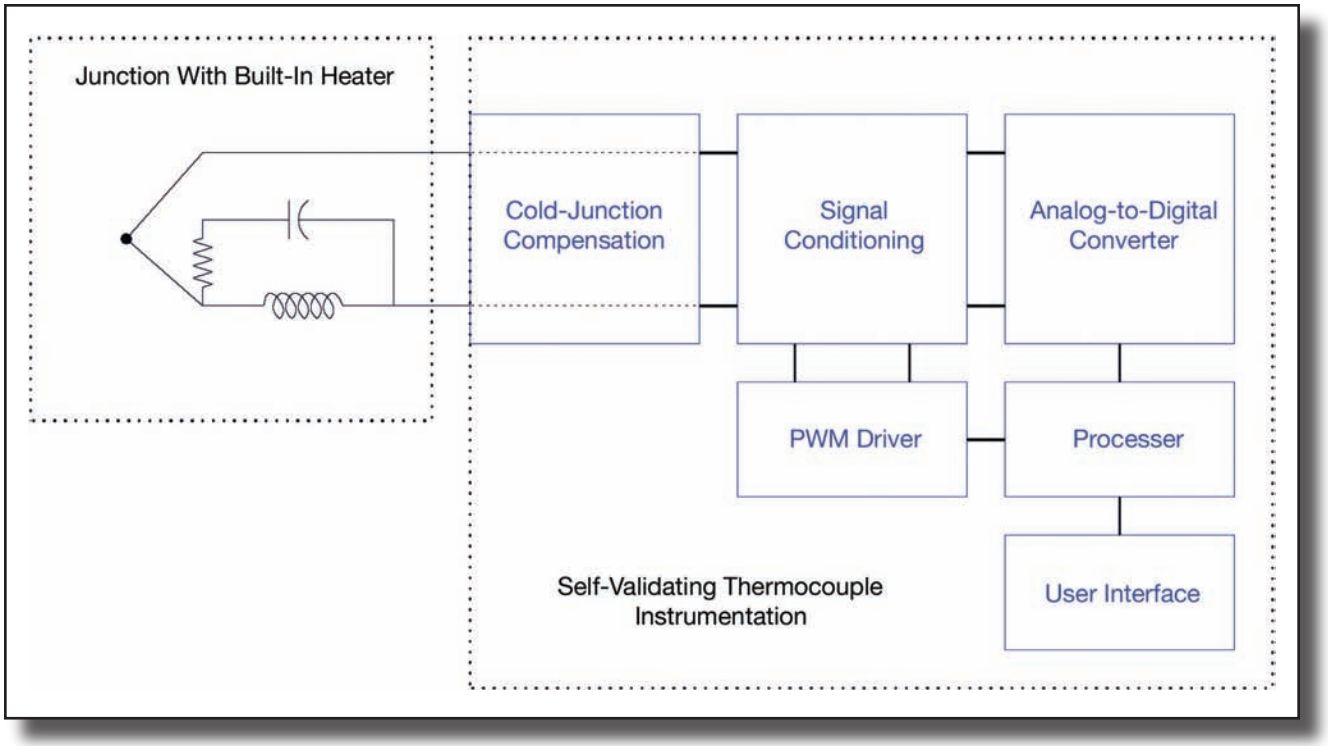

Self-Validating Thermocouple architeture.

The design uses a series of statistical tools to evaluate the correct state of the system. So upon power-up, the user can select to start a diagnosis/monitoring sequence, in which the PWM signal will be used to estimate the time constants corresponding to the correct configuration. The user may also use previous diagnostic values, which are stored in electrically erasable programmable read-only memory (EEPROM) so they are available every time the device powers up.

User Interface: The circuit board has a USB module for communication between the user and the microprocessor. Addressable Universal Synchronous Asynchronous Receiver Transmitter (USART) is the communication protocol used for this interface. The SVT will provide data to the user periodically (as defined by the user). The data could be either obtained automatically by the system (scheduled) for later analysis or requested by the user at any time (on demand).

Contact: José M. Perotti <Jose.M.Perotti@nasa.gov>, NASA DX-E3, (321) 867-6746

Participating Organizations: NASA DX-E3 (Josephine B. Santiago) and ASRC Aerospace (Dr. Carlos T. Mata and Carlos E. Zavala)

NASA Engineering Shuttle Telemetry Agent

Integrated System Health Management Technologies

The Engineering Development Directorate at KSC has designed, developed, and deployed a rule-based agent to monitor the Space Shuttle's ground processing telemetry stream. The NASA Engineering Shuttle Telemetry Agent (NESTA) increases situational awareness for system and hardware engineers during ground processing of the Shuttle's subsystems. The agent provides autonomous monitoring of a telemetry stream, known as the Shuttle Data Stream, and automatically alerts system engineers when predefined criteria are met (Figure 1). Efficiency and safety are improved through increased automation.

Sandia National Laboratory's Java Expert System Shell (Jess) is employed as the rule engine. Jess's predicate logic lends itself well to capturing the heuristics and specifying the engineering rules of this spaceport domain. The declarative paradigm of the rule-based agent yields a highly modular and scalable design, spanning multiple subsystems of the Shuttle. Several hundred monitoring rules have been written thus far, with corresponding notifications sent to Shuttle engineers.

Java classes were developed to parse and decode the Shuttle Data Stream and represent measurements as facts in Jess's working memory. To interface Jess's rule engine with the Shuttle Data Stream, each data measurement is modeled and implemented as a Java bean. Within Jess, each Java bean corresponds to what is known as a shadow fact. A Jess shadow fact is a mirror image of a Java bean, such as a pressure measurement, within Jess's working memory. All shadow facts are registered listeners of their Java bean counterparts. Thus, whenever a measurement changes in the data stream, a property change event is automatically generated for the given measurement and its sibling shadow fact is updated in Jess's working memory.

After a shadow fact is updated, the Jess pattern matcher determines if the premises of any rules match the new or modified facts. Rules are compared to working memory to identify premises that are matched by the data in working memory. For NESTA, this data represents measurements from the Shuttle Data Stream and rules represent data monitoring criteria submitted by NASA Shuttle and system engineers. An action handler class was developed and is used to build and send the notification message to the Shuttle

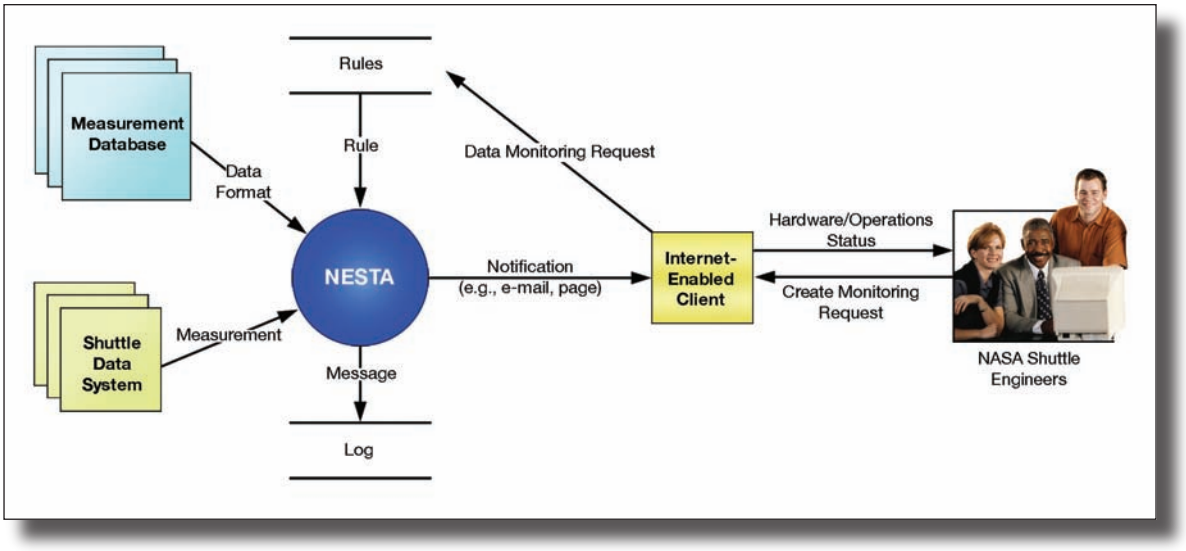

Figure 1. Context diagram.

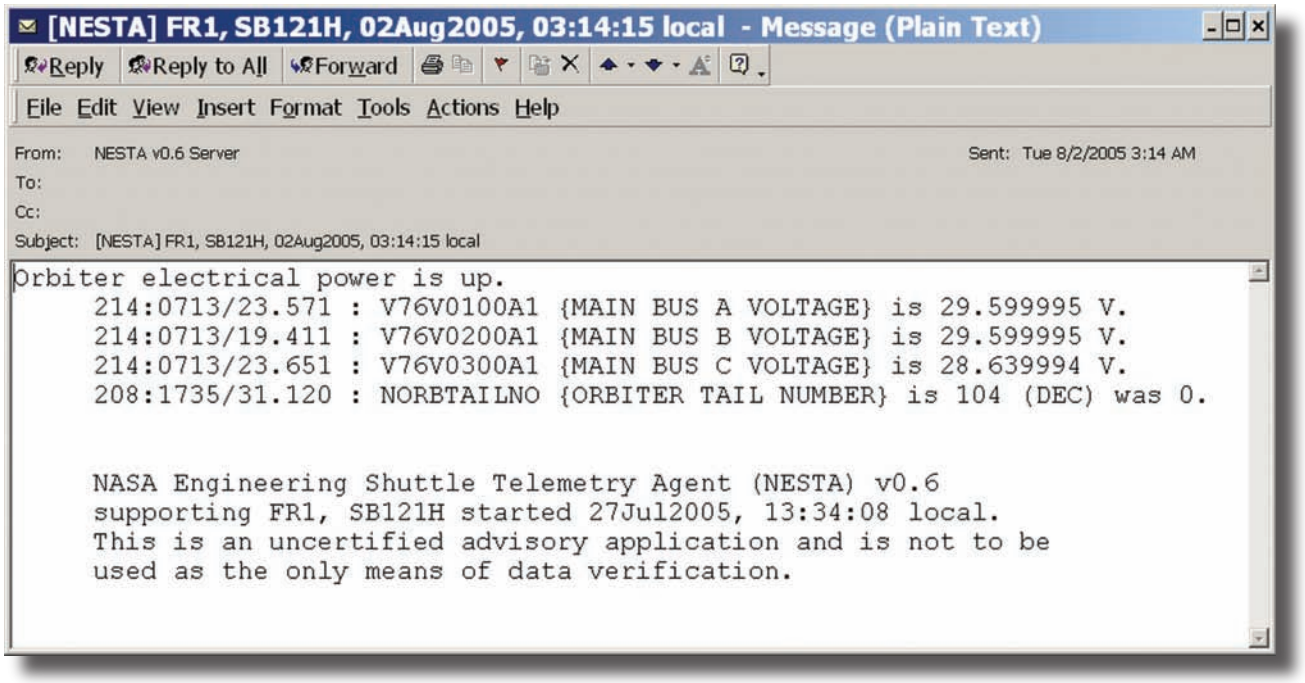

Figure 2. NESTA e-mail message.

engineer whenever a rule fires. Figure 2 shows an actual e-mail message generated by NESTA when an Orbiter was powered on.

Key accomplishments:

- Allows a NASA engineer to specify rules to be applied to measurements published in the Shuttle Data Stream.
- Generates near real-time notifications and alerts in the form of e-mails or wireless pages. Notifications may include a text message and measurement values and may be sent to multiple users when the rule's premises are satisfied.
- Monitors an arbitrary number of Shuttle Data Stream sources. This includes four control rooms used for checkout and launch of the Shuttle and its components.
- Processes multiple types and subtypes of measurements, including discretes (i.e., Boolean measurements), analogs (i.e., floating-point measurements), and digital patterns (i.e., integer measurements).
- Allows users to create and modify multiple monitoring requests without restarting NESTA.

Key milestones:

- Identify knowledge patterns and develop sophisticated graphical user interfaces to allow Shuttle engineers to create, modify, and delete rules. Add XML representations for rules.
- Investigate truth maintenance systems to enable nonmonotonic and model-based reasoning.

Contact: Glenn S. Semmel <Glenn.S.Semmel@nasa.gov>, NASA DX-E1, (321) 861-2267

Participating Organizations: NASA PH-K2 (Kevin E. Smith) and University of Central Florida (Dr. Ladislau L. Bölöni)

NESTA
NASA Engineering
Shuttle Telemetry Agent

Appendix A

KSC High-Priority Technology Needs

Articles from the KSC Technology Development and Application 2005 Report are listed under the applicable technology need.

Hazardous-Leak Detection and Isolation

Contamination Detection/Reduction/Cleaning

Integrated System Health Management Technologies

Corrosion Control

Task/Process Modeling and Simulation

Wire Inspection and Repair

- Next-Generation Wiring: Polyimide Wire Insulation Repair Material (p. 30)
- ATR-FTIR Analysis of Aging Space Shuttle Wire (p. 32)
- Variable-Pulse-Width Time Domain Reflectometry (p. 34)

Intelligent Work Instruction/Work Control Systems

- Dual-Role Taxonomy for Categorizing Factors Contributing to Adverse Safety Events (p. 134)

Propellant Loading/Servicing/Storage

- Assessing the Mechanics of Granular Materials Undergoing Narrow-Cavity Shear in Gravity (p. 82)
- Highly Reliable Liquid-Oxygen Pump (p. 84)
- Cryo-Tracker Mass Gauging System Testing in a Launch Vehicle Simulation (p. 86)
- Ray Trace Math Model and Windows Software Implementation for a Focused Infrared Lamp Protection System (p. 88)
- Remote Infrared Heating of the External Tank (p. 90)

Resource, Personnel, and/or Foreign Object Debris (FOD) Identification and Tracking

Communications Technology Upgrades

- Emerging Communication Technology (ECT) (p. 70)

Localized Weather Forecasting and Measurement

- Multistation Sonic Location of Lightning Strikes (p. 54)
- NASA Hail Monitor Development Progress (p. 56)
- Spectral Analysis Using a Second-Order Response Function (p. 58)

Self-Contained Atmosphere Protective Ensemble (SCAPE) Electrostatic Discharge (ESD) Control Enhancements

Nondestructive Composite Material and Bond Evaluation

Decision/Data Models and Analysis

- Computational Fluid Dynamics Analysis of Wind Flow Impact on the Vehicle Assembly Building (p. 40)
- Autonomous Flight Safety System (AFSS): Phase III (p. 68)
- Software Quality Diagnosis and Prognosis Model (p. 132)

Seamless Command and Control Coordination

- NASA Support of the March 2005 GlobalFlyer Mission (p. 64)
- Space-Based Telemetry and Range Safety (STARS) (p. 66)

Water Detection

Mission Data Feedback and Analysis

Minimally Intrusive Repair and Self-Healing Systems

Window Inspection

Improved Gaseous-Nitrogen Pipeline Filtration

Ding/Chip Tracking and Evaluation

Defect/Damage Location and Spacecraft Handling Systems
- Nonpyrotechnic Latch and Release System for Aerospace and Other Applications (p. 48)

Improved Helium Flow Rate and Quantity Measurements

Advanced Planning and Scheduling Tools

Hydrogen Vent Recovery

Spaceport/Range Situational Awareness

Helium Recovery and Purge Gas Substitution

Element and Gas Composition Sensors

Payload Environment Models

Flight Environment Measurement
- Evaluation of 3-D Thermal Boundary Layer Correction Factors for Circular Heat Flux Gauges Mounted in Flat Plate With Surface Temperature Discontinuity (p. 80)

Spacecraft Nutation Models
- Parameter Estimation of Spacecraft Fuel Slosh (p. 78)

Risk Assessment Tool
- High-Fidelity Aerothermal and Material-Response Analyses for Application to Engineering-Level Debris Survivability Tools (p. 74)

Large-Material and Equipment Handling
- High-Temperature Acoustic Liners (p. 42)
- Distribution of Forces in Granular Materials (p. 44)
- Physics of Rocket Exhaust Cratering (p. 46)

Modular Support Equipment

***In Situ* Resource (ISRU) Commodity Production**

Radiation Protection Technologies
- Analysis of a Lunar Base Electrostatic Radiation Shield Concept (p. 36)
- Analytical/Numerical Approximation of the Electric Field of a Conducting Torus (p. 38)

TDRSS-Compatible Transceiver

- Reconfigurable Wideband Digital Receiver and Transmitter Architecture for the Tracking and Data Relay Satellite System (TDRSS) (p. 60)
- Space-Based Telemetry and Range Safety Experiment on a Sounding Rocket (p. 62)

Unmanned Aerial Vehicle Platforms

Space and Air Traffic Management System

Efficient Lighting Systems

- Plant Lighting Systems (p. 114)

Remote Plant/Microorganism Health Sensing

- Using Noninvasive Techniques To Quantify the Effects of Mild Water Stress on Plants (p. 106)
- Bioluminiscent Monitoring System for Opportunistic Pathogens in the Spacecraft Environment (p. 108)
- Bioluminescent Biosensors for Monitoring Volatile Organic Compound Contaminants in the Spacecraft Environment (p. 110)
- Volatile-Organic-Compound Filter Cartridge for Biological Experiments in Space (p. 112)

Bioregenerative Life Support System Operation/Validation/Control

- Water Offset Nutrient Delivery Experiment (WONDER): Feedback Moisture Control for Porous-Tube and Substrate Nutrient Delivery Systems for Plant Growth in Space (p. 94)
- Passive Observatories for Experimental Microbial Systems (POEMS): Novel Payload Hardware for Microbial Growth in Space (p. 96)
- Development and Coupling of Metabolomics Capability With Transcriptomics To Dissect Cellular and Molecular Processes of Living Organisms (p. 98)
- Generation One Bioregenerative (GOBIO) Subsystem Interfacing Test Module: Project Background and Infrastructure (p. 100)
- Advanced Life Support (ALS) Project: Growth of Salad Crops for Long-Duration Space Exploration (p. 102)
- Capacitance-Based Moisture Sensing (p. 104)

Remote Payload Testing

Payload Mass and Center-of-Gravity (CG) Monitoring

Bird Abatement System

Thermal Protection System (TPS) Process Enhancement/Automation

Appendix B

Innovative Partnership Program

KSC is NASA's lead Center for developing technologies to support launch/landing and vehicle/payload processing. One of the primary missions of NASA's Innovative Partnership Program is to leverage technologies for its mission directorates, programs, and projects through investments and technology partnerships with industry, academia, Government agencies, and national laboratories. The benefits of these technology partnerships to NASA and its partners include an increased range of technology solutions, reduction in costs, accelerated maturation of technologies, and a larger pool of commercial providers. The Innovative Partnership Program also supports the transfer of technology developed in support of the Space Shuttle.

Technology Transfer

Home to world-class researchers, KSC offers a number of inventions and discoveries through its Technology Transfer Office. When discoveries are made or inventions are conceived at KSC, inventors promptly report these innovative technologies to the Technology Transfer Office to protect the Government's interests and to provide the widest practicable and appropriate dissemination for the benefit of the scientific, industrial, and commercial communities and the general public. In 2005, 143 innovations were reported to KSC's Technology Transfer Office by innovators.

Setra Systems offers NASA technology in air pressure calibrator
KSC's Technology Transfer Office executed an Exclusive Patent License Agreement with Setra Systems, a leading designer and manufacturer of pressure-, acceleration-, and weight-sensing devices, for the commercialization of the NASA-developed low-differential pressure transducer technology into a portable calibrator that can generate stable and extremely accurate pressure profiles. Setra will market the calibrator to pharmaceutical manufacturers for certifying their air-handling sensors to FDA standards.

Setra's calibrator incorporating the NASA technology.

Huff & Huff adapts NASA's groundwater remediation technology
A Nonexclusive Licensing Agreement was executed with Huff & Huff for the manufacture, use, and sale of NASA's Emulsified Zero-Valent Iron (EZVI) technology for groundwater remediation. Huff & Huff is an environmental consulting firm that provides remediation services across the country. Approximately 70 percent of the firm's market is in the private sector, with remediation being the largest part of the environmental work. EZVI reductively dehalogenates dense nonaqueous-phase liquid sources in polluted water. EZVI directly treats these contaminant sources, requires less treatment time, reduces treatment costs, and produces less toxic and more easily degradable by-products.

EZVI injection head at KSC.

Technology Infusion

NASA's current-to-voltage converter perfected by Detector Electronics
Detector Electronics Corporation acquired the rights to manufacture and sell the NASA-developed current-to-voltage converter. NASA will use the technology with its hydrogen detection systems at launch facilities. This upgrade from existing technologies improves the safety detection systems currently deployed at the KSC launch facilities and provides very accurate conversion throughout a wide temperature range. It simplifies system calibration with very high accuracy capability provided by a piecewise linearization software algorithm. This unique feature provides full electrical isolation and allows users to minimize/cancel the propagation of common problems (crosstalk, common-mode noise, etc.) between electronic systems.

NASA's scaling device manufactured by Armor Holdings
Armor Holdings International, a leading manufacturer of security products for law enforcement personnel, licensed the rights to manufacture and sell

NASA's laser scaling device and accompanying software, which were developed by engineers at KSC to address a specific Space Shuttle need. Several years ago, hail damaged several spots on the foam surface of the Space Shuttle External Tank. The operations team needed a way to measure the size of the damage sites, some of which were inaccessible, to determine if repairs were necessary. So, they photographed the surface remotely with a telephoto lens. To simplify and improve the analysis of the surface images, KSC engineers developed the laser scaling device, which projects a known pattern into the field of view of the camera.

Research and Development Partnerships

Through NASA Space Act Agreements, private companies can collaborate with NASA scientists, using NASA facilities, equipment, and technologies, to perform research and development.

Emission control system
KSC and Phoenix Systems International entered into a Space Act Agreement to continue the development of a catalytic oxidizing system that reduces nitrogen oxide and sulfur oxide emissions at power plants burning fossil fuel. This design effort builds on the work performed previously by Phoenix Systems, the exclusive licensee for 16 technologies in this area developed by scientists at KSC.

Improved flame-resistant materials
A Space Act Agreement between KSC and Great Lakes Chemical Company initiated a three-phase cooperative research and development project to scale up production, testing, and commercialization of an improved flame-retardant polymer material. This polymer can be added to a diverse matrix of thermoplastic polymers with appropriate dipole moment (e.g., nylons, polyesters, and acrylics), using common polymer-processing techniques. The resulting polymer is flame-retardant, with improved mechanical properties. Applications of this technology include protective garments, fabrics and panels used in airplanes, and electronics.

SBIR/STTR

KSC's Innovative Partnership Program is responsible for implementing the Small Business Innovation Research (SBIR) and Small Business Technology Transfer (STTR) programs. SBIR and STTR fulfill the missions and objectives of KSC, involving small, high-tech companies and research institutions in Government-sponsored research and development efforts, enabling innovations that also have potential commercial applications. As small businesses work to meet NASA's research and development needs, they stimulate growth in local economies and nearby business communities.

Automatic detection of control valve failures
Interface & Control Systems, Inc., (ICS) is a product development and engineering services firm specializing in real-time, embedded, and autonomous command and control software systems. KSC awarded ICS an STTR contract to automate the detection of mechanical failures in the Marrotta fuel control valves used in the Space Shuttle Main Engines. This project combines two cross-cutting technologies: Florida Institute of Technology's Adaptive Machine Learning algorithms and ICS's SCL, a rule-based expert system.

Food production in space
Aeroponics International's innovation is a flexible, self-contained, self-supporting, low-mass aeroponic crop production unit with integral environmental systems for the delivery and control of a nutrient mist to plant roots. The FLEX Aeroponic System model was developed for commercialization through a NASA SBIR Phase I contract for the research and development of a low-mass, inflatable aeroponic system for producing pesticide-free lettuces, grains, peppers, tomatoes, and other vegetables. The innovation addresses the need for water and nutrient delivery technologies for food production in space.

FLEX Aeroponic System for modular rapid pure food production for space and earth.

Assessing range operational performance
Knowledge Based Systems, Inc., (KBSI) has developed the Range Process Scheduling Tool (RPST). The RPST is intended for use by range planners and range technology portfolio managers to quantitatively assess range operational performance and the impact of range technology changes/upgrades on operational performance. RPST also addresses NASA's need for key enabling technology for modeling and analyzing future spaceports. KBSI was awarded Phase I, Phase II, and Phase III SBIR contracts. KBSI also developed the Tool Kit for Enabling Adaptive Modeling and Simulation (TEAMS). TEAMS provides space transportation system designers a knowledge-based infrastructure for quickly and easily developing, maintaining, and reconfiguring operations analysis models.

Simulation software maximizes resource use
SPACESIM is a computer model that simulates detailed operations processes for spaceports worldwide, allowing spaceport decision makers to improve launch vehicle throughput and maximize resource utilization. Nevins Software, Inc., developed the SPACESIM model under an SBIR contract with KSC.

Awards

KSC continues to provide incentives to innovators through Space Act Awards. The objectives of this program are to officially recognize and reward inventions and other scientific and technical contributions that have helped to achieve NASA's aeronautical, commercial, and space goals and to encourage the creation and reporting of similar contributions in the future. In 2005, 123 Space Act Awards, totaling $67,450, were presented to innovators of KSC's technologies, as well as 26 Board Action Awards, 2 Patent Application Awards, 17 Software Release Awards, and 21 NASA Tech Brief Awards.

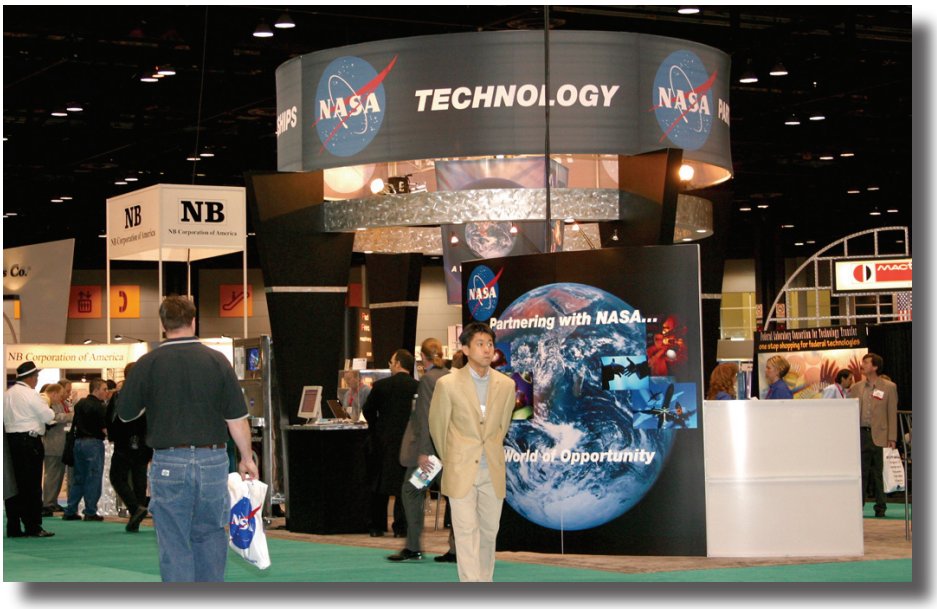

KSC Technology Transfer exhibit at the National Design Engineering Show in Chicago.

Appendix C

Transferring NASA Technology and Content Into High School Classrooms

The Education Technology Office at KSC focuses on promoting the transfer of NASA technology and content into education, while fostering student interest in science technology engineering and math careers. The Virtual Lab, with its simulation of a scanning electron microscope (SEM), provides an example of this focus.

While there are multiple uses for the SEM at NASA, high school and college students rarely have opportunities to work with these instruments because of their cost. To inspire the next generation of explorers, KSC has funded the development of a virtual SEM (VSEM) by the Beckman Institute for Advanced Science and Technology at the University of Illinois at Urbana-Champaign as part of NASA's Learning Technologies Project (LTP). LTP, funded by the Office of Education, conducts and facilitates educational projects at all levels of the American education system. The project funds activities that use the Internet and other technologies to foster reform and restructuring in math, science, computing, engineering, and technical education.

KSC's Virtual Lab is a suite of virtual microscopes and includes the VSEM, a virtual light microscope, a virtual atomic-force microscope, and a virtual energy-dispersive spectrometer with over 80 specimens. The latter two instruments are in development and will be available by September 2006. The open-source software is provided on <*SourceForge.net*>. Its open architecture makes extensive use of XML to allow easy integration of new specimens and downloads from multiple Web servers. In the Virtual Lab, flash animation and videos are included alongside the simulations to explain how the VSEM works, how specimens are prepared, and how the SEM is used at NASA. Students are then able to analyze NASA-related specimens, such as a section of Space Shuttle tile (see the figure). These specimens are rich with detail, allowing the students to magnify and pan around any area of interest because of the high-resolution, multidimensional nature of the images. The software, additional specimens, support information, and a developer's discussion forum are available at <*http://virtual.itg.uiuc.edu*>. The Virtual Lab has also demonstrated its usefulness within the scientific community and informal education in helping to communicate and share specimen data.

Teachers involved with the development of the Virtual Lab emphasized the importance of making science engaging, using materials that students can relate to beyond the classroom. The Virtual Lab has received national recognition for this role of hands-on learning in *Science Magazine* (April 8, 2005), which noted, "Many beginning students never get closer to an electron microscope than the photos in their textbooks. But anyone can get a sense of what the instrument can do by downloading this simulator from NASA's Kennedy Space Center."

The version of Virtual Lab developed in 2004–2005 was piloted in three high schools that are working to meet the needs of diverse populations of students from underserved areas (based on household income). In 2005, with funding by the BellSouth Foundation, researchers from the University of Central Florida (UCF) were able to test the software and work with teachers to develop materials to integrate the VSEM into high school biology classrooms. This study enabled us to better understand the needs of teachers and students in low-income high schools. This work would not have been possible without collaboration among KSC's Education Technology Office, KSC's Material Science group, the Beckman Institute, and UCF.

During our research in local high schools, we observed that teachers need flexible materials that they can adapt for their students. This insight has guided our current efforts.

Key accomplishments:

- Developed an online resource with nationally recognized models for assessment and instruction that will help teachers integrate the tool into their classrooms.
- Presented findings from studying the use of the Virtual Lab in low-income classrooms at the International Artificial Intelligence in Education Conference.
- Presented the VSEM at the Microscopy and Microanalysis 2005 conference and shared the Virtual Lab with experts in the fields of education and microscopy.

Key milestones:

- Integrate our focus into teacher education courses while working with teachers to continue developing materials for instruction and assessment.
- Promote the Virtual Lab and related materials to support classroom integration through regional conferences on science and technology related to education.
- Further the long-term goal of adapting Java-based teachable agents to guide student work with the Virtual Lab.

Contact: Theresa M. Schroeder <Theresa.M.Schroeder@nasa.gov>, NASA XA-D1, (321) 867-0590

Participating Organizations: University of Central Florida, College of Education (Dr. Laura N. Blasi and Yedong Tao) and Beckman Institute for Advanced Science and Technology at the University of Illinois at Urbana-Champaign (Glenn Fried and Ben Grosser)

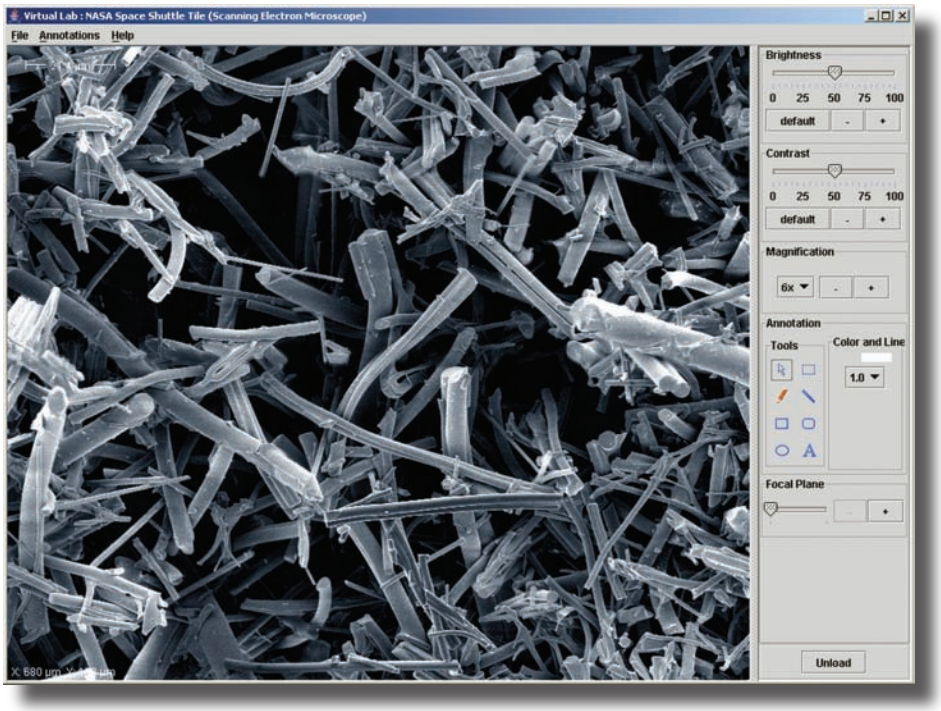

Space Shuttle tile specimen as viewed using the VSEM.

Appendix D

Kennedy Space Center Export Control

"It is the policy of the United States to sustain vigorous scientific enterprise. To do so involves sustaining the ability of scientists and other scholars freely to communicate research findings, in accordance with the applicable provision of the law, by means of publication, teaching, conferences, and other forms of scholarly exchange."

Export Administration Regulations(EAR, Section 2, Paragraph 12)

The U.S. Government controls exports of sensitive equipment, software and technology as a means to promote our national security interests and foreign policy objectives. Through the export control system, the U.S. Government can effectively provide for national security by limiting access to the most sensitive U.S. technology and weapons.

National Export Control Legislation and Regulations:

Arms Export Control Act of 1976	Export Administration Act of 1979
International Traffic in Arms Regulations (ITAR)	**Export Administration Regulations (EAR)**
Govern export of defense articles and services, to include most space-related technologies/systems.	Govern the majority of U.S. commercial exports (civil and dual-use) as well as International Space Station (ISS) hardware.
United States Munitions List (USML)	**Commerce Control List (CCL)**
<www.pmddtc.state.gov>	*<www.bis.doc.gov/>*

What is an Export?

- Traditional "shipments" of items through Center or commercial transportation to destinations outside the United States.
- Mailing, faxing, or e-mailing items outside the United States or to foreign persons within the United States.
- Hand-carrying items outside the United States.
- Verbal discussions with foreign nationals or presentations to groups that include foreign persons.
- Placing information in the public domain or on the World Wide Web, or posting data on ftp: sites, Internet chat rooms, or electronic bulletin boards.

With the exception of publicly available technical data and software, every commodity, piece of technical data, and software item in the economy—from pencils to missile guidance systems—is subject to the export control regulations.

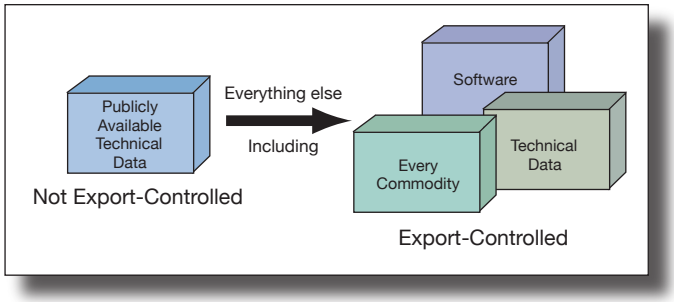

- The Departments of State and Commerce control the vast majority of all exports.
- All technology (e.g., articles, technical data, software, and defense services) must be classified and licensed for export unless an exemption or exception can be found.

NASA Kennedy Space Center – Export Control Office:

The NASA Kennedy Space Center Export Control Office assists with export control and export compliance matters in maintaining national security and limiting access to the most sensitive space technologies. The office is coordinated by Center Export Administrator Wayne Ranow. The Export Control Help Desk is operated William Collins, Anteon Corporation. The KSC Export Control Office furnishes export assistance with classifications, license, export training, and general answers related to export control matters. Please visit the following sites for all of your export control needs, training lessons, and export training certifications:

<https://satern.nasa.gov/elms/learner/login/jsp>, **(SATERN: To Obtain Export Training Certification)**

<http://exportcontrol.ksc.nasa.gov>, **(KSC: Export Training Purposes Only)**

Export Control Training Lessons	
Technical Exchange Information Lesson	KSC Export Control Basic Lesson
KSC Export Control Foreign National Visit Processing Lesson	KSC Export Control International Visitors – International Partners
Document Availability Authorization Lesson	

NASA Kennedy Space Center – Export Control Office Points of Contact	
Wayne Ranow, Center Export Administrator *<Wayne.Ranow-2@nasa.gov>* (321) 867-6066 Melanie Chan, Associate Center Export Administrator *<Melanie.R.Chan@nasa.gov>* (321) 867-6367	William Collins, Sr. Technical Director Anteon Corporation *<William.Collins-2@ksc.nasa.gov>* Export Hot Line: (321) 867-9209
Export Control Web Site *<http://exportcontrol.ksc.nasa.gov>*	

Index

Index

Index

REPORT DOCUMENTATION PAGE

Form Approved
OMB No. 0704-0188

1. REPORT DATE *(DD-MM-YYYY)*	2. REPORT TYPE	3. DATES COVERED *(From - To)*
01-03-2005	Technical	January 1, 2005 – December 31, 2005

4. TITLE AND SUBTITLE
Technology Development and Application 2005 Annual Report

5a. CONTRACT NUMBER

5b. GRANT NUMBER

5c. PROGRAM ELEMENT NUMBER

6. AUTHOR(S)

5d. PROJECT NUMBER

5e. TASK NUMBER

5f. WORK UNIT NUMBER

7. PERFORMING ORGANIZATION NAME(S) AND ADDRESS(ES)
NASA, John F. Kennedy Space Center
Kennedy Space Center, Florida 32899

8. PERFORMING ORGANIZATION REPORT NUMBER
NASA-TM-2006-214201

9. SPONSORING/MONITORING AGENCY NAME(S) AND ADDRESS(ES)
National Aeronautics and Space Administration
Washington, D.C. 20546

10. SPONSOR/MONITOR'S ACRONYM(S)

11. SPONSOR/MONITOR'S REPORT NUMBER(S)

12. DISTRIBUTION/AVAILABILITY STATEMENT
Unclassified – Unlimited
Subject Category:
Availability: NASA CASI (301) 621-0390

13. SUPPLEMENTARY NOTES

14. ABSTRACT
Successful technology development and application projects are critical to KSC. When advanced technologies are infused in spaceport and range systems, the outcomes are dramatically safer, more efficient, and more responsive operations for launch customers. Transformational spaceport and range technologies are required to enable space-craft processing and launch capabilities involving common, shared-usage equipment applicable to a wide range of vehicles and payloads. These advanced technologies will benefit any Earth spaceport, lunar base, or Mars base.

The KSC technology development and application team includes a variety of partnerships among civil servants, contractors, academic institutions, and commercial industries. KSC's technology development stakeholders include current space transportation programs, future space transportation programs/initiatives, and enabling technical programs. The KSC Technology Development and Application 2005 Annual Report encompasses the efforts of contributors to the KSC advanced technology development program and KSC technology transfer activities.

KSC Chief Technologist Dr. Dave Bartine, (321) 867-7069, is responsible for publication of this report and should be contacted for any desired information regarding KSC's Technology Development and Application activities.

15. SUBJECT TERMS
Technology Development and Application

16. SECURITY CLASSIFICATION OF:			17. LIMITATION OF ABSTRACT	18. NUMBER OF PAGES	19a. NAME OF RESPONSIBLE PERSON
a. REPORT	b. ABSTRACT	c. THIS PAGE			Dr. Dave Bartine
U	U	U	UU	1??	19b. TELEPHONE NUMBER *(Include area code)* (321) 867-7069

National Aeronautics and Space Administration

John F. Kennedy Space Center
Kennedy Space Center, FL 32899

www.nasa.gov

NASA Technical Memorandum 2006-214201